2002

DEVELOPMENT OF IMPROVED HEAD-DISK SPACING MEASUREMENT METHODS FOR MAGNETIC DISK DRIVES

LIU, XINQUN

DEVELOPMENT OF IMPROVED HEAD-DISK SPACING MEASUREMENT METHODS FOR MAGNETIC DISK DRIVES

by

XINQUN LIU

A thesis submitted to the University of Plymouth
in partial fulfilment for the degree of

DOCTOR OF PHILOSOPHY

Department of Communication and Electronic Engineering
Faculty of Technology

October 2002

DEVELOPMENT OF IMPROVED HEAD-DISK SPACING MEASUREMENT METHODS FOR MAGNETIC DISK DRIVES

XINQUN LIU

ABSTRACT

A detailed review of existing flying height or head disk spacing testing techniques has been made, and in-depth analyses of the working principles of the currently popular optical interferometry flying height testing methods are presented with simulation results. A new dual-beam normal incidence polarisation inteferometry method is then proposed. One advantage of this dual-beam polarisation interferometry is that it can be used for both the direct spacing measurement (DSM) method and relative displacement measuring (RDM) method. The RDM method is a good way to measure the head-disk spacing and the slider pitch or roll when a real magnetic disk is used for testing. The DSM method has the advantage that the absolute head-disk spacing can be observed and measured directly, especially in the case where it is difficult for the light beam to 'spot' the back surface of the head-slider. When used for the DSM method, the flying height can be measured down to contact without losing sensitivity. Slider pitch or roll can also be measured using the phase information. Another advantage of this polarisation interferometry is that, when used for the DSM method, with the measured intensity and phase information, the optical constants of the slider material can be determined, which is necessary to determine the flying height. By investigation of the application limits and potential problems of the intensity interferometry method, an improved intensity interferometry method is also proposed by using phase-shifting technique to improve the sensitivity of this method when the head-disk spacing is below 10 nm and near contact. An experimental testing system has been built to test the capability and effectiveness of the proposed interferometry methods. Experimental results are presented which show good agreement with the results gained from theoretical analyses and simulation.

TABLE OF CONTENTS

LIST OF FIGURES

LIST OF TABLES

ACKNOWLEDGEMENTS

This work has been conducted under the supervision of Professor Warwick Clegg, and I would like to express my great thanks for his tremendous support, encouragement and guidance from the beginning till the end. I would also like to thank Dr. Bo Liu and the Data Storage Institute of Singapore for their invaluable technical and financial support, which is greatly appreciated.

I would like to express my gratitude to all those people and organisations who have been associated with this project especially the following.

My second supervisor Dr. David Jenkins for his guidance and useful discussions.

Both academic members and technical staff at the Centre for Research in Information Storage Technology and DCEE for their support and friendship.

Mr. Adrian Mathews and Brian Pateman at the Workshop of the University of Plymouth. Without their industrious work and enthusiastic support, many of the mechanical parts for building up the opto-mechanical testing system would not have been available on time.

Mr. Chibesa Chilumbu, James Windmill, Glen Tunstall, Nick Fry, Phil Brown, Robert Windmill, Adrian Ambroze, James Slader, and Bill Mckee for their constant friendship.

Changchun Institute of Optics & Fine Mechanics, Chinese Academy of Sciences, for their support and encouragement.

Last but by no means least, I would like to thank my wife, my son, and my own and my wife's family. Without their continuous encouragement, support, love and understanding, this thesis would not have been finished.

AUTHOR'S DECLARATION

At no time during the registration for the degree of Doctor of Philosophy has the author been registered for any other University award.

This study was financed with the aid of research support from the Data Storage Institute of Singapore, the CVCP (ORS Award), the Faculty of Technology, University of Plymouth, and the British Council in Singapore. The author is extremely grateful for all these sources of support.

Six papers from this work have been presented at international conferences and published in the relevant journals. Copies of the published papers are included in the Publications section of this thesis.

The author also attended the 2000 International Conference on Magnetics, April 2000, Toronto, Canada.

Signed Xinqun Liu

Date 16/10/2002

1 Introduction

1.1 Overview

The need for ever-greater storage capacity has resulted in the data-storage recording densities of magnetic hard disk drives growing at a rate of about 60% every year in the past decade. In order to support these developments, work has been undertaken in parallel to improve the heads, media, channel, and electronics. However, one of the most critical and effective parameters in increasing areal density is the flying height or spacing between the read-write head and the recording disk medium. Since 1990, the flying height has been reduced from above 140nm to under 20nm for the leading-edge products of the magnetic recording industry, which is illustrated in Figure 1.1.

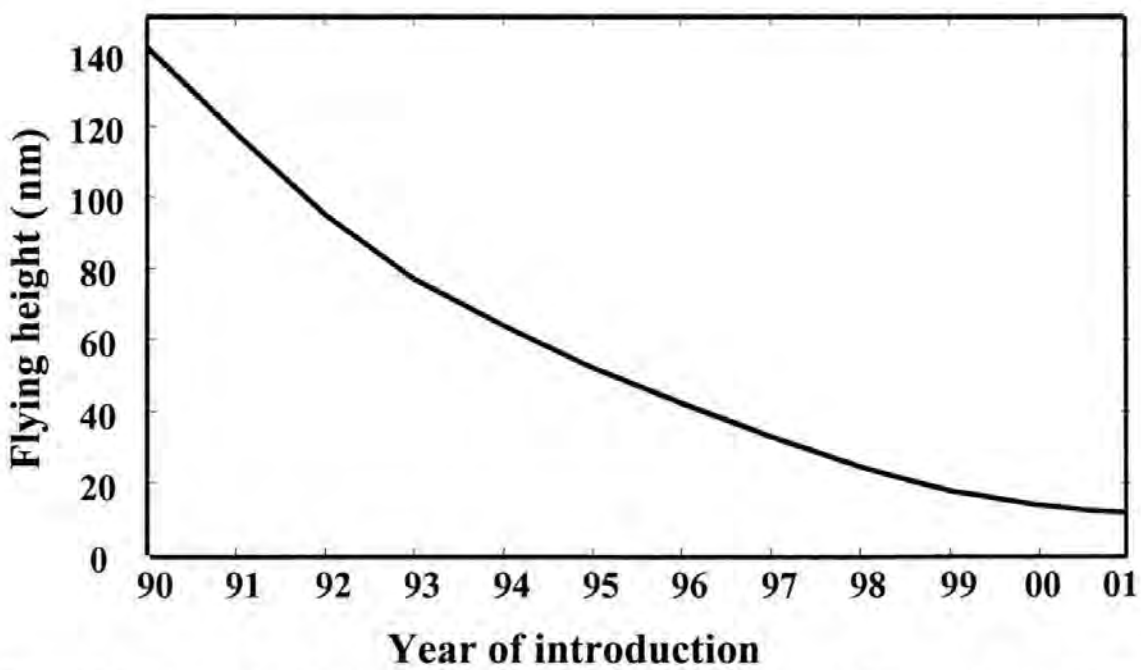

Figure 1.1 Flying height history for the leading-edge products of the magnetic recording industry

It is expected that the head-disk spacing will reduce from the current value of 20~30nm to a level of 5~10nm, as the technology moves from the current 10 Gb/in^2 areal density to beyond 40 Gb/in^2 areal density of commercial hard disk drives by the year 2004 [Liu et al., 1999].

Although it is very desirable to reduce the head-disk spacing or flying height to increase the recording areal density, head disk contact is undesirable during disk operation since that will deteriorate the tribological performance of the head disk interface and its reliability. Therefore, it becomes more and more important and necessary to make high accuracy head-disk spacing measurements and characterisation both in new read-write head product development and on the manufacturing line. This project was proposed from such a background to meet this technical challenge. The thesis is outlined as below:

Chapter 1 gives the backgroud of this research work and an overview of the development of magnetic hard disk drives.

Chapter 2 provides the theoretical basis being used in the optical flying height testing techniques through the whole thesis.

Chapter 3 gives a detailed review and analysis of several existing flying height or head medium spacing testing techniques. Simulation results for the theoretical analysis are also presented.

Chapter 4 describes the Improved Intensity Interferometry Method we have proposed for the measurement of head-disk spacing down to contact. In this chapter, two phase-shifting methods are given to improve the sensitivity of the intensity interferometry technique when the head-disk spacing is below 10 nm or near contact. Simulation results are also included.

Chapter 5 describes the Dual-Beam Normal Incidence Polarisation Inteferometry Method we have proposed. Simulation results for the theoretical analysis are presented through the whole chapter.

Chapter 6 presents the experimental system that has been built up to test the capability and effectiveness of the Improved Intensity Interferometry method and Normal Incidence Polarisation Interferometry method we have proposed.

Chapter 7 gives the experimental results and their analysis. The determination of the optical constants of the slider material and the initial phase of the interferometer is also presented in this chapter.

Chapter 8 presents the conclusions and recommendations for futher research.

1.2 Advances in HDD industry

Since the invention of the hard disk drive, it has undergone both evolutionary and revolutionary changes at a tremendous pace. The progress of areal data density is shown in Figure 1.2, which indicates an annual compound growth rate of about 30% in the 1970s and 1980s, but an even more astonishing rate of about 60% in the 1990s due to the introduction of magnetoresistive (MR) heads and partial-response maximum likelihood (PRML) detection channels.

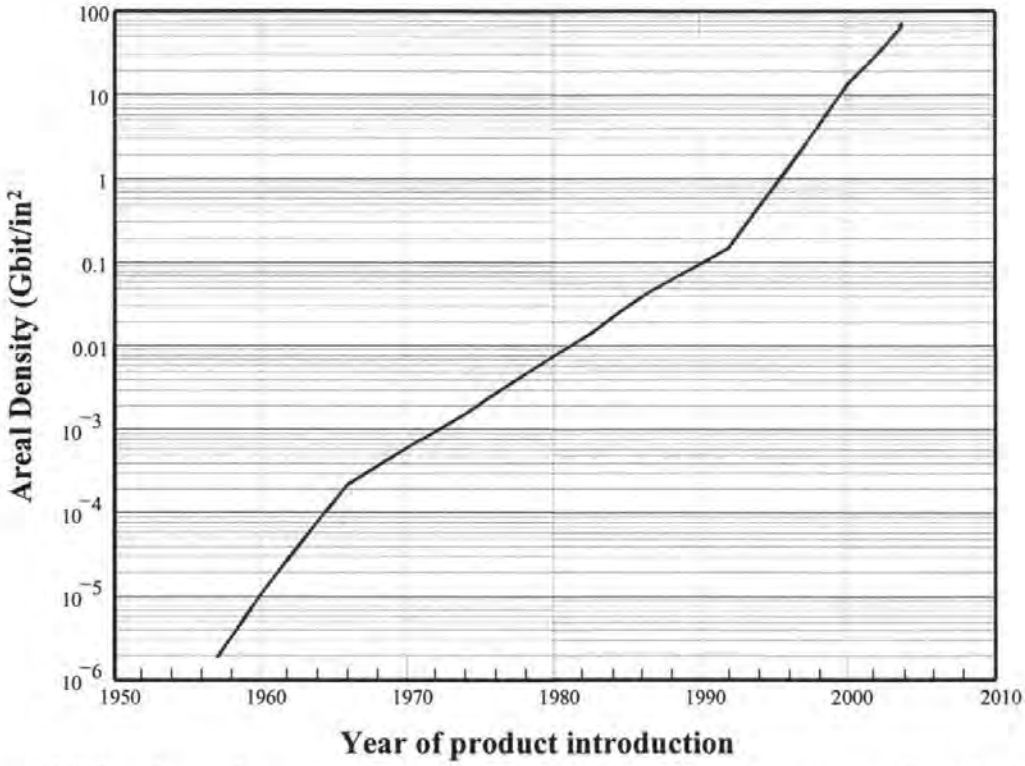

Figure 1.2 Leading-edge magnetic hard disk drive areal density vs. year of production introduction (including prediction) [Wang & Taratorin, 1999]. The line is for visual guidance only.

Hard disk drives, also called rigid disk files, were first developed by IBM, San Jose, California in the late 1950s. The very first hard disk drive was introduced in1956, which contained 50 disks with a diameter of 24 in., provided a data capacity of 5 MB and a data rate of 70.4 Kb/s. The areal density was about 2 Kb/in^2. In 1973, a generation of hard disk drive, the IBM 3340, also named Winchester was introduced, which contained two or four disks with a diameter of 14 in., providing a data capacity of 35 or 70 MB, a data rate of 6.4 Mb/s, and an areal density of 1.69 Mb/in^2. In 1997, the highest areal density of any hard disk drive reached 2.6 Gb/in^2, which was found in the IBM Travelstar 4GT. It had a data capacity of 4 GB and a data rate of 83.2 MB/s, and contained four disks with a diameter of 2.5 in. The following is news releases from IBM]:

In March 1998, IBM announced the highest capacity hard disk drive for notebook computers, Travelstar 6GT. It had a capacity of 6.4 GB and an areal density of 4.1 Gb/in^2.

In October 1998, IBM announced the highest capacity hard disk drive for premium notebook computers, the Travelstar 14GS. It had a capacity of 14.1 GB and an areal density of 5.0 Gb/in^2. Its Travelstar 10GT and travelstar 6GN had a capacity of 10.0 GB and 6.4 GB and an areal density of 5.6 Gb/in^2 and 5.7 Gb/in^2 respectively.

In November 1998, IBM announced its highest capacity desktop PC hard disk drive in the world, IBM Deskstar 25GP, the areal density of which is 3.74 Gb/in^2. It had a capacity of 25 GB, a data rate of 195.6 Mb/s, and contained 5 or 4 disk platters.

In June 1999, IBM announced the world's highest capacity hard disk drive for desktop PCs, Deskstar 37GP. It had a capacity of 37.5 GB, a data rate of 248 Mb/s, and an areal density of 5.3 Gb/in^2.

In October 1999, IBM announced the world's highest capacity server hard disk drive, Ultrastar 72ZX, which contained 11 disk platters, and had a capacity of 73.4 GB and areal density of 7.04 Gb/in^2.

In March 2000, IBM announced the highest capacity hard disk in the world drive for desktop computers, the Deskstar 75GXP. It contained 5 glass disk platters, and had a capacity of 75 GB, a data rate of 444 Mb/s, and an areal density of 11.2 Gb/in^2. Its Deskstar 40GV had an areal density of 14.3 Gb/in^2.

In April 2000, IBM announced it's world's highest capacity notebook computer hard disk drive, the Travelstar 32GH, which contained 4 glass disk platters and had a capacity of 32 GB and an areal density of 14 Gb/in^2. Both its Travelstar 30 GT and Travelstar 20 GN had an areal density of 17.1 Gb/in^2.

Let us now consider attainments in research: In February of 1999, Seagate set a new data-storage density mark of 16.3 Gb/in^2. In May, IBM demonstrated an even higher

data-storage density of 20 Gb/in^2. Five months later, IBM revealed their state-of-the-art hard disk drive with a data-storage density of 35.3 Gb/in^2. In March 2000, Seagate announced that they have demonstrated the world's highest areal density of 45 Gb/in^2. The current prediction is that if this trend of growth of continues, we should expect the data-storage density of commercial hard disk drives to be well in excess of 40 Gb/in^2 by the year 2004. In order to achieve such a high data-storage density, the corresponding head flying height is expected to be lower than 10 nm.

1.3 Physics of magnetic recording

1.3.1 Basic principles

Magnetic hard disk drives, floppy disk drives, and tape drives are all based on the same fundamental principle of magnetic recording which involves an inductive recording head (magnetoresistive (MR) read heads are also being used nowadays) and a recording medium, as shown in Figure 1.3. [Wang & Taratorin, 1999]

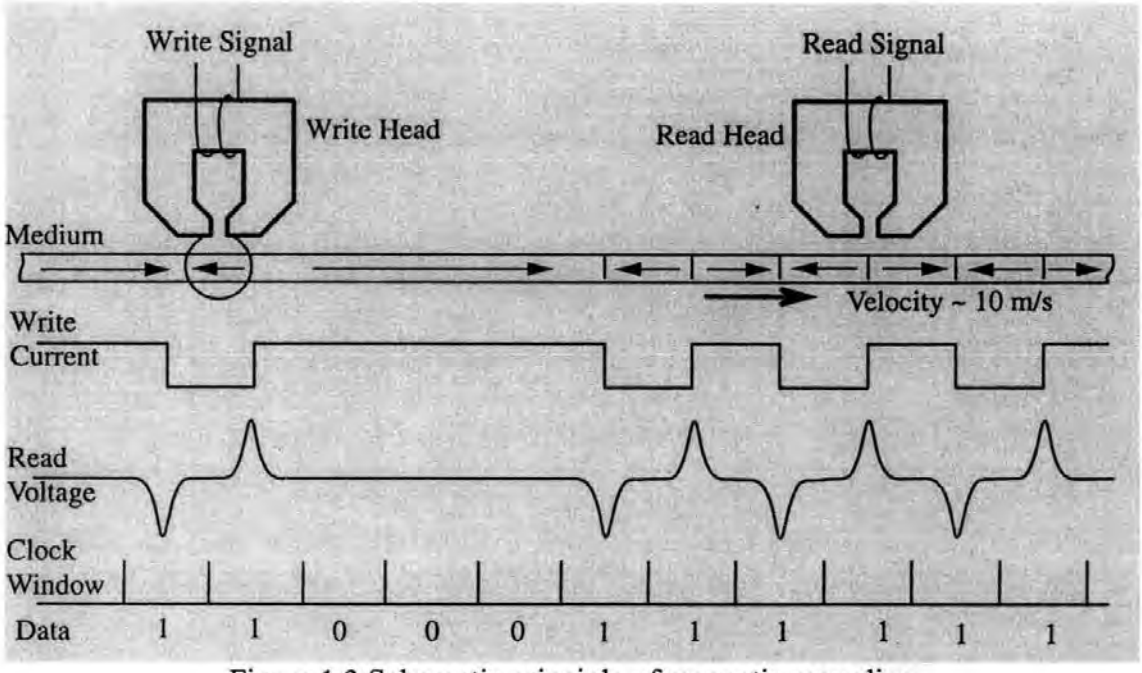

Figure 1.3 Schematic principle of magnetic recording

The inductive recording head is a transducer essentially consisting of some coils wound around a horseshoe-shaped soft magnetic material (with a low coercivity and high permeability) which has an air gap (called the head gap). The recording medium is made of a hard magnetic material with a large coercivity.

There are three possible modes of magnetic recording. One is the *longitudinal recording*, in which the medium magnetisation is parallel to the disk plane, as shown in Figure 1.3. The second mode is *perpendicular recording*, in which the medium magnetisation is normal to the disk plane. The third mode is *transverse recording*, where the medium magnetisation is normal to the page. At present, *longitudinal recording* is adopted in all commercial magnetic recording systems, *perpendicular recording* is still under research, while *transverse recording* is not being actively pursued due to various technical constraints.

During the write process, a write current is passed through the head coils to produce a magnetic write field in the medium near the head gap. The write field must be larger than the medium coercivity to magnetise the medium along the field direction. By switching the direction of the write current, magnetisation transitions can be written in the medium. In reality, the magnetic transition length is finite, but it is shown to be zero in Figure 1.3 for simplicity.

During the read process, the medium with written transitions is passed underneath the head gap. The relative motion between the head and the magnetostatic stray field produced by the magnetic transitions generates induced voltage pulses in the coils due to Faraday's law. Each transition corresponds to a voltage pulse that has finite amplitude and a finite half-amplitude pulse width PW_{50}, which limits how close the voltage pulses can be spaced and still be resolved.

In a simple coding scheme of digital magnetic recording called non-return-to-zero modified (NRZI) coding, the presence of a transition or a voltage pulse in a given clock

window (timing window) represents a "1", while the absence of a transition or pulse represents a "0". Therefore, the linear data density is fundamentally limited by the value of PW_{50}.

1.3.2 Overview of magnetic hard disk drives

Among the magnetic storage systems, magnetic hard disk drive is the dominant mass storage device for computers because of its storage capacity (>1 GB), low cost per megabyte (<$0.20/MB), reasonably fast access time (~10ms), and a relatively mature manufacturing infrastructure.

A magnetic disk drive is mainly composed of the following four parts:

1. *Magnetic read/write heads and magnetic disks (platters).* Each write/read head, which is too small to be visible to the eye, is located on the trailing edge of a *slider* (or called *head-slider*). The slider is mounted on the end of a stainless steel gimbal-suspension, forming the so-called *head-gimbal assembly* (HGA). The write/read head and a recording disk surface is often called a *head-disk assembly*.
2. *Data detection electronics and write circuit*, which are mostly located on a printed circuit board with many very-large-scale integrated (VLSI) chips.
3. *Mechanical servo and control system*, including spindles, actuators, suspensions, and control chips.
4. *Interface* to microprocessor, located at one edge of the printed circuit board, through which the microprocessor input information from or output information to the disk drives.

A photograph of a hard disk drive is shown in Figure 1.4.

Figure 1.4 A photograph of a hard disk drive (Courtesy of IBM Corporation)

The operation of the head-disk assembly is based on a self-pressured air bearing between the slider and the spinning disk. This air bearing maintains a constant separation called flying height between them, as shown in Figure 1.5. By positioning the head-slider along the radial direction, different data tracks can be written on the disk. Each data track is divided into many data sectors. The state-of-the-art flying height is of the order of 20nm, while the relative speed between slider and disk is extremely high (about 10 m/s or higher).

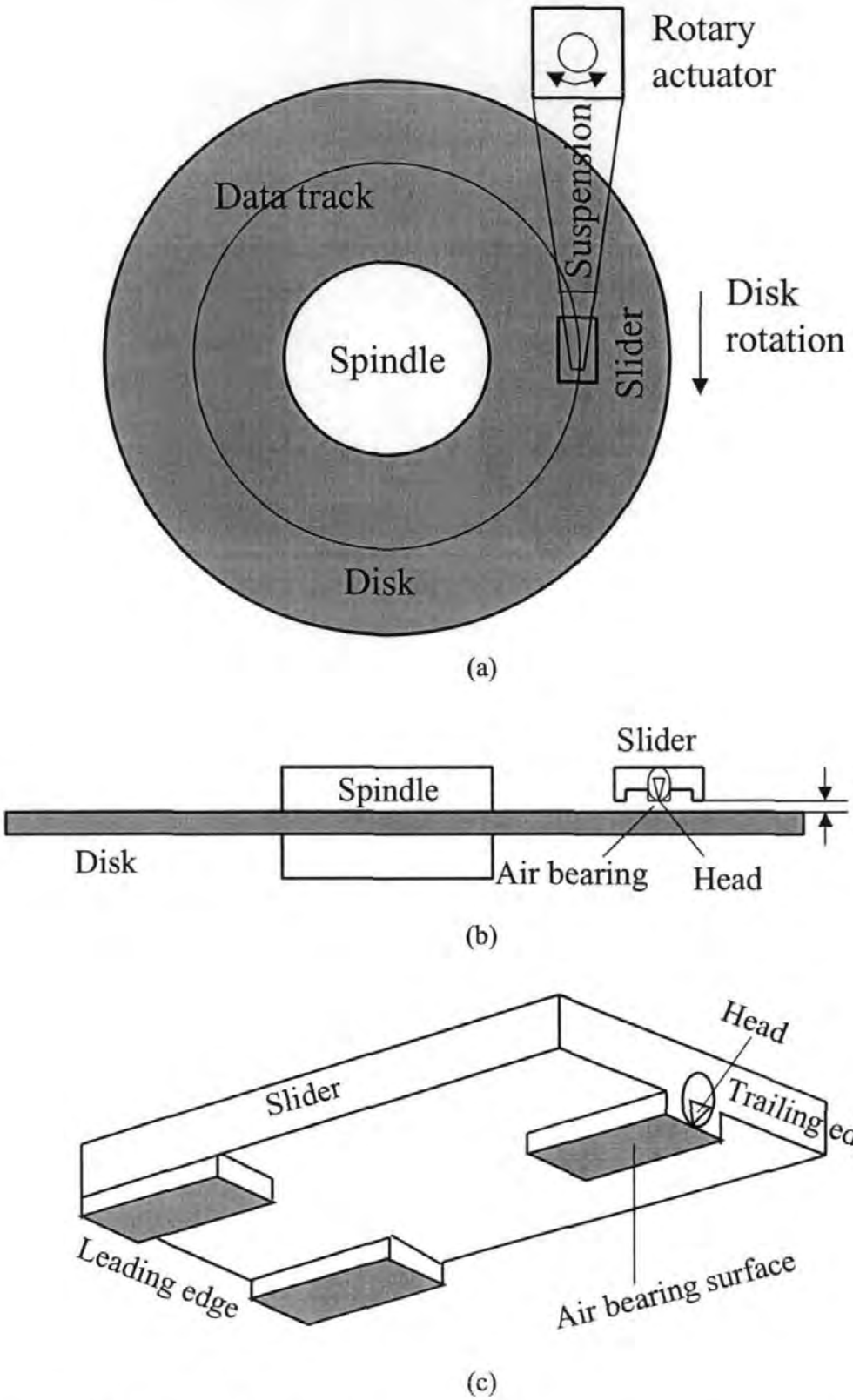

Figure 1.5 Schematic diagram of hard-disk assembly: (a) top view, (b) side view, (c) magnified view of slider.

1.4 Flying height and recording density

This section will illustrate that flying height is an important parameter of increasing the areal recording density. The read process in longitudinal magnetic recording will be analysed to demonstrate the relationship between the flying height and areal density, which is shown in Figure 1.6.

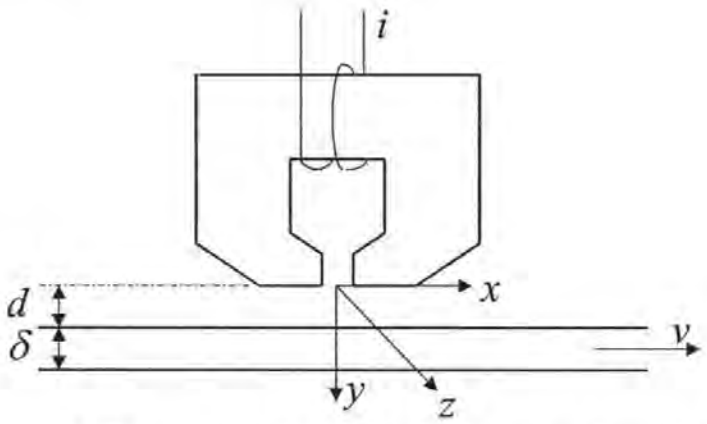

Figure 1.6 Read process in longitudinal magnetic recording

Reciprocity formula. When a magnetic recording medium with written magnetic transitions passes underneath an inductive recording head, the magnetic flux produced by each transition is picked up by the head. The variation of the magnetic flux produces an induced voltage in the head coil, that is, a readback signal. Assume that the head produces a field $H_x(x,y,z)$ in the x direction. Then, for a medium with magnetisation of M_x, the corresponding output voltage V_x at time t can be derived using *the principle of reciprocity* as below [Mee & Daniel, 1995]:

$$V_x(\bar{x}) = -\mu_0 v \int_{-w/2}^{+w/2} dz \int_{d}^{d+\delta} dy \int_{-\infty}^{+\infty} \frac{dM_x(x-\bar{x})}{d\bar{x}} \frac{H_x(x,y,z)}{i} dx \qquad (1.1)$$

where $\bar{x} = vt$

μ_0 = permeability of free space

v = medium velocity

w = track width

d = spacing from head to medium

δ = thickness of medium

i = current in head coil which produces above-mentioned field

Equation (1.1) can be simplified when the track width w is much larger than other dimensions in the system, hence it may be assumed that there is no variation of magnetisation with the z dimension. Thus the above formula can be simplified to

$$V_x(\bar{x}) = -\mu_0 vw \int_d^{d+\delta} dy \int_{-\infty}^{+\infty} \frac{dM_x(x-\bar{x})}{d\bar{x}} \frac{H_x(x,y)}{i} dx \tag{1.2}$$

This equation forms the basis for the study of the reproduce or read process and is often referred to simply as the reciprocity formula.

Readback from single transition. The real magnetic transition is not an infinitely sharp step transition, but rather a finite width transition, which is often approximated by an arctangent function:

$$M_x(x-\bar{x}) = \frac{2}{\pi} M_0 \tan^{-1}\left(\frac{x-\bar{x}}{a}\right) \tag{1.3}$$

where a is the transition parameter. It can be observed that the arctangent transition becomes a step transition if $a = 0$.

From the reciprocity formula, and Karlqvist equation for the head field expression, the readback voltage output produced in a short gap (almost zero gap-length) read head can be obtained to be [Mee & Daniel, 1995]:

$$V_x(\bar{x}) = \frac{-\mu_0 vwM_0 H_g g}{\pi i} \ln \frac{(a+d+\delta)^2 + \bar{x}^2}{(a+d)^2 + \bar{x}^2} \tag{1.4}$$

where H_g is the field in the gap, and g is the gap length.

The amplitude of this voltage output pulse is obtained by putting $\bar{x} = 0$ in the above equation, while pulse width is another important parameter as shown in Figure 1.7.

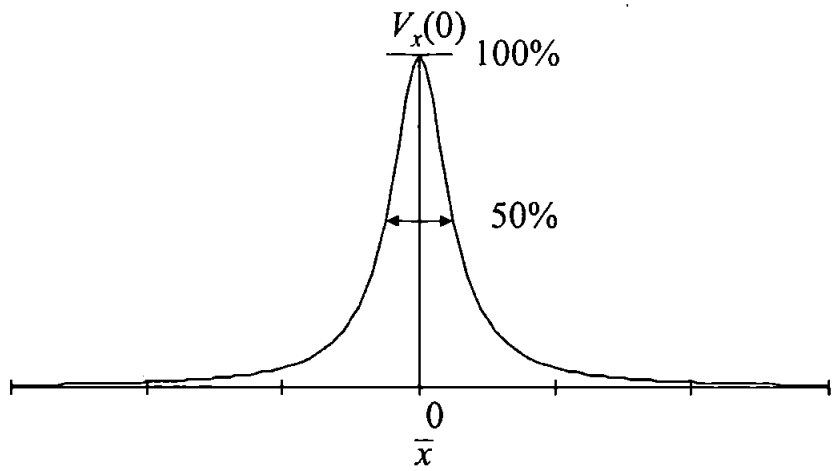

Figure 1.7 Readback voltage output pulse from a single transition

The pulse width at 50 percent of peak amplitude (PW_{50}) can be derived by solving the equation $V_x(0)/2 = V_x(\bar{x})$ as

$$PW_{50} = 2\sqrt{(d+a)(d+\delta+a)} \tag{1.5}$$

When the reproduce gap length is not negligible, a suitable approximation for PW_{50} in general case is given below:

$$PW_{50} = 2\sqrt{(d+a)(d+\delta+a)+g^2/4} \tag{1.6}$$

For thin media, equations (1.5) and (1.6) reduce to the following form:

$$PW_{50} = 2(d+a) \tag{1.7}$$

From equation (1.5)–(1.7), it is clearly seen that to increase the recording density, or to achieve a narrow readback voltage pulse, one of the most effective ways is to decrease the head-disk spacing or the flying height, assuming other parameters can not be changed. A similar result can also be obtained in the reproduce process using MR read heads [Wang & Taratorin, 1999]. These are the reasons why the flying height of the hard disk drive is getting lower and lower.

1.5 Hard disk drive head disk interface

A schematic of the head gimbal assembly (HGA) of the hard disk drive is shown as in Figure 1.8.

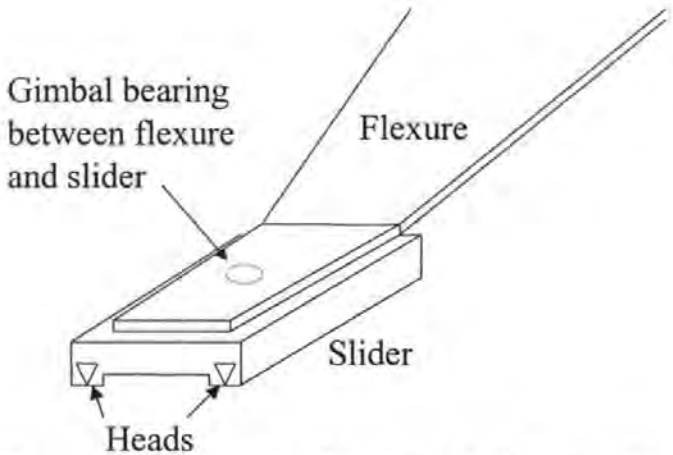

Figure 1.8 A schematic of the head gimbal assembly

The disk head slider is attached to a thin leaf spring (referred to as load beam and/or flexure) suspension, which supports the slider over the disk surface in an attitude that in part determines its flying characteristics. The suspension design allows the head slider to move freely around the load point and permits freedom of motion in the vertical direction as well as rotational motions about the pitch and roll axes—pitch and roll. The flying attitude of the air-bearing slider is usually described by three important parameters: the trailing-edge air film thickness or flying height, pitch angle, and roll angle. Lower air film thickness or flying height are achieved by changing one or more of the many slider parameters in a way that reduces the load bearing capacity of the slider.

The governing equations and analysis for a particular kind of slider can be found in the literature [White, 1984; Hu & Bogy, 1997]. For a conventional two-rail taper-flat slider (e.g. IBM 337-type), from a theoretical point of view, the flying height and the pitch and roll angles can be determined by a number of equations. To show this, the relevant parameters are marked in Figure 1.9.

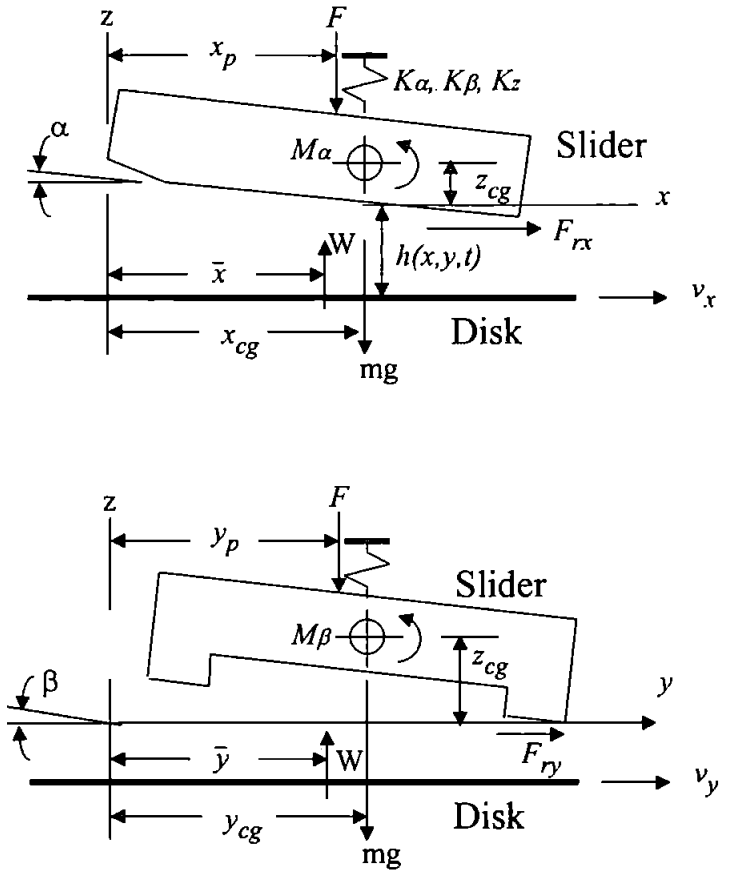

Figure 1.9 Physical model of a head slider flying above a rigid disk surface. Flexure damping coefficients (C_z, C_α, C_β) are not shown [White, 1984].

The air-bearing film will be determined by the following modified Reynolds equation [Bhushan, 1996]:

$$\frac{\partial}{\partial x}[ph^3(1+\frac{6aMp_a h_m}{ph})\frac{\partial p}{\partial x}]+\frac{\partial}{\partial y}[ph^3(1+\frac{6aMp_a h_m}{ph})\frac{\partial p}{\partial y}]$$
$$=6\eta_a[\frac{\partial}{\partial x}(v_x ph)+\frac{\partial}{\partial y}(v_x ph)]+12\eta_a\frac{\partial}{\partial t}(ph) \tag{1.8}$$

where x and y are the spatial coordinates, t is the time, a is the surface correction coefficient, M is the Knudsen number at ambient conditions, p_a is the ambient pressure, h_m is a reference film thickness, η_a is the viscosity at ambient conditions, v_x and v_y are the disk velocity components in x and y directions (if the skew angle of the head slider is zero, v_y will be zero.), p is the local pressure of the air, and h is the local air film thickness or flying height.

The rigid body motion equations for the head slider attached to the flexture that provides three degrees of freedom are given by:

$$m\frac{d^2z}{dt^2} + C_z\frac{dz}{dt} + K_z z + mg + F = W(t) \tag{1.9a}$$

$$I_\alpha\frac{d^2\alpha}{dt^2} + C_\alpha\frac{d\alpha}{dt} + K_\alpha\alpha + M_\alpha + (F + K_z z)(x_{cg} - x_p) + F_{rx}z_{cg} = (x_{cg} - \bar{x})W(t) \tag{1.9b}$$

and

$$I_\beta\frac{d^2\beta}{dt^2} + C_\beta\frac{d\beta}{dt} + K_\beta\beta + M_\beta + (F + K_z z)(y_{cg} - y_p) + F_{ry}z_{cg} = (y_{cg} - \bar{y})W(t) \tag{1.9c}$$

where the bearing load is:

$$W(t) = \int_0^B\int_0^L (p - p_a)dxdy \tag{1.9d}$$

the load point location (air-film centre of pressure) can be determined from:

$$\bar{x}(t) = \frac{1}{W(t)}\int_0^B\int_0^L x(p - p_a)dxdy \tag{1.9e}$$

and

$$\bar{y}(t) = \frac{1}{W(t)}\int_0^B\int_0^L y(p - p_a)dxdy \tag{1.9f}$$

and the resultant fluid friction forces in the x and y direction are given by:

$$F_{rx} = \int_0^B\int_0^L\left\{\frac{\eta_a v_x}{h[1 + (2aMp_a h_m / ph)]} + \frac{h}{2}\frac{\partial p}{\partial x}\right\}dxdy \tag{1.9g}$$

and

$$F_{ry} = \int_0^B\int_0^L\left\{\frac{\eta_a v_y}{h[1 + (2aMp_a h_m / ph)]} + \frac{h}{2}\frac{\partial p}{\partial y}\right\}dxdy \tag{1.9h}$$

where B and L are the bearing breadth and length of the slider, C_z, C_α and C_β are the flexture's damping coefficients, K_z, K_α and K_β are the flexture's stiffness coefficients,

F is the applied force at the pivot location x_p and y_p, I_α and I_β are the slider's moments of inertia, M_α and M_β are the static moments, m is the slider's mass, x_{cg}, y_{cg} and z_{cg} are the coordinates of the slider's mass centre, α is the pitch angle, and β is the roll angle. Full analysis of the slider dynamics requires a simultaneous solution of equation (1.7) and (1.8), which can be found in the literature [White & Nigam, 1980; White, 1984; Aruga et al., 1986; Hendriks, 1988; Bhushan, 1996], though it is very complicated.

2 Theoretical Basis for Optical Flying Height Testing

This chapter provides the theoretical basis to be used in the optical flying height testing techniques through the whole thesis. In the first section, wave reflection, refraction, and wave propagation in a stratified medium are described. Optical interferometry is briefly described in the second section. The application of Jones vectors is discussed in the third section, which is particularly useful in describing and analysing monochromatic polarised light [Azzam & Bashara, 1987]. [Born & Wolf, 1989] and [Boef, 1991] are extensively referenced in this chapter.

2.1 Reflection and refraction of a plane wave

2.1.1 The law of reflection and refraction

When a plane wave is incident on a boundary between two homogeneous media of different optical properties, it is split into two waves: a reflected wave propagating back into the first medium and a transmitted wave proceeding into the second medium, which is shown in Figure 2.1.

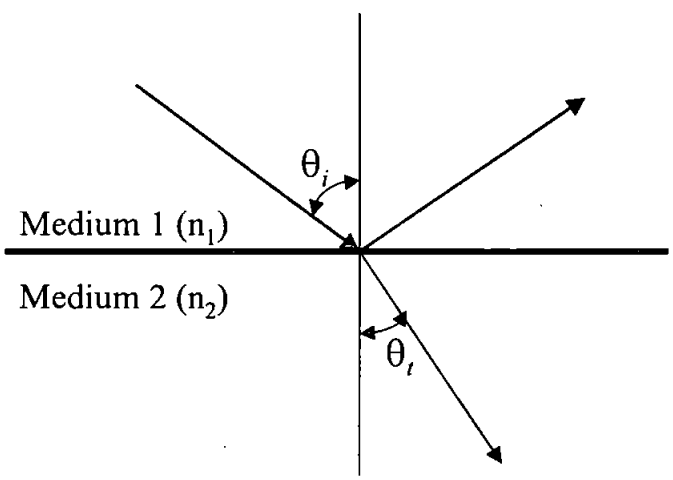

Figure 2.1 Reflection and refraction of a plane wave.

The quantitative relationship between incident angle θ_i and refractive angle θ_t in Figure 2.1 is called the *law of refraction* (or Snell's law of refraction), which is given by:

$$n_1 \sin\theta_i = n_2 \sin\theta_t \tag{2.1}$$

where n_1 and n_2 are called the indices of refraction (or refractive indices) of the first and second media.

2.1.2 Fresnel formulae

Now we consider the amplitudes of the reflected and the transmitted waves. Let $\mathbf{A}_{\parallel}$ and $\mathbf{A}_{\perp}$ denote the complex amplitudes of the electric fields of the parallel and perpendicular components of the incident wave (relative to the plane of incidence). The quantitative relationships between the amplitudes of the transmitted and reflected waves, and that of the incident wave are called the *Fresnel formulae*, which are given by [Moller, 1988]:

$$\mathbf{T}_{\parallel} = \frac{2n_1 \cos\theta_i}{n_2 \cos\theta_i + n_1 \cos\theta_t} \mathbf{A}_{\parallel} \tag{2.2a}$$

$$\mathbf{T}_{\perp} = \frac{2n_1 \cos\theta_i}{n_1 \cos\theta_i + n_2 \cos\theta_t} \mathbf{A}_{\perp} \tag{2.2b}$$

$$\mathbf{R}_{\parallel} = -\frac{n_2 \cos\theta_i - n_1 \cos\theta_t}{n_2 \cos\theta_i + n_1 \cos\theta_t} \mathbf{A}_{\parallel} \tag{2.2c}$$

$$\mathbf{R}_{\perp} = \frac{n_1 \cos\theta_i - n_2 \cos\theta_t}{n_1 \cos\theta_i + n_2 \cos\theta_t} \mathbf{A}_{\perp} \tag{2.2d}$$

where $\mathbf{T}_{\parallel}$ and $\mathbf{T}_{\perp}$ denote the complex amplitudes of the parallel and perpendicular component of the transmitted wave. $\mathbf{R}_{\parallel}$ and $\mathbf{R}_{\perp}$ denote the complex amplitudes of the

parallel and perpendicular component of the reflected wave. By using the law of refraction, the *Fresnel formulae* can be written in the following alternative form:

$$\mathbf{T}_{\parallel} = \frac{2\cos\theta_i}{(n_2/n_1)\cos\theta_i + \sqrt{1-[(n_1/n_2)\sin\theta_i]^2}}\mathbf{A}_{\parallel} \tag{2.3a}$$

$$\mathbf{T}_{\perp} = \frac{2\cos\theta_i}{\cos\theta_i + (n_2/n_1)\sqrt{1-[(n_1/n_2)\sin\theta_i]^2}}\mathbf{A}_{\perp} \tag{2.3b}$$

$$\mathbf{R}_{\parallel} = \frac{-(n_2/n_1)\cos\theta_i + \sqrt{1-[(n_1/n_2)\sin\theta_i]^2}}{(n_2/n_1)\cos\theta_i + \sqrt{1-[(n_1/n_2)\sin\theta_i]^2}}\mathbf{A}_{\parallel} \tag{2.3c}$$

$$\mathbf{R}_{\perp} = \frac{\cos\theta_i - (n_2/n_1)\sqrt{1-[(n_1/n_2)\sin\theta_i]^2}}{\cos\theta_i + (n_2/n_1)\sqrt{1-[(n_1/n_2)\sin\theta_i]^2}}\mathbf{A}_{\perp} \tag{2.3d}$$

For normal incidence, $\theta_i = 0$ and $\theta_t = 0$, and (2.2a) ~ (2.2d) reduce to:

$$\mathbf{T}_{\parallel} = \frac{2n_1}{n_1 + n_2}\mathbf{A}_{\parallel} \tag{2.4a}$$

$$\mathbf{T}_{\perp} = \frac{2n_1}{n_1 + n_2}\mathbf{A}_{\perp} \tag{2.4b}$$

$$\mathbf{R}_{\parallel} = \frac{n_1 - n_2}{n_2 + n_1}\mathbf{A}_{\parallel} \tag{2.4c}$$

$$\mathbf{R}_{\perp} = \frac{n_1 - n_2}{n_1 + n_2}\mathbf{A}_{\perp} \tag{2.4d}$$

2.1.3 Reflectivity and transmissivity

When we examine how the energy of the incident field is divided between the reflected field and transmitted field, we define the following rations which are called *reflectivity* and *transmissivity* respectively [Born & Wolf, 1989]:

$$R = \frac{J^{(r)}}{J^{(i)}} = \frac{|\mathbf{R}|^2}{|\mathbf{A}|^2} \quad \text{and} \quad T = \frac{J^{(t)}}{J^{(i)}} = \frac{n_2\cos\theta_t}{n_1\cos\theta_i}\frac{|\mathbf{T}|^2}{|\mathbf{A}|^2} \tag{2.5}$$

where **A**, **R**, and **T** are the amplitudes of the electric fields of incident wave, reflected wave and transmitted wave respectively, and $J^{(i)}$, $J^{(r)}$, and $J^{(t)}$ are the amount of energy per unit area of the boundary per second for incident wave, reflected wave, and transmitted wave respectively. It can be easily verified that

$$R + T = 1 \tag{2.6}$$

which is in agreement with the law of conservation of energy.

The reflectivity and transmissivity depend on the polarisation of the incident wave. They can be expressed in terms of the reflectivity and transmissivity associated with polarisations in the parallel and perpendicular directions respectively as:

$$R_{\parallel} = \frac{J_{\parallel}^{(r)}}{J_{\parallel}^{(i)}} = \frac{|\mathbf{R}_{\parallel}|^2}{|\mathbf{A}_{\parallel}|^2} \quad \text{and} \quad T_{\parallel} = \frac{J_{\parallel}^{(t)}}{J_{\parallel}^{(i)}} = \frac{n_2 \cos\theta_t}{n_1 \cos\theta_i} \frac{|\mathbf{T}_{\parallel}|^2}{|\mathbf{A}_{\parallel}|^2} \tag{2.7}$$

$$R_{\perp} = \frac{J_{\perp}^{(r)}}{J_{\perp}^{(i)}} = \frac{|\mathbf{R}_{\perp}|^2}{|\mathbf{A}_{\perp}|^2} \quad \text{and} \quad T_{\perp} = \frac{J_{\perp}^{(t)}}{J_{\perp}^{(i)}} = \frac{n_2 \cos\theta_t}{n_1 \cos\theta_i} \frac{|\mathbf{T}_{\perp}|^2}{|\mathbf{A}_{\perp}|^2} \tag{2.8}$$

Again it is not difficult to verify that:

$$R_{\parallel} + T_{\parallel} = 1, \qquad R_{\perp} + T_{\perp} = 1 \tag{2.9}$$

For normal incidence, the distinction between the parallel and perpendicular components disappear, and the reflectivity and transmissivity become:

$$R = \left(\frac{n_1 - n_2}{n_1 + n_2} \right)^2, \text{ and } \quad T = \frac{4 n_1 n_2}{(n_1 + n_2)^2} \tag{2.10}$$

It can be seen from (2.8) that:

$$\lim_{n_1 \to n_2} R = 0, \qquad \lim_{n_1 \to n_2} T = 1 \tag{2.11}$$

Similar results also hold for the limiting values of $R_{\parallel}$ and $T_{\parallel}$, and $R_{\perp}$ and $T_{\perp}$, as can be seen from (2.7) and (2.8). Therefore, the smaller the difference between the optical densities of the two media, the less energy is carried away by the reflected wave.

It can be verified that when

$$\tan\theta_i = n_2 / n_1, \tag{2.12}$$

the reflectivity of the parallel wave, $R_{\parallel}$, becomes zero. The angle θ_i given by (2.12) is called the *Brewster angle*. In this case, the reflected light has no component in the plane of incidence, and the reflected and transmitted rays are perpendicular to each other.

When a light wave propagates from an optically denser medium into a less dense medium, i.e., $n_1<n_1$, if the angle of incidence θ_i equals the critical value $\overline{\theta_i}$ given by

$$\sin\overline{\theta_i} = n_2 / n_1 \tag{2.13}$$

then $\theta_t = 90°$, so that the light emerges in a direction tangent to the boundary. If θ_i exceeds the limiting value $\overline{\theta_i}$, no light enters the second medium. All the incident light is then reflected back into the first medium and this is called *total internal reflection*.

2.1.4 Wave propagation in a stratified medium

A medium whose properties are constant throughout each plane perpendicularly to a fixed direction is called a *stratified medium*. The theory of stratified media is very important in optics in connection with *multi-layers*, i.e., a succession of thin plane-parallel films. Such films can be produced with the help of high-vacuum deposition techniques, and their thickness can be controlled with very high accuracy. They have many useful applications such as *antireflection films*, *reflection enhancement films*, optical filters, etc. In this subsection, we will just consider the resulted thin film equations, which will be used for the derivation of flying height or head disk spacing in later chapters.

Consider a plane wave propagating through a homogeneous film as shown in Figure 2.2.

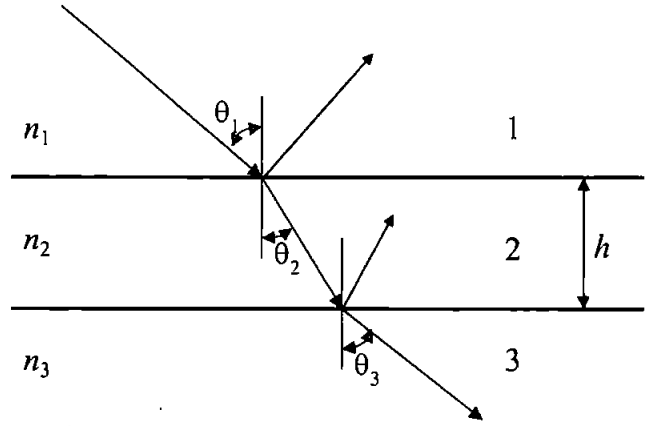

Figure 2.2 Propagation of an electromagnetic wave through a homogeneous film

Let **A**, **R**, and **T** denote as before the amplitudes of the electric vectors of the incident, reflected and transmitted waves. $r = \frac{\mathbf{R}}{\mathbf{A}}$ and $t = \frac{\mathbf{T}}{\mathbf{A}}$ are called the reflection and transmission coefficients of the film respectively. It can be derived that r and t can be expressed as [Born & Wolf, 1989]:

$$r = \frac{r_{12} + r_{23}e^{2i\beta}}{1 + r_{12}r_{23}e^{2i\beta}} \tag{2.14}$$

$$t = \frac{t_{12}t_{23}e^{2i\beta}}{1 + r_{12}r_{23}e^{2i\beta}} \tag{2.15}$$

where $\beta = \frac{2\pi}{\lambda_0} n_2 h \cos\theta_2$, λ_0 is the wavelength in vacuum, h is the thickness of the film, n_i (i=1, 2, 3) are refractive indices (or called optical constants) of the media, θ_i (i=1, 2, 3) are angles shown in Figure 2.2, and the coefficients r_{12}, t_{12}, and r_{23}, t_{23} associated with the reflection and transmission at the first and second surfaces are expressed by:

$$r_{12} = \frac{n_1 \cos\theta_1 - n_2 \cos\theta_2}{n_1 \cos\theta_1 + n_2 \cos\theta_2} \tag{2.16}$$

$$t_{12} = \frac{2n_1 \cos\theta_1}{n_1 \cos\theta_1 + n_2 \cos\theta_2} \tag{2.17}$$

$$r_{23} = \frac{n_2 \cos\theta_2 - n_3 \cos\theta_3}{n_2 \cos\theta_2 + n_3 \cos\theta_3} \tag{2.18}$$

$$t_{23} = \frac{2n_2 \cos\theta_2}{n_2 \cos\theta_2 + n_3 \cos\theta_3} \tag{2.19}$$

For dielectric media, i.e., n_i (i = 1, 2, 3) are real numbers, the reflectivity and transmissivity can be given as:

$$R = |r|^2 = \frac{r_{12}^2 + r_{23}^2 + 2r_{12}r_{23}\cos 2\beta}{1 + r_{12}^2 r_{23}^2 + 2r_{12}r_{23}\cos 2\beta} \tag{2.20}$$

$$T = \frac{n_3 \cos\theta_3}{n_1 \cos\theta_1} \frac{t_{12}^2 t_{23}^2}{1 + r_{12}^2 r_{23}^2 + 2r_{12}r_{23}\cos 2\beta} \tag{2.21}$$

It is not difficult to calculate that $R + T = 1$. The phase changes for the reflected and transmitted waves can also be derived from (2.14) and (2.15) as:

$$\delta_r = \arg(r) = \tan^{-1} \frac{r_{23}(1 - r_{12}^2)\sin 2\beta}{r_{12}(1 + r_{23}^2) + r_{23}(1 + r_{12}^2)\cos 2\beta} \tag{2.22}$$

$$\delta_t = \arg(t) = \tan^{-1}\left(\frac{1 - r_{12}r_{23}}{1 + r_{12}r_{23}} \tan\beta\right) \tag{2.23}$$

Hence the relationship between the film thickness and the reflectivity, transmissivity, and phase change can be calculated.

2.2 Optical interferometry

The intensity I of light has been defined as the time average of the amount of energy which crosses a unit area in unit time perpendicular to the direction of the energy flow. For a plane wave, the intensity is given by [Born & Wolf, 1989] as:

$$I = \frac{c}{4\pi}\sqrt{\frac{\varepsilon}{\mu}}\left\langle \vec{E}^2 \right\rangle \tag{2.24}$$

where c is the velocity of light in the vacuum, ε is known as the *dielectric constant* (or permittivity), μ is called the *magnetic permeability*, $\langle \bullet \rangle$ denotes time average, and $\vec{E}$ is the *electric vector* of the wave. Since we will be comparing intensities in the same medium, we can take the quantity $\langle \vec{E}^2 \rangle$ as a measure of intensity. To facilitate calculations on optical interferometry the electric field of the light wave will be described with complex quantities. For a monochromatic light wave, the electric vector $\vec{E}$ can be represented as:

$$\vec{E} = \mathrm{R}\{\mathbf{A}e^{i\omega t}\} = \frac{1}{2}\left[\mathbf{A}e^{i\omega t} + \mathbf{A}^* e^{-i\omega t}\right] \tag{2.25}$$

A is complex amplitude of the light wave. $\mathrm{R}\{\bullet\}$ represents the real part of a complex variable. From (2.25),

$$\vec{E}^2 = \frac{1}{4}(\mathbf{A}^2 e^{2i\omega t} + \mathbf{A}^{*2} e^{-2i\omega t} + 2\mathbf{A} \bullet \mathbf{A}^*) \tag{2.26}$$

Taking the time average over a large interval, compared with the period $T = 2\pi/\omega$, we have:

$$\langle \vec{E}^2 \rangle = \frac{1}{2}\mathbf{A} \bullet \mathbf{A}^* = \frac{1}{2}|\mathbf{A}|^2 \tag{2.27}$$

So the intensity of the light wave can be represented as:

$$I = |\mathbf{A}|^2 \tag{2.28}$$

When two monochromatic waves $\vec{E}_1$ and $\vec{E}_2$ from the same source, with amplitudes of $\mathbf{A}_1$ and $\mathbf{A}_2$ respectively, are superimposed at a certain point P, the total electric field at this point is:

$$\vec{E} = \vec{E}_1 + \vec{E}_2 \tag{2.29}$$

such that

$$\vec{E}^2 = \vec{E}_1^2 + \vec{E}_2^2 + 2\vec{E}_1 \bullet \vec{E}_2 \tag{2.30}$$

The intensity of the combined light wave $\vec{E}_1$ and $\vec{E}_2$ at point P can be derived as:

$$I = I_1 + I_2 + 2\sqrt{I_1 I_2}\cos\phi \tag{2.31}$$

where $I_1 = |\mathbf{A}_1|^2$ and $I_2 = |\mathbf{A}_2|^2$ are the intensities of the two waves at point P respectively, and ϕ is the phase difference between the two waves. If a photo-detector (PD) is positioned at position P and the photo current is amplified with an amplifier, the output voltage of this amplifier will be given by:

$$\begin{aligned} V_{out} &= K[I_1 + I_2 + 2\sqrt{I_1 I_2}\cos\phi] \\ &= V_1 + V_2\cos\phi \end{aligned} \tag{2.32}$$

where the value of the proportionality factor K depends on the photo-detector efficiency and the amplifier gain.

2.3 Polarisation interferometry

2.3.1 Jones representation of polarised light

The electric field $\vec{E}$ of a polarised monochromatic light propagating in the z-direction is given by:

$$\vec{E} = \mathrm{R}\{\mathbf{A}e^{i\omega t}\} = \mathrm{R}\{\mathbf{E}e^{-ikz}e^{i\omega t}\} \tag{2.33}$$

where ω is the angular frequency of the light wave, and k is the wave-number of the light in the medium. The complex vector $\mathbf{E}$ is called the *Jones vector* and has two components $\mathbf{E}_x$ and $\mathbf{E}_y$ given by:

$$\mathbf{E}_x = |\mathbf{E}_x|e^{i\delta_x} \tag{2.34}$$

$$\mathbf{E}_y = |\mathbf{E}_y|e^{i\delta_y} \tag{2.35}$$

Here δ_x and δ_y are phase constants. From (2.33) to (2.35), it can be seen that $\vec{E}$ can be considered as a linear superposition of two light waves plane polarised in the x and y direction respectively:

$$\vec{E} = \mathrm{R}\{(\mathbf{E}_x\vec{x} + \mathbf{E}_y\vec{y})e^{-ikz}e^{i\omega t}\} \tag{2.36}$$

where $\vec{x}$ and $\vec{y}$ are unit vectors pointing in the x and y directions respectively. The polarisation state of $\vec{E}$ is determined by the amplitudes $|\mathbf{E}_x|$ and $|\mathbf{E}_y|$, and the phase difference $(\delta_x - \delta_y)$ between the two polarisation components. Since only the phase difference between $\mathbf{E}_x$ and $\mathbf{E}_y$ is relevant here, δ_x is often set to zero for convenience. The decomposition of $\vec{E}$ in two plane-polarised waves is shown in Figure 2.3.

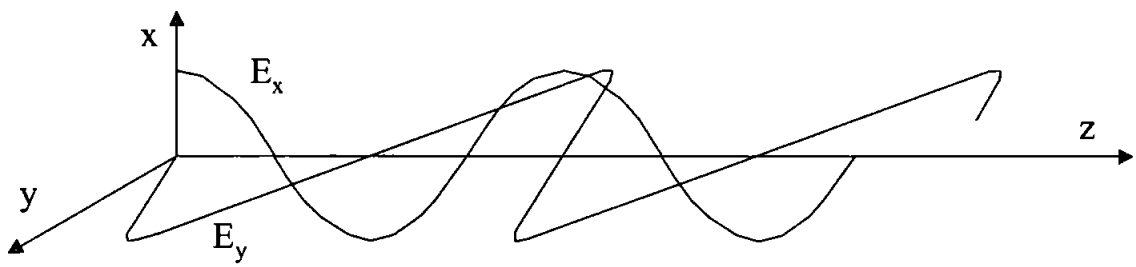

Figure 2.3 Decomposition of a monochromatic polarised light wave into two plane-polarised waves.

Jones vectors of some polarisation states that are frequently encountered are listed in Table 2.1.

Polarisation state	Jones vector
Linear horizontally polarised (LHP) in x – z plane	$\begin{pmatrix} A \\ 0 \end{pmatrix}$
Linear vertically polarised (LVP) in y – z direction	$\begin{pmatrix} 0 \\ A \end{pmatrix}$
Linearly 45° polarised	$\begin{pmatrix} A \\ A \end{pmatrix}$
Linearly -45° (or 135°) polarised	$\begin{pmatrix} A \\ -A \end{pmatrix}$
Right circularly polarised	$\begin{pmatrix} A \\ iA \end{pmatrix}$

Left circularly polarised	$\begin{pmatrix} A \\ -iA \end{pmatrix}$

Table 2.1 Jones vectors of some frequently encountered polarisation states

If a light beam passes an optical element (e.g., a polariser or wave plate), the state of polarisation and the corresponding Jones vector may change. Within the context of the Jones representation, we can associate the optical element with a matrix J that operates on the Jones vector $\mathbf{E}_i$ of the incident beam. The Jones vector $\mathbf{E}_o$ of the light beam after passing the optical element is then given by:

$$\mathbf{E}_o = J \cdot \mathbf{E}_i \tag{2.37}$$

The matrix J is a square $2*2$ matrix called *Jones matrix*. Generally its four elements are complex numbers. The corresponding Jones matrices of some frequently used optical elements are listed in Table 2.2.

Optical element	**Jones matrix**
Polariser with transmission axis in x-direction	$J_p(0°) = \begin{pmatrix} 1 & 0 \\ 0 & 0 \end{pmatrix}$
Polariser with transmission axis in y-direction	$J_p(90°) = \begin{pmatrix} 0 & 0 \\ 0 & 1 \end{pmatrix}$
Polariser with transmission axis 45°	$J_p(45°) = \frac{1}{2}\begin{pmatrix} 1 & 1 \\ 1 & 1 \end{pmatrix}$
Polariser with transmission axis 135° (or -45°)	$J_p(-45°) = \frac{1}{2}\begin{pmatrix} 1 & -1 \\ -1 & 1 \end{pmatrix}$
Quarter-wave plate, fast axis in x-direction	$J_{wp}(\frac{\lambda}{4}, 0°) = \begin{pmatrix} i & 0 \\ 0 & 1 \end{pmatrix}$
Quarter-wave plate, fast axis in y-direction	$J_{wp}(\frac{\lambda}{4}, 90°) = \begin{pmatrix} i & 0 \\ 0 & -1 \end{pmatrix}$
Quarter-wave plate, fast axis in 45° with respect to horizontal direction	$J_{wp}(\frac{\lambda}{4}, 45°) = \frac{1}{\sqrt{2}}\begin{pmatrix} 1 & i \\ i & 1 \end{pmatrix}$
Quarter-wave plate, fast axis in -45° with respect to horizontal direction	$J_{wp}(\frac{\lambda}{4}, -45°) = \frac{1}{\sqrt{2}}\begin{pmatrix} 1 & -i \\ -i & 1 \end{pmatrix}$
Half-wave plate, fast axis in 22.5° with respect to horizontal direction	$J_{wp}(\frac{\lambda}{2}, 22.5°) = \frac{1}{\sqrt{2}}\begin{pmatrix} 1 & 1 \\ 1 & -1 \end{pmatrix}$

Table 2.2 Jones matrices of some optical elements

The intensity I of a polarised beam can be easily derived from its Jones vector $\mathbf{E}$, which can be given by:

$$I = |\mathbf{E}|^2 = \mathbf{E}^T \cdot \mathbf{E}^* \tag{2.38}$$

The derivation process is similar to that for equation (2.28), and can be found in [Boef, 1991].

Two laser beams having Jones vector $\mathbf{E}_1$ and $\mathbf{E}_2$ are said to be orthogonally polarised if:

$$\mathbf{E}_1^T \cdot \mathbf{E}_2^* = 0 \tag{2.39}$$

2.3.2 Polarisation interferometry

Consider a pair of orthogonally polarised beams originated from the same source, which is usually referred to as reference beam and object beam respectively in an interferometer. For description simplicity, we assume that the reference beam $\vec{E}_r$ is polarised in the z-x plane, the object beam $\vec{E}_o$ is polarised in the z-y plane, and both beams are perfectly aligned and propagate in the z-direction. The Jones vectors of $\vec{E}_r$ and $\vec{E}_o$ are given respectively by:

$$\mathbf{E}_r = \begin{pmatrix} A_r \\ 0 \end{pmatrix} e^{i\phi_r} \tag{2.40}$$

$$\mathbf{E}_o = \begin{pmatrix} 0 \\ A_o \end{pmatrix} e^{i\phi_o} \tag{2.41}$$

Thus the Jones vector $\mathbf{E}$ of the combined reference and object beam $\vec{E}$ can be given as:

$$\mathbf{E} = \begin{pmatrix} A_r e^{i\phi_r} \\ A_o e^{i\phi_o} \end{pmatrix} \tag{2.42}$$

At this stage, no interference between $\vec{E}_r$ and $\vec{E}_o$ happens because they are orthogonally polarised. This can also be seen from the following expression of the intensity I of the combined beam $\vec{E}$:

$$I = |\mathbf{E}|^2 = A_r^2 + A_o^2 \tag{2.43}$$

If the combined reference and object beam passes a polariser with its transmission axis set at +45° to the x-axis, both beams will have the same polarisation state and interference between them becomes visible. If the Jones vector of the beam transmitted through the polariser is denoted by $\mathbf{E}_+$, then

$$\mathbf{E}_+ = \frac{1}{2}\begin{pmatrix} 1 & 1 \\ 1 & 1 \end{pmatrix} \cdot \mathbf{E} = \frac{1}{2}\begin{pmatrix} A_r e^{i\phi_r} + A_o e^{i\phi_o} \\ A_r e^{i\phi_r} + A_o e^{i\phi_o} \end{pmatrix} \tag{2.44}$$

The intensity I_+ of the transmitted beam can be obtained as:

$$I_+ = |\mathbf{E}_+|^2 = A_r^2 + A_o^2 + 2A_r A_o \cos(\phi_o - \phi_r) \tag{2.45}$$

If the polariser's transmission axis is set to −45° relative to the x-axis, the Jones vector of the transmitted beam then becomes:

$$\mathbf{E}_- = \frac{1}{2}\begin{pmatrix} 1 & -1 \\ -1 & 1 \end{pmatrix} \cdot \mathbf{E} = \frac{1}{2}\begin{pmatrix} A_r e^{i\phi_r} - A_o e^{i\phi_o} \\ -A_r e^{i\phi_r} + A_o e^{i\phi_o} \end{pmatrix} \tag{46}$$

Thus the intensity I_- of the transmitted beam can be obtained as:

$$I_- = |\mathbf{E}|^2 = A_r^2 + A_o^2 - 2A_r A_o \cos(\phi_o - \phi_r) \tag{47}$$

From (45) and (47), it can be seen that in both cases interference between the reference and object beams occurs, although the interference terms have opposite sign.

3 Flying Height Testing Methods – analysis and review of existing techniques

3.1 Overview

Because of its importance, many contributions have been made to the development of methods for the measurement and characterisation of the flying height or the spacing between the head slider and the disk medium. Over the past few decades, a variety of methods have been developed and utilised to measure this parameter. These can be classified into two general categories: optical interferometry methods and electrical methods. Optical interferometry is a well established technique to measure film thickness. As early as 1919, interference colours were used to measure the thickness of lubricating films on glass. The extension of its use to the measurement of lubrication film for rolling element bearing applications was made by Archard and Kirk [1963] and later by Cameron and Gohar [1966] and Foord et al. [1969–1970]. Since then, the optical technique has been extensively used for various tribological applications, including the head-medium interface. There are a number of optical interferometry methods that have been used for the measurement of the head disk spacing. One classical and popular method is the intensity-based interferometry technique, in which both monochromatic light and white light, have been used for the light source. Modern electronics and computer techniques have made the testing accuracy of this intensity interferometry method much higher than before. Polarisation interferometry is another popular method in which both intensity and phase information are utilised to determine

the flying height. The main advantage of this method is that it is able to overcome the loss of sensitivity of the intensity interferometry method when the flying height is near-contact. The above two methods can be called the direct spacing measuring (DSM) methods [Liu et al, 2000] in which a special transparent glass disk is used in place of the real magnetic disk, and the flying height is determined by analysing the interference phenomena between the slider and the rotating glass disk [Ohkubo & Kishigami, 1988; Lacey et al., 1992; de Groot, 1998a]. Other optical testing methods include Laser Doppler Interferometry (LDI), Phase Demodulated Laser Interferometry (PDLI), etc., in which the head-disk spacing is determined by measuring the relative motion between the head-slider and the disk by using dual-beam interferometry [Briggs & Talke, 1989; McMillan & Talke, 1994; Lee & Wu, 1995; Staudenmann, 1998]. These methods can be called relative displacement measuring (RDM) method, in which a real magnetic disk and head-slider assembly can be employed. The DSM method has the advantage that the absolute head-disk spacing can be directly measured, while the RDM method has the advantage of using the real magnetic disk. Typical techniques among the electrical methods are the capacitance probe technique [Sonnenfield, 1993] and the readback transducer method [Shi et al., 1987]. The electrical resistance or acoustic emission measurement techniques are other electrical methods for the measurement of frequency and intensity of the contacts between the asperities of the surfaces of the head slider and disk.

In the following sections, a detailed review and analysis is given of several flying height or head-medium spacing testing techniques.

3.2 Traditional optical interferometry technique

A typical situation where interference occurs is shown in Figure 3.1. A thin parallel film

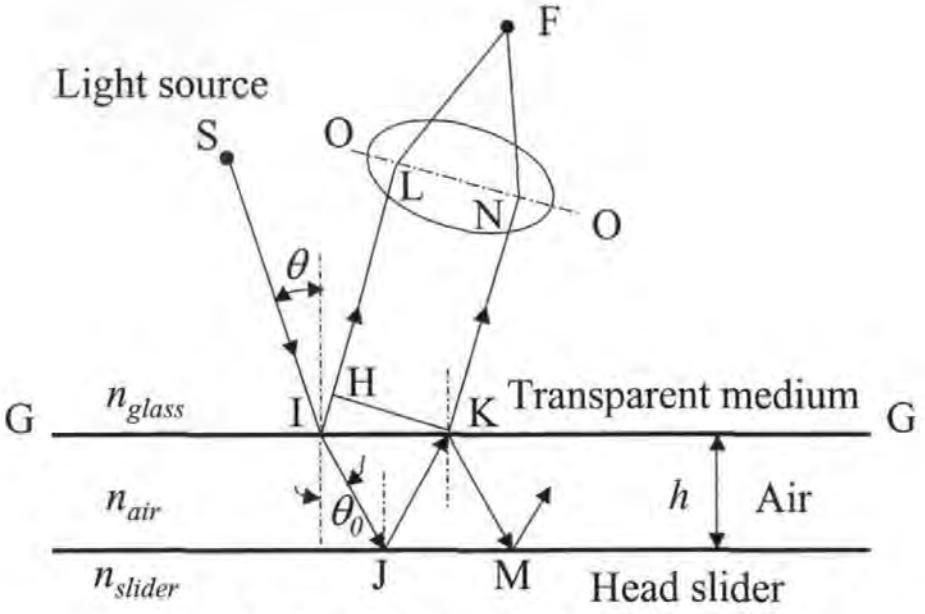

Figure 3.1 Parallel plate optical interferometry

of air is bounded on one side by the transparent medium (e.g. glass disk) and on the other side by the air-bearing surface of the head slider. The refractive indices of the glass and air are n_{glass} and n_{air} respectively and it is known that $n_{glass} > n_{air}$. Monochromatic light of wavelength λ originated from the source S is divided into a transmitted ray IJ and a reflected ray IL at the glass-air interface AA. IJ is reflected at J and emerges along KN parallel to IL. For the purpose of simplifying the explanation, we neglect the reflected ray KM, although multiple reflections should be accounted for to get maximum accuracy. After superposition at F, the two parallel rays IL and KN give rise to interference phenomena due to their path difference. Referring to Figure 3.1, the optical path difference δ is obtained as:

$$\delta = 2n_{air}\,\mathrm{IJ} - \mathrm{IH} + del \tag{3.1}$$

where *del* is the additional delay caused by the advance in the phase produced by the reflection at the air slider interface at J. Using Snell's law of refraction, it follows from equation (3.1) that

$$\delta = 2n_{air} h \cos\theta_0 + del \tag{3.2}$$

where θ_0 is the angle of incidence of the beam in the air film. It is common knowledge that if the two rays are in phase after superposition, maximum reinforcement occurs. On the other hand, if the path-length difference leads to a phase difference of 180°, annihilation occurs. So the resulting beam is of maximum intensity if the path difference δ is a multiple of wavelength λ, that is

$$\lambda = m\lambda, \qquad m=1,2,3,\cdots\cdots \tag{3.3a}$$

On the other hand, the minimum intensity occurs if

$$\delta = \frac{2m+1}{2}\lambda, \qquad m=1,2,3,\cdots\cdots \tag{3.3b}$$

In the instance of the head slider being a dielectric material, the phase change on reflection from the air-slider interface will be 180°, that is, $del = \lambda/2$. Since the refractive index of air is 1, for normal incidence, the bright fringes are located at the film thickness corresponding to

$$h = \frac{2m+1}{4}\lambda, \qquad m = 0,\ 1,\ 2,\ 3,\ \cdots\cdots \tag{3.3c}$$

while the dark fringes will be located at

$$h = m\frac{\lambda}{2}, \qquad m = 0,\ 1,\ 2,\ 3,\ \cdots\cdots \tag{3.3d}$$

If the light source is white rather than monochromatic, the interference pattern from a thin film will consist of continuous colour fringes instead of alternating bright and dark fringes of the monochromatic light. Each wavelength of the white light forms its own interference pattern. Hence the colour of the interference pattern at any point is due to the superposition of those colours whose wavelength intensities are strengthened through constructive interference, and the absence of those colours the wavelength intensities of which are weakened because of destructive interference at that particular film thickness. From Newton's colour chart, it is known that the colour is a function of

the film thickness. The zero spacing corresponds to a very dark (almost black) fringe. As the spacing increases, a sequence of well-defined colours appears beginning with grey, followed consecutively by white, yellow, orange, red, violet, indigo, blue, green, etc. At spacing larger than 1 μm, the contrast becomes weaker, and at a distance over 1.5 μm, only alternating green and red colours remain.

For visual measurement of air-film thickness of less than 1.5 μm, this white light interferometry is normally used. In white light interferometry, for a film thickness from 0 to 0.5 μm, only one single wavelength in the visible spectrum gains maximum intensity. The colours are quite pure and distinct, except from 0 to 0.15 μm, where the wavelengths in the visible spectrum reach their first intensity maximum so close together that the combined interference pattern appears as one fringe, changing from black at zero through grey to white at 0.125 μm before the first yellow occurs at 0.175 μm. From 0.5 to 1.0 μm, there are two wavelengths in the visible spectrum that reach a maximum intensity at any given film thickness. From 1.1 to 1.5 μm, there are three such wavelengths, and so on. As the number of wavelengths that reach their maxima simultaneously increases, the colour of the interference fringe appears less distinct, until the superposition is such that the result is practically white illumination. By comparison of the colour of the fringes with the Newton's fringe chart (called the calibration chart), a minimum film thickness of about 0.05 μm can be readily detected. The accuracy and resolution are about 0.025 μm for film thickness between 0.05 and 0.5 μm. This resolution decreases to about 0.10 μm at a film thickness of about 1.5 μm. It is clear that the most useful operating range for this white light interferometry method lies within the spacing range from 0.05 μm to 1.0 μm [Lin & Sullivan, 1972; Tanaka et al., 1984; Mitsuya & Ohkubo, 1987].

The drawback of the white light interferometry method discussed above is apparent: first, the resolution is too low, second, its measurement speed is too slow and dynamic measurement of flying height is impossible. This problem can be overcome by using an interferometry method in which monochromatic light and a solid state photodiode detector are employed [Fleischer & Lin, 1974; Nigam, 1982; Mizoshita et al., 1985; Best et al., 1986; Yamada et al., 1986]. The intensity of the monochromatic interference fringe between the glass disk and the head slider is converted into electrical signals by a photo-detector. Referring to Figure 3.1 again, as the head medium spacing changes, the intensity at the detector positioned at F is given to be

$$I = I_1 + I_2 + 2\sqrt{I_1 I_2}\cos\left(\frac{2\pi}{\lambda}\delta\right) \tag{3.4a}$$

where I_1 is the intensity of light reflected from the glass disk surface (IL) and I_2 is the intensity of light reflected from the slider's air bearing surface (KN).

The maximum intensity occurs when $\cos(2\pi\delta/\lambda) = 1$, and the minimum intensity occurs when $\cos(2\pi\delta/\lambda) = -1$. Therefore,

$$\begin{aligned} I_{max} &= I_1 + I_2 + 2\sqrt{I_1 I_2} \\ I_{min} &= I_1 + I_2 - 2\sqrt{I_1 I_2} \end{aligned} \tag{3.4b}$$

The clarity of fringes is usually described by their visibility:

$$\gamma = \frac{I_{max} - I_{min}}{I_{max} + I_{min}} = \frac{2\sqrt{I_1 I_2}}{I_1 + I_2} \tag{3.5}$$

which has a maximum of one when $I_1 = I_2$. Although high reflectivities of the surfaces are not a necessary requirement for this two-beam interferometry to achieve a good visibility, they are important to make an efficient use of the total light input, and obtain sharpened fringes of good visibility.

If the phase shift on reflection from the air slider interface is known ($d = \lambda/2$ for the head slider being dielectric material), the average film thickness can be calculated from

(3.4a) using the dc part of the intensity signal. The ac intensity fluctuations are caused by the dynamic vibrations of the slider [Best et al., 1986]. If the values of I_{max} and I_{min} of the dc intensities are known, dynamic measurement can be calibrated in peak-to-peak height without the knowledge of d. Figure 3.2 shows the simulation result of the dc output of the photo-detector as a function of flying height.

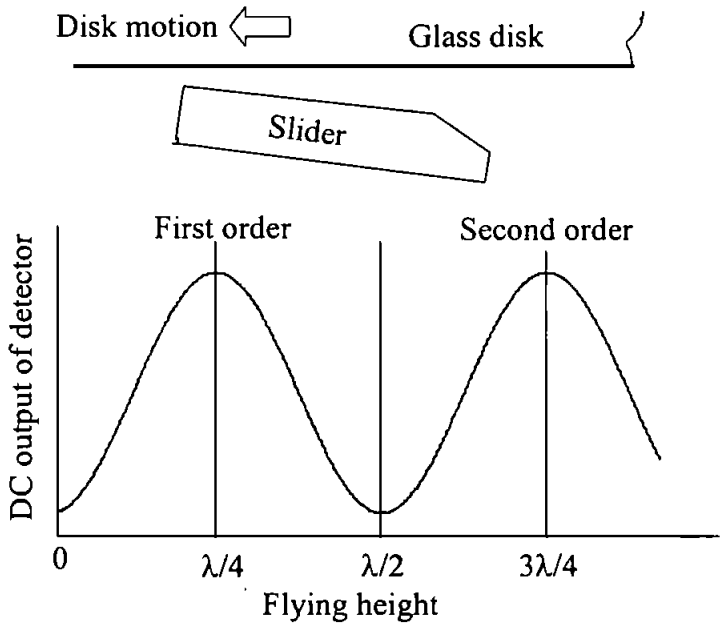

Figure 3.2 dc output of the photo-detector as a function of flying height

From [Best et al., 1986], the flying height variation Δh, causing an observed intensity fluctuation ΔI about an average intensity $\bar{I}$, is given to first order by

$$\Delta I = \pm 4\pi \cos\theta \frac{\sqrt{4I_1 I_2 - (\bar{I} - I_1 - I_2)^2}}{\lambda} \Delta h \qquad (3.6)$$

where θ is the angle of incidence. The sign of this equation depends on which quadrant the data are taken in. The maximum ΔI for a given Δh occurs when $\bar{I} = I_1 + I_2$ (i.e. the mid value points between I_{max} and I_{min} of the dc intensity curve). Second order effects become important when the dynamic data are taken near the maximum or minimum of the dc intensity curve.

Fleischer and Lin (1974) used a light source of HeNe laser operating in the infrared region with a wavelength of 3.391 μm. Indium arsenide (InAs) photo-voltaic detectors operating in current mode were used to measure the intensity of the light. Nigam (1982), Mizoshita et al. (1985) and Best et al. (1986) used monochromatic light in the visible range of about 545 nm and silicon photodiode detectors. Resolution of these measurement systems is determined by a number of factors such as the photo-detector noise, and non-uniformity of the glass disk, etc. For a typical head slider and fused quartz disk, rather high resolution was obtained. Dynamic vibration of the head slider to 100KHz was measured (Best et al., 1986). In fact, the techniques discussed here have led to the modern intensity interferometry flying height testing method which is to be analysed in the later section of this chapter.

3.3 Laser Doppler interferometry

Laser Doppler interferometry has been used to measure the dynamics of the head slider in a hard disk drive [Miu et al., 1984; Bogy & Talke, 1985; Miu & Bogy, 1986; Riener & Talke, 1988; Riener et al., 1988; Briggs & Talke, 1989]. This technique can be used to measure both out-of-plane and in-plane movement of the slider with virtually no restriction to slider or disk material. Laser Doppler vibrometry (LDV) is used to measure the out-of-plane velocities of the four corners from which the out-of-plane velocity of the geometric centre as well as the pitch and roll of the slider can be calculated. Laser Doppler anemometry (LDA) measures in-plane velocity of the four corners, which give the radial and tangential velocities of the geometric centre and the yaw of the slider. In addition, LDV has been used to measure disk runout and the vibrations of the suspension and actuator. These measurements are useful to determine the natural frequencies of the air bearing, the rotating disk, the actuator, and the suspension arm (Bogy & Talke, 1985).

LDV is based on the fact that an acousto-optically modulated light beam, when reflected from a moving surface, is frequency modulated by the motion of the surface. Such a phenomenon is a particular case of the well-known Doppler effect. The frequency modulation is proportional to the velocity component of the moving surface parallel to the direction of the light beam, which is normally incident on the surface. In conventional interferometry, the resolution limit is related to the wavelength of light, but in the case of LDV, the resolution limit is a function only of the resolution capability of the frequency demodulator.

Figure 3.3 shows a schematic diagram of the optical and electronic systems of the LDV. A vertical polarised monochromatic light from a HeNe laser is separated by a beam splitter into a reference beam and a signal beam. The signal beam is 40MHz frequency shifted by using an acousto-optical modulator, and is circularly polarised as it exits the quarter-wave plate. The light is then focused by use of an objective lens into a 25 μm spot on the back surface of the object to be measured (head slider in our case). The reflected beam becomes horizontally polarised as it returns through the quarter-wave plate again and is then recombined with the orthogonally polarised reference beam at the polarising beam splitter. Thereafter, the polarisation of the combined beam is rotated by 45°, and the beam is separated into two components. Two photo-detectors are used to detect the frequency-modulated signals A and B superimposed on the carrier frequency of 40MHz. Finally, the signals are passed through a differential amplifier and a modulation analyser for frequency demodulation. The output of this instrument is proportional to the normal velocity of the measured surface [Miu et al., 1984; Miu & Bogy, 1986].

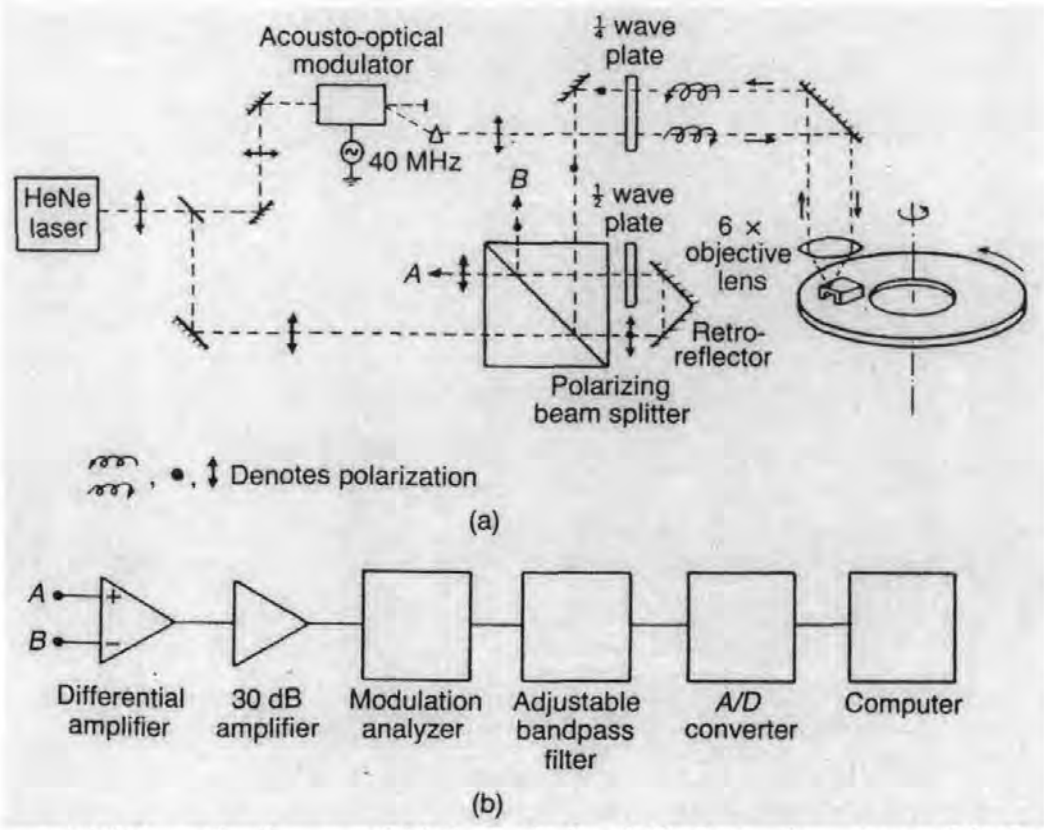

Figure 3.3 Schematic diagram of (a) the optical and (b) electronic systems of the Laser Doppler Vibrometer [Bogy & Talke, 1985]

Figure 3.4 shows an optical schematic of the LDA. A HeNe laser beam is split into two beams, one of which is frequency shifted at 40 MHz. Both beams are then focused on the back surface of the object to be measured (head slider in our case), where they interfere and create a sequence of moving interference fringes. The intensity of the light collected in the photo-multiplier is modulated by the light scattered from the moving asperities onto the backside of the slider. When a particle crosses the fringe pattern with a certain velocity, it scatters light at the frequency proportional to its velocity component orthogonal to the fringe lines, and inversely proportional to the fringe spacing. Due to the 40 MHz pre-shift of the laser beam, the fringes move with a constant speed, and the Doppler frequency appears as a frequency modulation on the 40 MHz signal after detection by the photo-multiplier tube.

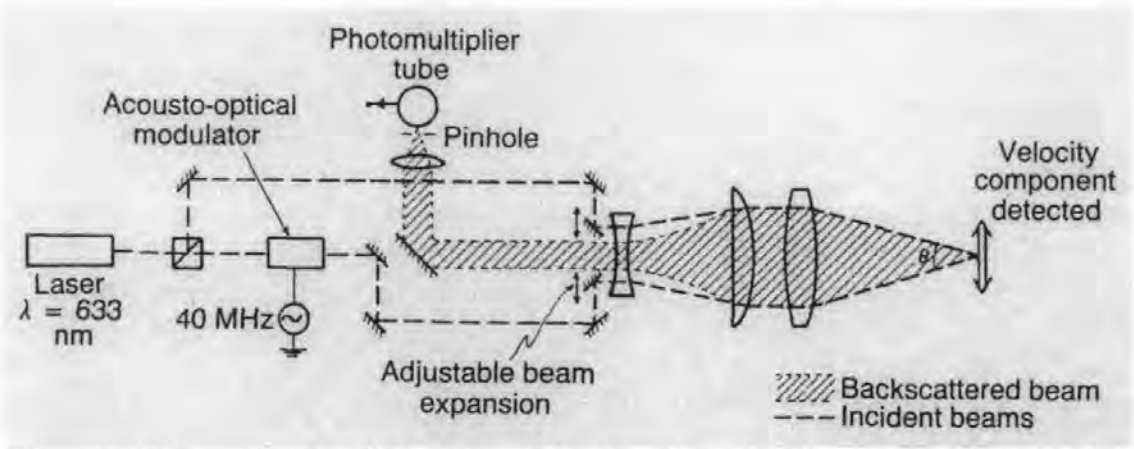

Figure 3.4 Schematic of optical system of the Laser Doppler Anemometer [Bouchard et al., 1985b]

3.4 Capacitance technique

The measurement of capacitance between two sliding surfaces has been extensively used to measure film thickness. Crook (1958, 1961) used the capacitance technique to measure the film thickness in the contact zone between oil lubricated rollers. Archard and Kirk (1961) also used this technique to measure the film thickness between oil lubricated crossed cylinders. Licht (1968) used the capacitance technique to measure dynamic air film thickness in self-acting foil bearings. This technique has also been used in head medium interfaces.

Neglecting edge effects, the capacitance between the two parallel flat plats of area A and spacing h is given by

$$C = \varepsilon_0 A / h \tag{3.7}$$

Regardless of edge effects, the capacitance C of a plate oriented with arbitrary pitch angle α and roll angle β relative to the disk (see Figure 1.9) can be written as (Millman et al., 1986)

$$C = \varepsilon_0 \int_0^B \int_0^L \frac{dxdy}{h_m' + x\tan\alpha - y\tan\beta} \tag{3.8}$$

where ε_0 is the dielectric constant of the ambient air and L and B are the length and width of the rail. The minimum film thickness h_m is related to the effective minimum film thickness $h_m^{'}$ by the following relation:

$$h_m^{'} = h_m + \frac{t_l}{\varepsilon_l} + \frac{t_c}{\varepsilon_c} \tag{3.9}$$

so that the lubricant and magnetic coating thickness (t_l, t_c) can be included with their corresponding dielectric constants ε_l and ε_c. Millman et al. (1986) derived the following expression from equation (3.8):

$$\begin{aligned} C = \frac{\varepsilon_0}{\tan\theta}\Bigg\{ & \left[B + \frac{\tan\alpha}{\tan\beta}\left(L + \frac{h_m^{'}}{\tan\alpha}\right)\right]\left[\ln\left(\frac{B\tan\beta}{\tan\alpha}\left(L + \frac{h_m^{'}}{\tan\alpha}\right)\right)\right] \\ & - \left(B + \frac{h_m^{'}}{\tan\beta}\right)\left[\ln\left(\frac{B\tan\beta}{\tan\alpha} + \frac{h_m^{'}}{\tan\alpha}\right)\right] \\ & - \left[\frac{\tan\alpha}{\tan\beta}\left(L + \frac{h_m^{'}}{\tan\alpha}\right)\right]\left[\ln\left(L + \frac{h_m^{'}}{\tan\alpha}\right)\right] + \left(\frac{h_m^{'}}{\tan\beta}\right)\left[\ln\left(\frac{h_m^{'}}{\tan\alpha}\right)\right]\Bigg\} \end{aligned} \tag{3.10}$$

This equation has three unknowns ($h_m^{'}$, $\tan\alpha$, and $\tan\beta$) and can be solved numerically if the capacitance is known at three different locations. At each location, the film thickness variation, h_m, causing an observed capacitance fluctuation, ΔC, is given by [Best, 1987]

$$\Delta C = \frac{\varepsilon_0 LB}{h_m^{'}(h_m^{'} + \alpha L + \beta B)}\Delta h \tag{3.11}$$

As an alternative, the capacitance probe can be mounted on one of the surfaces to measure film thickness against a conducting surface [Briggs & Herkart, 1971; Feliss & Talke, 1977].

3.5 Readback transducer method

The readback transducer method is a non-invasive flying height testing methods by which the flying height or head-disk spacing is determined from the readback signal. This includes the amplitude of readback signal measurement method, the PW_{50} (pulse width at 50% of the peak value) of readback signal measurement method, and the thermal signal detection method.

3.5.1 Amplitude of readback signal measurement method

This method is used to measure the head-disk spacing change by detecting the variation of the readback signal amplitude [Shi et al., 1987; Eaton & Baldwinson, 1997; Schardt, 1998; Novotny & Hsiao, 1998]. The magnitude of the readback signal depends on many parameters. Assuming longitudinal magnetisation and unit permeability of the recording medium, Wallace (1951) derived the following equation for the readback voltage of a sinusoidally recorded signal:

$$e(t) = 4\pi(10^{-8})N\alpha W\left(\frac{\mu}{1+\mu}\right)Mv(1-e^{-2\pi\delta/\lambda})G(\lambda)e^{-2\pi d/\lambda}\cos\left(\frac{2\pi vt}{\lambda}\right) \qquad (3.12)$$

where

e	voltage of readback signal (V)
t	time (s)
N	number of turns of the readback coil
α	head efficiency
W	head width (cm)
μ	core permeability
M	peak remanent magnetisation of the recording medium (EMU/cc)
v	tangential velocity (cm/s)
δ	medium thickness (cm)

λ wavelength of recorded signal (cm)

$G(\lambda)$ gap factor

d spacing between the head and medium (cm)

For a given disk file operating at a given track, the quantities N, α, μ, ν, λ are constants. Let E denote the amplitude of $e(t)$, then from (3.12)

$$E = f(M,\delta)\exp(-2\pi d/\lambda) \tag{3.13}$$

where $f(M,\delta)$ is a function deducible from (3.12). Since $f(M,\delta)$ is non-negative, it can be further written as

$$f(M,\delta) = C\exp[-2\pi s(M,\delta)/\lambda] \tag{3.14}$$

where C is a positive constant. Thus,

$$E = C\exp[-2\pi(d+s)/\lambda] \tag{3.15}$$

Here we may view $s(M,\delta)$ as a "virtual spacing variation" introduced by the non-uniform M and δ, and we note that d and s linearly superpose. We will neglect s in the following further discussion.

Now let d_0 denote an arbitrary reference spacing (not necessarily the steady flying height), Δd the spacing variation, and A the amplitude modulation of the readback signal resulting from the spacing variation defined by

$$d = d_0 + \Delta d \tag{3.16}$$

and

$$A = [E(d) - E(d_0)]/E(d_0) \tag{3.17}$$

then it follows from (3.15)~(3.16) that

$$\Delta d = -\frac{\lambda}{2\pi}\ln(1+A) = -\frac{\lambda}{2\pi}\ln\frac{E(d)}{E(d_0)} = -\frac{v}{2\pi f}\ln\frac{E(d)}{E(d_0)} \tag{3.18}$$

where f is the recording frequency.

From (3.18), it is seen that the head-disk spacing change can be determined by measuring the amplitude of the readback signal before and after the change.

3.5.2 PW_{50} of readback signal measurement method

The PW_{50} of readback signal measurement method is based on the detection of the pulse width of the read-back signal. Since the head disk spacing variation provides a proportional change in pulse width by measuring the pulse width change, flying height variation can be determined [Klaassen & van Peppen, 1994]. In Chapter 1, from equation (1.7), it has been shown that under some conditions, PW_{50} has a linear relationship with head disk spacing or flying height. Below is another rational derivation of the relationship between the flying height change and the pulse width variation.

A readback signal is shown in Figure 3.5, which is supposed to be read from a series of

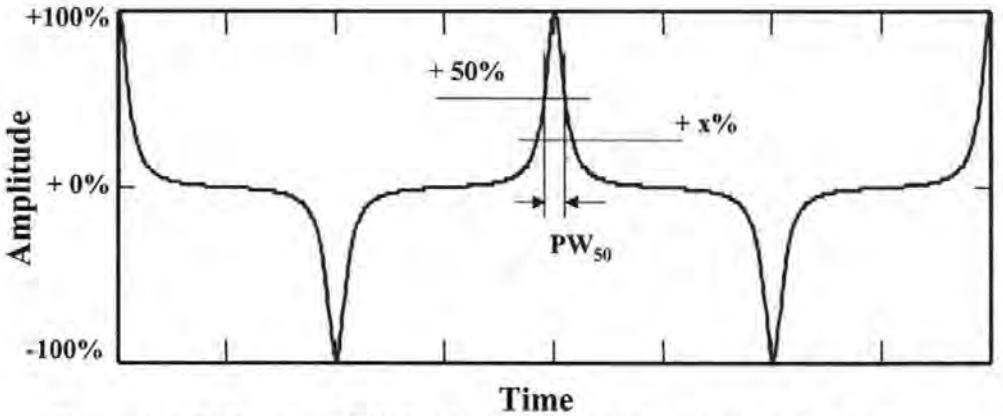

Figure 3.5 Definition of PWx, the pulse width at a slicing level of $x\%$ $(-100 \le x \le +100)$.

isolated transitions written on the disk. The shape of this waveform will be characterised by its pulse width PWx at x percent $(-100 \le x \le +100)$ of the peak to base-line amplitude. The pulse length at x percent is represented by PLx which is the length of the pulse projected along the track. For a disk travelling at velocity v with respect to the head, PLx = vPWx. Wallace (1951) demonstrated that the magnetic spacing loss can be represented by a non-causal (no phase shift) low-pass filter, whose

cutoff frequency decreases with increasing flying height. For an increase of Δd in the flying height d, this "spacing loss filter" has a transfer function $H(\omega)$ given by:

$$H(\omega) = \exp(-\Delta d|\omega|/v) = \exp(-2\pi\Delta d/\lambda) \tag{3.19}$$

where λ is the wavelength along the track of a sinusoidal signal at an angular frequency ω. This filter is applied to the readback signal at flying height d to arrive at the signal at flying height $d + \Delta d$.

For pulses with Lorentzian shape (which is usually the close approximation of the readback signal shape), we can easily calculate what happens to the pulse width as we vary the flying height. A Lorentzian readback pulse shape is given by:

$$e(t) = \frac{e(0)}{1 + \left(\frac{2t}{PW_{50}}\right)^2} \tag{3.20}$$

where $e(0)$ is the peak amplitude, and PW_{50} is the pulse width at half maximum value. The Fourier transform of this Lorentzian pulse is:

$$F_i(\omega) = \frac{\pi}{2} e(0) PW_{50} \exp(-|\omega| PW_{50}/2) \tag{3.21}$$

Filtering the Lorentzian pulse of (3.20) by the spacing loss filter of (3.19) produces an output pulse whose Fourier transform $F_o(\omega)$ is equal to the product of $F_i(\omega)$ and $H(\omega)$:

$$F_o(\omega) = \frac{\pi}{2} e(0) PW_{50} \exp\left[-\left(\frac{PW_{50}}{2} + \frac{\Delta d}{v}\right)|\omega|\right] \tag{3.22}$$

Transforming $F_o(\omega)$ back to the time domain reveals the Wallace spacing loss weighted pulse:

$$e'(t) = \frac{e'(0)}{1 + \left(\frac{2t}{PW'_{50}}\right)^2} \tag{3.23}$$

which, again, has a Lorentzian shape. A Lorentzian pulse is obviously shape invariant under the Wallace head medium spacing loss.

The pulse width at half maximum value is now :

$$PW'_{50} = PW_{50} + 2\frac{\Delta d}{v} = \frac{PL_{50} + 2\Delta d}{v} \tag{3.24}$$

From this we conclude that (for Lorentzian pulses) a pulse width measurement yields an incremental measurement of flying height d. If we conduct a difference measurement before and after a change of Δd in the flying height d the increment in pulse width is:

$$\Delta PW_{50} = PW'_{50} - PW_{50} = S_{50}\frac{\Delta d}{v} \tag{3.25}$$

where the measurement sensitivity factor S_{50} is defined as:

$$S_{50} = \frac{\Delta PL_{50}}{\Delta d} \tag{3.26}$$

For a Lorentzian pulse obviously $S_{50} = 2$. More generally, for a slicing level of x percent, it can be shown that for Lorentzian pulse:

$$\Delta PW'_x = PW'_x - PW_x = 2\frac{\Delta d}{v}\sqrt{\frac{100 - |x|}{|x|}} \tag{3.27}$$

and therefore, the sensitivity factor at slicing level x is given by:

$$S_x = \frac{\Delta PL_x}{\Delta d} = 2\sqrt{\frac{100 - |x|}{|x|}} \tag{3.28}$$

It looks from equation (3.28) that the sensitivity S_x increases when lowering the slicing level x. However, the uncertainty in the measurement will also increase duo to baseline noise and the more shallow slope of the readback pulse towards its base (see Figure 3.5).

Klaassen and van Peppen (1994) provided a method and circuitry, which can directly measure the pulse width from isolated read-back pulse signals. Some advanced Digital

Storage Oscilloscopes/Disk Drive Analyzers (e.g. products of Lecroy and Tektronix) have functions that enable measurement of the PW_{50} from isolated read-back pulse signals. Zhu et al. (1998) also tried to provide a digital sampling technique to measure the PW_{50} of isolated readback pulse signals. It was claimed the method could be used under relatively low sampling rate. Li et al. (2001) provided a parameter estimation method which can be used to determine the PW_{50} without the restriction of isolated readback pulse signals.

3.5.3 Thermal signal detection method

The thermal signal detection is another head-disk spacing measurement method proposed in recent years. It is intended to be used for the measurement of disk topography or dynamic flying height by detecting and processing the readback signal from a magnetoresistive (MR) head in a hard disk drive [Abraham, 1996; Smith, 1999; Sundaram et al., 1999]. Changes in flying height or head-disk spacing modulate both the envelope of the readback signal and its mean value. To clarify the statement, we introduce two nomenclatures: magnetic spacing and thermal spacing, although both of them mean the flying height or head-disk spacing. While the envelope is related to the magnetic spacing, the mean value is a function of the thermal spacing. The thermal spacing signal is the result of Joule heating, whereby some of the thermal energy generated in the MR head dissipates into the air film between the head and disk. Changes in head flying height alter the heat transfer and hence the temperature and resistance of the MR head. Abraham (1996) has shown that the MR head voltage resulting from thermal spacing can be approximated as:

$$e_{thermal}(t) = C_0 + C_1 \beta I^3 R^2 d(t) \tag{3.29}$$

where $e_{thermal}$ is the MR voltage due to its temperature, t is time, C_0 and C_1 are constants that depend on the geometry and thermal properties of the MR element and adjacent shields, β is the temperature coefficient of resistance for the MR material, I and R are the MR current and electrical resistance respectively, and d is the head disk spacing or flying height. From (3.29), we note that the flying height can be determined from the measured thermal signal. However, most disk drives use an arm-mounted electronic module circuitry (AEM), which is used to amplify the head output signal, and usually includes a high pass filter. The filter provides the necessary AC coupling for the read channel, but also distorts the thermal signal. The AEM output signal is the convolution of $e_{thermal}$ and the impulse response of the filter. Assuming a high pass filter with a single pole, f_a, and gain G, the AEM output voltage will be [Abraham, 1996]:

$$e_{AEM}(t) = G\int_{-\infty}^{\infty} e_{thermal}(t-\tau)[\delta(\tau) - \exp(-f_a\tau)]d\tau \tag{3.30}$$

The transfer function for an inverse filter that will correct for the AEM filter is then given by:

$$H_{INV}(s) = \frac{1}{G}\frac{s+f_a}{s+f_b} \tag{3.31}$$

where f_b is a suitably chosen pole, so that the inverse filter can be easily realised as an analogue circuit if desired. If the AEM output voltage is sampled with a fixed sampling time interval, the true thermal signal of the MR head can be estimated by applying the matched z-transform to (3.31) and using the resulting infinite impulse response (IIR) digital filter to process the sampled sequence $e_{AEM}(n)$.

3.6 Modern optical flying height testing techniques

The Data Storage Industry has relied for some time on *direct spacing measuring* (DSM) optical testers for quantifying flying height in production and in developing new designs [de Groot, 1998a]. DSM optical testers employ a rotating transparent glass substrate in place of the real magnetic disk, and determine the flying height by analysis of the interference phenomena between the head slider and the glass [Ohkubo & Kishigami, 1988; Lacey et al., 1992; de Groot et al., 1996a; Erickson & Lauer, 1997]. Up to now, the methods that are widely accepted by industry, and have also been utilised in the popular commercial flying height testers, are Intensity Interferometry and Polarization Interferometry. These will now be analysed and described in detail below.

3.6.1 Intensity Interferometry

Intensity Interferometry is one of the popular methods used by the majority of the industry to determine the absolute flying height. Its popularity is based on its accuracy, no modification to the slider, and ability to view the complete air-bearing surface. The operating principle of this technique is straightforward: A mechanism loads the slider onto a rotating glass disk, the light source illuminates a measurement point on the slider, and the thin film of the air bearing modulates the reflected light over portions of the modulation curve. The flying height is determined by measuring the reflected intensity. Single-wavelength testers are limited by the periodicity of the interference, which introduces ambiguities and a severe loss of measurement sensitivity near the extrema of the curve, i.e. when the flying height is very low. To overcome this problem, a variety of so-called white-light systems could be adopted, such as the computerised system of Fridge and Miller (1986) using an arc lamp and a spectrophotometer, the tunable monochromater of Lin (1973) and the variable filter wheel of Nigam (1982). The principal drawback of white-light systems is that they are too slow. The solution to this

problem is to settle on a small number of discrete wavelengths and measure the corresponding intensities directly, rather than scanning through the spectrum. Fukuzawa, et al. (1996) of IBM adapted this concept to disk drive sliders, and in 1992, Phase Metrics Corporation introduced a high speed (e.g. >100kHz) design for single point measurement [Lacey et al., 1992]. This three-wavelength compromise has rapidly become the dominant technology for flying height testing. In the meanwhile, considerations were made and incorporated to these intensity-based flying height testers to compensate the Phase Change on Reflection Phenomenon (PCOR) [Lacey et al, 1993; Lue & Lacey, 1994; Li, 1996; Li & Menon, 1996; Li, 1997], which requires an entirely separate ellipsometric analysis to determine the PCOR for each of the three wavelengths.

Figure 3.6 shows the schematic of a modern intensity interferometry flying-height tester.

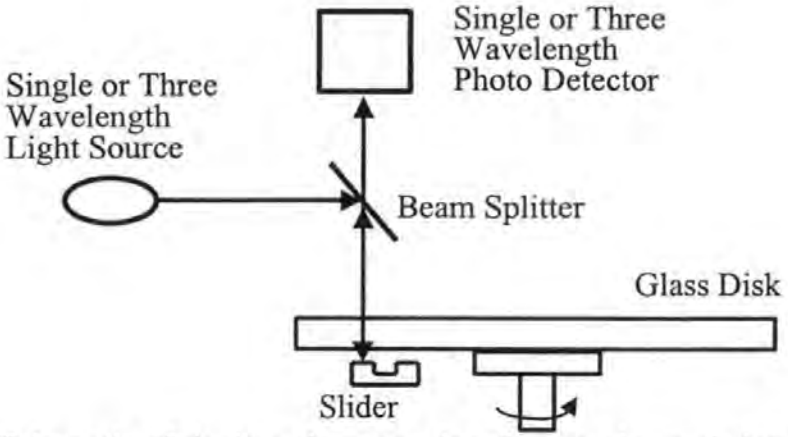

Figure 3.6 Schematic of single or three-wavelength monochromatic interferometer

3.6.1.1 Single Reflection

A beam of light E_i emitted from the light source transmits into the glass disk, as conceptually illustrated in Figure 3.7. At the glass air interface, E_{r1}, A portion of E_i, is

reflected back into the glass disk. The remaining light E_{t1} transmits through the air spacing between the glass disk and the slider air-bearing surface. Similar to that at the

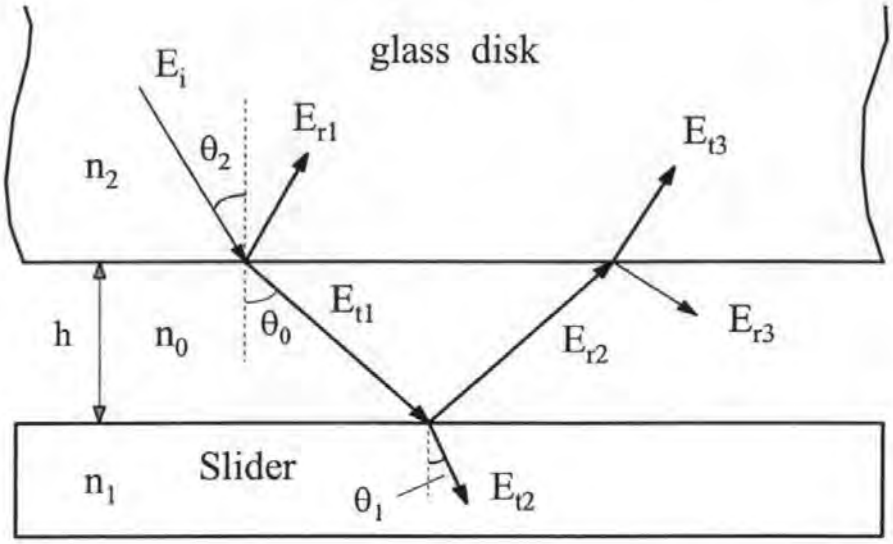

Figure 3.7 Light beam at disk slider interface

glass air interface, a portion of E_{t1}, labelled as E_{t2}, is reflected off at the air slider interface. E_{t3} of this reflected light transmits into the glass disk, and interferes with E_{r1}. For such a single reflection at normal incidence, the intensity of the interfered light beam is

$$I_s = I_{r1} + I_{t3} + 2\sqrt{I_{r1} I_{t3}} \cos\left(\frac{4\pi}{\lambda} h + \phi_s\right) \tag{3.32}$$

where $I = \langle E^2 \rangle \equiv$ time average of the electric field squared, I_s is the intensity of the interfered light beam, λ is the wavelength of the light, h is the head disk spacing or flying height, and ϕ_s is the phase shift of light when it is reflected off the slider air-bearing surface. This phase shift is caused by the discontinuity of the light wave when it is reflected off the slider air-bearing surface. This phase shift can be calculated from

$$\phi_s = \pi - \tan^{-1}\left(\frac{2n_0 k_1}{n_0^2 - n_1^2 - k_1^2}\right) \tag{3.33}$$

where n_0 is the real index of the air above the slider and $(n_1 + ik_1)$ is the complex index of the slider material [Born & Wolf, 1989]. If the slider is made of a dielectric material, this phase shift will be π (180°). Because the popularly-used slider material (Al_2O_3/TiC ceramic) is not completely dielectric $(k_1 \neq 0)$, equation (3.33) does not yield a value of π for ϕ_s. A typical flying height tester using this single reflection theory is the Phase Metrics Dynamic Flying Height Tester (DFHT) [Lacey et al., 1992; McMillan & Talke, 1994]. Nigam (1982) used this in his system as well.

3.6.1.2 Multi-reflection

In a real flying height testing system, at the slider disk interface, the light beam actually experiences a multi-reflection. In such an instance, the intensity of the interfered light I_m should be

$$I_m = I_0 \left| \frac{r_{20} + r_{01} \exp(i\delta)}{1 + r_{20} r_{01} \exp(i\delta)} \right|^2 \tag{3.34}$$

where $\delta = \frac{4\pi h}{\lambda} \cos\theta_0$, h and θ_0 are as shown in Figure 3.7, r_{20} is the reflection coefficient of the glass air boundary, r_{01} is of the air slider boundary, and I_0 is the intensity of the incident light [Born & Wolf, 1989].

For normal incident light,

$$I_m = I_0 \frac{{r_{20}}^2 + |r_{01}|^2 + 2r_{20}|r_{01}|\cos(\delta + \phi_s)}{1 + {r_{20}}^2 |r_{01}|^2 + 2r_{20}|r_{01}|\cos(\delta + \phi_s)} \tag{3.35}$$

where $\phi_s = \pi - \tan^{-1}\left(\frac{2n_0 k_1}{{n_0}^2 - {n_1}^2 - {k_1}^2} \right)$, $r_{20} = \frac{n_2 - n_0}{n_2 + n_0}$, $r_{01} = \frac{n_0 - (n_1 + ik_1)}{n_0 + (n_1 + ik_1)}$, n_2 is the refractive index of the glass disk.

Using a signal processing algorithm, Fukuzawa et al. (1996) adopted this multi-reflection theory in their flying height measurement apparatus. The new products of the

Phase Metrics Dynamic Flying Height Tester (DFHT) also use this for the determination of flying height [Lacey & Ross, 1995].

The measurement error of the flying height tester created by using the single reflection theory can be evaluated through the simulation method as below. Equation (3.32) can be further written as

$$\frac{I_s}{I_0} = r_1^2 + (t_1|r_2|t_1')^2 + 2r_1t_1|r_2|t_1'\cos(\frac{4\pi n_0}{\lambda}h + \phi_s) \tag{3.36}$$

where $t_1 = \frac{2n_2}{n_0 + n_2}$, $t_1' = \frac{2n_0}{n_0 + n_2}$.

Assume that the refractive index of the glass disk is 1.5, the index of the slider is $2 + i0$, and the light wavelength λ=670nm, then from (3.35) and (3.36), the interference intensities for single and multiple reflections as functions of flying height can be plotted as in Figure 3.8.

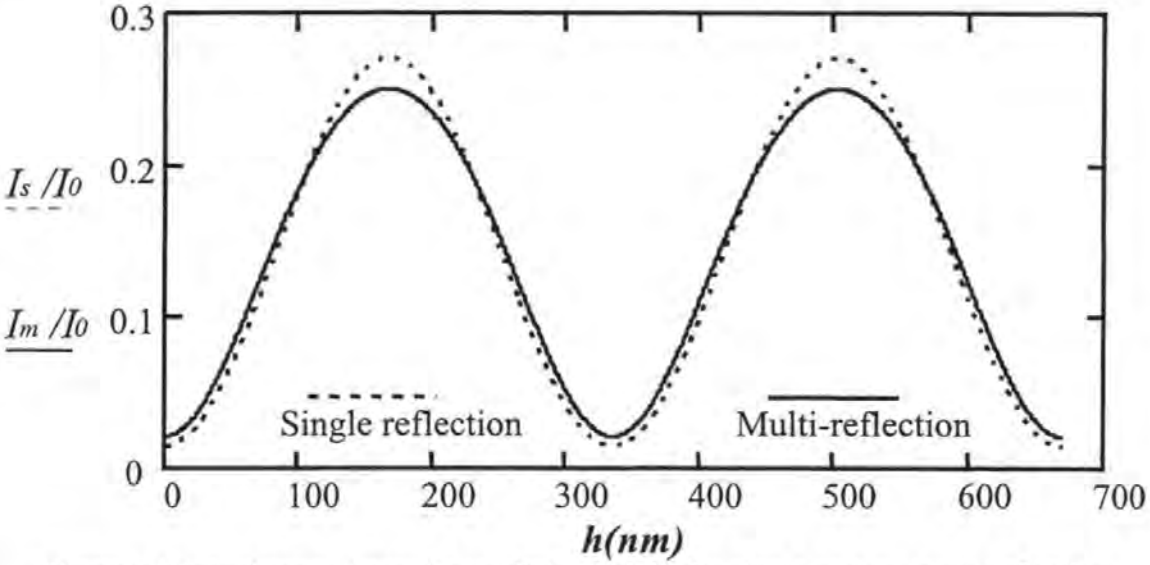

Figure 3.8 Interference intensity vs. flying height for single and multiple reflection

Because the flying height is determined using the normalised intensity detected in a flying height tester, for the purpose of error analysis, the normalised interference intensity curves are plotted below in Figure 3.9.

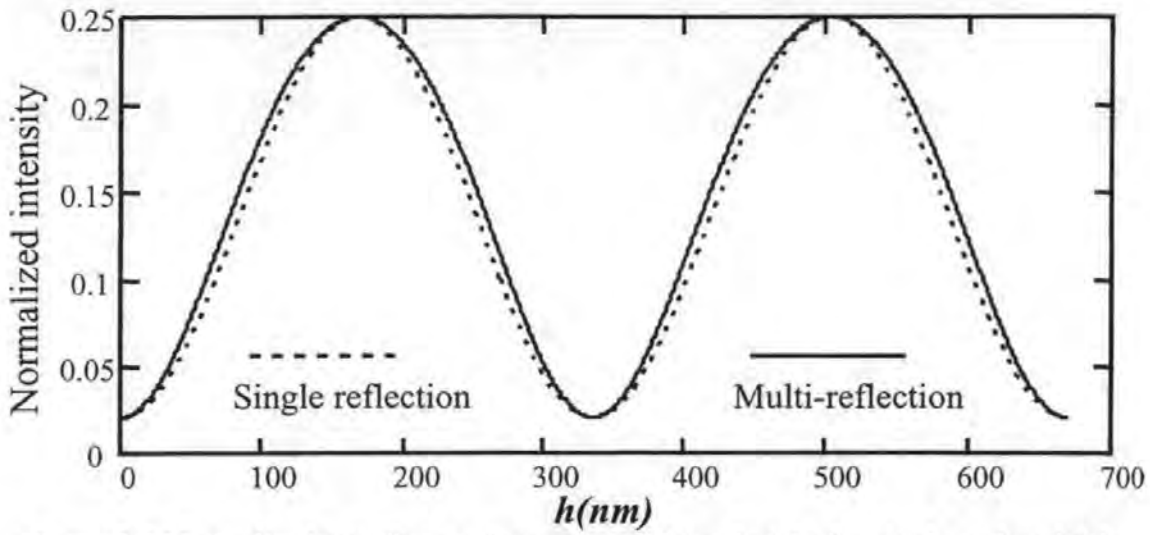

Figure 3.9 Normalised interference intensity vs. flying height for single and multiple reflection

From Figure 3.9, we can see that although the intensity of the reflected light decays very quickly after the first reflection, the importance of the multi-reflection cannot be ignored. If the single reflection model is used, a flying height measurement error of about 7 nm will be introduced at about 67 nm nominal flying height. This error diminishes as the flying height becomes smaller. This error can be evaluated from the measurement error as a function of normalised intensity, which is plotted in Figure 3.10.

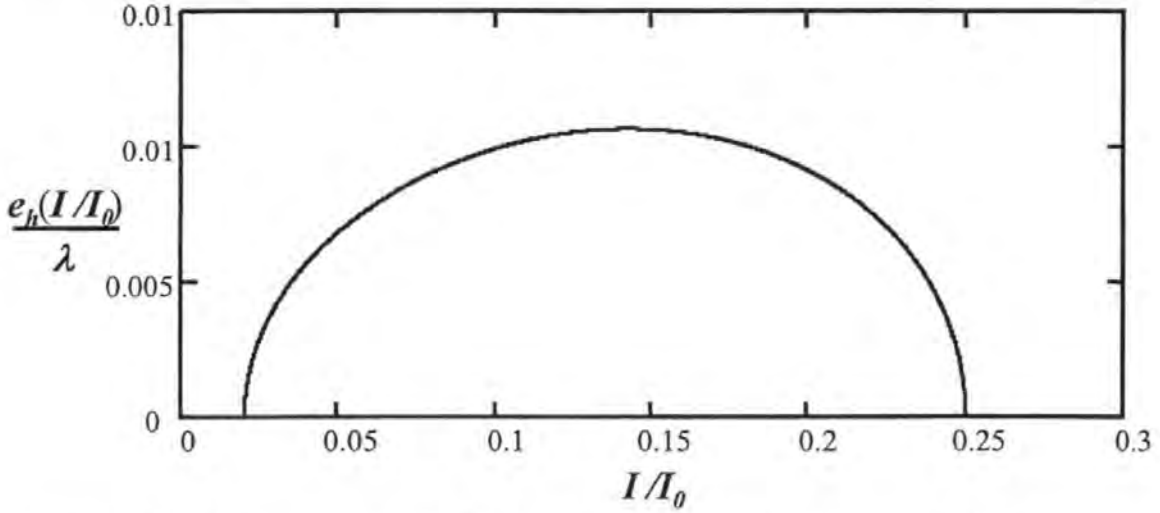

Figure 3.10 Measurement error as a function of normalised intensity when single reflection is used

3.6.2 Polarisation Interferometry

As stated by de Groot [1996b], a fundamental difficulty of Intensity Interferometry relates to the loss of measurement sensitivity near contact. The intensity modulation for all wavelengths has a vanishing derivative at low flying height. It became evident to many researchers that simply measuring the reflected intensity from the slider-glass interface is not adequate for production testing of the next generation of disk drives in which head-sliders fly very near to contact, i.e., in the 5 to 20nm height range, even in the presence of substantial PCOR. Attention then shifted to a radically new way for the measurement of flying height.

3.6.2.1 Sommargren's PSI method

It is known that two-beam Phase Shifting Interferometry (PSI) is accurate to the nanometre level, with uniform sensitivity over the entire measurement range [Hariharan, 1985]. For conventional PSI, the reflections from the head slider and the disk surface must be separated. This is not so easy, since the distance between the slider and the disk is extremely small. In 1986, Sommargren proposed the use of a polarisation beam-splitter coating on the transparent disk, to separate the reflections from the disk surface and the slider by means of polarisation encoding [Sommargren, 1986]. A modulator shifts the relative phases of the polarisation components to generate a time-varying sinusoidal interference signal at the detector. The starting phase of the signal is linearly proportional to the flying height, and does not lose sensitivity at contact. However, there are important practical problems associated with manufacture and durability of the coating.

Sommargren (1993) also proposed a dual-beam PSI geometry that avoids any disk coatings. As shown in Figure 3.11, a polarising beam splitter PBS_1 divides the source light into two parallel beams having orthogonal polarisations. Both beams are incident

on the disk surface at Brewster's angle, so that the p-polarised beam passes the glass disk completely without reflection, while the s-polarised beam is partially reflected.

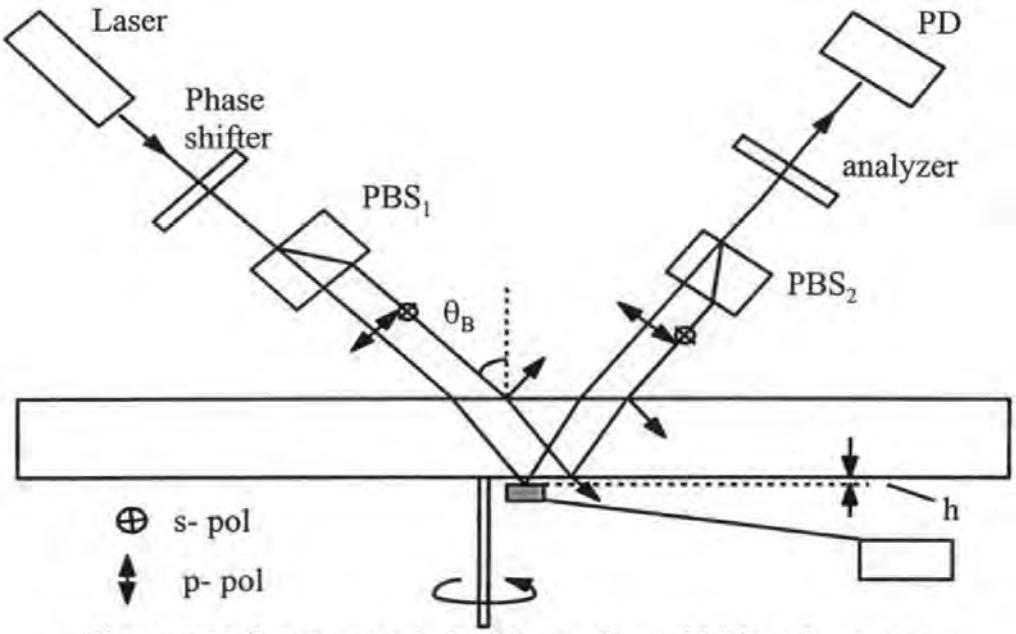

Figure 3.11 Sommargren's dual-beam phase-shift interferometer

The p-polarised beam passing through the disk illuminates the slider, while the other polarised beam serves as a reference. The p-polarised beam (measurement beam) reflected from the slider air bearing surface, and the s-polarised beam (reference beam) reflected from the bottom surface and passing through the top surface of the glass disk, are recombined by the polarising beam splitter PBS_2. The combined beam, having two orthogonally-polarised components, then passes through the analyser which preferably has its polarisation axis at 45° to each of the polarisation components. Both components of the transmitted beam are now having the same polarisation state and will optically interfere. The phase difference between these two waves is related to the flying height h. The complex amplitudes of these waves are given by

$$\begin{aligned} E_m &= A_m e^{-ik(Z_m+2h\cos\theta_B)-i\phi} \\ E_r &= A_r e^{-ikZ_r-2\pi n/N} \end{aligned} \tag{3.37}$$

where A_m and A_r are related to the reflectivities of the slider and the lower surface of the glass disk respectively, $k = 2\pi/\lambda$ (λ is the wavelength of the beam), $Z_m(x,y)$ and $Z_r(x,y)$ are the optical path lengths travelled by each wave through the glass disk, ϕ is the phase change on reflection from the slider surface, $2\pi n/N$ (N=4, n = 0,1,2,3) is produced by the phase shifter, which varies the relative phase of the orthogonal polarisation components of the beam. The intensity of the image at the photo-sensing device is given by

$$I(x,y) = A_m^{\,2} + A_r^{\,2} + 2A_mA_r\cos[k(Z_m - Z_r) + 2kh\cos\theta_B + \phi - 2\pi n/N] \qquad (3.38)$$

The optical path difference $(Z_m - Z_r)$ through the glass disk is due to manufacturing imperfections (flatness, parallelism, homogeneity).

The phase shifter is controlled so that the phase between polarisation components is shifted by $\pi/2$ each time after a frame of intensity is taken. To determine the flying height, h, four frames $(N = 4)$ of the intensity are collected and stored by computer, one for each distinct phase shift (n = 0,1,2,3) of phase shifter. These intensities are given by

$$I_0 = C_1 + C_2\cos(2kh\cos\theta_B + \phi) \qquad (3.39a)$$

$$I_1 = C_1 + C_2\sin(2kh\cos\theta_B + \phi) \qquad (3.39b)$$

$$I_2 = C_1 - C_2\cos(2kh\cos\theta_B + \phi) \qquad (3.39c)$$

and

$$I_3 = C_1 - C_2\sin(2kh\cos\theta_B + \phi) \qquad (3.39d)$$

If the intensity is integrated over an integral number of revolutions, the dependence on the optical path difference $(Z_m - Z_r)$ only influences the constant C_2 and not the argument of the cosine. The phase $\Phi(x,y)$ is calculated by the computer at each point in the image of the slider using

$$\Phi(x,y) = \tan^{-1}[(I_1 - I_3)/(I_0 - I_2)] \tag{3.40a}$$

$$\Phi(x,y) = 2kh\cos\theta_B + \phi \tag{3.40b}$$

After the phase change on reflection, ϕ, is determined, the flying height, h, can be calculated. With this method, since the distance, h, is calculated at each point on the air bearing surface of the slider, the following steady state information can be readily obtained from $h(x,y)$ (but the accuracy can not be guaranteed).

(a) The flying height from smallest value of h, and the location of the smallest distance;

(b) Pitch and roll of the slider air bearing surface;

(c) Shape changes of the air bearing surface of the slider caused by flying.

However, there are important limitations that slowed practical implementation. For instance, the opto-mechanical geometry makes the system sensitive to the disturbances resulting from the optical path length variations of the two beams, which will inevitably affect the measurement accuracy and resolution of the system. Dynamic measurement of the flying height is also impossible because the integrated (sum or average) intensity is employed.

3.6.2.2 de Groot's polarisation interferometry

Despite the practical difficulties of the PSI techniques outlined above, convinced by Sommargren's case for phase detection in flying height testing, de Groot (1996a, 1996b) proposed a polarisation interferometry method which includes phase detection as well as intensity detection without any special modifications to the glass disk. Figure 3.12 shows the basic optical geometry of the polarisation interferometer for flying height testing.

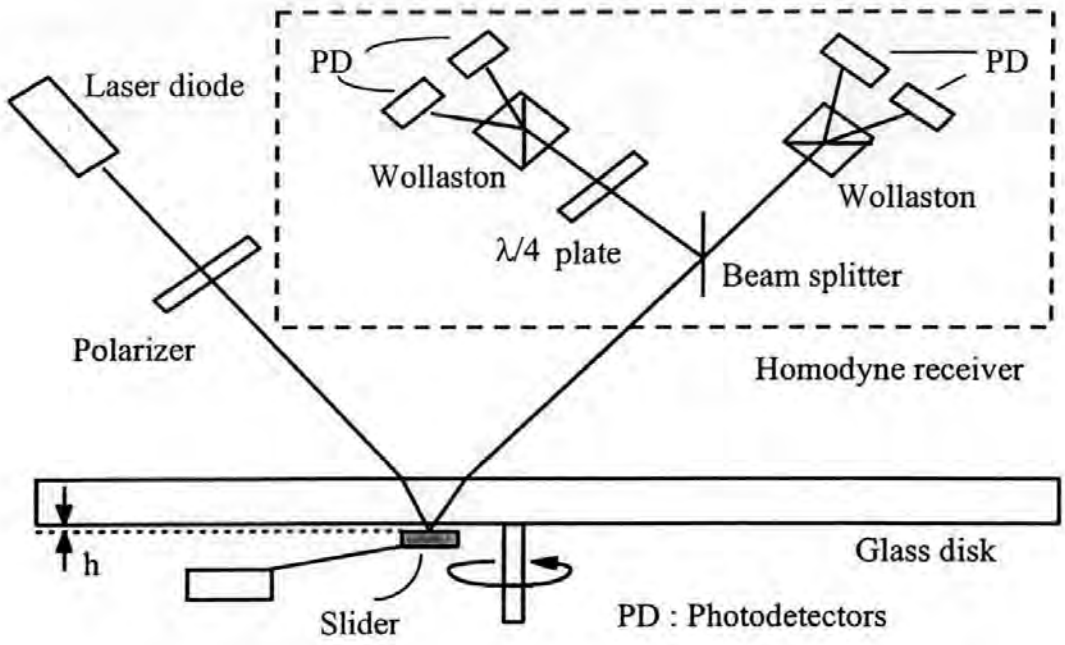

Figure 3.12 Polarisation interferometer for flying height testing

The oblique beam incidence defines two orthogonal polarisation components *s* and *p*, where *p* polarisation is parallel to the plane of incidence. By using Jones' vectors, the electric field of the incident beam can be written as

$$\mathbf{E} = \begin{pmatrix} \mathbf{E}_s \\ \mathbf{E}_p \end{pmatrix} \tag{3.41}$$

For example, if the incident beam is linearly polarised with equal *s* and *p* components, then $|\mathbf{E}_s| = |\mathbf{E}_p| = 1/\sqrt{2}|\mathbf{E}|$. The electric field components $\mathbf{E}_s$ and $\mathbf{E}_p$ are complex numbers, so that any relative phase shift between the two polarisation components can be represented as a complex phase angle. The combined reflections from the slider surface and the surface of the glass disk modify the polarisation state of the beam. The electric field of the reflected beam is given by

$$\mathbf{E}' = S\mathbf{E} \tag{3.42}$$

where

$$S = \begin{pmatrix} r_s & 0 \\ 0 & r_p \end{pmatrix} \tag{3.43}$$

and r_s, r_p are the effective reflectivities of the slider-glass combination (interface), which can be represented by the standard thin-film equations for layered media and are given by [Born & Wolf, 1989]

$$r_s(\beta) = \frac{r_{1s} + r_{2s}\exp(i\beta)}{1 + r_{1s}r_{2s}\exp(i\beta)} \tag{3.44a}$$

$$r_p(\beta) = \frac{r_{1p} + r_{2p}\exp(i\beta)}{1 + r_{1p}r_{2p}\exp(i\beta)} \tag{3.44b}$$

where the phase term β is given by

$$\beta = 2kh\cos(\theta) \tag{3.45}$$

The reflection coefficients r_{1s} and r_{1p} are for the glass-air boundary, and r_{2s} and r_{2p} for the air-slider boundary. The phase β depends on the wave number $k = 2\pi/\lambda$, the angle of incidence θ, and the flying height h. The normalised intensity of the reflected beam is

$$I(\beta) = I_s(\beta) + I_p(\beta)) \tag{3.46}$$

where

$$I_s(\beta) = |r_s(\beta)|^2 \tag{3.47a}$$

$$I_p(\beta) = |r_p(\beta)|^2 \tag{3.47b}$$

The phase difference between the two polarisation components of the reflected beam is

$$\phi(\beta) = \arg[r_s(\beta)] - \arg|r_p(\beta)| \tag{3.48}$$

The intensity $I(\beta)$ and the phase difference $\phi(\beta)$ are measured with a homodyne interferometric receiver which basically consists of a polariser, a beam splitter, two Wollaston prisms, one $\lambda/4$ plate and four photodetectors as shown in Figure 3.12. The components of this homodyne receiver are selected and arranged so that the four intensities I_1, I_2, I_3, I_4 detected by the four photodetectors correspond to a sequence of four interference signals separated in phase by exactly $\pi/2$ radians and are given by

$$I_1 = \alpha\left(I_s + I_p + 2\sqrt{I_s I_p}\cos\phi\right) \tag{3.49a}$$

$$I_2 = \alpha\left(I_s + I_p - 2\sqrt{I_s I_p}\cos\phi\right) \tag{3.49b}$$

$$I_3 = \alpha\left(I_s + I_p + 2\sqrt{I_s I_p}\sin\phi\right) \tag{3.49c}$$

$$I_4 = \alpha\left(I_s + I_p - 2\sqrt{I_s I_p}\sin\phi\right) \tag{3.49d}$$

where α is a constant coefficient. Then the phase difference between the s and p polarisation components can be extracted by means of the formula

$$\phi = \tan^{-1}\left(\frac{I_3 - I_4}{I_1 - I_2}\right) \tag{3.50}$$

Figure 3.13 and Figure 3.14 show the plots of the intensity $I(\beta)$ and the phase $\phi(\beta)$ as functions of flying height.

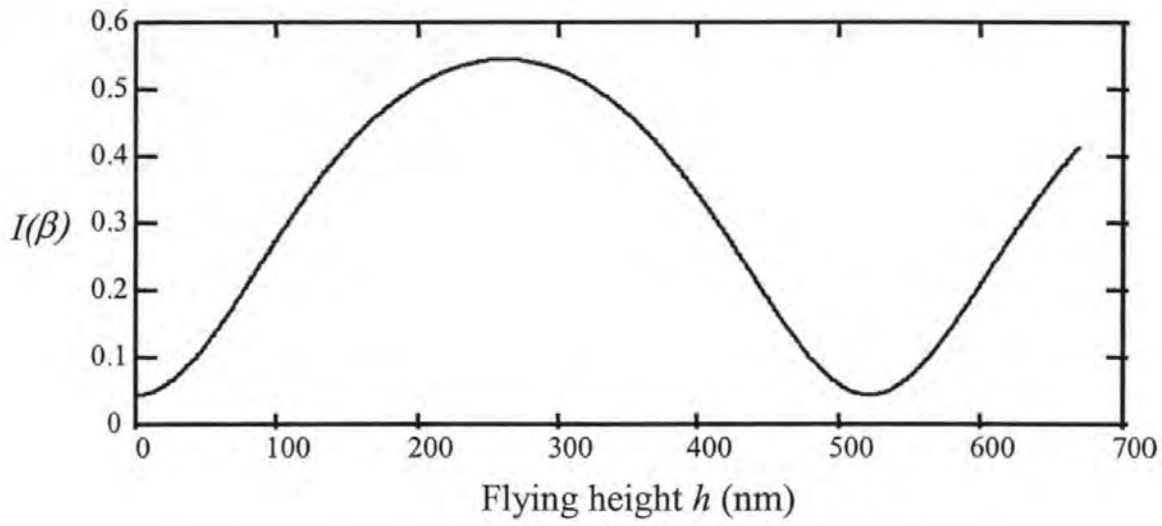

Figure 3.13 Reflected intensity as a function of flying height

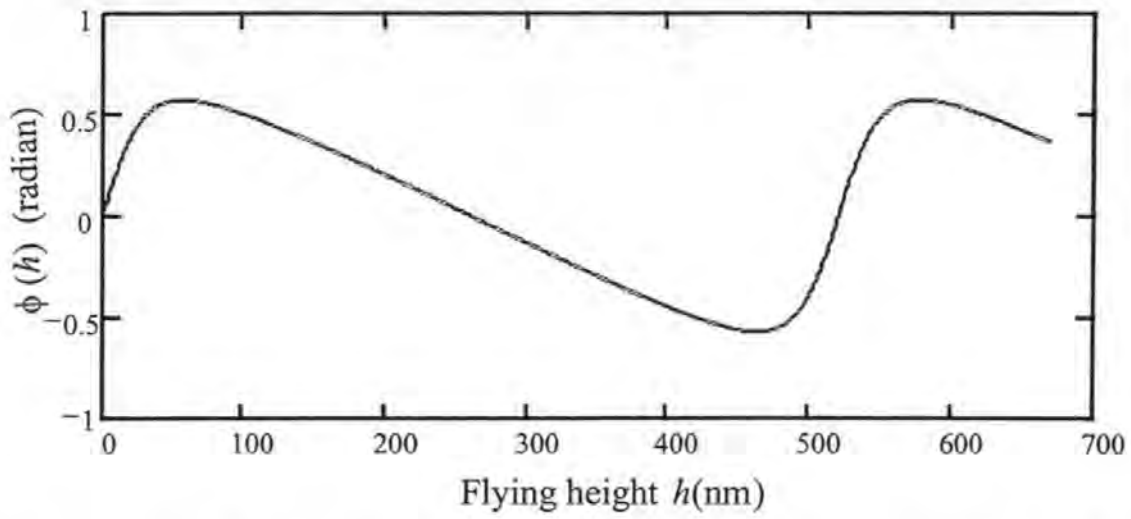

Figure 3.14 Phase difference between the two polarisation components as a function of flying height

What is important about the intensity and phase curves of this polarisation interferometer is that they are complementary. When the intensity curve has a steep slope, the phase is fairly constant; when the intensity is nearly constant, the phase is changing rapidly. Using both curves together means that there is always a way to measure flying height with good sensitivity. Of particular importance is the region near zero flying height, where the intensity $I(\beta)$ varies slowly and is therefore a poor measure of flying height, whereas the phase $\theta(\beta)$ varies rapidly in this region, with maximum sensitivity at contact (if neglecting the phase change on reflection effect).

The additional benefit of this methodology is that it also provides a method and means for the determination of the complex refractive index of the slider surface, which is also inevitable in the flying height measurement.

3.7 Scattered total internal reflection method

A totally different optical flying height testing method has been under research in recent years ago [Sides & Lo, 1996; Lo & Sides, 1997; Guerra, 1998; Walker & Sides, 2000], which is called the scattered total internal reflection (SCATIR) method. Instead of using optical interference phenomenon, SCATIR employs measuring scattered photons from

an evanescent wave to determine the flying height or head disk spacing. The principle is as follows: when a light beam propagates from a dense medium (glass disk) to a less dense medium (air) with an incident angle greater than the critical angle, total reflection occurs at the interface between the two media. When such a total reflection takes place, a surface wave called evanescent wave is formed in the second (less dense) medium near the interface. If a third medium (head slider) is present and is disseminative, light from the incident beam will be scattered and the intensity of the scattering depends on the separation between the first and third media. This is shown in Figure 3.15.

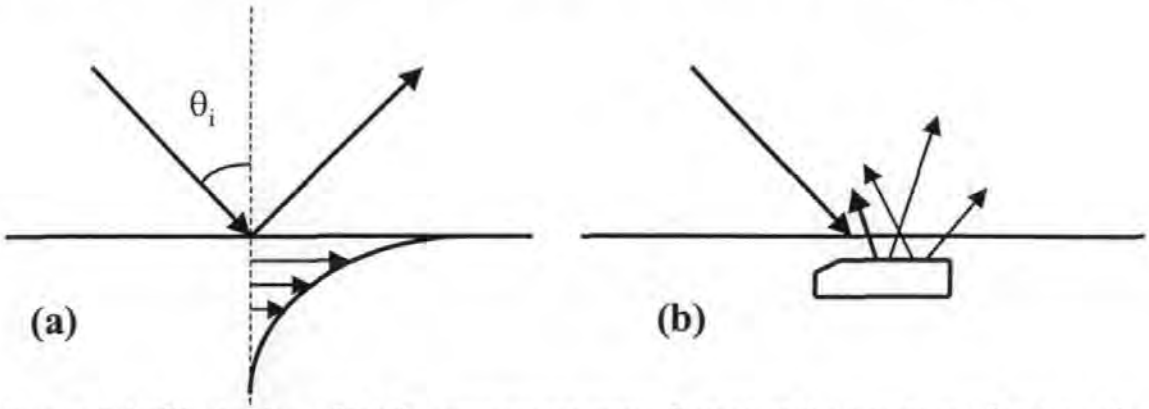

Figure 3.15 Illustration of (a) the evanescent wave formed at the interface of two media, and (b) the scattering of the evanescent wave off a slider.

The spacing between the glass disk and the head slider or flying height can be determined from [Walker & Sides, 2000]

$$I(h) = I_0 \exp(-h/\delta) \tag{3.51}$$

where

$$\delta = \frac{\lambda}{4\pi\sqrt{n_1^2 \sin^2\theta_i - n_2^2}} \tag{3.52}$$

and I is the intensity of illumination (W/m^2), I_0 is a pre-exponential constant (W/m^2), h is the flying height (m), δ is the decay constant (m), λ is the wavelength of the incident light (m), n_1 is the refractive index of the glass disk, n_2 is the refractive index

of air, and θ_i is the angle of incidence. This method is still under research for its capability and accuracy for measurement of head-disk spacing below 25nm.

4 Improved Intensity Interferometry Method for Measuring Head-Disk Spacing Down to Contact

In section 3.6.1, we have given an in-depth analysis of the working principle of the intensity interferometry flying height testing technique. In this chapter, we will first provide an investigation to the application limit and potential problems of this intensity interferometry method, and the approach which needs to be used to ensure this intensity-based method can be correctly implemented in practice. Then phase-shifting methods are proposed to improve the sensitivity of this technique when the head-disk spacing is below 10 nm or near contact. This is based on fabricating the glass testing disk to have a specified thickness, or having it coated with a specified thickness of thin carbon film.

4.1 Application limit and potential problems

As stated in section 3.6.1, in intensity interferometry flying height testers, a normal incident beam is usually employed. At the disk-slider interface, the light beam experiences multiple reflections as shown in Figure 3.7. According to the standard thin-film equation, the intensity of the interfered light reflected from the interface is given by equation (3.35), which is the theoretical basis and working principle of all the current modern intensity interferometry flying height testers.

We have seen in this case, only reflections at the disk-slider interface are considered. That is, only a single layer reflection effect is taken into account. This may not be

sufficient, especially when a laser is used as the light source, in which case the light's coherent length is much longer. Consider the slider and glass disk interface again in Figure 4.1, where the glass disk is about 3 mm thick. If the coherent length of the

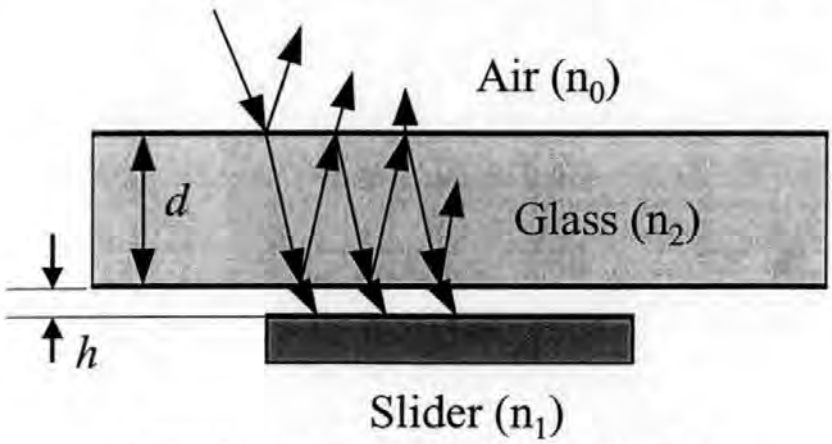

Figure 4.1 Two-layer reflection consideration

light beam is longer than a few times the double thickness of the glass disk, the two-layer reflection effect should be considered. In this case, the intensity of the returned beam from the glass disk will be given by:

$$I(N) = I_0 \left| r_{02} + t_{02} t_{20} r(h) \exp(i \frac{4\pi n_2 d}{\lambda}) \sum_{m=2}^{N-2} [r_{20}{}^m r^m(h) \exp(i \cdot m \frac{4\pi n_2 d}{\lambda})] \right|^2 \qquad (4.1)$$

where $r(h) = \dfrac{r_{20} + r_{01} \exp(i \frac{4\pi h}{\lambda})}{1 + r_{20} r_{01} \exp(i \frac{4\pi h}{\lambda})}$ is the reflectivity of the disk-slider interface according to the standard thin film equation, $r_{02} = \dfrac{n_0 - n_2}{n_0 + n_2}$, $t_{02} = \dfrac{2n_0}{n_0 + n_2}$, $t_{20} = \dfrac{2n_2}{n_0 + n_2}$, h is the flying height, d is the thickness of the glass disk, and N is the reflection cycles the beam is assumed to have experienced between the two surfaces of the glass disk within its coherent length. From (4.1), It can be seen that the intensity of the interfered beam returned from the glass disk is not only dependent on the head-disk spacing h, but also dependent on the glass disk thickness d. Figure 4.2 (a–c) shows the plots of the intensities as functions of flying height for three different glass disk thickness, d.

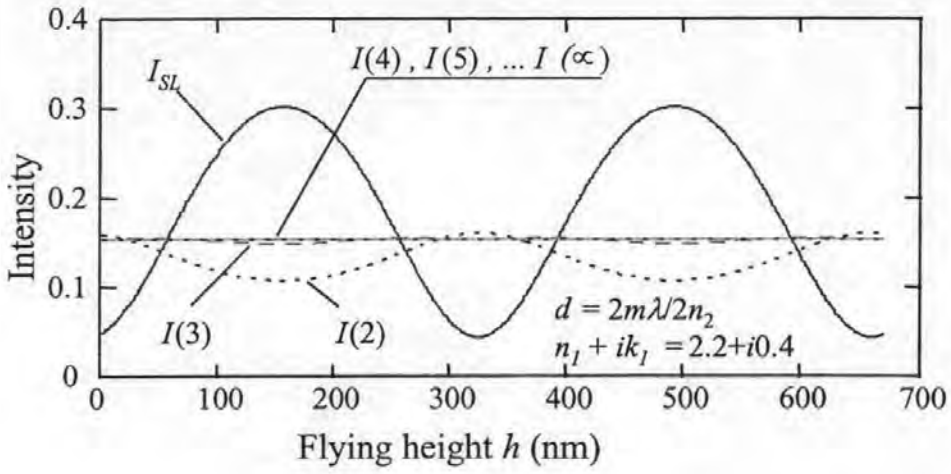

(a)

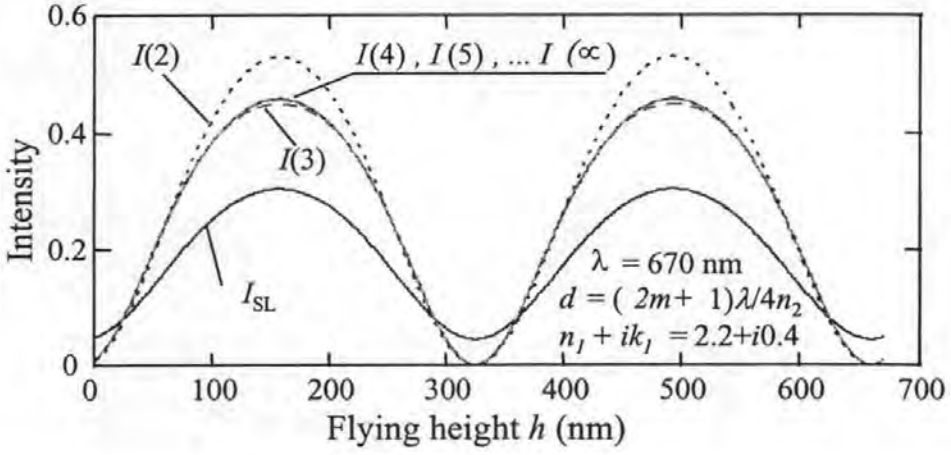

(b)

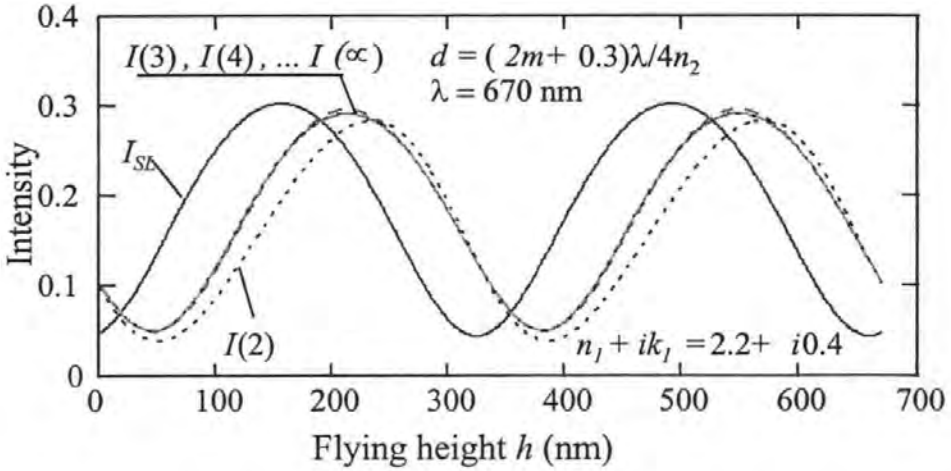

(c)

Figure 4.2 Intensity curves of single layer and multi-layer reflections as functions of flying height.

In Figure 4.2, m is a positive integer, I_{SL} (intensity of single layer reflections) is the intensity of the light reflected from the slider-disk interface regardless of the effect of multi-reflection between the two glass-disk surfaces. $I(2)$, $I(3)$, ..., and $I(\infty)$ (intensity of multi-layer reflections) are the intensities of the beam returned from the glass disk when the reflection cycles between the two glass-disk surfaces are assumed to be $N = 2, 3, ...,$ and ∞. From Figure 4.2, we notice that the intensity curve of the returned beam from the glass disk, when multi-reflection happens between the two glass-disk surfaces (multi-layer reflections), is totally different from the one when only single layer reflections is considered. This is true especially when a laser is used as the light source, in which case the coherent length of the light beam is longer than a few times the double thickness of the glass disk. To deal with this problem, an effective way is to make an efficient anti-reflection coating at the top surface of the glass disk, so that the effect of multi-reflection between the two glass-disk surfaces can be neglected, and the single layer reflection equation (3.35) can be employed to determine the flying height.

According to equation (3.35), the intensity as a function of flying height is re-drawn in Figure 4.3.

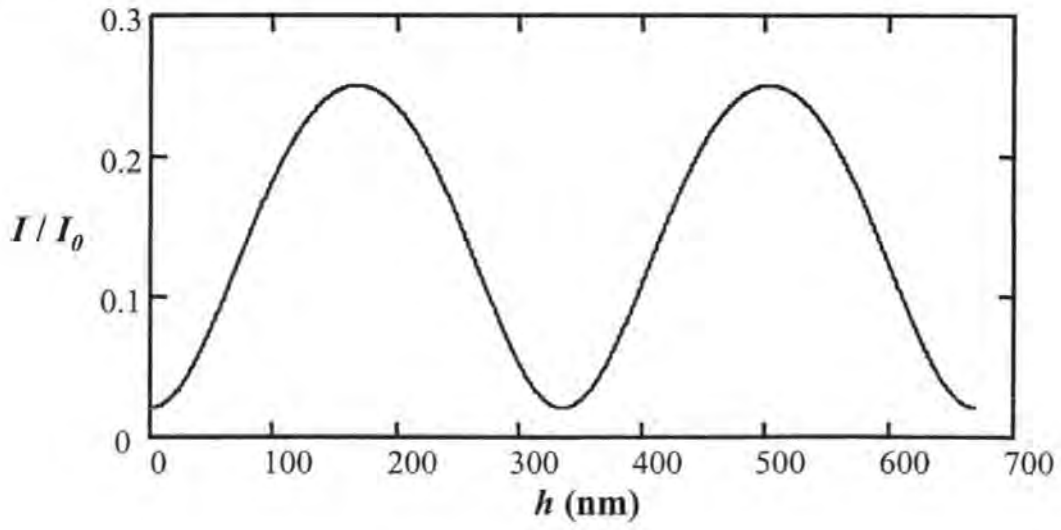

Figure 4.3 Intensity curve of single layer reflections as a function of flying height h.

From this commonly-used intensity curve, it can be seen that using this intensity interferometry technique, the flying height could be measured down to around 10 nm with acceptable precision. However, when the spacing is reduced to under 10 nm, the sensitivity of this intensity-based technique worsens considerably. By calculation, it can be found that the maximum sensitivity occurs at about 63 nm of flying height with a sensitivity value (intensity changing rate with respect to flying height) of 2.45×10^{-3}/nm. At a flying height of 10 nm, the sensitivity reduces to 6.5×10^{-4}/nm, only about a quarter of the maximum value. Although the phase change on reflection phenomenon (PCOR), when the slider material is not completely dielectric, can alleviate the situation, the sensitivities of the intensity curve in the near contact area are still not good enough for precise head disk spacing measurement.

4.2 Improving the sensitivity near contact

Since the intensity-based interferometry technique is a simple and accurate flying height testing method, and has been widely employed by the disk industry, it is useful to determine if ways can be found to increase the sensitivity near contact. To deal with this problem, we find that if the phase of the intensity curve is shifted, the sensitivity around the near-contact area can be improved. Two methods to enable this are presented below.

4.2.1 Using glass disks of specified thickness

Again, from the intensity curves in Figure 4.2, we have seen that the effect of the multi-reflection between the two glass-disk surfaces has already performed this function, if a light source of long coherent length, e.g., a laser, is used. In fact, by numerical evaluation, we found that if the glass disk is manufactured or modified to have a thickness within $\frac{\lambda}{4n_2}(2m+1.3)$ to $\frac{\lambda}{4n_2}(m+1.8)$, where *m is an integer,* the intensity

curve of the two-layer reflections, according to (4.1), is advantageously phase-shifted relative to the intensity curve of the single layer reflections, and can be used for determining the head-disk spacing down to contact. This is shown in Figure 4.4 where the disk thickness is $\frac{\lambda}{4n_2}(2m+1.5)$. We can see from Figure 4.4 that when the intensity curve I_s is changing slowly, where the flying height is below 10 nm, the curve I_d has very good sensitivity because of its strong rate of change with flying height.

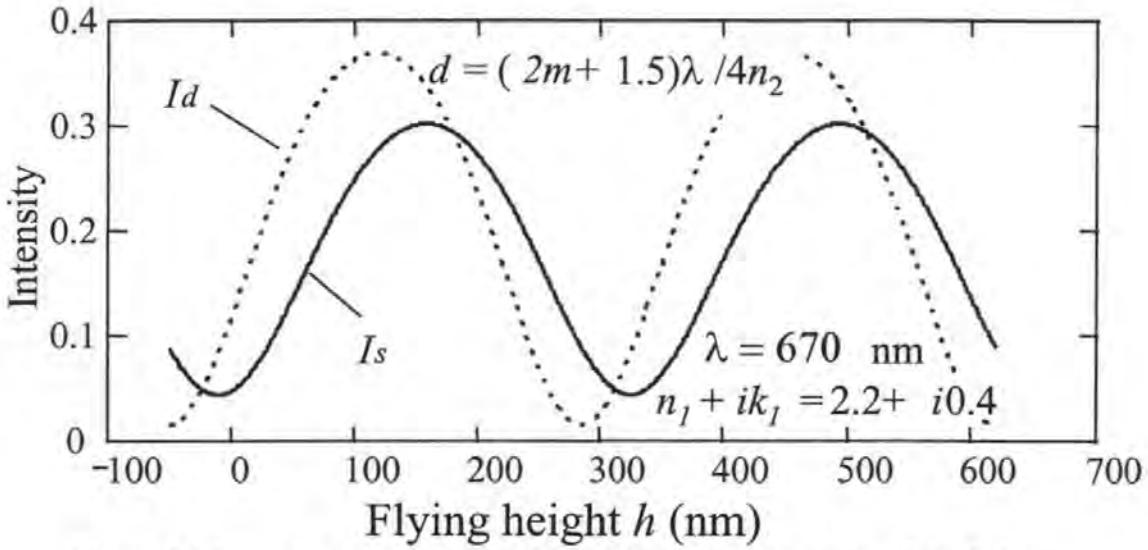

Figure 4.4 Intensity curves as functions of flying height. I_s is of single layer reflections, I_d is of two-layer reflections which can be used to determine the head-disk spacing down to contact.

Since for present technology, it is difficult to manufacture a glass disk with small enough thickness tolerance, e.g. ±2nm, for the whole disk, a realistic way of putting this method into practical use is by utilising small areas of the disk where the thickness can be controlled to very small tolerance.

4.2.2 Using glass disks with carbon-coating

In this method, we utilise a glass disk with an anti-reflection coating on one surface and a carbon coating on the other surface (working surface). In this case, the light beam will

experience two-layer reflections as well, and the intensity of the returned beam from the disk-slider interface will be given by:

$$I_C = I_0 \left| \frac{r_{23} + r_{L2} \exp(i4\pi n_3 d_1 / \lambda)}{1 + r_{23} r_{L2} \exp(i4\pi n_3 d_1 / \lambda)} \right|^2 \tag{4.2}$$

where $r_{L2} = \frac{r_{30} + r_{01} \exp(i4\pi n_0 h / \lambda)}{1 + r_{30} r_{01} \exp(i4\pi n_0 h / \lambda)}$, $r_{23} = \frac{n_2 - (n_3 + ik_3)}{n_2 + (n_3 + ik_3)}$, $r_{30} = \frac{n_3 + ik_3 - n_0}{n_3 + ik_3 + n_0}$, d_1 is thickness of the carbon coating film, and $(n_3 + ik_3)$ is the refractive index of the carbon coating layer. Again by numerical evaluation, we found if the carbon coating thickness d_1 is selected from 0.03λ to 0.08λ, the intensity curve will also be advantageously phase-shifted relative to the intensity curve of the single layer reflections, and can be used to determine the head-disk spacing down to contact. This is shown in Figure 4.5, where the carbon coating thickness is assumed to be 0.035λ.

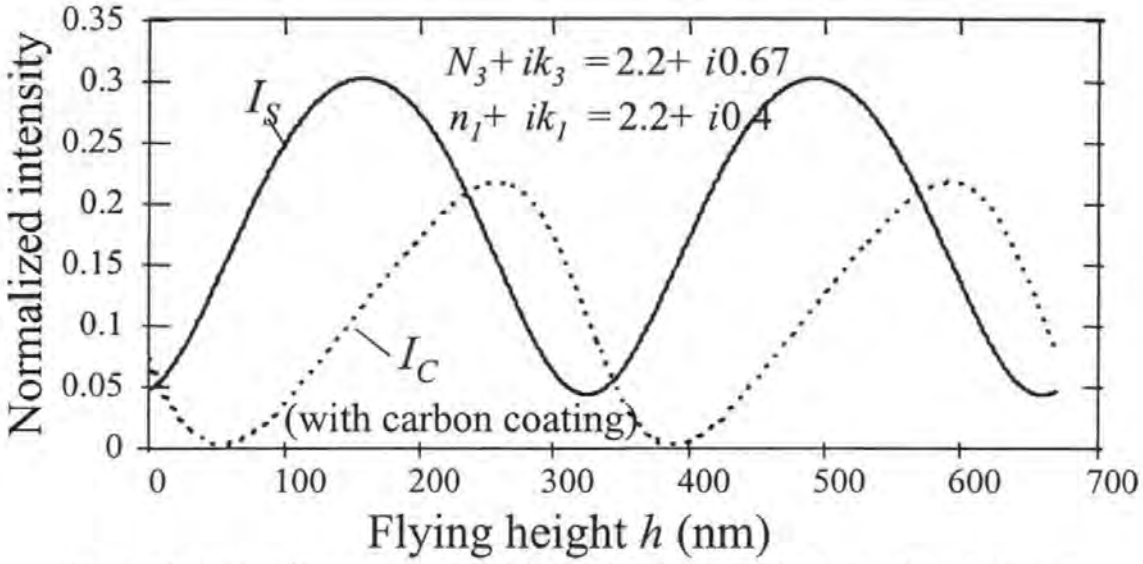

Figure 4.5 Intensity curves as functions of flying height. I_s is of single layer reflections, and I_C is of using carbon coating glass disk, with d_1=23nm.

This method can be used for the whole disk, since making a carbon coating with thickness tolerance of ±2nm is quite practical, and in this case, the maximum theoretical flying height error caused will be 0.8 nm. However, if the tolerance of the carbon

coating cannot be sufficiently controlled for the whole disk, which is required for accurate measurement purpose, then small areas of the disk can be used.

5 Dual Beam Normal Incidence Polarisation Interferometry Method

From **Chapter 3**, we know that using the currently available intensity interferometry flying height testers, the flying height can be measured down to around 10 nm with acceptable accuracy. But when the spacing is reduced to under 10 nm, the sensitivity of this intensity-based interferometry technique worsens considerably. To cope with this fundamental limitation of intensity interferometry related to the loss of measurement sensitivity near contact, an *oblique incidence polarisation interferometry* method was developed, in which intensity information and phase information are used together to determine the flying height down to contact. However, since the light beam is obliquely incident on the glass disk, the sensitivity of its intensity channel is reduced by a factor of $1/\cos\theta$ ($\theta \approx 50°$) compared with that of the normal incidence.

In addition to the above mentioned disadvantages for both the intensity interferometry and oblique incidence polarisation interferometry methods, because they can only perform one point measurement at one time, neither of these two methods can perform dynamic multidimensional characterisation of head-disk spacing or dynamic measurement of the head slider's pitch and roll, which is very important for the study of head-slider dynamics. Besides, although these two methods are widely accepted by industry because of their accuracy and direct observation and measurement of the head-disk spacing, when a real head and magnetic disk assembly needs to be tested for the flying height, they become unsuitable because specially-made transparent glass disk must be employed in place of the real magnetic disk.

Considering the measurement condition of whether a real magnetic disk or a special glass disk is used, we can divide the methods into relative displacement measuring (RDM) method and direct spacing measuring (DSM) method. In RDM method, a real magnetic disk and head-slider are employed. The head-disk spacing is determined by measuring the relative motion between the head-slider and the disk by using dual-beam interferometry. In the DSM method, a special transparent glass disk is used in place of the real magnetic disk, and the flying height is determined by analysing the interference phenomena between the slider and the rotating glass disk. The DSM method has the advantage that the absolute head-disk spacing can be directly measured, while the RDM method has the advantage of using the real magnetic disk. It will be highly advantageous if a testing instrument can accommodate both techniques.

Based on all these consideration, we proposed a dual-beam polarisation interferometry method which possesses all the preferred abilities mentioned above.

5.1 Dual-beam normal incidence polarisation interferometry

The schematic diagram of our dual-beam normal incidence polarisation interferometer for head-disk spacing measurement is as shown in Figure 5.1. Instead of using one or more acousto-optical modulators (AOM), this polarisation interferometer configuration utilises two orthogonally-polarised light beams to remove the directional ambiguity of the flying height change. The main part of the interferometer utilises a polarising beam splitter PBS_1, two quarter-wave plates QW_1 and QW_2, two mirrors M_1 and M_2, and a

non-polarising beam splitter $NPBS_1$ as both a beam splitter and phase shifter.

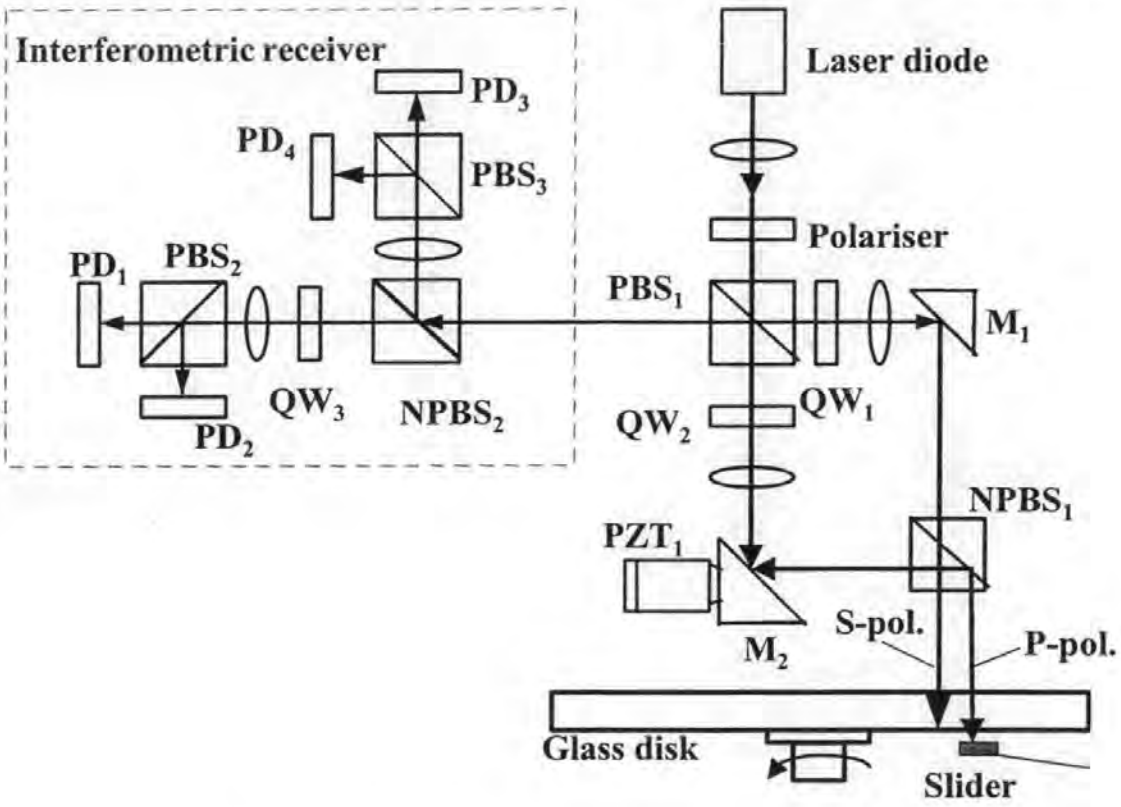

Figure 5.1 Dual-beam normal incidence polarisation interferometer

The fast axes of QW_1 and QW_2 are turned 45° with respect to the reference plane (paper plane). The use of a polarising beam splitter PBS_1 is inevitable to build up a polarisation interferometer, and also prevent the returning beam from feeding back to the laser diode. Mirror M_2 is driven by a piezoelectric translator PZT_1, which can be used to perform system calibration. M_2 can also be micro-positioned manually to adjust the spacing of the two measurement beams. A laser diode or monochromatic light source can be used. The light beam passes through the linear polariser and enters the polarising beam splitter PBS_1. The beam is then split into two linearly polarised beams. The p-polarised object beam passes through the quarter-wave plate QW_2, becoming circularly polarised, reflected by mirror M_2, and is focused onto the slider's air-bearing surface. The reflected beam passes QW_2 again, becoming s-polarised, and is then reflected to the interferometric receiver. The s-polarised reference beam passes through quarter-wave

plate QW_1, becoming circularly polarised, reflected by mirror M_1, and is focused onto an adjacent point on the glass disk. The reflected beam passes QW_1 again, becoming p-polarised, then passes through PBS_1 and also enters the interferometric receiver. Note that the two incident beams to the glass disk, after passing the two quarter-wave plates, are not linearly polarised, but we still use p-pol and s-pol to simply indicate the two polarised beams. The interferometric receiver is used to measure the intensity of the returned interfered beam and the phase difference between the two polarised beams. According to the optical parts being used and their orientation, there are a few variations to the construction of the receiver. The interferometric receiver in Figure 5.1 consists of a non-polarising beam splitter $NPBS_2$, two polarising beam splitters PBS_2 and PBS_3 both seated (rotated) 45° with respect to the reference plane (paper plane), a quarter-wave plate QW_3 with its fast axis in the s-polarised direction, and four photo-detectors. To ease the mounting of the mechanical parts, an alternative construction of the receiver was used in our experimental system, which will be reiterated in Chapter 6. The interferometric receiver is the key part of this interferometer to obtain the intensity and phase information of the returned beam so as to determine the head-disk spacing. Further details and working principle will be given in Chapter 6.

Let us consider Figure 5.1 again. The polarising beam splitter PBS_1 splits the incoming laser beam into a reference beam and an object beam. The ratio of intensities of these two beams, determined by the polarisation plane of the beam entering the PBS, can be conveniently adjusted by rotating the collimator in its mount. After the spacing of the two measurement beams is settled and the calibration by using PZT_1 is finished, there will be an initial phase difference θ_0 between the two beams, which is introduced by the optical path difference of the two beams. If the phase shift resulted from the head disk spacing or flying height is designated by θ, the total phase difference between the two

beams will be $(\theta + \theta_0)$, which can be measured/determined by the interferometric receiver.

5.2 Single-layer reflection

We have seen from Chapter 4 that multi-layer reflections in the disk-slider interface should be considered if multi-reflection between the two surfaces of the glass disk happens. This will be discussed in Section 5.3 for our dual-beam normal incidence polarisation interferometry. In this section, single layer reflections will be considered. To ensure single layer reflections happen, anti-reflection coatings must be applied to the top surface of the glass disk if a long coherent length light source is used.

5.2.1 Flying height measurement

The measurement beam (p-pol beam) is focused onto the air-bearing surface of the head-slider and the reference beam (s-pol beam) is focused onto an adjacent point on the glass disk, which is shown in Figure 5.2 where h still represents the head-disk spacing to be measured.

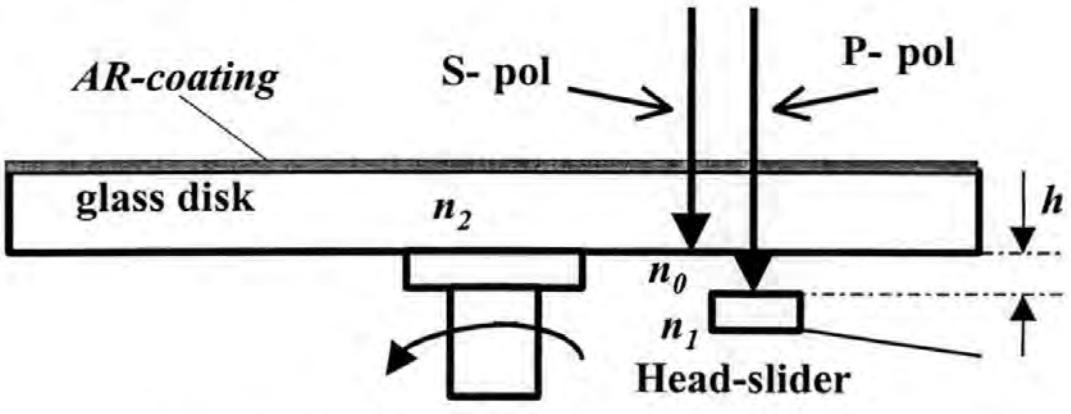

Figure 5.2 Flying height measurement (single layer reflections)

According to the standard thin-film equation [Born & Wolf, 1989], the reflection coefficient of the p-pol beam is

$$r_p = \frac{r_{p20} + r_{p01}\exp(i\beta_p)}{1 + r_{p20}r_{p01}\exp(i\beta_p)} \tag{5.1}$$

where $r_{p20} = \frac{n_2 - n_0}{n_2 + n_0}$, $r_{p01} = \frac{n_0 - (n_1 + ik_1)}{n_0 + (n_1 + ik_1)}$, $\beta_p = \frac{4\pi}{\lambda} n_0 h$, λ is the wavelength, h is the head-disk spacing, and n_2, n_0 and $(n_1 + ik_1)$ are the refractive indices of the glass disk, air, and slider material respectively. So the intensity and phase change of the reflected p-pol light are

$$I_p = I_{p0}\left|r_p\right|^2 \tag{5.2}$$

$$\phi_p = \arg(r_p) \tag{5.3}$$

where I_{p0} is the intensity of the incident p-pol beam.

The intensity and phase change of the reflected s-pol beam are

$$I_s = I_{s0}\left|r_{s20}\right|^2 \tag{5.4}$$

$$\phi_s = \arg(r_{s20}) \tag{5.5}$$

where $r_{s20} = \frac{n_2 - n_0}{n_2 + n_0}$, I_{s0} is the intensity of the incident s-pol beam.

Therefore, the intensity I and the phase difference ϕ between the two polarisation components of the returned beam are:

$$I = I_{p0}\left|\frac{r_{p20} + r_{p01}\exp(i\beta_p)}{1 + r_{p20}r_{p01}\exp(i\beta_p)}\right|^2 + I_{s0}\left|r_{s20}\right|^2 \tag{5.6}$$

$$\phi = \arg(r_{s20}) - \arg\left(\frac{r_{p20} + r_{p01}\exp(i\beta_p)}{1 + r_{p20}r_{p01}\exp(i\beta_p)}\right) + \theta_0 \tag{5.7}$$

where θ_0 is the initial phase difference between the two beams. In real flying height testing, I_{p0} and I_{s0} should be adjusted as equal as possible. But it will not affect the measurement result if they are not strictly equal. The intensity I and phase difference ϕ

can be detected by the interferometric receiver as shown in Figure 5.1. They can be measured as:

$$I = I_s + I_p \tag{5.8}$$

$$\phi = \tan^{-1}\left(\frac{I_2 - I_1}{I_3 - I_4}\right) \tag{5.9}$$

where I_1, I_2, I_3 and I_4 are the intensities detected by the four photo-detectors respectively.

From (5.6) and (5.7), the intensity I and the phase difference $\theta = (\phi - \theta_0)$ as functions of head-disk spacing h are plotted in Figure 5.3, where the refractive index of glass disk is 1.5, the index of head-slider is $n_1 + ik_1 = 2.2 + 0.4i$, the wavelength of light source (e.g. laser diode) is 670 nm, and $I_0 = I_{p0} = I_{s0}$ is assumed.

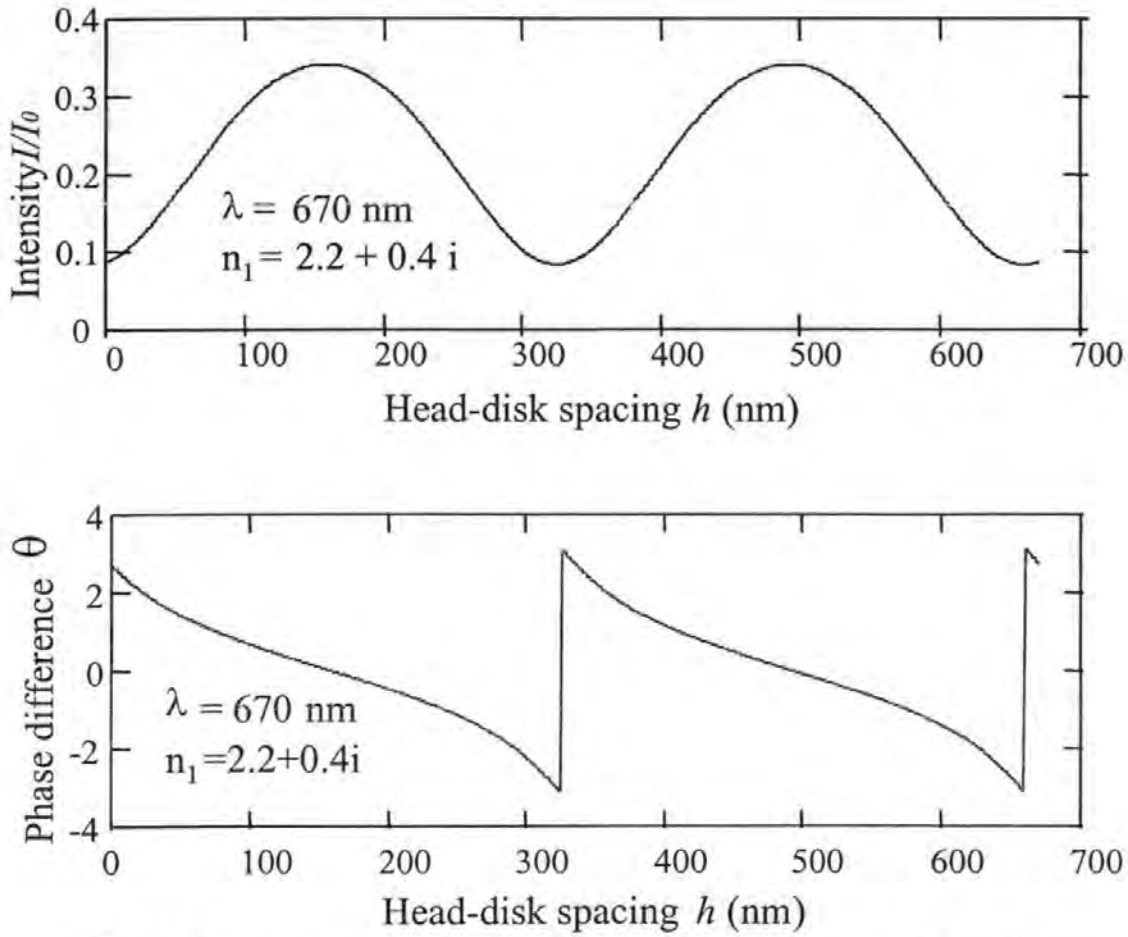

Figure 5.3 Intensity and phase difference as functions of head-disk spacing.

From the intensity curve and phase-difference curve in Figure 5.3, we can see that the phase information is useful to determine the flying height when the intensity curve is getting flat, i.e., when the sensitivity of intensity curve is getting poor. With the measured intensity and phase information, the head-disk spacing can be determined in a number of ways. First, analytically, we can use the phase value alone to determine the flying height all the way down to contact, since the whole phase curve has fairly good sensitivity. Second, we can use the intensity value in the area where its sensitivity is high, and in the area where its sensitivity is low, we use phase value. Third, we can also calculate the flying height by minimising the difference between measured and theoretical values of both the intensity and phase [de Groot et al., 1996a]. Details about which methods should be used will be discussed separately in Chapter 7.

5.2.2 Slider pitch/roll measurement

To measure slider pitch and roll, the s-pol beam is focused on one point of the slider air bearing surface, while the p-pol beam is focused on another point of the slider air bearing surface, distinct from the first point, as shown in Figure 5.4.

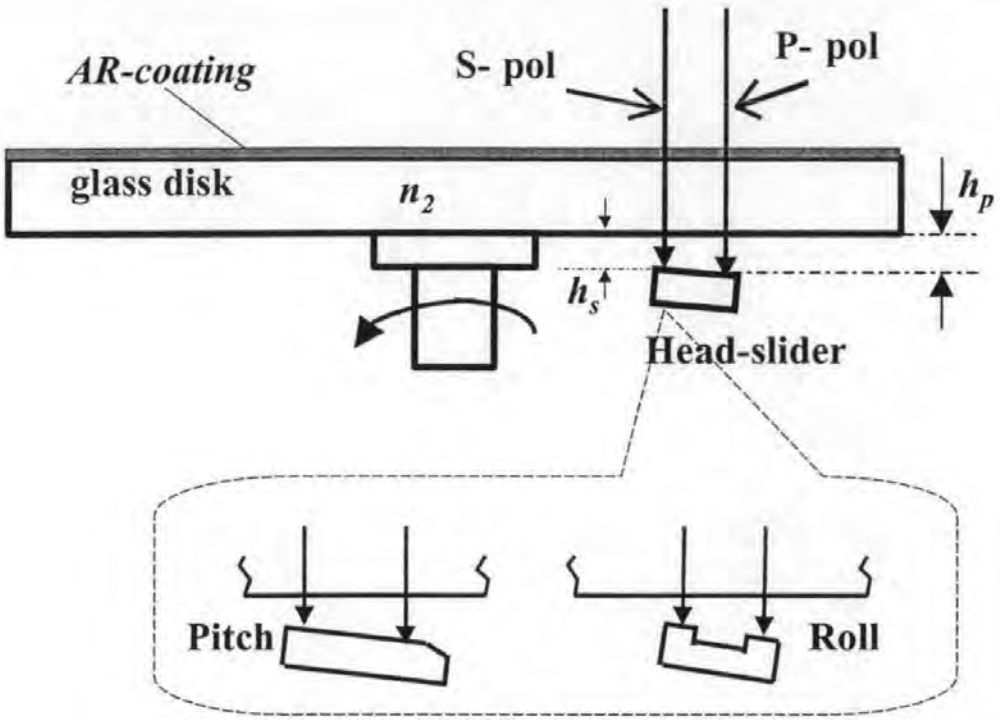

Figure 5.4 Head-disk spacing pitch and roll measurement

Suppose the s-pol beam experiences a flying height of h_s, the p-pol beam experiences a flying height of h_p, and the two polarised beams both experience single layer reflections at the slider-disk interface, the reflection coefficients of the two polarised beams are then given by:

$$r_s = \frac{r_{s20} + r_{s01}\exp(i\frac{4\pi}{\lambda}n_0 h_s)}{1 + r_{s20}r_{s01}\exp(i\frac{4\pi}{\lambda}n_0 h_s)} \tag{5.10}$$

$$r_p = \frac{r_{p20} + r_{p01}\exp(i\frac{4\pi}{\lambda}n_0 h_p)}{1 + r_{p20}r_{p01}\exp(i\frac{4\pi}{\lambda}n_0 h_p)} \tag{5.11}$$

where $r_{s20} = \frac{n_2 - n_0}{n_2 + n_0}$. The intensity and phase change of the reflected s-pol beam are:

$$I_s = I_{s0}|r_s|^2 \tag{5.12}$$

$$\phi_s = \arg(r_s) \tag{5.13}$$

The intensity and phase change of the reflected p-pol beam are

$$I_p = I_{p0}\left|r_p\right|^2 \tag{5.14}$$

$$\phi_p = \arg(r_p) \tag{5.15}$$

Using the interferometric receiver shown in Figure 5.1, the intensity I and phase difference ϕ between the two polarisation components of the returned beam can be measured.

According to (5.12), (5.14), (5.13), and (5.15), the intensity and phase change of the reflected s-pol or p-pol beams as functions of flying height are plotted in Figure 5.5 and Figure 5.6, where the refractive index of the glass disk is 1.5, the complex refractive index of the slider is $(2+0.2i)$, the wavelength of the laser light source is 670 nm, and $I_{p0} = I_{s0} = 1$ is assumed.

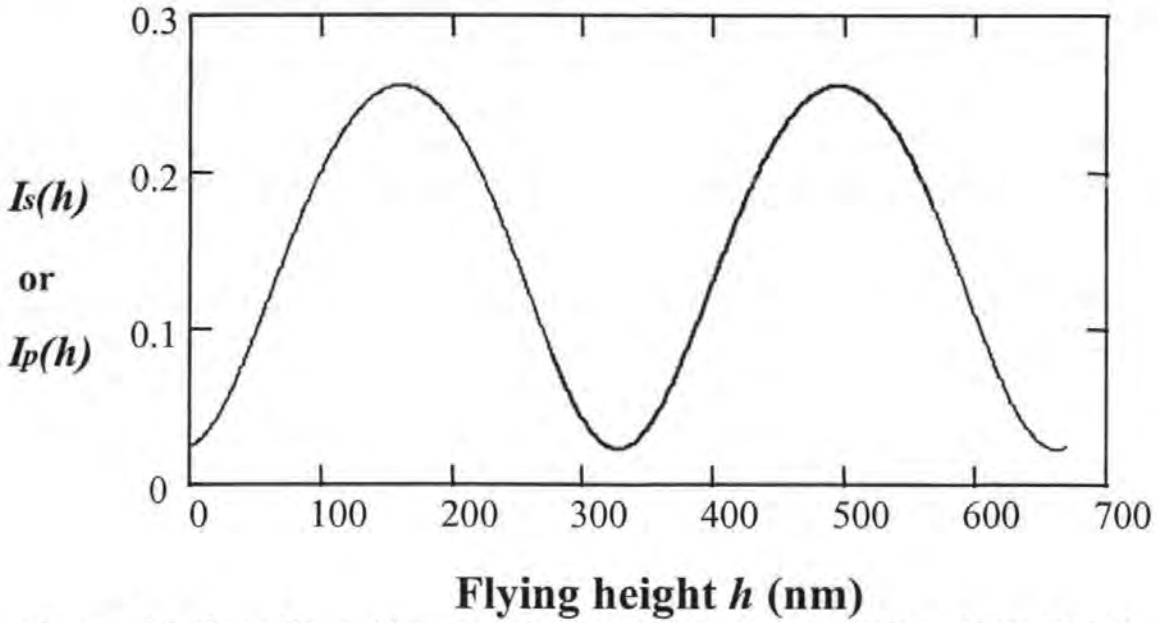

Figure 5.5 Reflected intensities of s-pol and p-pol beams as a function of flying height

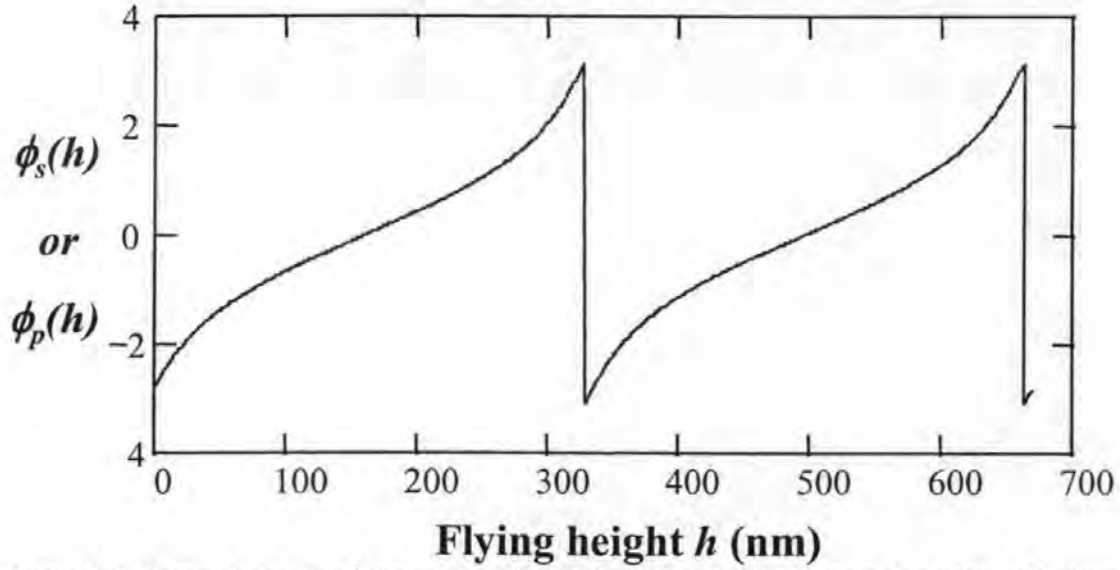

Figure 5.6 Phase changes of the reflected s-pol and p-pol beams as a function of flying height

What we are interested in here is how to get $\Delta h = (h_s - h_p)$ from the measured information $(I_s + I_p)$ or $(\phi_s - \phi_p)$. Apparently, it is impossible to get Δh from the intensity $(I_s + I_p)$, and directly from $(\phi_s(h) - \phi_p(h))$. However, if the flying height is known, $\Delta h = (h_s - h_p)$ can be obtained from the phase information. To determine it qualitatively, we can approximate the relationship between the phase difference and the slider's pitch or roll as linear. To determine it quantitatively, we need to first measure the flying height, so the changing rate of the height at this point can be determined. The slider's pitch or roll can then be determined linearly from the measured phase difference value by using this changing rate.

5.3 Multi-layer reflection

If no anti-reflection coating is made to the top surface of the glass disk, multiple reflections between the two surfaces of the glass disk will occur, and multiple-layer reflections should be considered in the disk-slider interface. This is the case especially when long coherent length light sources (e.g. laser) are used. Here we will discuss this multi-reflection for our dual-beam normal incidence polarisation interferometry.

5.3.1 Flying Height Measurement

As shown in Figure 5.7, the p-pol beam is focused on one point of the slider air bearing surface, while the s-pol beam is focused on an adjacent point on the glass disk. Since both the two beams are normally incident to the glass disk surface and the slider air bearing surfaces, the s-pol beam will experience multiple reflections between the top surface and bottom surface of the glass disk (single layer), while the p-pol beam will experience more complicated two-layer multiple reflections.

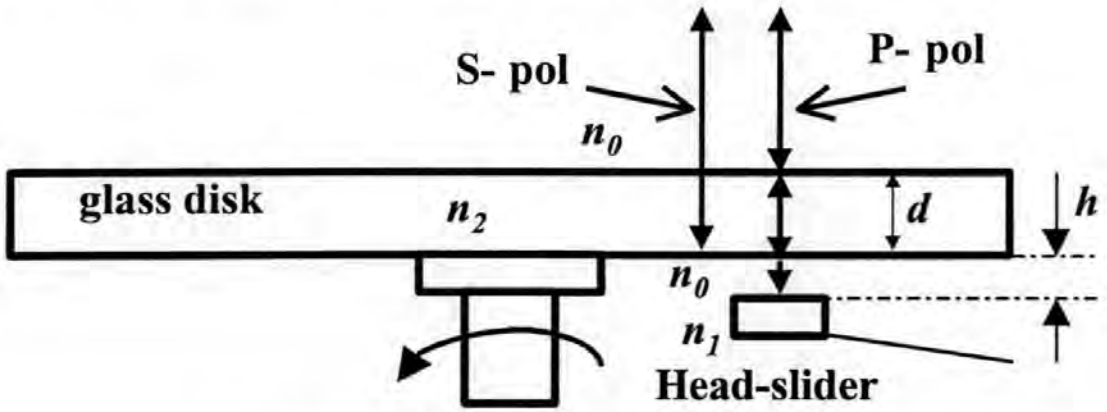

Figure 5.7 Flying height measurement (two layer reflections)

Upon reflection from the glass disk, the reflection coefficient of the s-pol beam is given by

$$r_s = \frac{r_{s02} + r_{s20}\exp(i\beta_s)}{1 + r_{s02}r_{s20}\exp(i\beta_s)} = |r_s|\exp(i\phi_s) \tag{5.16}$$

The intensity and phase change of the reflected s-pol beam are

$$I_s = I_{s0}|r_s|^2 \tag{5.17}$$

$$\phi_s = \arg(r_s) \tag{5.18}$$

where $r_{s02} = \frac{n_0 - n_2}{n_0 + n_2}$, $r_{s20} = \frac{n_2 - n_0}{n_2 + n_0}$, $\beta_s = \frac{4\pi}{\lambda} n_2 d$ and I_{s0} is the intensity of the incident s-pol beam. For the p-pol beam, two-layer reflections should be considered.

First, the effective reflection coefficient of the one-layer glass-slider combination is given by:

$$r_{pe} = \frac{r_{p20} + r_{p01}\exp(i\beta_{p1})}{1 + r_{p20}r_{p01}\exp(i\beta_{p1})} \tag{5.19}$$

where $r_{p20} = \frac{n_2 - n_0}{n_2 + n_0}$, $r_{p01} = \frac{n_0 - n_1}{n_0 + n_1}$ and $\beta_{p1} = \frac{4\pi}{\lambda} n_0 h$. Therefore the two-layer reflection coefficient of the p-pol beam on reflection from the glass disk is given by

$$r_p = \frac{r_{p02} + r_{pe}\exp(i\beta_{p2})}{1 + r_{p02}r_{pe}\exp(i\beta_{p2})} \tag{5.20}$$

The intensity and phase change of the reflected p-pol beam are given by

$$I_p = I_{p0}\left|r_p\right|^2 \tag{5.21}$$

$$\phi_p = \arg(r_p) \tag{5.22}$$

where $r_{p02} = \frac{n_0 - n_2}{n_0 + n_2}$, $\beta_{p2} = \frac{4\pi}{\lambda} n_2 d$ and I_{p0} is the intensity of the incident p-pol beam. Using the interferometric receiver shown in Figure 5.1, the intensity I and the phase difference ϕ between the two polarisation components of the returned beam can be measured, where I_1, I_2, I_3, and I_4 are the intensities detected by the four photo detectors.

It is seen that another important parameter, the glass disk thickness d, has been introduced to the intensity and phase equations. Apparently, it is still possible for the flying height to be determined from either the intensity information or phase information detected by the interferometric receiver if the glass disk thickness d is known. However, since this parameter will significantly affect the intensity and phase curves, we will consider this below.

A.

Set $d = \frac{m\lambda}{4n_2}$.

When m is an even number, from (5.16), it is known that the reflectivity of the glass disk $|r_s|^2$ is zero. That is, the glass disk is totally transparent to the light beam. There will be no interfered beam returning back from the disk slider interface. In this case, no intensity and phase information can be used to determine the flying height.

B.

When m is odd, from (5.16), the reflectivity of the glass disk, $|r_s|^2$, has its maximum value:

$$|r_s|^2 = \left(\frac{n_1^{\,2} - n_2^{\,2}}{n_1^{\,2} + n_2^{\,2}} \right)^2 \tag{5.23}$$

In this case, the evolution of the intensity $I = I_s + I_p$ and phase difference $\theta = \phi_s - \phi_p$ as functions of flying height are shown in Figure 5.8 and Figure 5.9, where the refractive index of the glass disk is 1.5, the index of slider is $(2 + 0.2i)$, $I_{p0} = I_{s0} = I_0$, and the wavelength of the light beam is 670 nm. From Figure 5.8 and Figure 5.9, we can see that the intensity curve has a good sensitivity and can be used to determine the flying height. However, the phase curve has poor sensitivity for some head-disk spacings, so it is less useful to determine the flying height.

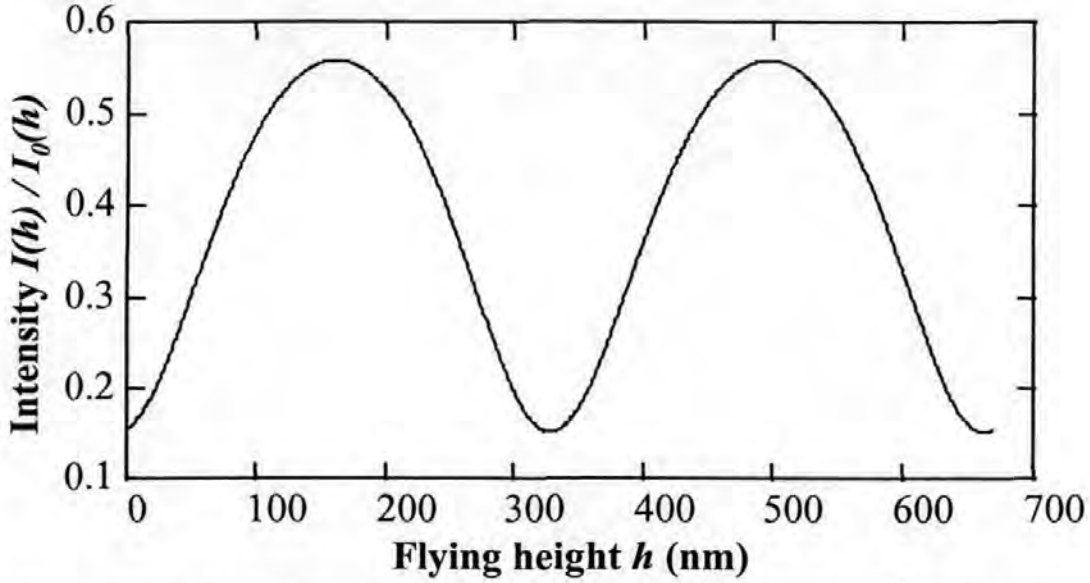

Figure 5.8 Reflected intensity as a function of flying height, $d = \frac{m\lambda}{4n_2}$, m is odd.

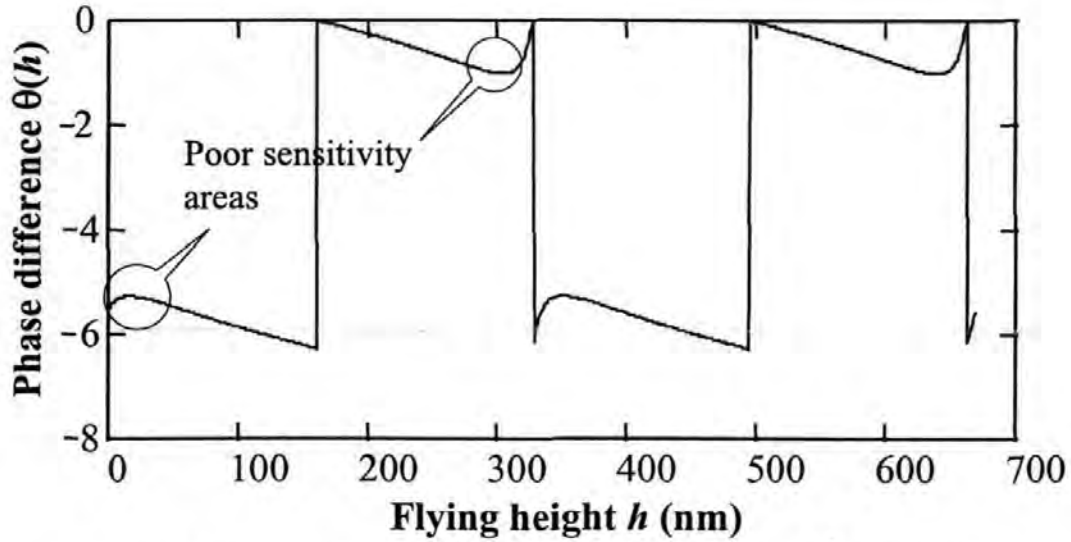

Figure 5.9 Phase difference between the two beams, $d = \frac{m\lambda}{4n_2}$, m is odd.

C.

From the following simulation results, it can be seen that if the glass disk thickness d is properly chosen, both the intensity and phase information will be useful for measuring the flying height.

For example, if m is even,

when d is chosen to be $d = \frac{(m+0.1)\lambda}{4n_2}$, from (5.17), the intensity of the reflected s-pol beam is $I_s = 0.00423 I_{s0}$;

and when d is chosen to be $d = \frac{(m+0.2)\lambda}{4n_2}$, from (5.17), the intensity of the reflected s-pol beam is $I_s = 0.0163 I_{s0}$.

The plots of intensity $I = I_s + I_p$ and phase difference $\theta = \phi_s - \phi_p$ as functions of flying height are shown in Figure 5.10 and Figure 5.11.

From Figure 5.10 and Figure 5.11, we see that when the intensity curve is nearly constant, the phase curve has a fairly steep slope, and the whole phase curve has a fairly good sensitivity (changing rate with respect to flying height). So in this case, both the intensity and phase information are useful in determining the flying height, although the sensitivities of intensity curves and phase curves are different for different values of disk thickness d.

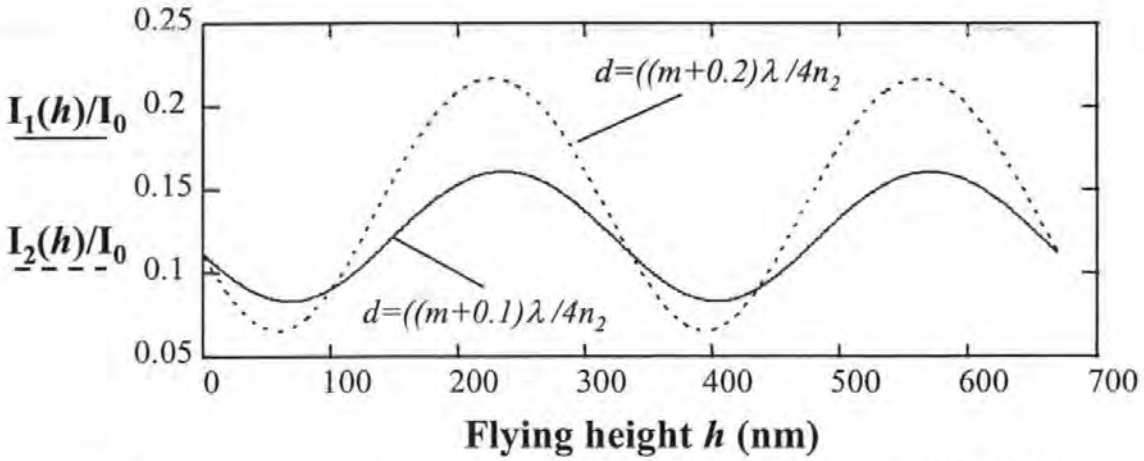

Figure 5.10 Reflected intensities as functions of flying height when $d = \frac{(m+0.1)\lambda}{4n_2}$ and $d = \frac{(m+0.2)\lambda}{4n_2}$ respectively, m is even, $n_2 = 1.5$, and $\lambda = 670$ nm.

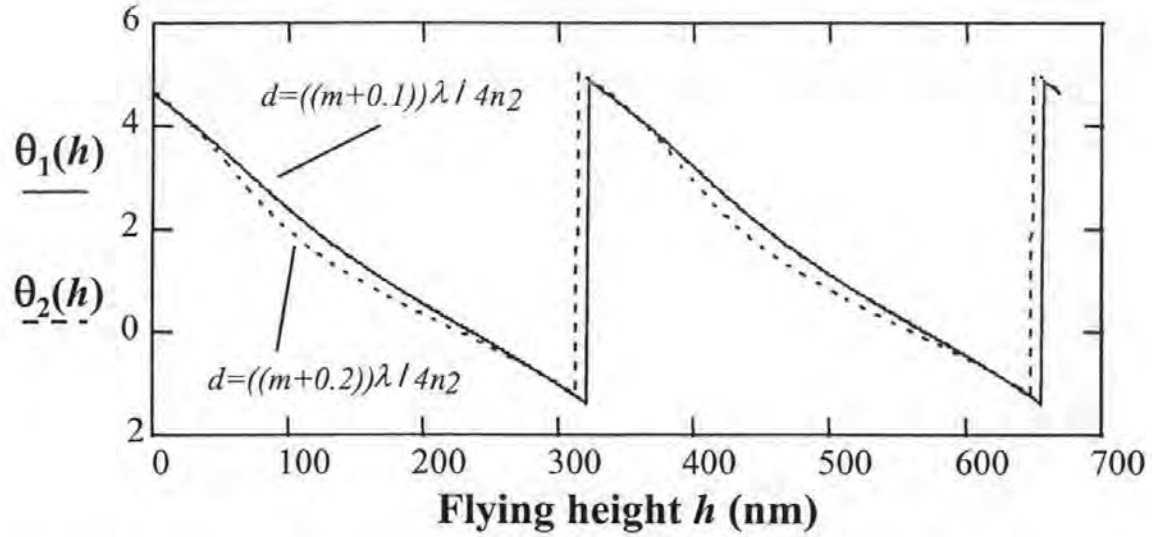

Figure 5.11 Phase differences between the two beams as functions of flying height when $d = \dfrac{(m+0.1)\lambda}{4n_2}$ and $d = \dfrac{(m+0.2)\lambda}{4n_2}$ respectively, m is even, $n_2 = 1.5$, and $\lambda = 670$ nm.

Additional curves are presented in Figure 5.12 and Figure 5.13, where the disk thickness d is chosen to be $d = \dfrac{(m+0.3)\lambda}{4n_2}$ and $d = \dfrac{(m+0.4)\lambda}{4n_2}$. Similar results are obtained.

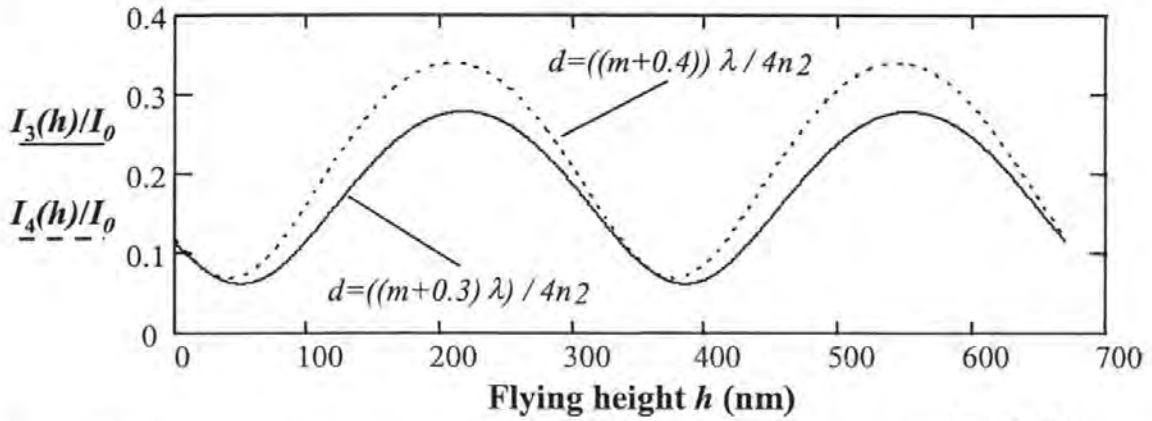

Figure 5.12 Reflected intensities as functions of flying height when $d = \dfrac{(m+0.3)\lambda}{4n_2}$ and $d = \dfrac{(m+0.4)\lambda}{4n_2}$ respectively, m is even, $n_2 = 1.5$, and $\lambda = 670$ nm.

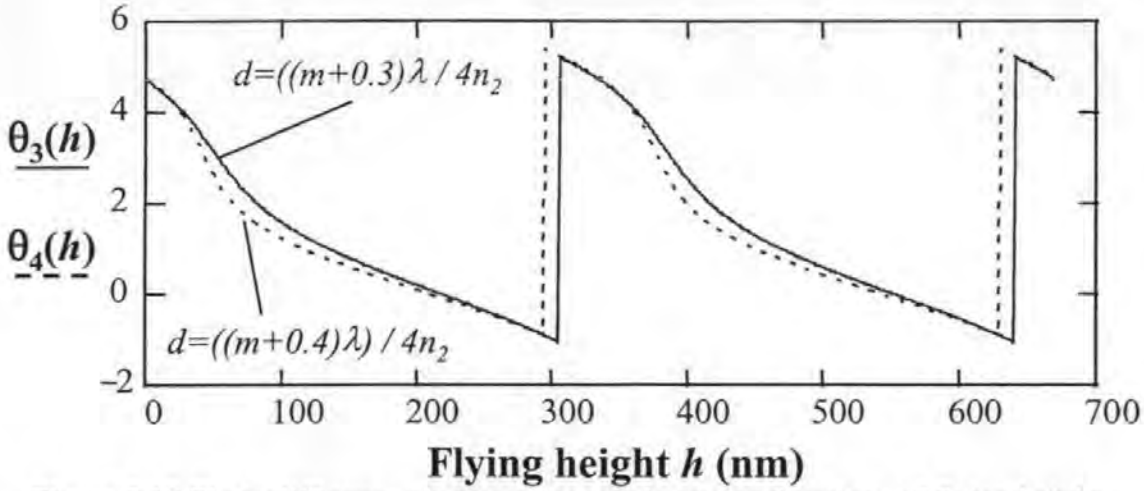

Figure 5.13 Phase differences between the two beams as functions of flying height when $d = \frac{(m+0.3)\lambda}{4n_2}$ and $d = \frac{(m+0.4)\lambda}{4n_2}$ respectively, m is even, $n_2 = 1.5$, and $\lambda = 670$ nm.

From above analysis and computer simulation, we can conclude that whether this methodology works or not depends on whether we can control the glass disk thickness d (strictly speaking, this should be the optical path length) to be a constant of useful value. If this cannot be guaranteed, the method will not be practical since the intensity and phase difference of the returned interfered light beams will vary with d.

5.3.2 Slider pitch/roll measurement

As shown in Figure 5.14, the s and p polarised beams are focused onto two different points on the slider's air bearing surface.

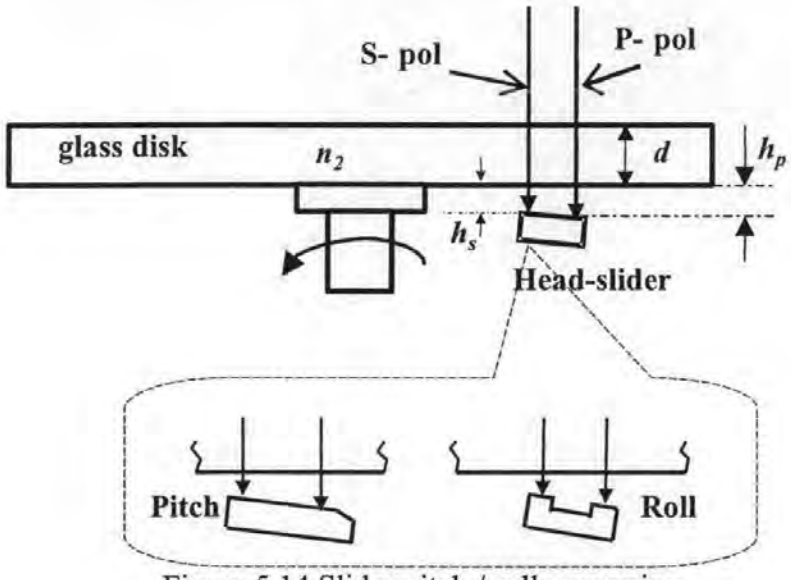

Figure 5.14 Slider pitch / roll measuring

Suppose the s-pol beam experiences a flying height of h_s, and the p-pol beam experiences a flying height of h_p. Both s-pol beam and p-pol beam will experience two-layer reflections between the glass disk, the air gap, and the slider air-bearing surface. The two-layer reflectiion coefficient of s-pol beam, upon reflection from the glass disk, is given by:

$$r_s = \frac{r_{s02} + r_{se}\exp(i\frac{4\pi}{\lambda}n_2 d)}{1 + r_{s02}r_{se}\exp(i\frac{4\pi}{\lambda}n_2 d)} \tag{5.24}$$

where

$$r_{se} = \frac{r_{s20} + r_{s01}\exp(i\frac{4\pi}{\lambda}n_0 h_s)}{1 + r_{s20}r_{s01}\exp(i\frac{4\pi}{\lambda}n_0 h_s)} \tag{5.25}$$

The reflection coefficient of p-pol beam upon reflection from the glass disk is given by:

$$r_p = \frac{r_{p02} + r_{pe}\exp(i\frac{4\pi}{\lambda}n_2 d)}{1 + r_{p02}r_{pe}\exp(i\frac{4\pi}{\lambda}n_2 d)} \tag{5.26}$$

where

$$r_{pe} = \frac{r_{p20} + r_{p01}\exp(i\frac{4\pi}{\lambda}n_0 h_p)}{1 + r_{p20}r_{p01}\exp(i\frac{4\pi}{\lambda}n_0 h_p)} \tag{5.27}$$

The intensity and phase change of the reflected s-pol beam are:

$$I_s = I_{s0}|r_s|^2 \tag{5.28}$$

$$\phi_s = \arg(r_s) \tag{5.29}$$

The intensity and phase change of the reflected p-pol beam are:

$$I_p = I_{p0}|r_p|^2 \tag{5.30}$$

$$\phi_p = \arg(r_p) \tag{5.31}$$

As in Section 5.2.2, our interest is how to determine $\Delta h = (h_s - h_p)$ from the measured intensity or phase information. We known that the only way to get Δh is from the measured phase information $(\phi_s(h) - \phi_p(h))$ if the glass disk thickness d is a constant, so that the flying height at that point can be measured, as stated in Section 5.3.1.

Another extreme condition is when the glass disk thickness is chosen to be $d = \frac{m\lambda}{4n_2}$ where m is even. In this case, the glass disk is totally transparent to the light beam. The phase difference between the two polarisation components upon reflection from the glass disk becomes:

$$\phi_s - \phi_p = \frac{4\pi}{\lambda}n_0(h_s - h_p) \tag{5.32}$$

Therefore $\Delta h = (h_s - h_p)$ can be directly obtained from the measured phase information $(\phi_s - \phi_p)$. In fact, on this occasion, the phase change ϕ_s and ϕ_p becomes linear, as shown in Figure 5.15, according to (5.29) and (5.31).

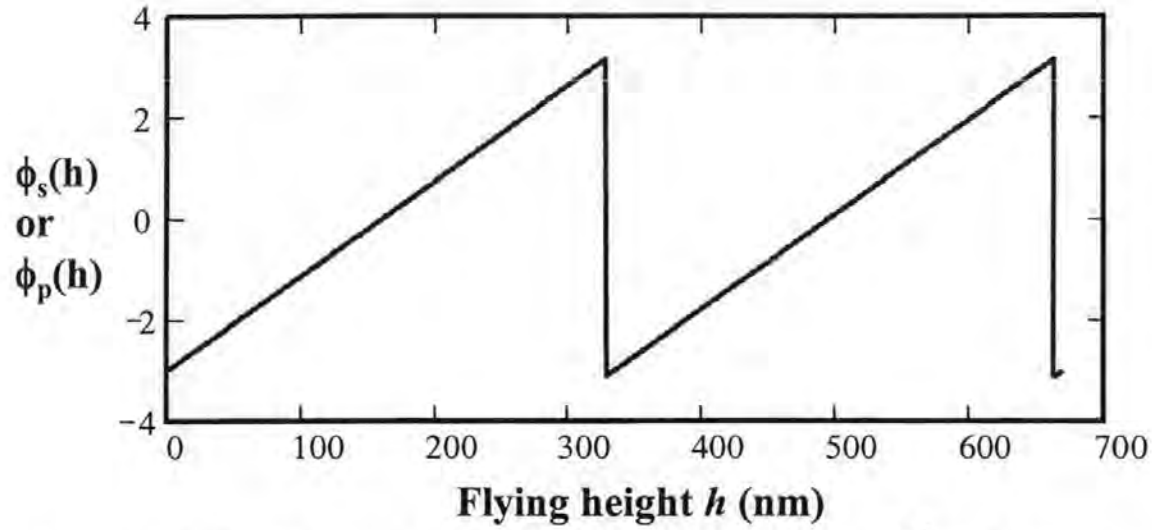

Figure 5.15 Phase change as functions of flying height when $d = \frac{m\lambda}{4n_2} d$, m is even.

The same problem exists as to whether we can manufacture the glass disk to the value we specified with acceptable tolerance. If this cannot be guaranteed, this method will not be practical.

5.4 Relative displacement measuring method

When this dual-beam polarisation interferometer is used in RDM method, real magnetic disk is used. The measurement beam is focused on the back surface of the head-slider and the reference beam is focused on an adjacent point on the disk, which is shown in Figure 5.16, where h is the head-disk spacing to be measured.

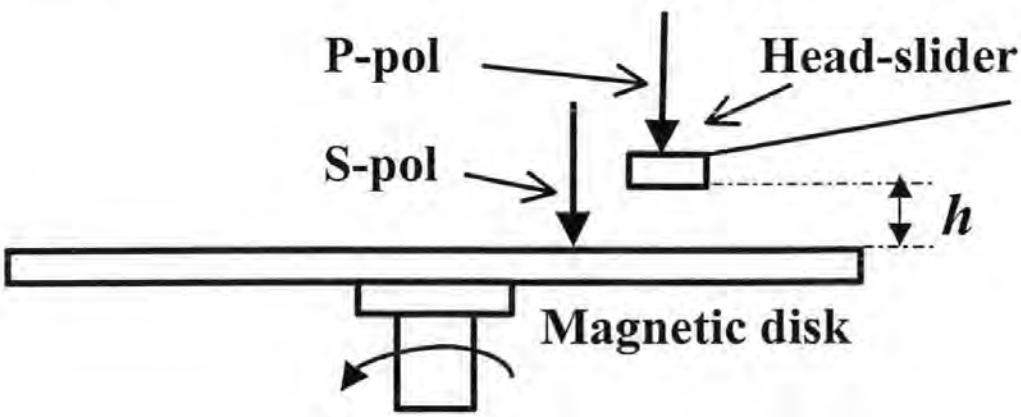

Figure 5.16 Relative displacement measuring method

The head-disk spacing h has a simple relationship with the phase difference ϕ detected by the interferometric receiver:

$$4\pi h/\lambda + \theta_0 = \phi \tag{7}$$

where λ is the wavelength of the laser and θ_0 is the initial phase difference between the two beams.

5.5 Summary

The RDM method is a good way to measure the head-disk spacing and the slider's pitch or roll because a real magnetic disk can be used. However, although a special glass disk must be used, the DSM method sometimes is more popular because the absolute head-disk spacing can be observed and measured directly, especially in the case where it is difficult for the light beam to 'spot' the back surface of the head-slider. From the above theoretical analysis and simulation results, we have seen that in DSM method, the single-layer reflection method can be used to measure the flying height down to contact using both intensity and phase information. Slider pitch and roll can also be measured using the phase information. The multi-layer reflection method could be used to measure the flying height and slider's pitch and roll if the thickness of the glass disk can be manufactured to a useful value. However, for present technology, it is difficult to manufacture a glass disk with small enough thickness tolerance, e.g. ±2nm, for the whole disk. The tip and tilt when the glass disk is rotating will also introduce a varying optical path through the disk for the light beams. These factors will inevitably introduce serious noise to the intensity and phase difference detected by the interferometric receiver, so there exist practical problems for the application of this multi-layer reflection method. A compromise of applying this method is using small areas of the disk where the thickness can be controlled and measured accurately. An advantage of

this dual beam polarisation interferometry is that it can be used for both the DSM and RDM methods.

A further benefit of this normal incidence polarisation method is that, with the measured intensity and phase information, it is also possible to use a similar method as in [de Groot, 1998a] to determine the optical constants of the slider, which is necessary to determine the flying height. This will be discussed in Chapter 7.

6 Experimental Set-up

This chapter presents the experimental system that has been built to test the capability and effectiveness of the Improved Intensity Interferometry method and Normal Incidence Polarisation Interferometry method we proposed in **Chapter 4** and **Chapter 5**. The general layout of the experimental testing system is shown in Figure 6.1.

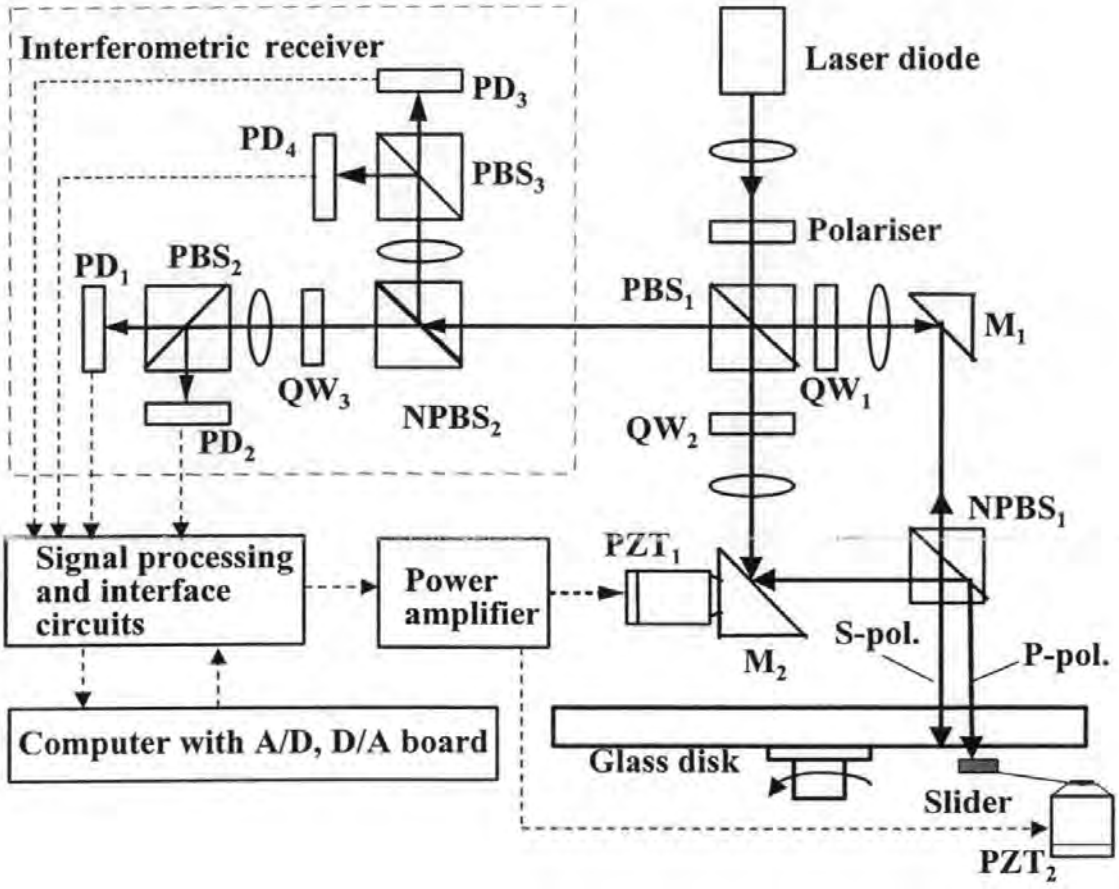

Figure 6.1 General layout of experimental testing system

The main part of the dual-beam interferometer and the interferometric receiver has been described in **Section 5.1**. Here, a 670 nm wavelength laser diode is used as the light source. The output signals from the photo-detectors of the interferometric receiver are amplified and equalised, then sampled by the PC computer through 12-bit A/D converters on an analogue I/O board. The sampling rate of the A/D converters will

determine the measurement bandwidth of the system. The A/D converter board with a sampling rate of 5MS/s is commercially available at present, which is fast enough to measure the dynamics of the head-disk spacing and its variation. The second piezoelectric translator PZT2 is used to move the head-slider vertically relative to the disk surface to simulate the head-disk spacing variation. The piezoelectric translators are controlled by the computer, through 12-bit D/A converters on the analogue I/O board and high voltage amplifiers. The photographs of the experimental testing system are shown in Figure 6.2 and Figure 6.3.

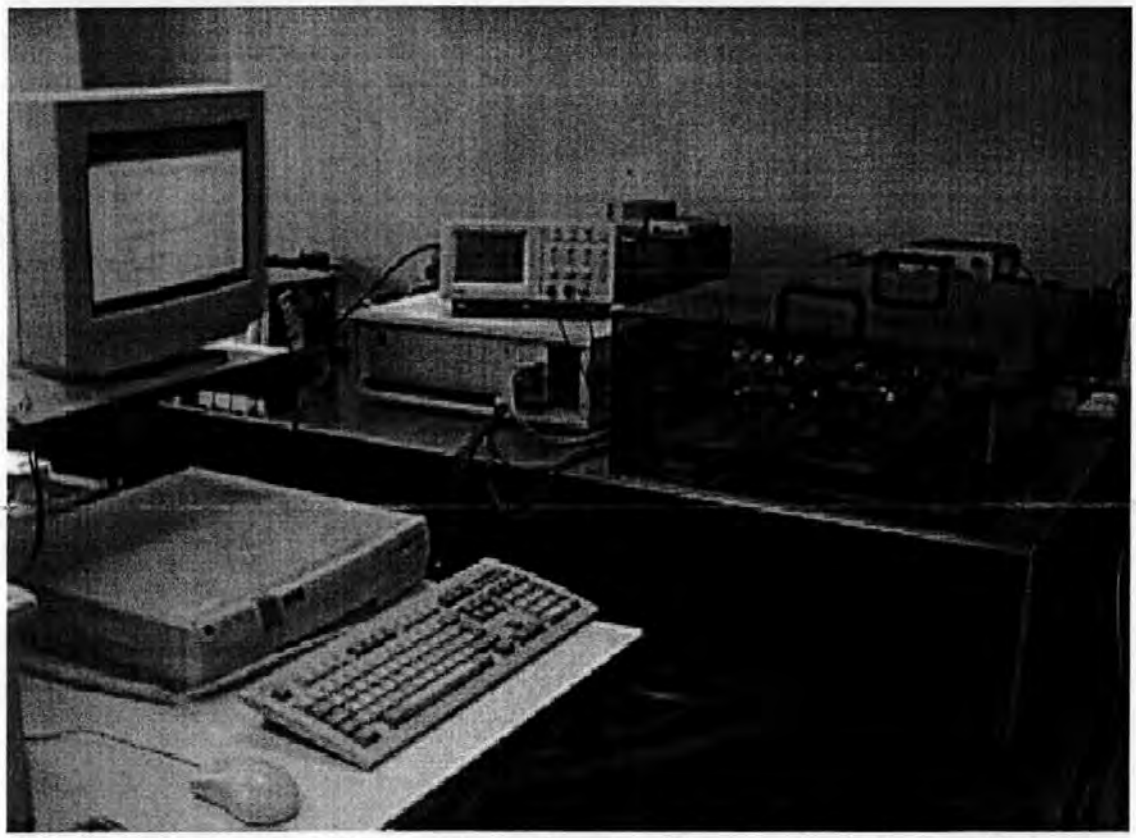

Figure 6.2 Photograph of the experimental system (Opto-mechanical part with a cover)

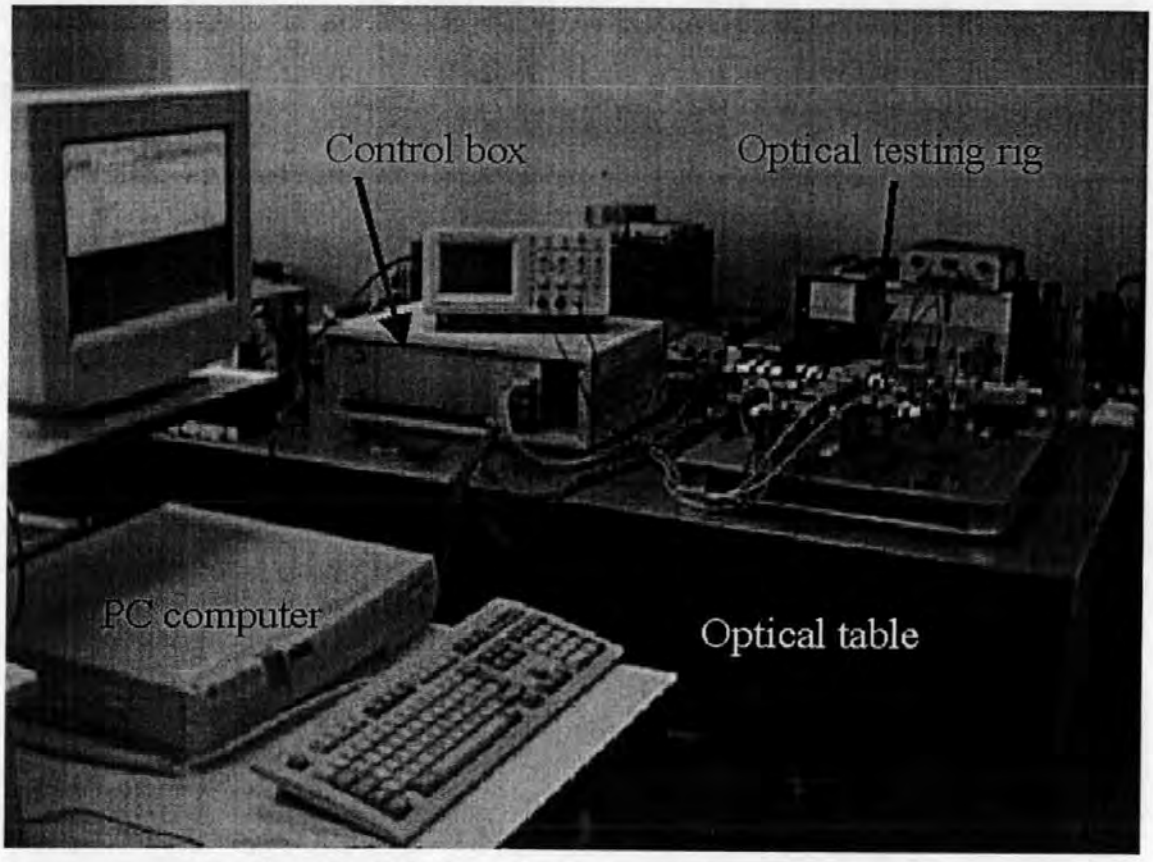

Figure 6.3 Photograph of the experimental system

6.1 Working principle of the interferometric receiver

In Figure 6.1, both PBS_2 and PBS_3 are seated (rotated) 45° with respect to the reference plane (paper plane). If we assume that the reflected beam returned from PBS_1 to the interferometric receiver is

$$\mathbf{E}^r = \begin{pmatrix} E_p \\ E_s \end{pmatrix} = \begin{pmatrix} A_p \\ A_s e^{i\phi} \end{pmatrix} \tag{6.1}$$

the beam passing through PBS_3 will be

$$E_3 = J_p(45°)E^r = \frac{1}{2}\begin{pmatrix} 1 & 1 \\ 1 & 1 \end{pmatrix}\begin{pmatrix} A_p \\ A_s e^{j\phi} \end{pmatrix} = \frac{1}{2}\begin{pmatrix} A_p + A_s e^{j\phi} \\ A_p + A_s e^{j\phi} \end{pmatrix} \tag{6.2}$$

the beam reflected out from PBS_3 will be

$$E_4 = J_p(-45°)E^r = \frac{1}{2}\begin{pmatrix} 1 & -1 \\ -1 & 1 \end{pmatrix}\begin{pmatrix} A_p \\ A_s e^{j\phi} \end{pmatrix} = \frac{1}{2}\begin{pmatrix} A_p - A_s e^{j\phi} \\ -(A_p - A_s e^{j\phi}) \end{pmatrix} \tag{6.3}$$

where $J_p(45°)$ and $J_p(-45°)$ are jones matrices given in Table 2.2 in Chapter 2.

Then the intensities of the beams detected by PD_3 and PD_4 can be derived as

$$P_3 = |\mathbf{E}_3|^2 = 2(A_p{}^2 + A_s{}^2 + 2A_pA_s\cos\phi) \tag{6.4}$$

$$P_4 = |\mathbf{E}_4|^2 = 2(A_p{}^2 + A_s{}^2 - 2A_pA_s\cos\phi) \tag{6.5}$$

In the same way, the intensities detected by PD_1 and PD_2 can be derived as

$$P_1 = |\mathbf{E}_1|^2 = (A_p{}^2 + A_s{}^2 - 2A_pA_s\sin\phi) \tag{6.6}$$

$$P_2 = |\mathbf{E}_2|^2 = (A_p{}^2 + A_s{}^2 + 2A_pA_s\sin\phi) \tag{6.7}$$

Therefore, the phase difference can be derived from

$$\phi = \tan^{-1}\frac{P_2 - P_1}{P_3 - P_4} \tag{6.8}$$

This interferometric receiver construction is perfect. It uses minimum number of optical parts. However, as our present optical testing rig is horizontally mounted on a honeycomb breadboard, the mechanical spacing restrains PBS_2 and PBS_3 being rotated 45°. To accommodate this situation, the construction of interferometric receiver is modified as shown in Figure 6.4, which is used in our experimental system.

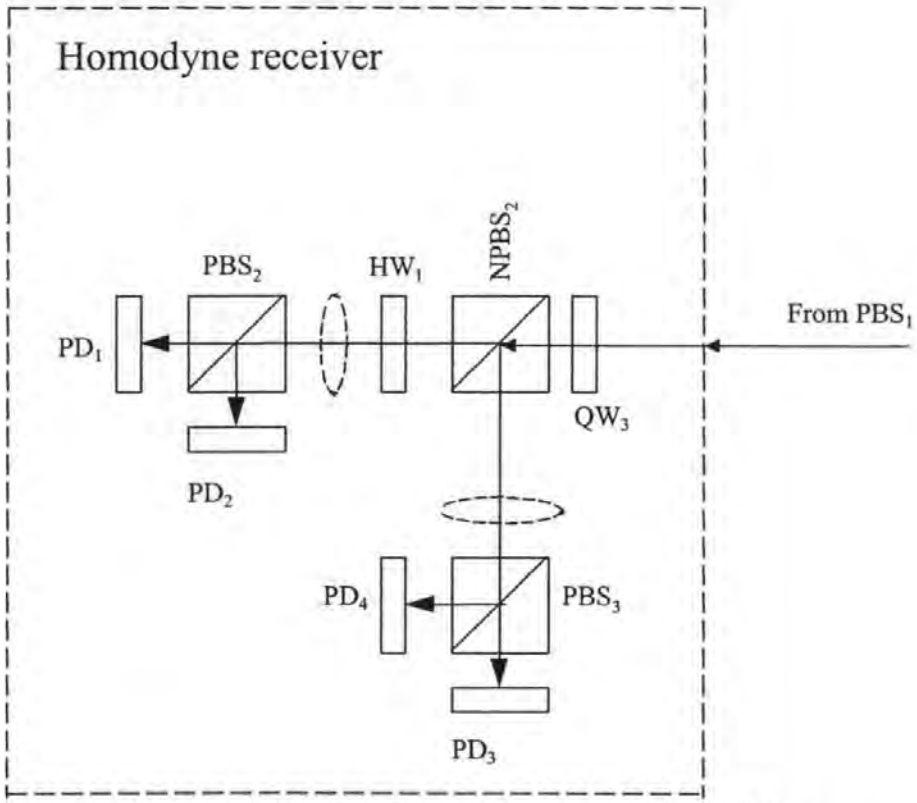

Figure 6.4 Another form of interferometric receiver

In this receiver construction, quarter wave plate QW_3 is moved to before $NPBS_2$, with its fast axis in 45° with respect to the reference plane, and a half-wave plate HW_1 is added before PBS_2 with its fast axis in 22.5° with respect to the reference plane. In the same way as above, by using jones matrices $J_{wp}(\frac{\lambda}{4}, 45°)$, $J_{wp}(\frac{\lambda}{2}, 22.5°)$, $J_p(0°)$ and $J_p(90°)$ given in Table 2.2, the intensities of the beams detected by the four photo detectors will become:

$$P_1 = \frac{1}{2}(A_p{}^2 + A_s{}^2 + 2A_pA_s\cos\phi) \tag{6.9}$$

$$P_2 = \frac{1}{2}(A_p{}^2 + A_s{}^2 - 2A_pA_s\cos\phi) \tag{6.10}$$

$$P_3 = \frac{1}{2}(A_p{}^2 + A_s{}^2 - 2A_pA_s\sin\phi) \tag{6.11}$$

$$P_4 = \frac{1}{2}(A_p{}^2 + A_s{}^2 + 2A_pA_s\sin\phi) \tag{6.12}$$

And the phase difference can be derived from

$$\phi = \tan^{-1} \frac{P_4 - P_3}{P_1 - P_2} \tag{6.13}$$

6.2 Optical testing rig

The photograph of the optical testing rig is shown in Figure 6.5. The whole optical testing rig is mounted on a honeycomb breadboard from Thorlab, which makes it movable when needed. The honeycomb breadboard sits on an air cushioned optical table in the lab. This can further reduce the environmental effects to the testing system.

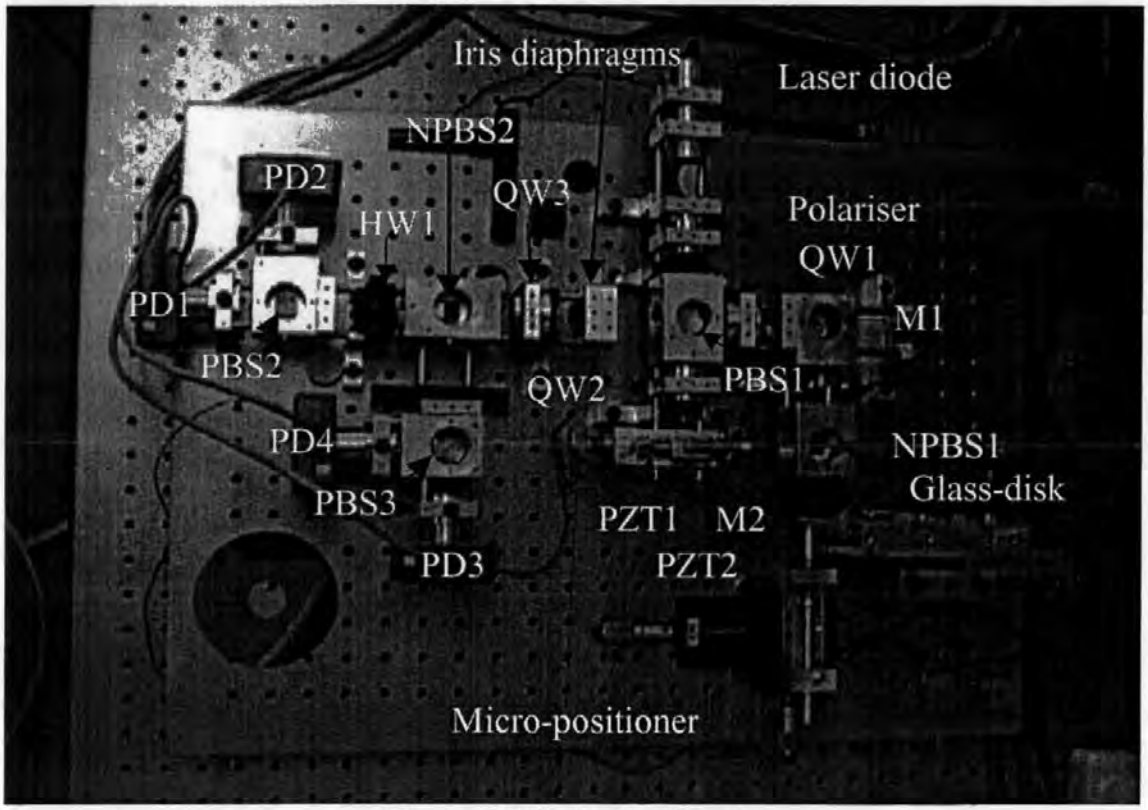

Figure 6.5 Optical testing rig

The main optical components used in the system are listed in Table 6.1.

Component name	Parameters	Part designator in the diagrams/photographs	Provider
Polarization filter	400-800nm	Polariser	Spindler & Hoyer

(Polariser)			
Non-polarised beam splitter (NPBS)		$NPBS_1$, $NPBS_2$	Spindler & Hoyer
Iris diaphragms	Iris diaphragms	Iris diaphragms	Spindler & Hoyer
Polarising beam splitter (PBS)	Broad band, 12mm cube	PBS_1~PBS_3	OptimaResearch
Quarter waveplate (QW).	676.4nm, to be mounted in 25mm diameter mount.	QW_1~QW_3	OptimaResearch
Laser diode	3mW, 670nm.	Laser diode	RS
Photo detector	720nm peak sensitivity wavelemgth	PD_1~PD_2	HAMAMATSU Photonics

Table 6.1 Main optical components used in the experimental testing system

All the mechanical parts of the testing rig were manufactured in the workshop at the University of Plymouth. Mechanical drawings of the main parts are given in Appendix1.

We can take a further look at the main part of the interferometer, which is shown in Figure 6.6.

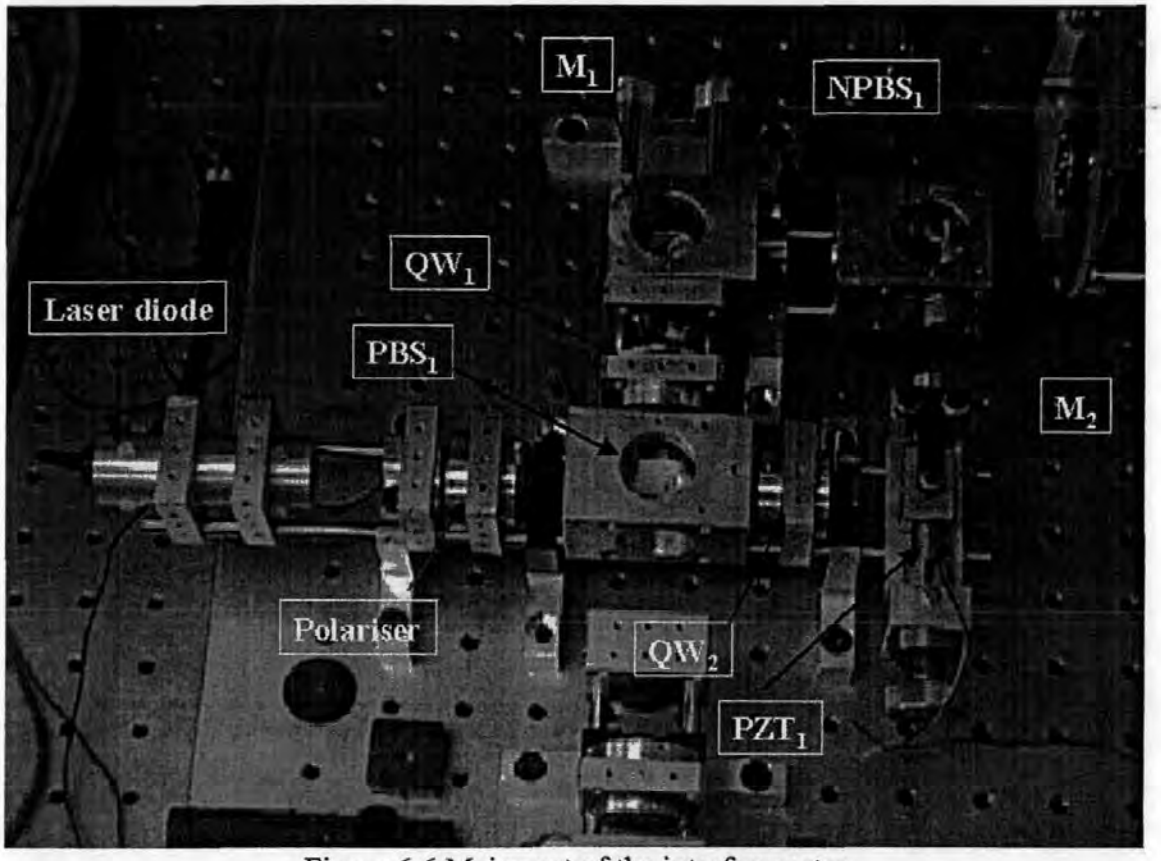

Figure 6.6 Main part of the interferometer

The photograph of interferometric receiver is show in Figure 6.7.

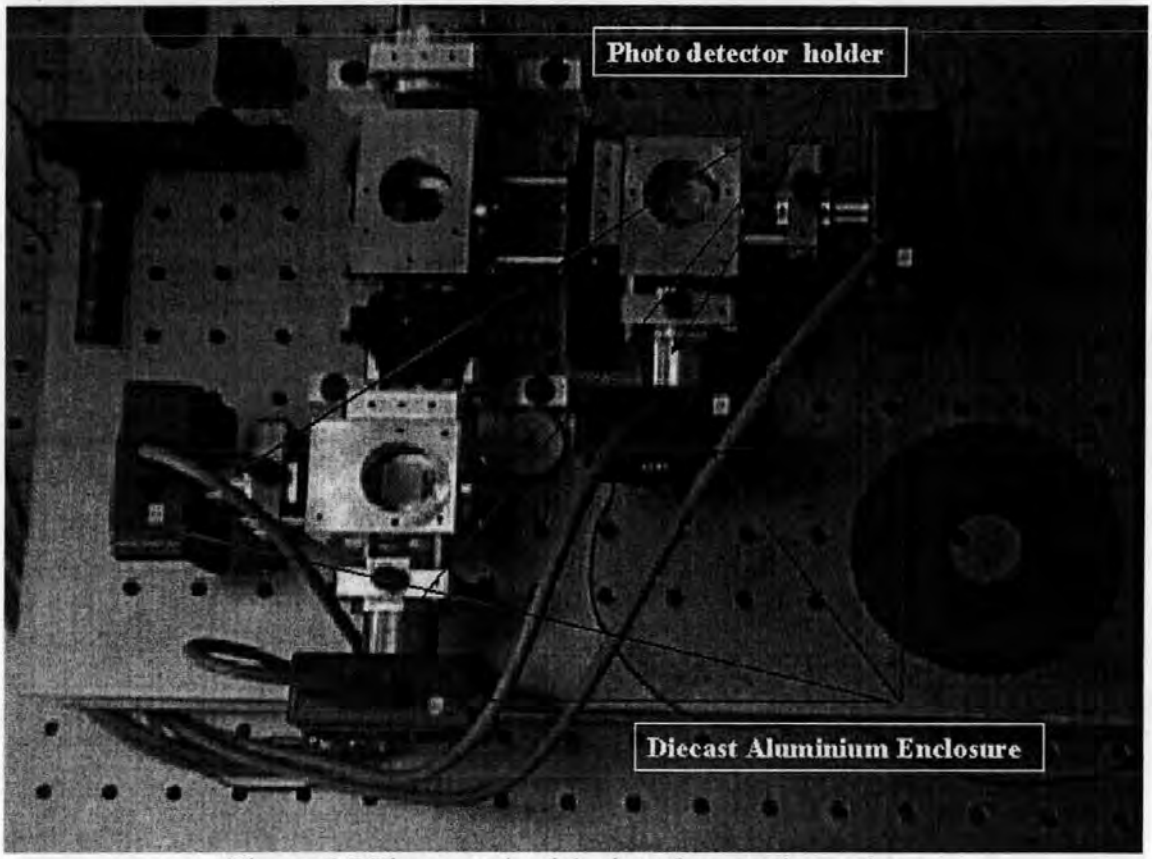

Figure 6.7 Photograph of the interferometric receiver

The glass testing disks are manufactured and provided by Changchun Institute of Optics & Fine Mechanics (CIOM), Chinese Academy of Sciences. There are two types of glass disks used in the experiment, the parameters of which are listed in Table 6.2.

	Diameter	**Thickness**	**Surface Roughness**	**Flatness**	**Anti-reflection coating**
Glass disk #1	95mm	3mm	< 2nm rms	<120nm Peak-to-valley	AR-coating to one side of surface: residual reflectance<0.1%
Glass disk #2	95mm	3mm	< 2nm rms	<120nm Peak-to-valley	no AR-coating

Table 6.2 Parameters of the glass disks

The photograph of one of the glass disks is show in Figure 6.8.

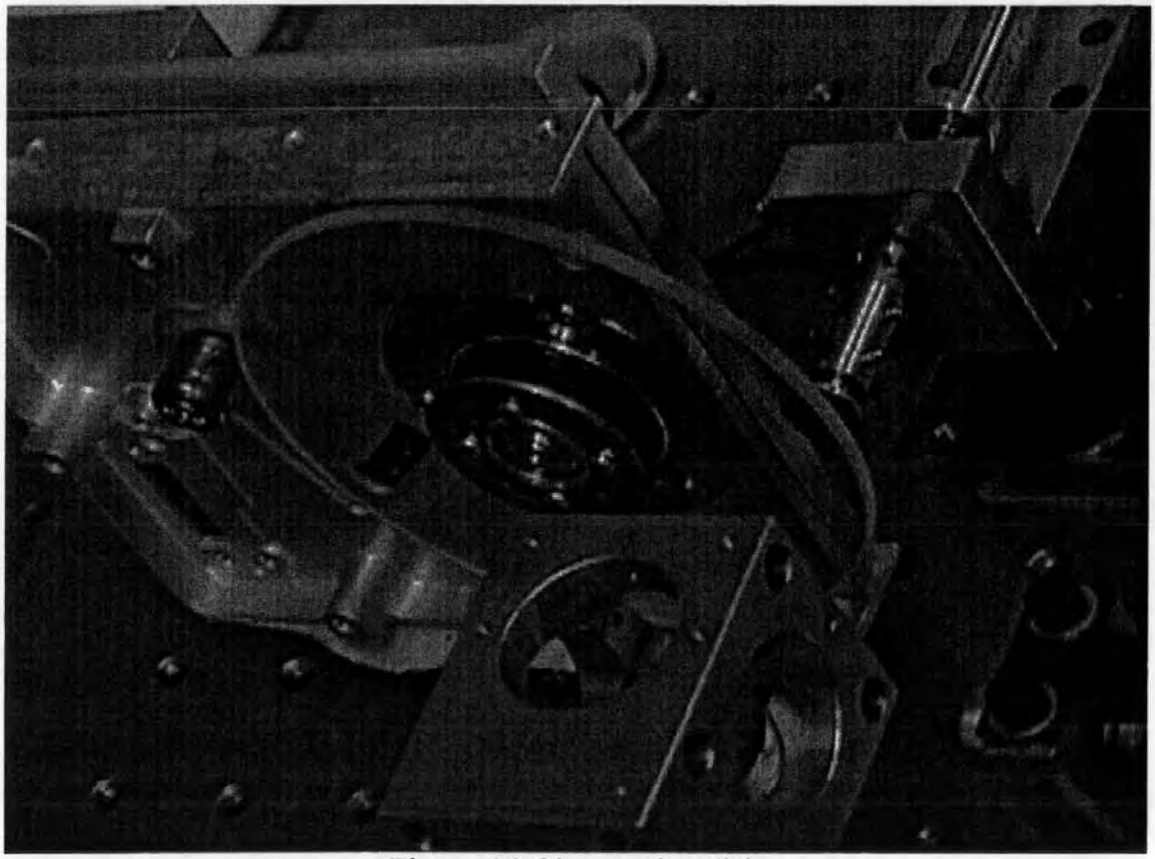

Figure 6.8 Glass testing disk

Piezoelectric translator PZT_1 is employed to move mirror M_2. This can be used for system calibration when measurement is going to be carried out. The photograph is shown in Figure 6.9.

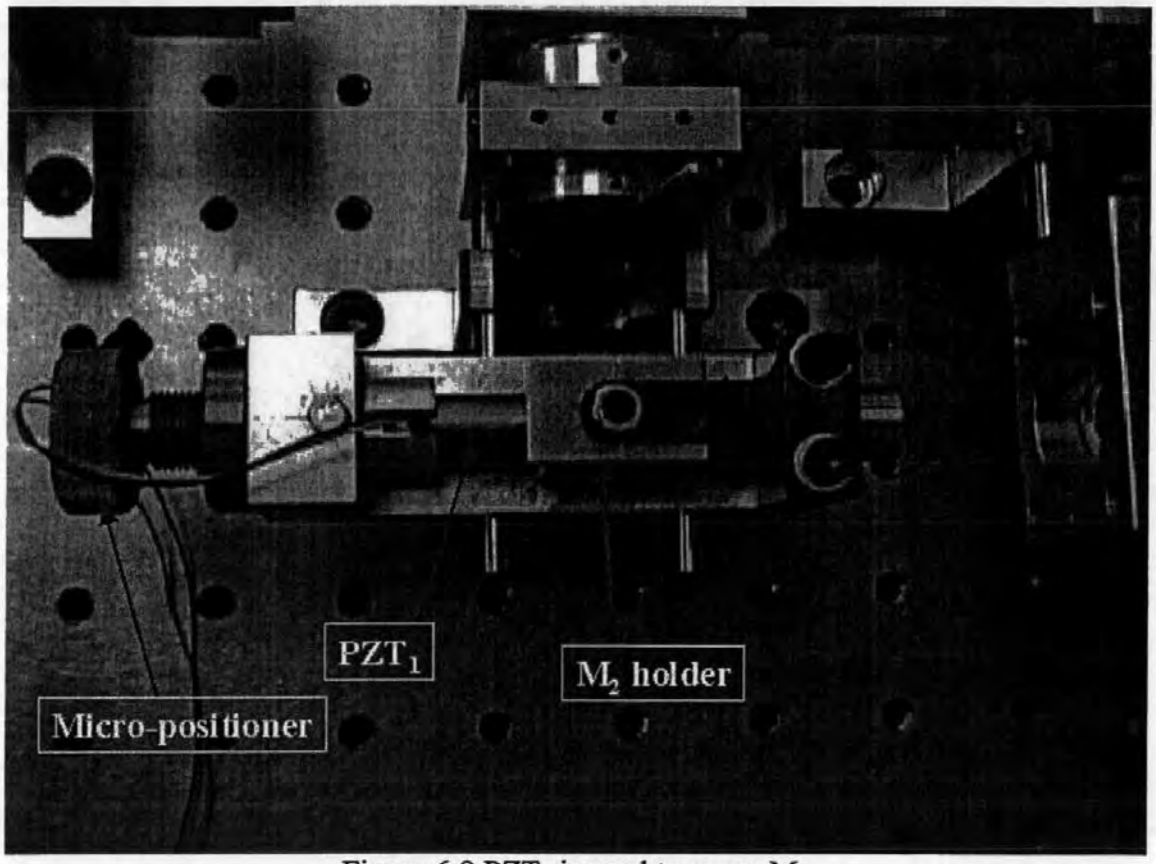

Figure 6.9 PZT_1 is used to move M_2

Piezoelectric translator PZT_2 is used to move the head-slider sample to simulate the flying height or head disk spacing change. The photograph is shown in Figure 6.10.

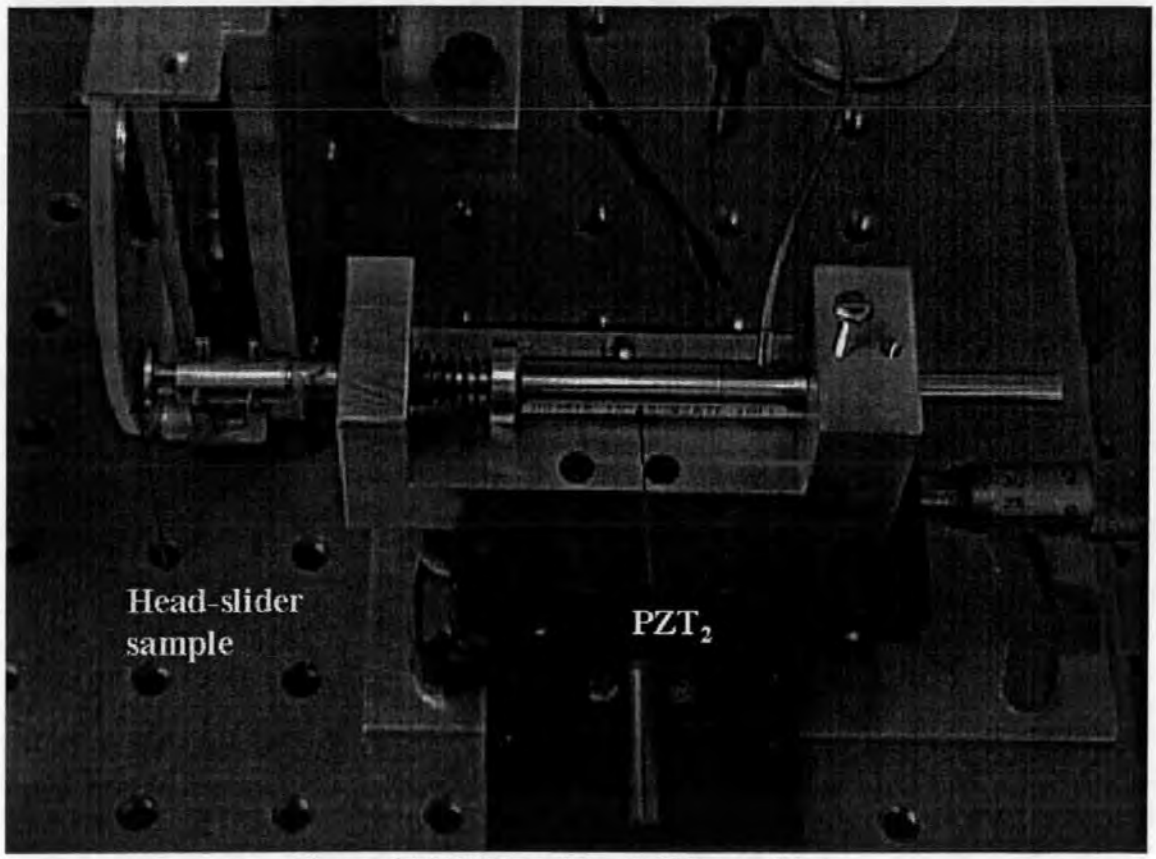

Figure 6.10 PZT_2 and head slider positioner

6.3 Tips on optical testing rig adjustment

6.3.1 Laser beam alignment adjustment

Adjust the laser centring screws untill the laser beam hits the centres of both the linear Polariser and QW_2.

6.3.2 PBS_1, $NPBS_2$, PBS_2, and PBS_3 adjustment.

Place a mirror at QW_1 and WQ_2 respectively (or just using QW_1 and QW_2 since they also reflect part of the incidence beams). Adjust PBS_1 until the two reflected beams overlap at the centre position of PD_1.

Next adjust $NPBS_2$ until the beam hits the centre position of PD_3.

Then adjust PD_2 and PD_4 respectively until the beams hit the centre position of PD_2 and PD_4 respectively.

6.3.3 Mirror1, Mirror2, and $NPBS_1$ adjustment

Put the glass disk (or hard disk) on its position, adjust Mirror1 until the reflected beam hits the centre position of PD_1. Adjust Mirror2 or/and $NPBS_1$ to make the reflected beam also hit the centre position of PD_1.

6.3 Control electronics and data acquisition

The main electronic circuits for the experimental flying height testing system can be divided into three parts: power supply, high voltage amplifier, and signal processing.

6.3.1 Power Supply

In this experimental flying height testing system, two piezoelectric translators from Physik Instrumente, PZT_1 and PZT_2, are employed. PZT_1 is used to move mirror M_2 to make phase shifting between the two polarised beams. This can be used for system calibration when making real flying height measurement. PZT_2 is used to move the head slider sample to simulate flying height variation in our experimental system. The main parameters of the two piezoelectric translators are given in Table 6.3.

Part Number	P830.10 (PZT_1)	P820.20 (PZT_2)
Open loop travel @ 0 to 100V	15 ± 20% μm	30 ± 20% μm
Open loop resolution	0.15 nm	0.3 nm
Force generation (blocked)	1500 ± 20% N	180 ± 20% N
Push/pull force capacity	1500/5 N	50/10 N
Length L	22 ± 0.3 mm	44 ± 0.3 mm

Table 6.3 Parameters of the piezoelectric translators

The piezoelectric translators require a voltage range of 0V ~ 100V to drive. Since the piezoelectric elements act like capacitors, the current needed from the power supply is very low. This makes it possible to use integrated circuit amplifiers to form the interface

between the low voltage signals from the computer and the high driving voltages for the PZT translators. As it is difficult to find a low noise, ±120Vdc ~ ±150Vdc, 50W power supply at an acceptable price to power the amplifier, a self-made power supply was built by using commercially available dc-dc converter modules by wiring them up in series to produce the required voltage. The dc-dc converters used here are VI-J64-CY supplied by Vicor, which has 300Vdc input, and 48V/50W output (can be trimmed). By combining four of these modules and using the VI-FKE6-CUX, 300Vdc front end power supply (also from Vicor), an output voltage of ±120V is produced. Diagrams of the high voltage power supply are shown in Figure 6.11 and Figure 6.12.

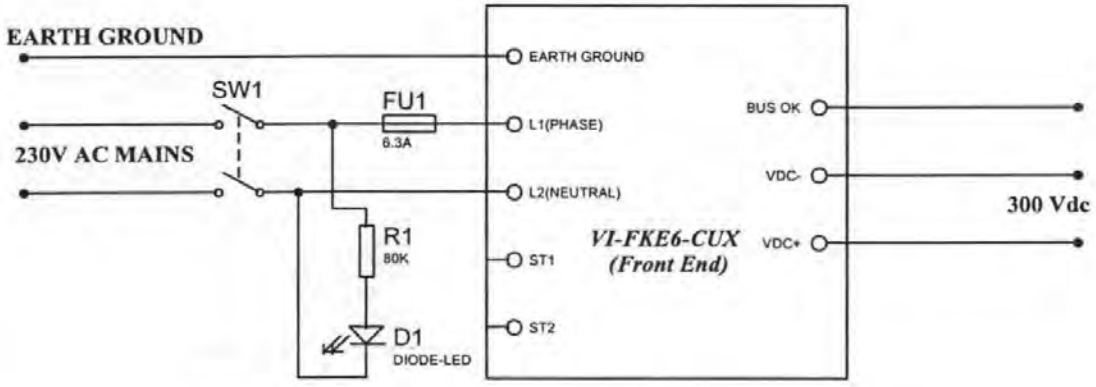

Figure 6.11 Circuit diagram of the 300V dc front end

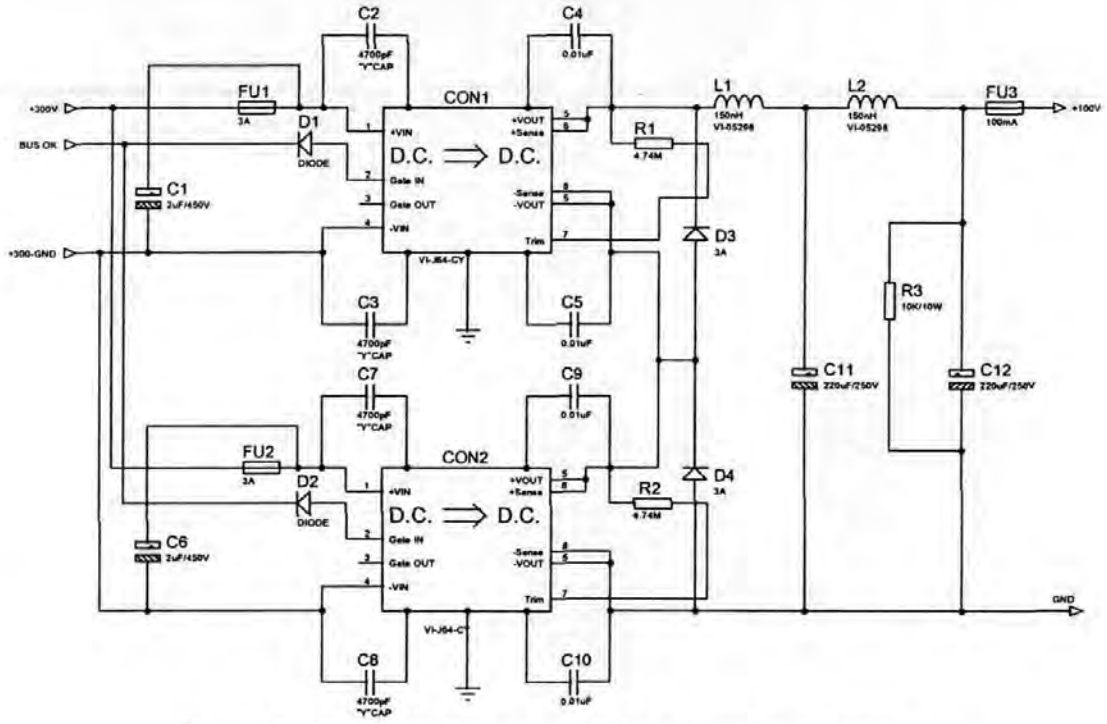

Figure 6.12 Circuit diagram of high voltage power supply

Two of the circuits shown in Figure 6.12 are connected to form a ±120 Vdc power supply.

6.3.2 High voltage amplifier

The piezoelectric translators PZT_1 and PZT_2 are driven by voltages of 0 to 100 Vdc from high power amplifiers, and can provide a largest movement of approximately 15μm and 30μm respectively when no external loads are applied. The amplifiers for the two PZT translators are built up with two high voltage amplifiers PA84 supplied by APEX Microtechnology, which is shown in Figure 6.13.

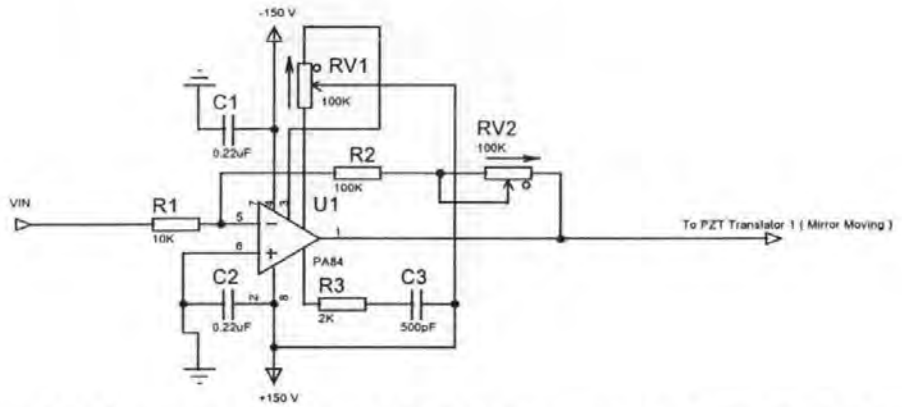

Figure 6.13 Circuit diagram of the high voltage amplifier for driving the PZT

Two of the circuit shown in Figure 6.13 are built to drive the two piezoelectric translators respectively. R3 and C3 are used for phase compensation (see APEX hand book). The gain of both the amplifier circuits is adjusted to 10.

The input voltage signals to the two amplifiers are produced by the computer via four D/A converters on the analogue I/O board. Two 12-bit D/A converters provide two coarse input voltages and two 8-bit converters provide two fine input voltages, which are added up separately using operational amplifiers to produce two input voltage signals for the two high voltage amplifiers used to drive PZT_1 and PZT_2 respectively. This is shown in Figure 6.14.

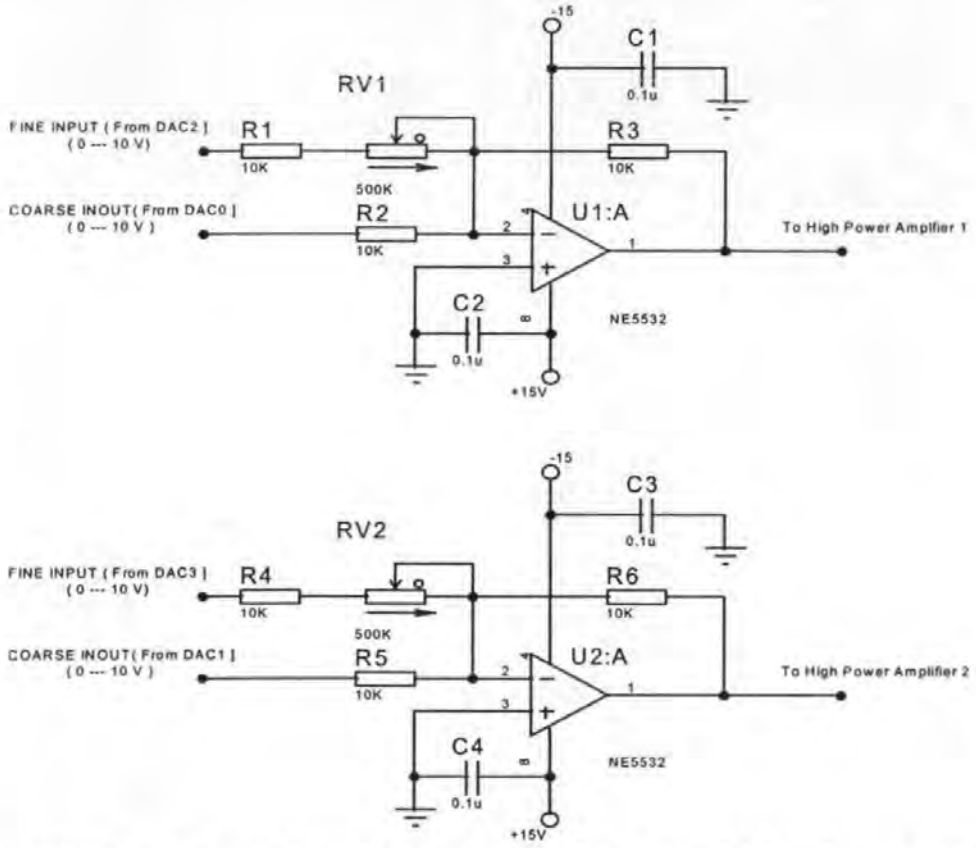

Figure 6.14 Circuits to produce the input signals for the two high voltage amplifiers

The resolutions of the movement of the piezoelectric translators can be calculated (or predicted) theoretically. For example, in non-load condition, PZT_2 will produce 30 μm movement on 100 Vdc voltage applied. Therefore, the movement produced by one input code of the coarse D/A converter will be: $\frac{30\times1000}{4096}\approx 7.32\text{nm}$. Similarly, if the variable resistor RV2 is adjusted to be 460K, the movement produced by one input code of the fine D/A converter will be $\frac{30\times1000}{256}\bullet\frac{10}{10+460}\approx 2.49\text{nm}$. In real applications, since there is usually external load applied to the piezoelectric translators, this calculation can only serve as a theoretical guidance. In our testing experiments, the amplification factor of the amplifier in Figure 6.13 was also changed from 10 to 1 when conducting high-resolution movement. This makes the PZT movement resolution become 10 times higher.

6.3.3 Signal processing circuits

The photo detectors used in the interferometric receiver are S1226-44BK Si Photodiodes from Hamamatsu Photonics. The circuits for photo detectors are shown below in Figure 6.15.

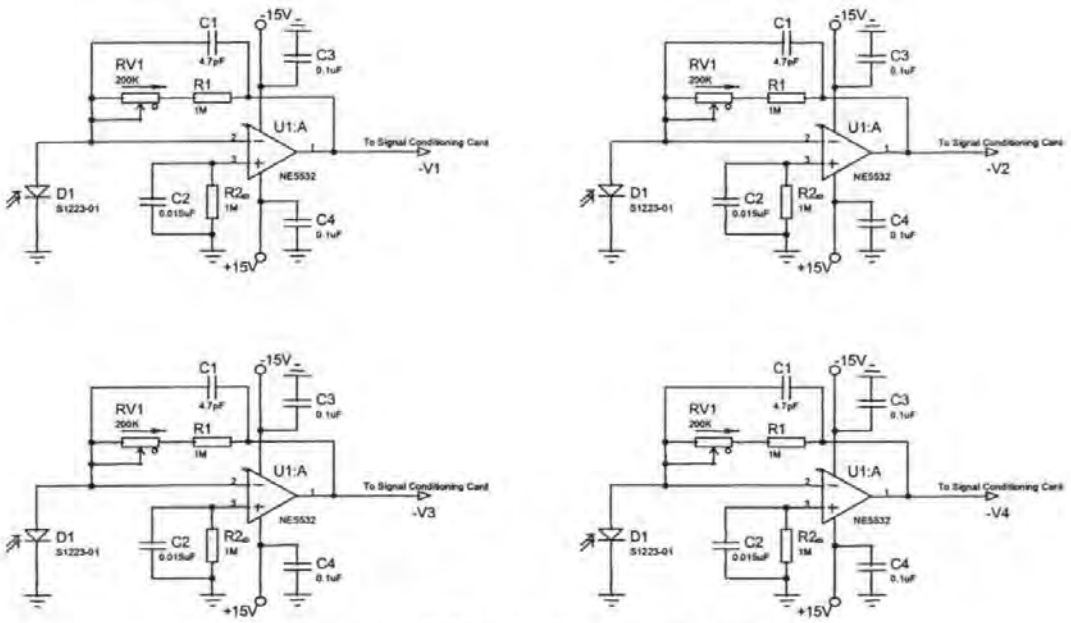

Figure 6.15 Circuits for photo detectors

The four circuits are identical, each of which is placed in the diecast aluminium enclosure to isolate (or reduce) the noises and interferences. The output voltage signals from the photo detector circuits then enter the signal conditioning circuits, which consist of four operational amplifier circuits as shown below in Figure 6.16.

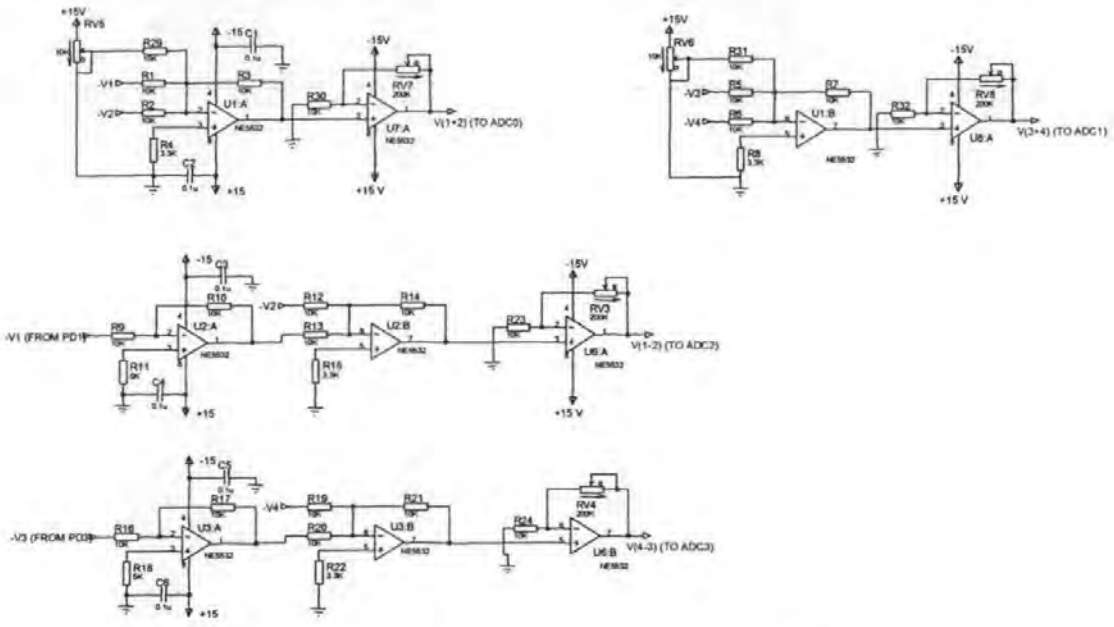

Figure 6.16 Signal conditioning circuits

The final output signals V(1+2), V(3+4), V(1-2), and V(4-3) are sampled by the computer via four A/D converter channels on the analogue I/O board. Except for the photo detector circuits, all the other circuits are designed on PCBs of standard Euro-card size (200mm × 160mm), which are fitted in the control box as shown below in Figure 6.17.

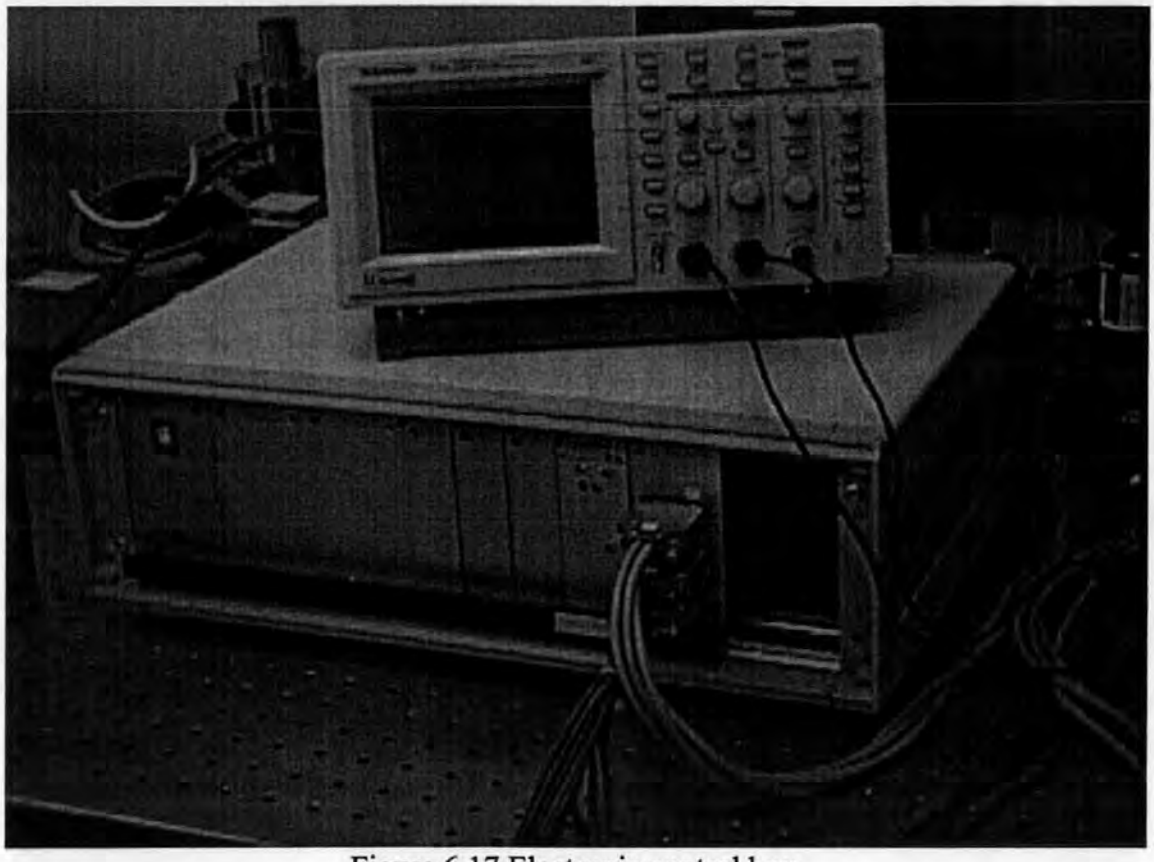

Figure 6.17 Electronic control box

6.3.4 Analogue I/O board

The analogue I/O board used in the experimental system is PC-30C from Amplicon Liveline Limited. The PC-30C board was a full size, low cost, high accuracy analogue and digital I/O board for IBM PC, PC/XT, PC/AT, PS/2 model 25, PS/2 model 30 and compatible series of computers. It can be plugged into any of the fully-bussed slots in a PC/XT/AT, PS/2 model 25 or 30, or compatible computer.

6.3.4.1 A/D subsystem

The A/D subsystem's major component is a monolithic analogue to digital converter. It allows for 16 single-ended inputs, and can be configured for unipolar (input range of 0 to 10V) or bipolar (input range of +/-5V or +/-10V) operation.

Key specifications:

- A/D resolution: 12 Bits

- Non-linearity: Less than ±0.75 LSB
- A/D full scale input ranges: 0 to +10V, –5 to +5V and –10 to +10V.
- Number of A/D inputs: 16 single ended.
- A/D throughput rate: 100 KHz

The four channels of A/D input in our experimental system are all configured as –10 to +10V.

6.3.4.2 D/A subsystem

The D/A subsystem consists of two 12-bit D/A converters, DAC0 and DAC1, and two 8-bit D/A converters, DAC2 and DAC3. Digital outputs are received from the host processor and converted to analogue voltage outputs required by the application. The four DACs are independent on each other, and can operate at a throughput of up to 130KHz. Output ranges are independently configurable as 0 to +10V unipolar, or as ± 10V bipolar. Here we use 0 to +10V output range.

Key specifications of DAC0 and DAC1:

- D/A resolution: 12Bits.
- D/A non-linearity: Within 0.01% FSR.
- Full scale output ranges:0 to +10V, –10 to +10V.
- D/A throughput: 130 KHz.

Key specifications of DAC2 and DAC3:

- D/A resolution: 8 Bits.
- D/A non-linearity: Within 0.38% FSR.
- Full scale output ranges:0 to +10V, –10 to +10V.
- D/A throughput: 130 KHz.

6.3.4.3 Software support

Supplied with the PC-30 board is a set of real time device drivers for use with a wide variety of software. These device drivers are written in C, and are callable from Microsoft C, Microsoft FORTRAN, Microsoft PASCAL, Turbo C, and Turbo Pascal version 4 and 5.

7 Experimental Results and Analysis

This chapter gives the experimental results and their analysis of this research work. Section 7.1 presents the flying height testing results of using the relative displacement measurement method. Section 7.2 gives the measurement results when using the direct spacing measurement method. Determination of the optical constants of the slider material and the initial phase of the interferometer is given in Section 7.3.

7.1 Relative displacement flying height measuring method

Results of using relative displacement measuring method are presented in this section. The method has been described in Section 5.4 of Chapter 5. In the experiment, PZT2 is used to move the head slider sample to simulate the flying height variation, and a piece of disk or mirror is used in the place of the real disk. We first make experiments to test the general noise level of the system or the system measurement error. In this experiment, PZT1 and PZT2 are both held stationary. The sampling rate of the A/D converter is set to 50kHz. The measurement result is shown in Figure 7.1.

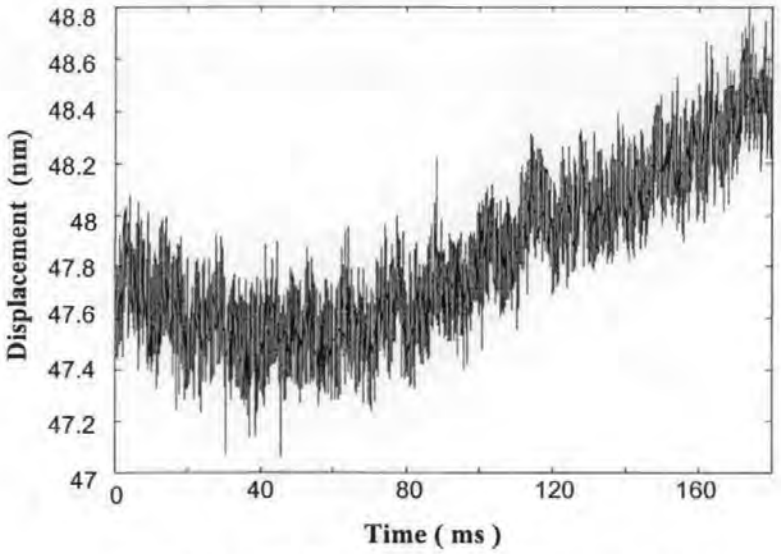

(a) The plot of 9000 points sampled data

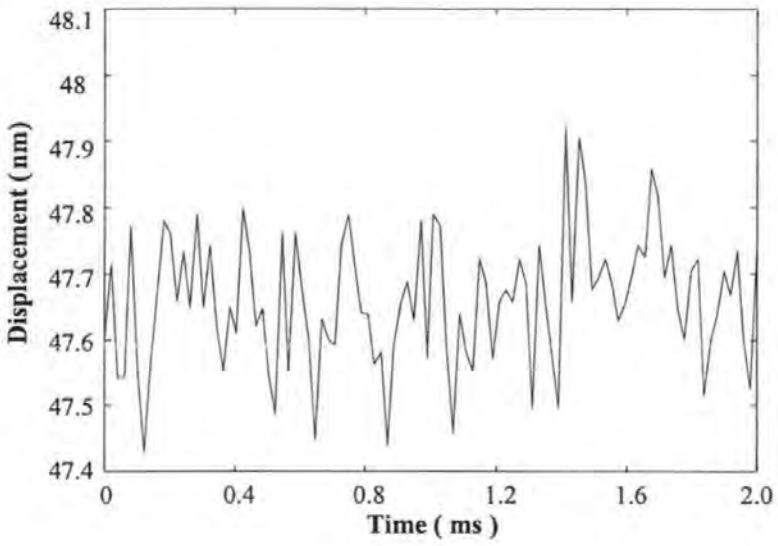

(b) Expanded version of plot (a)

Figure 7.1 System measurement error and general noise level

From Figure 7.1, we can see that the system measurement error is composed of both low and high frequency components. The low-frequency noise can be observed from Figure 7.1 (a), which most likely results from background vibration, thermal drift, air current disturbances etc. The magnitude of noise level caused by these can be well above 1 nm. In fast-changing displacement measurement cases, this low-frequency

noise can be eliminated by simple signal processing. The high-frequency noise comes from the laser diode, the photo-detectors, and the system's electronics. The peak-to-peak magnitude of this noise level is about 0.3 nm, which can be seen from Figure 7.1 (b).

We now conduct further experiments in which we use PZT2 to move the sample in a saw-wave form with several different amplitudes from about 4.75μm down to 1 nm. The measurement results are shown in Figure 7.2 to Figure 7.6 for successively smaller displacements. The measurement was conducted by using the C program A3.1 in Appendix 3.

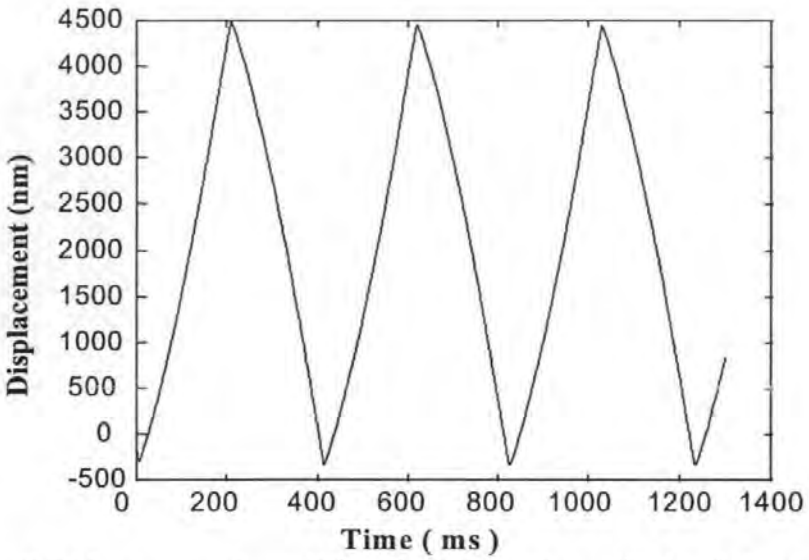

Figure 7.2 Measurement result for displacement amplitude of about 4.75 μm

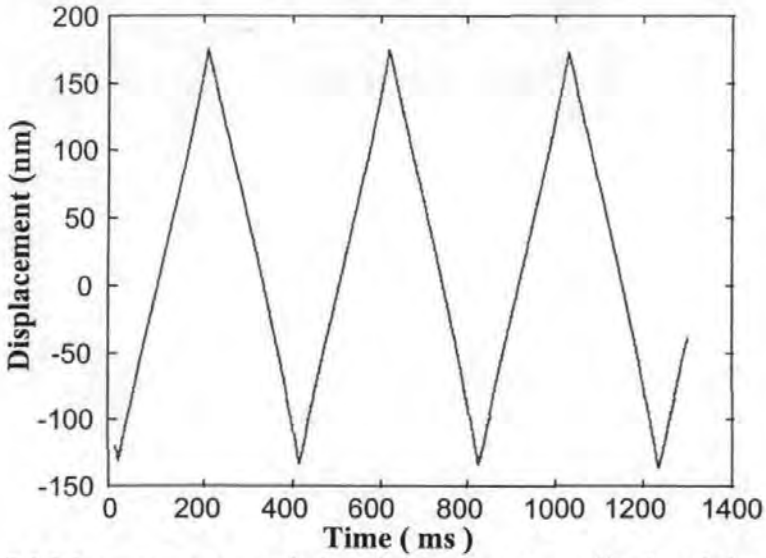

Figure 7.3 Measurement result for displacement amplitude of about 300 nm

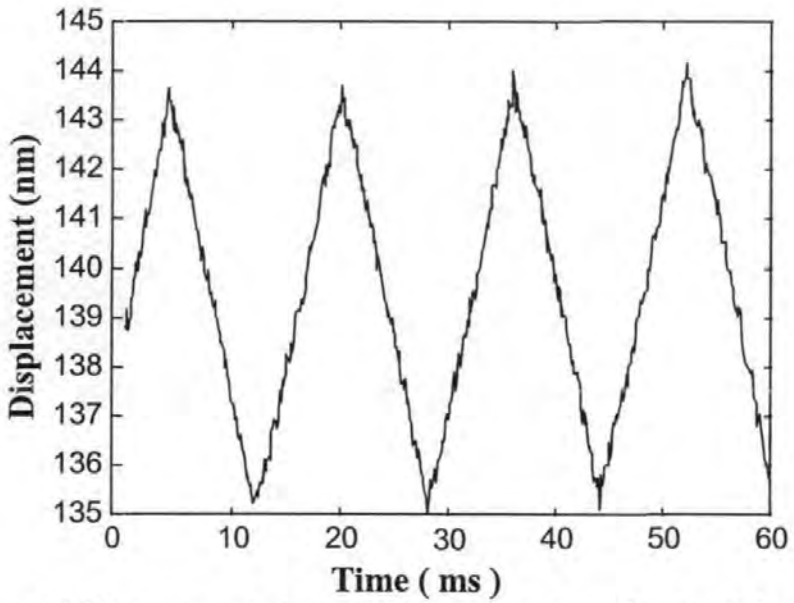

Figure 7.4 Measurement result for displacement amplitude of about 8.5 nm

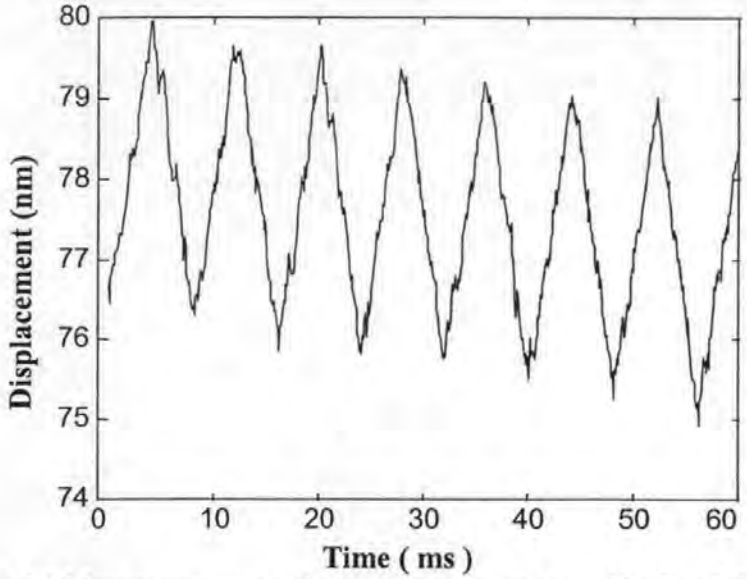

Figure 7.5 Measurement result for displacement amplitude of about 3.5 nm

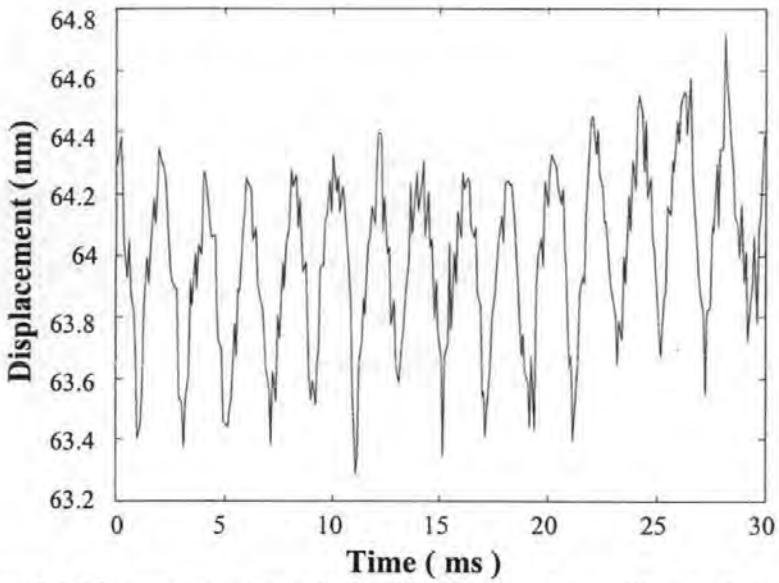

Figure 7.6 Measurement result for displacement amplitude of about 0.8 nm

From the experimental results shown above, it can be seen that the displacements with different magnitudes are measured with rather satisfying precision. Theoretically, a 12-bit A/D converter can provide a measurement resolution as good as $\lambda/4096$. However, because of system noises, the system in its present configuration has a general measurement resolution of about 0.5 nm. This will be further improved by carefully refining the system electronics and mechanics. The system measurement bandwidth can also be increased by using a higher sampling rate A/D board.

7.2 Direct spacing measurement method

Details of this method have been described in subsection 5.2.1 of Chapter 5. Again, to test the ability and effectiveness of this interferometer, we make the following experiments. The 3mm thick glass disk with antireflection coating is held in stationary state. The PZT_2 translator is used to move the head-slider in saw-wave form to simulate the head-slider flying height variation. Several experiments were conducted and the measured intensity and phase information were saved in a few data files using the C program A3.2 in Appendix 3. As described in subsection 5.2.1, with the measured intensity and phase information, the head-disk spacing can be determined in several ways. Here we give details of these methods and make our points about which method is better to be used.

7.2.1 Flying height determination from phase information

From Equation (5.7), it was derived that the flying height h can be expressed as the following equations:

$$h = -\frac{670}{4\pi}\cdot 2\cdot tan^{-1}\left[\frac{6n^2\cos\phi_p - 6\cos\phi_p + 6k^2\cos\phi_p + 13k\sin\phi_p}{9k^2\sin\phi_p + 9n^2\sin\phi_p - 4\sin\phi_p - 12k\cos\phi_p} \right. \\ \left. \frac{-\sqrt{25n^2\cos^2\phi_p + 72k^2 - 97n^2 + 36 + 72n^2k^2 + 36k^4 + 36n^4}}{}\right] \tag{7.1}$$

$$h = \frac{670}{4\pi}\cdot 2\cdot\left[\pi - tan^{-1}\left[\frac{6n^2\cos\phi_p - 6\cos\phi_p + 6k^2\cos\phi_p + 13k\sin\phi_p}{9k^2\sin\phi_p + 9n^2\sin\phi_p - 4\sin\phi_p - 12k\cos\phi_p} \right. \right. \\ \left. \left. \frac{-\sqrt{25n^2\cos^2\phi_p + 72k^2 - 97n^2 + 36 + 72n^2k^2 + 36k^4 + 36n^4}}{}\right]\right] \tag{7.2}$$

where 670 is the wave-length of the laser diode, $\phi_p = \left(-\phi^M - \theta_0\right)$, ϕ^M is the measured phase difference between the two polarising beams by the interferometric receiver. The initial phase difference θ_0 can be measured either directly at the beginning of the flying height testing by using the phase equation, or by using the method of minimising the difference between the measured and theoretical values of both intensity and phase, which will be detailed in Section 7.3.

If the flying height range is known, equation (7.1) can be used to determine the flying height below about $\lambda/4$ unambiguously (or determine the spacing between $m\lambda$ and $m\lambda+\lambda/4$ unambiguously, here m is an integer). Similarly, equation (7.2) can be used to determine the flying height in the range from about $\lambda/4$ to $\lambda/2$ unambiguously (or determine the spacing between $m\lambda+\lambda/4$ and $m\lambda+\lambda/2$ unambiguously, here m is an integer). Since the phase curve repeated periodically with a period of $\lambda/2$, if the flying height changes continuously, either equation (7.1) or (7.2) can be used to determine the flying height change unambiguously to any range. The flying height variation measurement results of the experiments are shown in Figure 7.7 to Figure 7.9, where we assumed the optical constants of the head-slider are n=2.79, and k=0.0998, which can also be measured using the method described in Section 7.3.

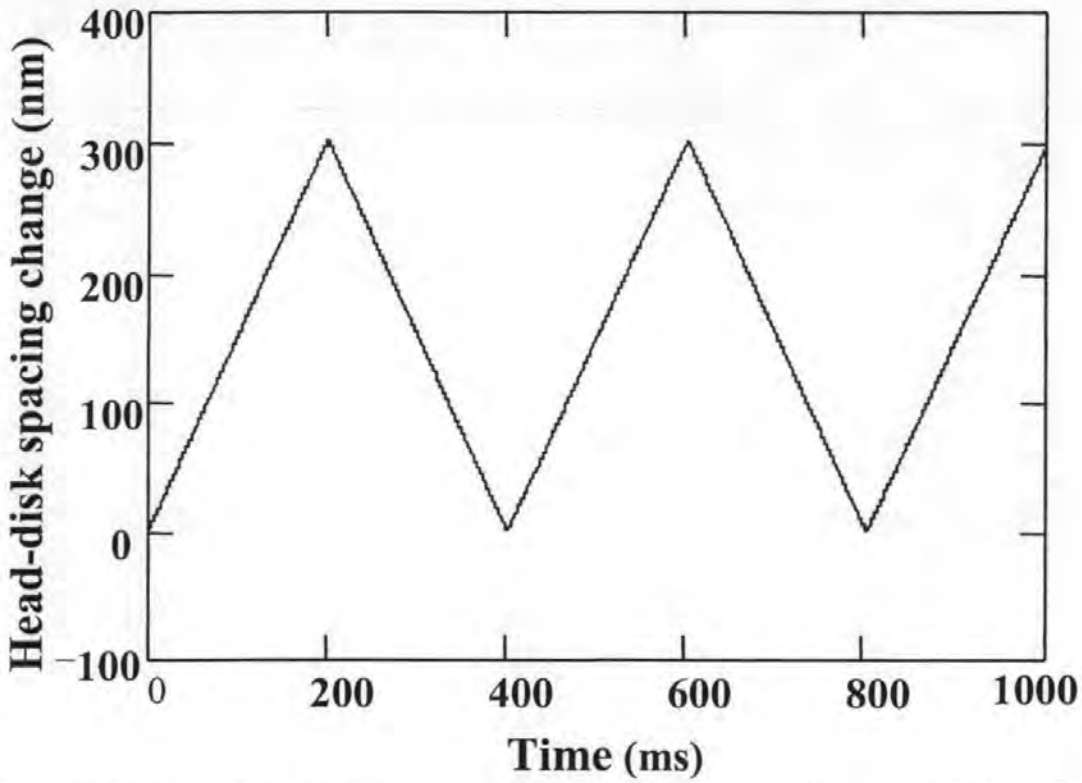

Figure 7.7 Measured head-disk spacing change with an amplitude of about 300nm in DSM method

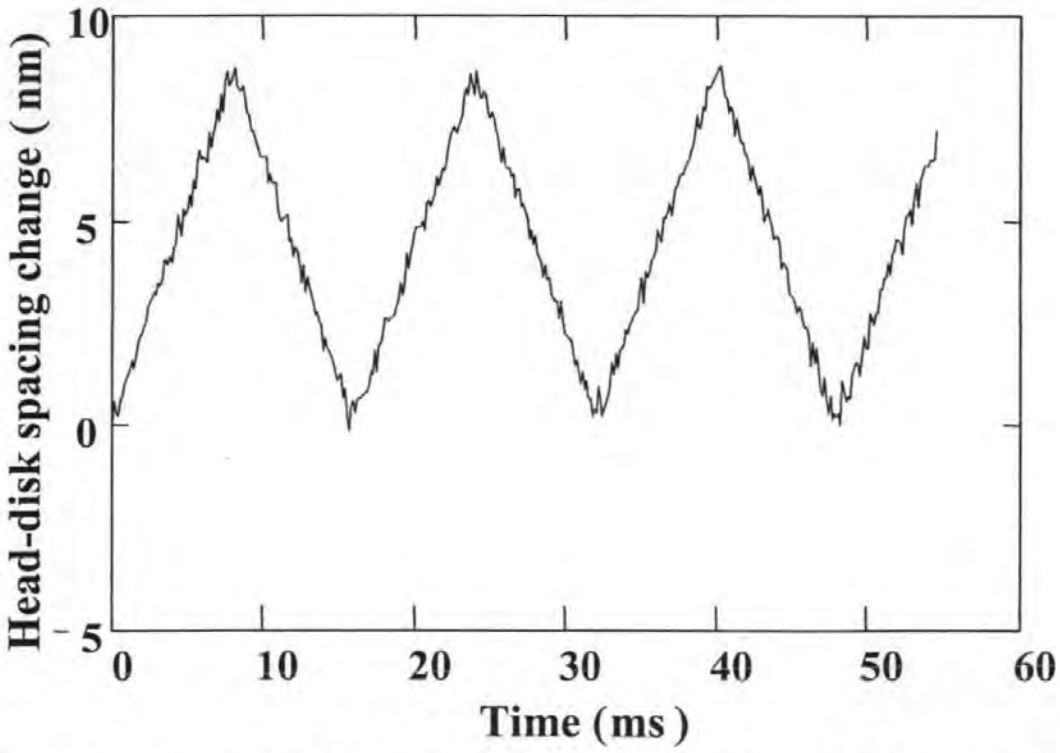

Figure 7.8 Measured head-disk spacing change with an amplitude of about 8.5nm in DSM method

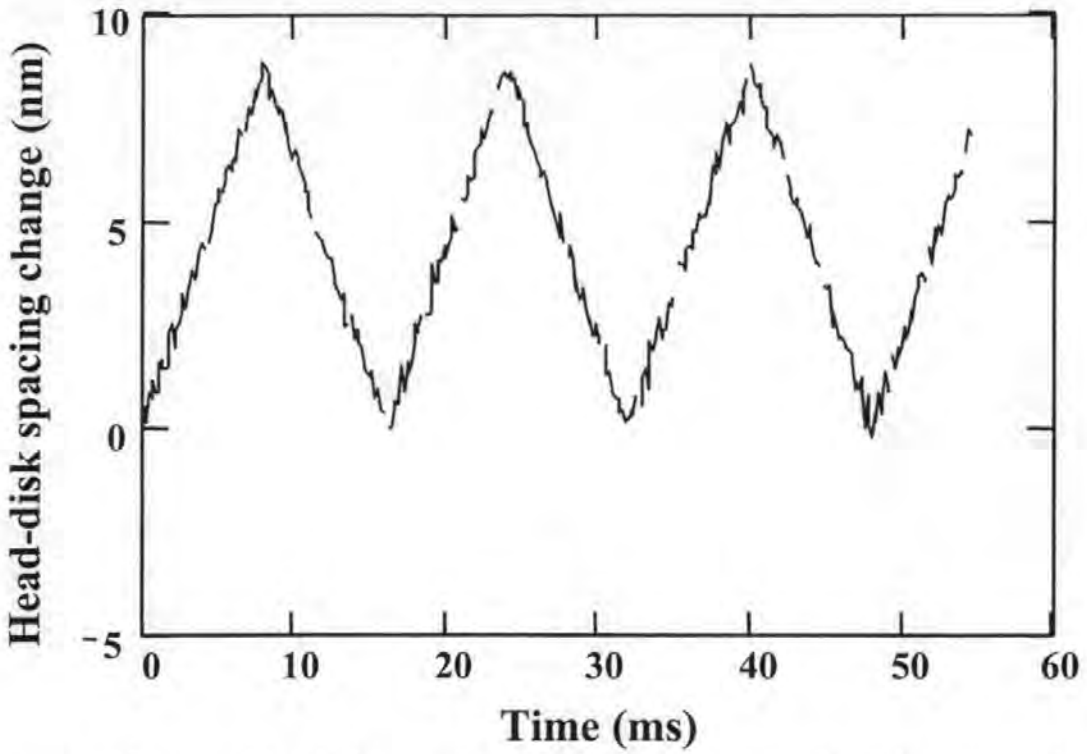

Figure 7.9 Measured head-disk spacing change with an amplitude of about 8.5nm in DSM method (repeated experiment)

From the above results, it is seen that by using the phase information alone, the flying height can be determined with very good accuracy and precision.

7.2.2 Flying height determination from intensity information

Because of the nature of the intensity curve (which can be found from Figure 5.3), the head disk spacing can be determined unambiguously in the range between $m\lambda$ and $m\lambda+\lambda/4$ from the intensity information if the direction of the spacing change is known before hand (Note: here m is an integer). If the direction of the spacing change is not known, the phase information must also be used to determine the direction.

From Equation (5.6), the following expressions can be derived to determine the flying height h from the measured intensity:

$$h = -\frac{2 \cdot 670}{4\pi}\left[tan^{-1}\left[\frac{-5k + 5kI + \sqrt{72I + 156n - 72k^3 - 72I^3k^2 - 241n^2}}{\frac{-36I^2k^4 - 156I^3n^3 - 36I^2n^4 + 72n^4I + 156k^2n + 72k^4I - 72k^2n^2}{4I - 4 - 9k^2 - 9n^2 + 12n + 9k^2I + 12nI + 9n^2I}} \right.\right.$$

$$\left.\left. \frac{-156I^3n - 36k^4 + 144k^2n^2I - 156I^2k^3n - 72I^2k^2n^3 + 156n^3}{-36n^4 - 36I^2 + 144k^3I - 94n^2I - 36 - 241n^2I^2} \right]\right] \tag{7.3}$$

$$h = -\frac{2 \cdot 670}{4\pi}\left[-\pi + tan^{-1}\left[\frac{-5k + 5kI - \sqrt{72I + 156n - 72k^3 - 72I^3k^2 - 241n^2}}{\frac{-36I^2k^4 - 156I^3n^3 - 36I^2n^4 + 72n^4I + 156k^2n + 72k^4I - 72k^2n^2}{4I - 4 - 9k^2 - 9n^2 + 12n + 9k^2I + 12nI + 9n^2I}} \right.\right.$$

$$\left.\left. \frac{-156I^3n - 36k^4 + 144k^2n^2I - 156I^2k^3n - 72I^2k^2n^3 + 156n^3}{-36n^4 - 36I^2 + 144k^3I - 94n^2I - 36 - 241n^2I^2} \right]\right] \tag{7.4}$$

Note that the I in (7.3) and (7.4) is the normalised measured intensity based on the following equation:

$$I = (I^M - I^M_{min})\frac{I^T_{max} - I^T_{min}}{I^M_{max} - I^M_{min}} + I^T_{min} \tag{7.5}$$

where I^M is the measured intensity, I^M_{min} and I^M_{max} are the minima and maxima of the measured intensity curve respectively, and I^T_{min} and I^T_{max} are the minima and maxima of the theoretical intensity curve respectively. I^M_{min} and I^M_{max} can be obtained during the calibration process before the measurement. I^T_{min} and I^T_{max} can be obtained from

equation (5.6) by setting I_{p0} and I_{s0} to 1, or just using the simplified equation (7.6) below for simplicity.

$$I^T = \left| \frac{r_{p20} + r_{p01}\, exp(i\beta_p)}{1 + r_{p20} r_{p01}\, exp(i\beta_p)} \right|^2 \tag{7.6}$$

It is not very difficult to verify that the minimum and maximum intensity values occur at $\beta_p = tan^{-1}\left(\frac{2n_0k_1}{n_0^2 - n_1^2 - k_1^2}\right)$ and $\beta_p = \pi + tan^{-1}\left(\frac{2n_0k_1}{n_0^2 - n_1^2 - k_1^2}\right)$ respectively.

If the flying height range is known, equation (7.3) can be used to determine the spacing in the range between $m\lambda$ and $m\lambda+\lambda/4$, while equation (7.4) can be used to determine the spacing in the range between $\lambda/4+m\lambda$ and $m\lambda+\lambda/2$ (Note: here m is an integer). From the intensity curve in Figure 5.3, we have known that the curve has very poor sensitivity in the area near the extremum points. The following experiment was conducted to see the result of extracting the head-disk spacing variation from the measured intensity information. The head slider was made linear movement by PZT_2. The extracted spacing variation curves by using equation (7.3) and (7.4) are shown in Figure 7.10 and Figure 7.11 respectively.

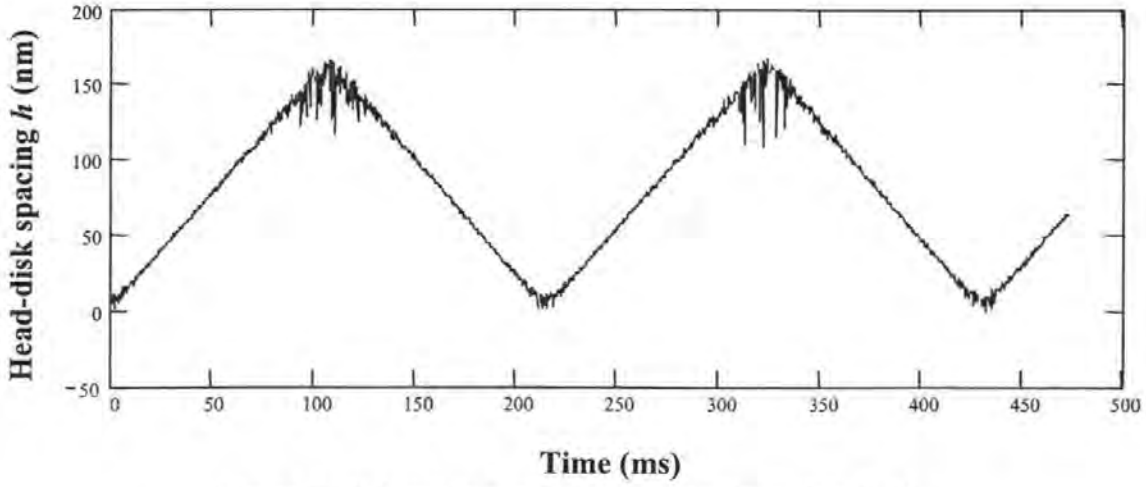

Figure 7.10 Spacing variation extracted by using (7.3)

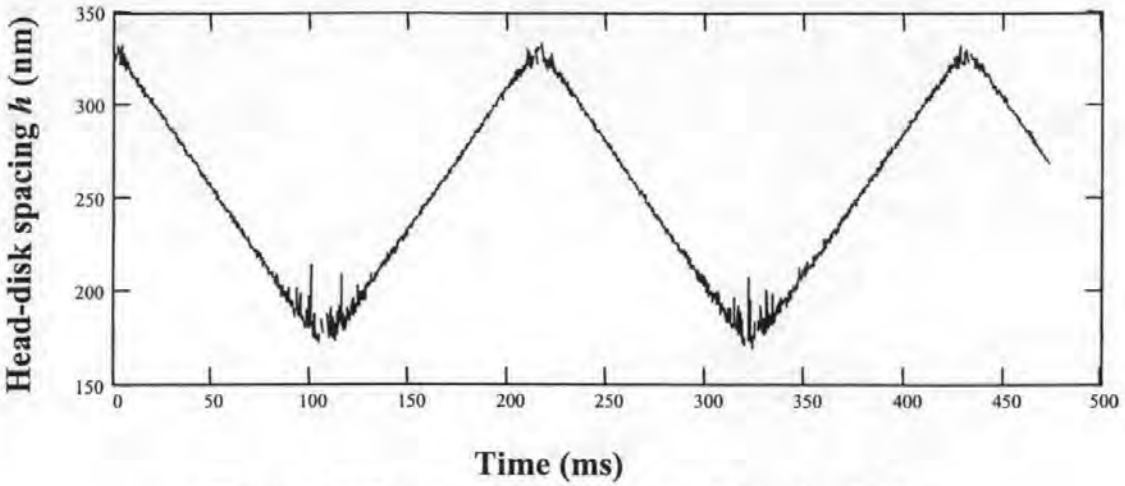

Figure 7.11 Spacing variation extracted by using (7.4)

From Figure 7.10 and Figure 7.11, it can be seen that because there are areas where the sensitivity of the intensity curve is very poor (there are points where the sensitivity is zero), a small noise will result in a large deviation of the measured spacing variation from the actual value.

7.2.3 Flying height determination by optimisation

Similar to the method used by de Groot [de Groot et al., 1996a], we can also calculate the flying height by minimising the difference between measured and theoretical values of both the intensity and phase. The merit function can be defined in a number of forms such as:

$$\begin{aligned}\chi(h) = &\left[(I+a)sin\left(\phi^M - \theta_0\right) - \left(I^T(h)+a\right)sin\left(\phi^T(h) - \theta_0\right)\right]^2 \\ &+ \left[(I+a)cos\left(\phi^M - \theta_0\right) - \left(I^T(h)+a\right)cos\left(\phi^T(h) - \theta_0\right)\right]^2\end{aligned} \tag{7.7}$$

where a is a constant parameter that can be chosen from, e.g., 0 to 0.5 depending on the optimisation result, I is the normalised measured intensity based on (7.5), ϕ^M is the measured phase difference between the two polarising beams, I^T is the theoretical intensity represented by (7.6), and ϕ^T is the theoretical phase difference between the two polarising beams represented by equation (5.7). For every pair of measured

intensity I^M and phase difference ϕ^M, flying height h can be derived by minimising merit function (7.7) (assume n and k are known).

The merit function can also be defined in other forms such as:

$$\chi(h) = \left[I - I^T(h)\right]^2 + \alpha\left[\phi^M - \phi^T(h)\right]^2 \tag{7.8}$$

where α is a weighting constant that can be set to, e.g., 1.0.

For C programming purpose, the theoretical intensity expression (7.6) is expanded as below:

$$I = \left(I_r^T\right)^2 + \left(I_i^T\right)^2 \tag{7.9}$$

where

$$I_r^T = \frac{\left(\left(1-n_1^2-k_1^2\right)\sin\left(\beta_p\right) - 2k_1\cos\left(\beta_p\right)\right)\left(\left(1+n_1\right)^2 + k_1^2 + 0.2\left(1-n_1^2-k_1^2\right)\cos\left(\beta_p\right)\right)}{\left(\left(1+n_1\right)^2 + k_1^2 + 0.2\left(1-n_1^2-k_1^2\right)\cos\left(\beta_p\right) + 0.4k_1\sin\left(\beta_p\right)\right)^2}$$
$$+ 0.4k_1\sin\left(\beta_p\right)\Big) - \left(0.2\left(1+n_1\right)^2 + 0.2k_1^2 + \left(1-n_1^2-k_1^2\right)\cos\left(\beta_p\right) + 2k_1\sin\left(\beta_p\right)\right)$$
$$+ \left(0.2\left(1-n_1^2-k_1^2\right)\sin\left(\beta_p\right) - 0.4k_1\cos\left(\beta_p\right)\right)$$
$$\underline{\left(0.2\left(1-n_1^2-k_1^2\right)\sin\left(\beta_p\right) - 0.4k_1\cos\left(\beta_p\right)\right)} \tag{7.10}$$

$$I_i^T = \frac{\left(0.2\left(1+n_1\right)^2 + 0.2k_1^2 + \left(1-n_1^2-k_1^2\right)\cos\left(\beta_p\right) + 2k_1\sin\left(\beta_p\right)\right)\left(\left(1+n_1\right)^2 + k_1^2 + \right.}{\left(\left(1+n_1\right)^2 + k_1^2 + 0.2\left(1-n_1^2-k_1^2\right)\cos\left(\beta_p\right) + 0.4k_1\sin\left(\beta_p\right)\right)^2}$$
$$0.2\left(1-n_1^2-k_1^2\right)\cos\left(\beta_p\right) + 0.4k_1\sin\left(\beta_p\right)\Big) + \left(\left(1-n_1^2-k_1^2\right)\sin\left(\beta_p\right) - 2k_1\cos\left(\beta_p\right)\right)$$
$$+ \left(0.2\left(1-n_1^2-k_1^2\right)\sin\left(\beta_p\right) - 0.4k_1\cos\left(\beta_p\right)\right)$$
$$\underline{\left(0.2\left(1-n_1^2-k_1^2\right)\sin\left(\beta_p\right) - 0.4k_1\cos\left(\beta_p\right)\right)} \tag{7.11}$$

We have known from Section 7.2.2 that the sensitivity of the intensity curve is very poor in some areas and it is difficult to derive the correct flying height from the measured intensity in these areas. Hence it is not difficult to predict that using the optimisation method, it is also difficult to obtain the correct flying height in these areas if the intensity information is involved in the merit function.

7.3 Optical constants and initial phase determination

We have mentioned in Section 5.5 that using our dual beam normal incidence polarisation interferometer, it is also possible for the optical constants of the slider material to be determined. In conventional optical flying height testers, an ellipsometer is usually required to do this job.

7.3.1 Initial phase determination

There are two methods to determine the initial phase θ_0 of the interferometer. The first method is measuring θ_0 directly before the start of the flying height measurement. To do this, the head slider is removed from the measurement position, hence the two polarising beams will be purely reflected by the glass disk surface, and the phase difference measured by the interferometric receiver will be the initial phase we need.

The second method is by using optimisation. This will be detailed in the next section.

7.3.2 Optical constants determination

If the initial phase difference θ_0 and optical constant n and k are unknown, the following optimisation method can be used to determine them from the measured intensity and phase difference information. To do this, we need to have a group of measured intensity and phase differences at different flying heights. This can be done during the flying height measurement process, or in our experimental simulation by recording the intensity and phase difference measured by the interferometric receiver while changing the head disk spacing using PZT_2. The merit function can be defined as:

$$\chi = \sum_{j=1}^{N} \left(I_j^M - I_j^{TN} \right)^2 \tag{7.12}$$

where N is the number of measurement or sampling points, I_j^M is the jth measured intensity value, I_j^{TN} is the normalised theoretical intensity value corresponding to the jth sampling point, which is given by:

$$I_j^{TN} = (I_j^T(n,k,\phi_j^M - \theta_0) - I_{min}^T)\frac{I_{max}^M - I_{min}^M}{I_{max}^T - I_{min}^T} + I_{min}^M \tag{7.13}$$

where ϕ_j^M is the jth measured phase difference value, I_{min}^M, I_{max}^M, I_{min}^T and I_{max}^T are the minima and maxima of the measured and theoretical intensity curves which has been described in Section 7.2.2, and $I_j^T(n,k,\phi_j^M - \theta_0)$ is the theoretically derived intensity value corresponding to the jth sampling or measurement point, which can be obtained by using equation (5.6) and (5.7), or for simplicity, by using the following two equations (7.14) and (7.15):

$$\phi_j^M = -arg(\frac{r_{p20} + r_{p01}\,exp(i\beta_p)}{1 + r_{p20}r_{p01}\,exp(i\beta_p)}) + \theta_0 \tag{7.14}$$

$$I_j^T(n,k,\phi_j^M - \theta_0) = \left|\frac{r_{p20} + r_{p01}\,exp(i\beta_p)}{1 + r_{p20}r_{p01}\,exp(i\beta_p)}\right|^2 \tag{7.15}$$

If θ_0 is known beforehand, the optimisation becomes two-parameter estimation for the optical constant n and k. If the optical constant n and k are known beforehand, the optimisation becomes simple one parameter determination for the initial phase difference θ_0. If the three parameters are all unknown, they can be determined in the optimisation process all together. To obtain an accurate and reliable estimation result, the number of measurement or sampling points N should be big enough, e.g., larger than 20.

7.3.3 Optimisation algorithm selection

[NR, 1992] provides exhaustive and mature optimisation algorithms with C program routines. For one-dimensional minimisation without calculation of the derivative, the Bracket method, Brent's method, or Golden Section Search method can be used. For one-dimensional minimisation with calculation of the derivative, a variant of Brent's method can be used, which makes limited use of the first derivative information.

For multidimensional minimisation without computation of first derivatives, the Downhill Simplex method and Powell's method are available. There are two major families of algorithms for multidimensional minimisation with calculation of first derivatives. The first family includes the Fletcher-Reeves algorithm and the Polak-Ribiere algorithm. The second family includes the Davidon-Fletcher-Powell algorithm and the Broyden-Fletcher-Goldfarb-Shanno algorithm. Both families require a one-dimensional minimisation sub-algorithm, which can itself either use, or not use, the derivative information.

To obtain the optical constants and initial phase (three unknown parameters) from the measurement data, a few minimisation algorithms were tried, which included the Downhill Simplex method, Powell's method, the Davidon-Fletcher-Powell algorithm, the Fletcher-Reeves algorithm and the Polak-Ribiere algorithm. Among these algorithms, Powell's method is the most effective (the quickest) to solve our problem, the Davidon-Fletcher-Powell algorithm is next fastest. The other methods did not work well at all.

The C program routines for Powell's method are listed in Section A3.3 of Appendix 3.

8 Conclusions and Future Work

8.1 Conclusions

A review of several existing flying height or head-medium spacing measurement techniques has been given, with analysis and simulation for each so that their advantages and limitations can be appreciated.

An investigation with more detailed analysis and simulation was made of the application limit and potential problems of the intensity interferometry method, and the approach which needs to be used to ensure that this intensity-based method can be correctly implemented in practice. Two phase-shifting methods have been proposed to improve the sensitivity of this technique when the head-disk spacing is below 10 nm or near contact, one of which is based on fabricating the glass testing disk to have a specified thickness, and an alternative of which requires it to be coated with a specified thickness of thin carbon film.

A Dual Beam Normal Incidence Polarisation Interferometry Method has been proposed as a new measuring system, with in-depth theoretical analysis and extensive simulation. These simulation results show that this polarisation interferometry method can be used to measure the flying height or head-disk spacing down to contact without losing sensitivity. The method is also easily adaptable to serving the slider's pitch and roll, and hence can be used for dynamic characterisation of the slider's behaviours, an important factor when performing e.g. fast track changing.

An important advantage of this dual beam interferometry method is that it can be used for both the direct spacing measurement (DSM) method and relative displacement measuring (RDM) method. The RDM method is a good way to measure the head-disk

spacing and the slider pitch or roll when a real magnetic disk is used for testing. Although a special glass disk must be used for the DSM method, it has the benefit that the absolute head-disk spacing can be observed and measured directly, especially in the case where it is difficult for the light beam to be reflected from the back surface of the head-slider because of the presence of the gimbal assembly. It is also possible for the slider pitch or roll to be measured using the phase information. An additional benefit of this polarisation interferometry method is that, with the measured intensity and phase information, the optical constants of the slider material can also be determined if they are unknown beforehand, which is necessary to determine the flying height.

Considerable work was undertaken to build up the experimental system to test the capability and effectiveness of the Improved Intensity Interferometry method and Normal Incidence Polarisation Interferometry method we have proposed. The experimental testing system can be divided into three parts: the optical testing rig itself, the control electronics which consists of signal processing circuits, high voltage amplifiers, and power supply, and a PC for overall control and data logging with an analogue I/O board and software control program written in C.

A large number of experiments were conducted for the RDM method and the DSM method. In all these experiments, the testing disk was held in a stationary state and a PZT translator was used to move the head-slider sample to simulate the flying height variation. Experimental results show that the head-disk spacing or flying height can be measured under these conditions with great precision. The system in its present configuration has a general measurement resolution of about 0.5 nm because of system noise. This, it is believed, could be further improved by carefully refining the system's electronics and mechanics.

8.2 Future work

From the experimental results in Chapter 7, it can be seen that the dual-beam normal incidence polarisation interferometry experimental testing system has a rather satisfying measurement precision. However, because of noise sources of various kinds, the experimental testing system in its present configuration has a general system noise of about 0.5 nm in magnitude. This needs to be further improved by carefully refining the system electronics, optics and mechanics if higher measurement resolution is desired.

The current experiments were made in the condition where the testing disk is held in a stationary state and a piezoelectric translator is used to move the head slider to simulate the head-disk spacing variation. Further experiments would be necessary on a high quality disk-testing spin stand, and in that case the set-up of the dual beam polarisation interferometry testing system needs to be modified to accommodate this different mechanical arrangement. The following issues should be considered in building up the testing system on the spin stand:

- The noise induced by the rotating testing disk (both electrical and mechanical) must be isolated from the interferometry testing system as much as possible.
- It will be inevitable for the interferometry testing system to pick up some of the residual noises induced by the working spin stand, so signal processing methods will need to be used to filter out such noise sources.
- The optical testing rig of the interferometry system should be made more compact to reduce mechanical vibrations in its structure. The adjustment of the optical system could be improved and parts of the system calibration could be made automatic.

With the modifications noted above, the system developed here would be close to commercial implementation. A further important area for future work is the proving

and refining of measurements of slider's dynamics – i.e. pitch and roll. Such measurements are not made by any system currently in commercial use, but would be an important addition to the knowledge of the slider's aerodynamic behaviour, especially during rapid track changes.

Appendix 1

Mechanical drawings

This appendix contains some drawings of the mechanical parts for the testing rig.

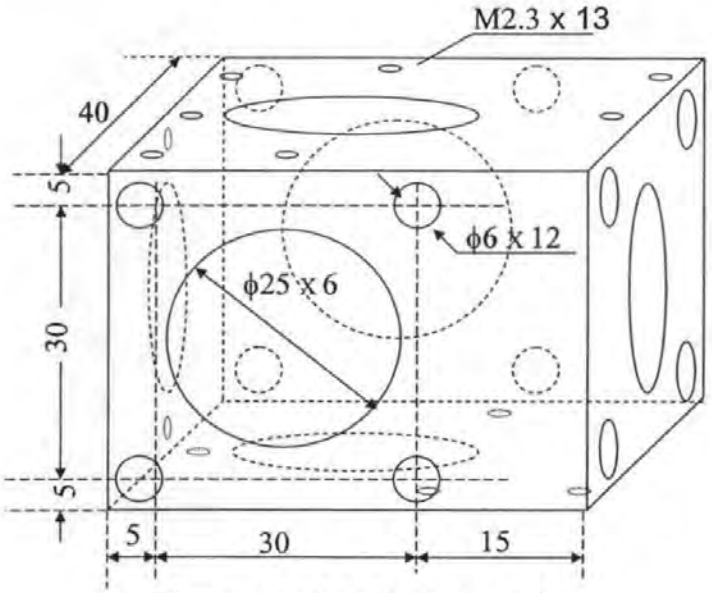

Figure A1.1 Mechanical part 1

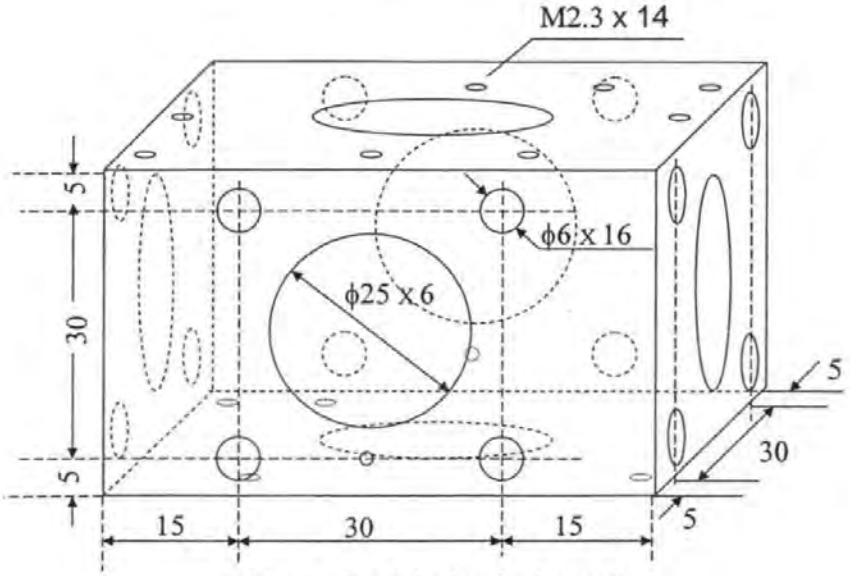

Figure A1.2 Mechanical part 2

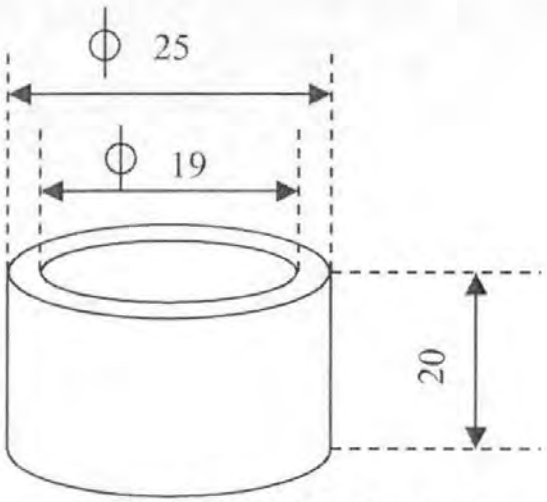

Figure A1.3 Mechanical part 3

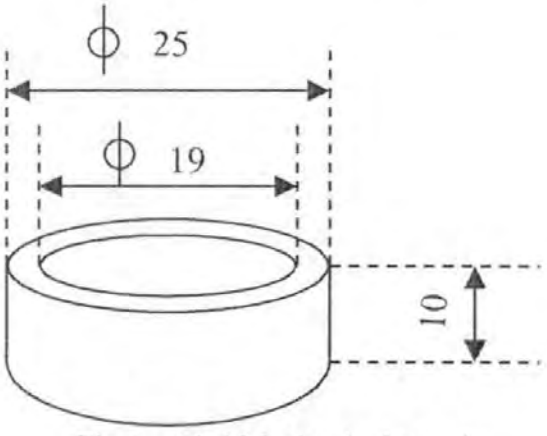

Figure A1.4 Mechanical part 4

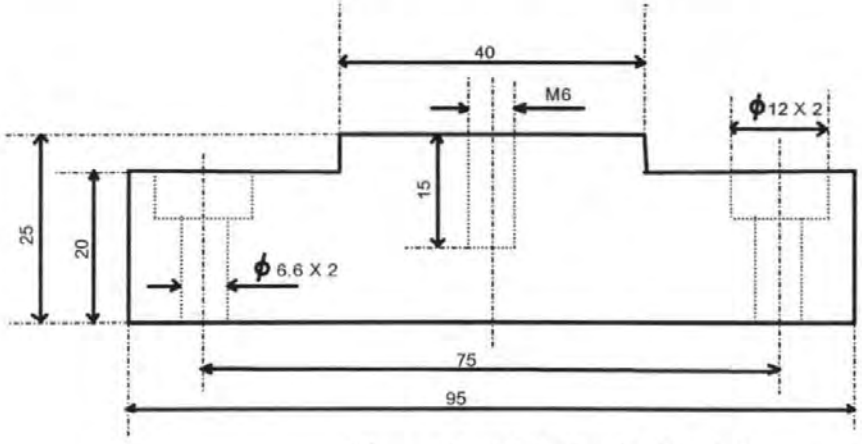

Figure A1.5 Mechanical part 5

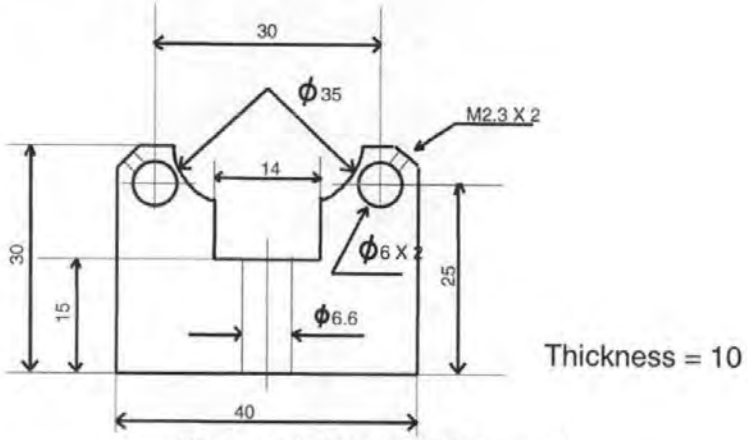

Figure A1.6 Mechanical part 6

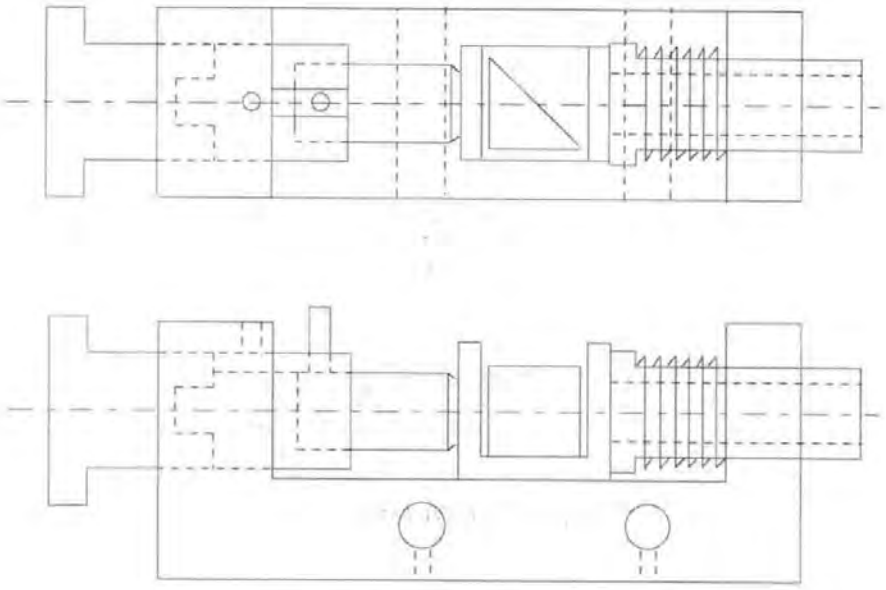

Figure A1.7 Mechanical part 7

Mechanical part 7 in Figure A1.7 is assembled from the following parts in Figure A1.8–1.11.

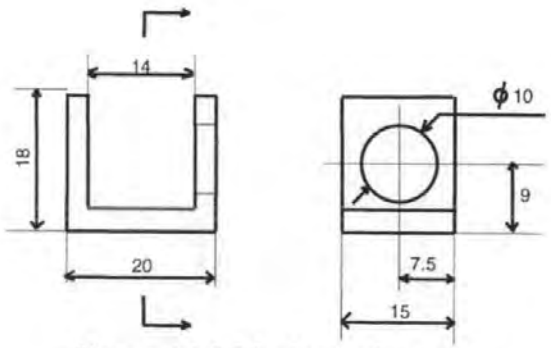

Figure A1.8 Mechanical part 7a

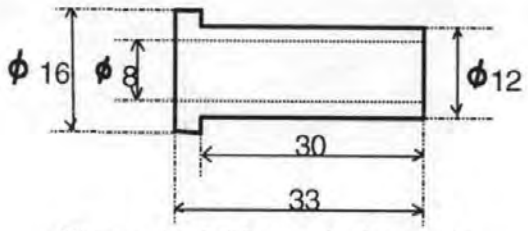

Figure A1.9 Mechanical part 7b

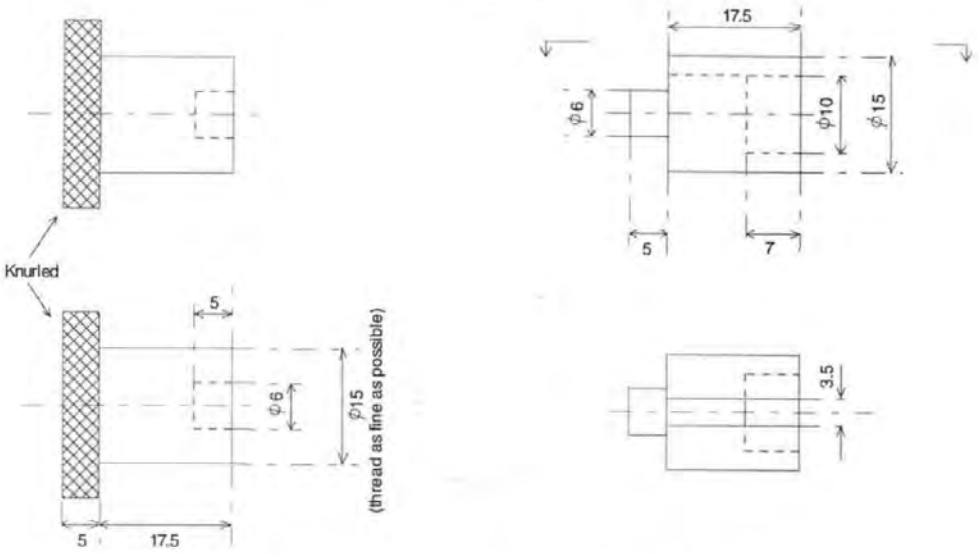

Figure A1.10 Mechanical part 7c

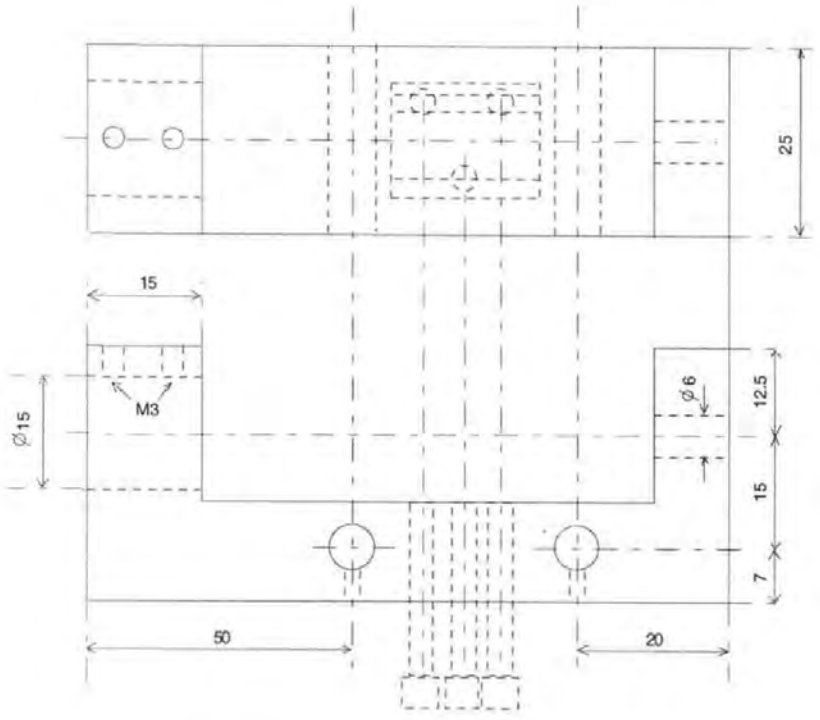

Aluminium
Quantity: 1

Figure A1.11 Mechanical part 7d

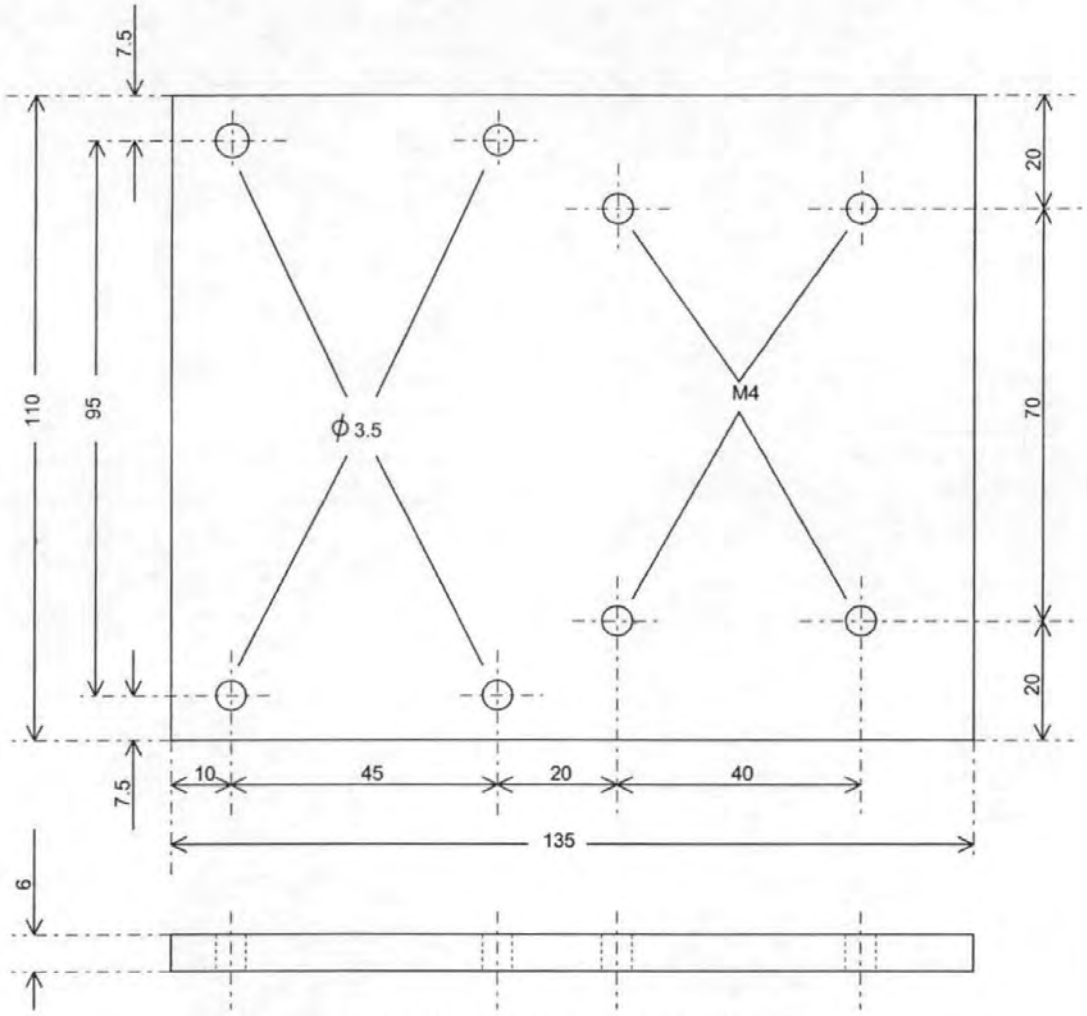

Figure A1.12 Hard disk drive holder (part 8a)

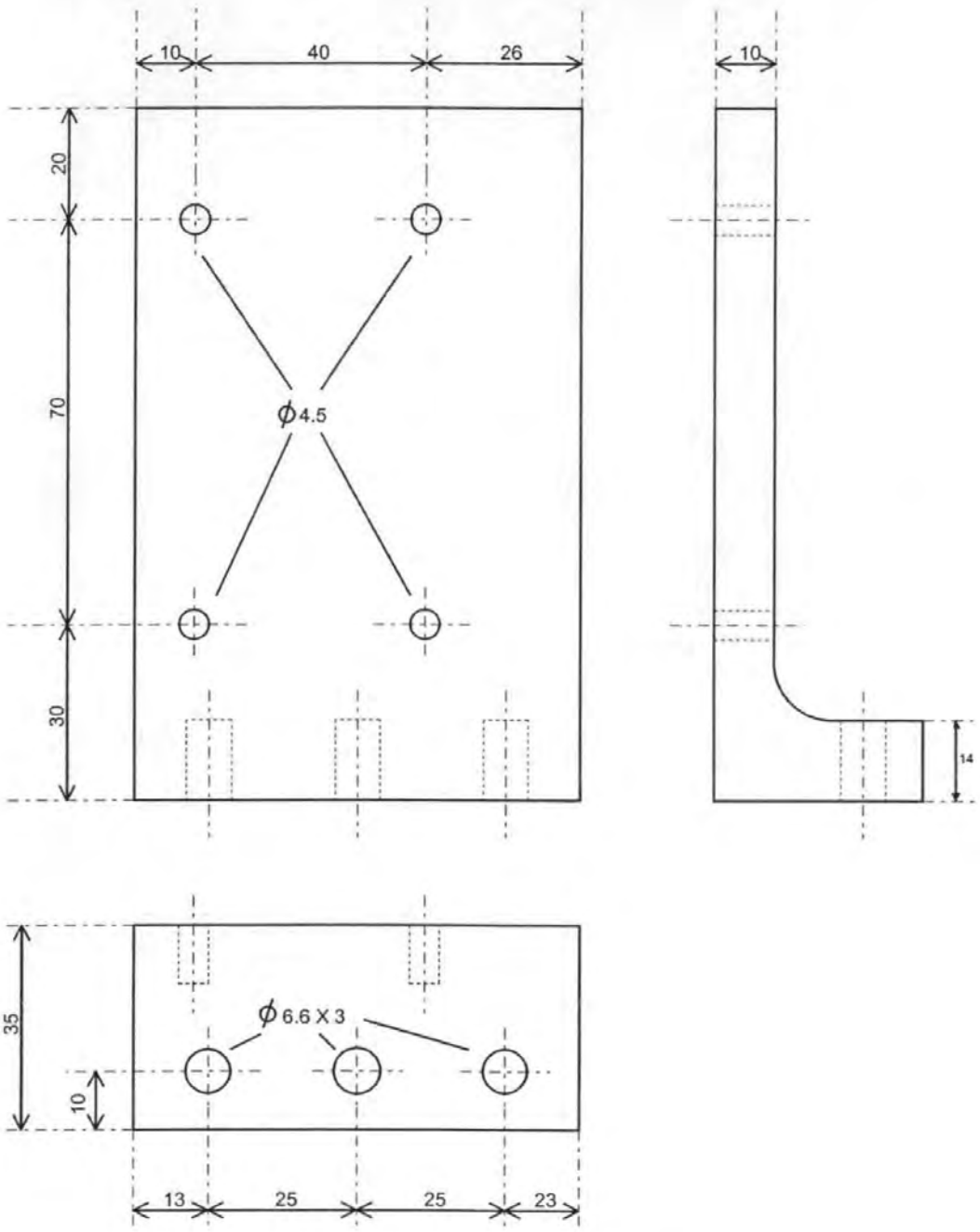

Figure A1.13 Hard disk drive holder (part 8b)

Appendix 2

Electronic circuit diagrams

This appendix contains the circuit diagrams, PCB layout, and system connections. The circuit diagrams are given on PCB basis.

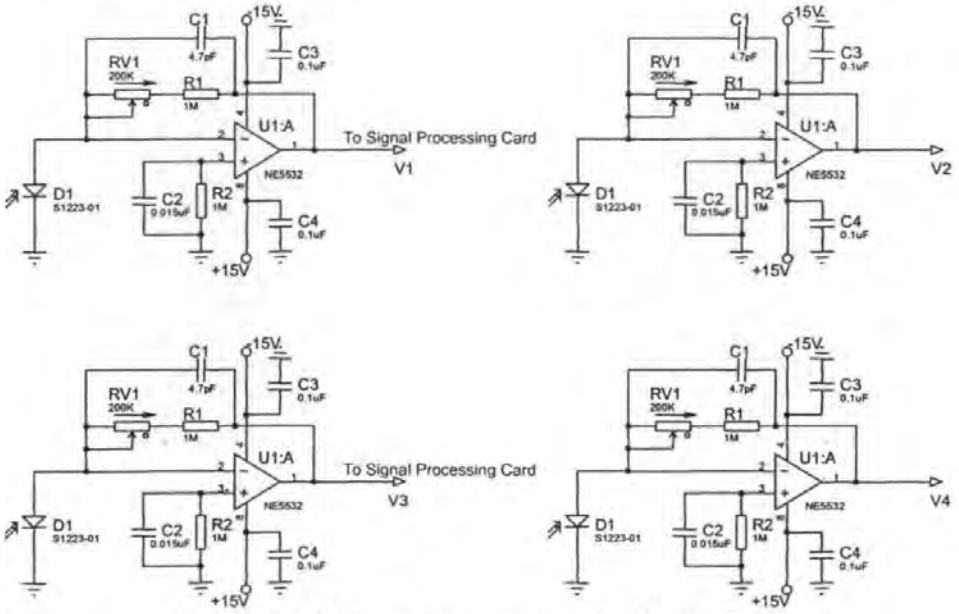

Figure A2.1 Photo detector circuit (Four PCBs)

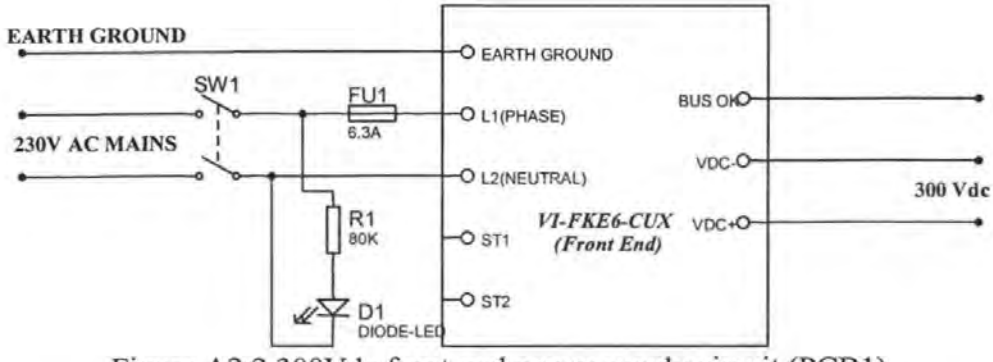

Figure A2.2 300Vdc front-end power supply circuit (PCB1)

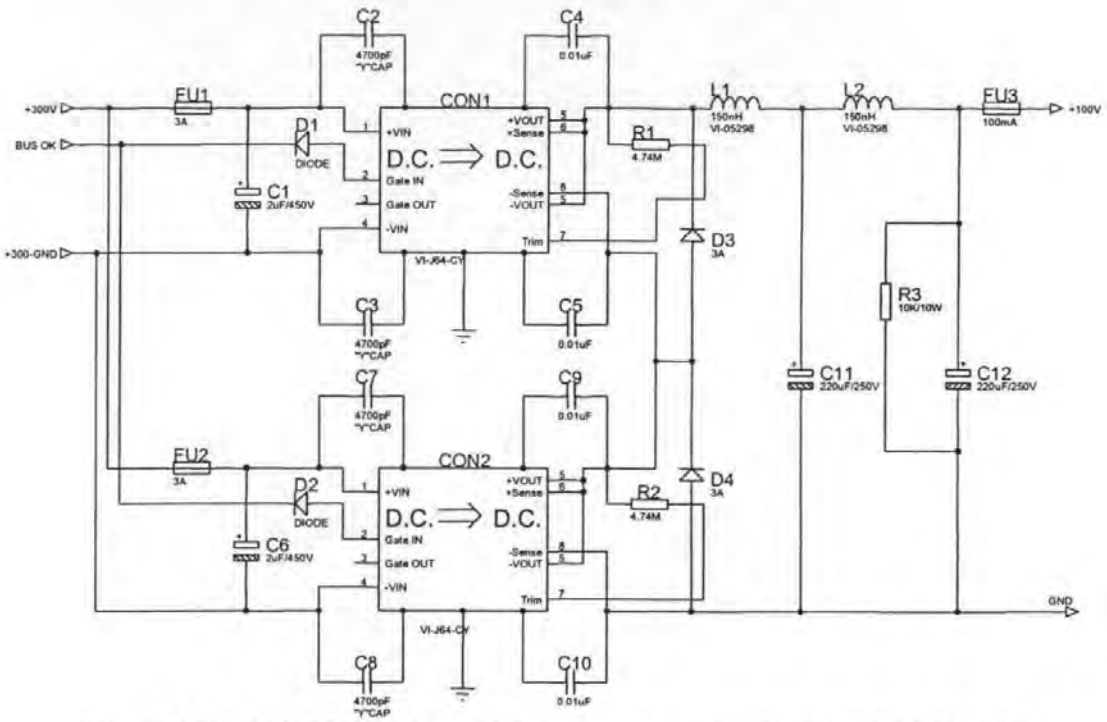

Figure A2.3 ±100Vdc high precision power supply circuit (PCB2/PCB3)

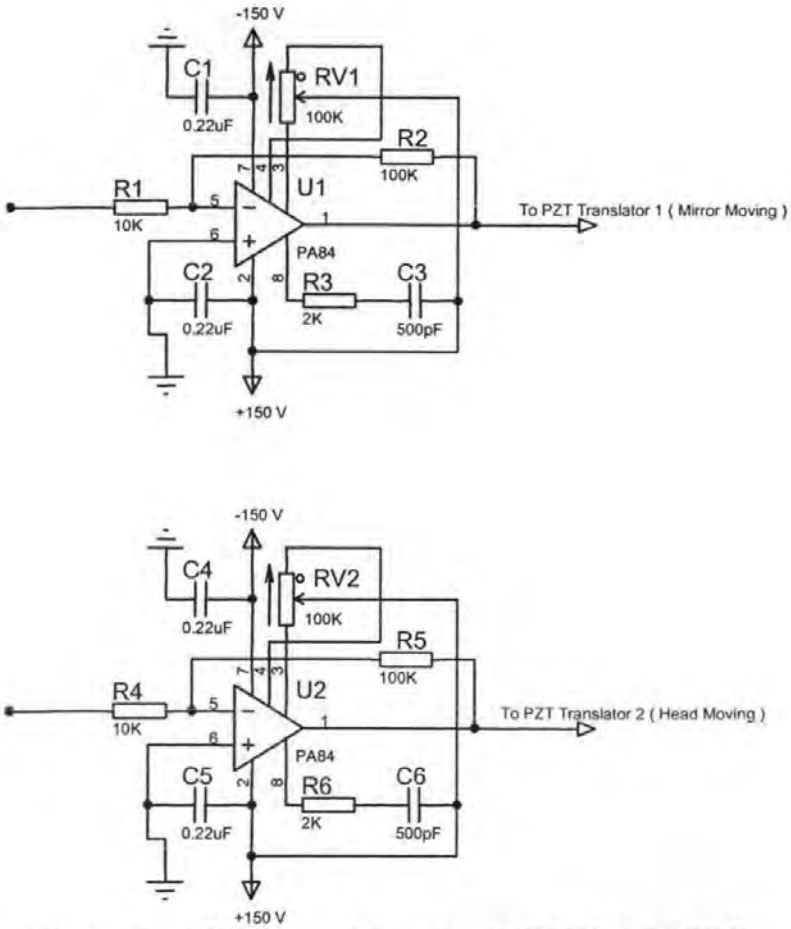

Figure A2.4 Power amplifier circuit (PCB4 and PCB5)

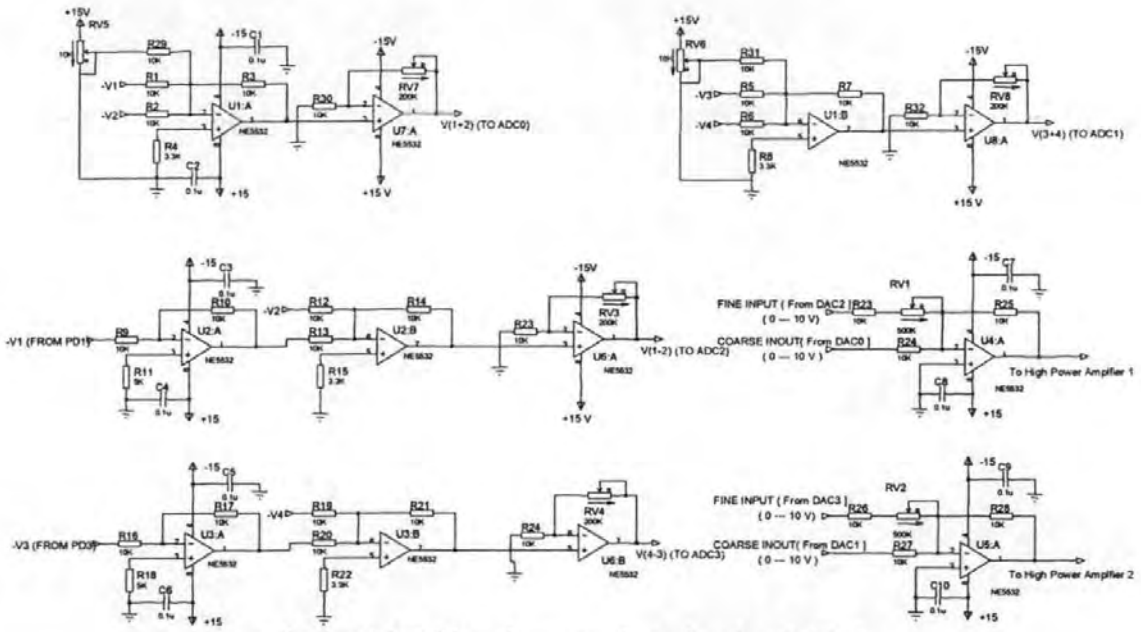

Figure A2.5 Signal processing circuits (PCB6)

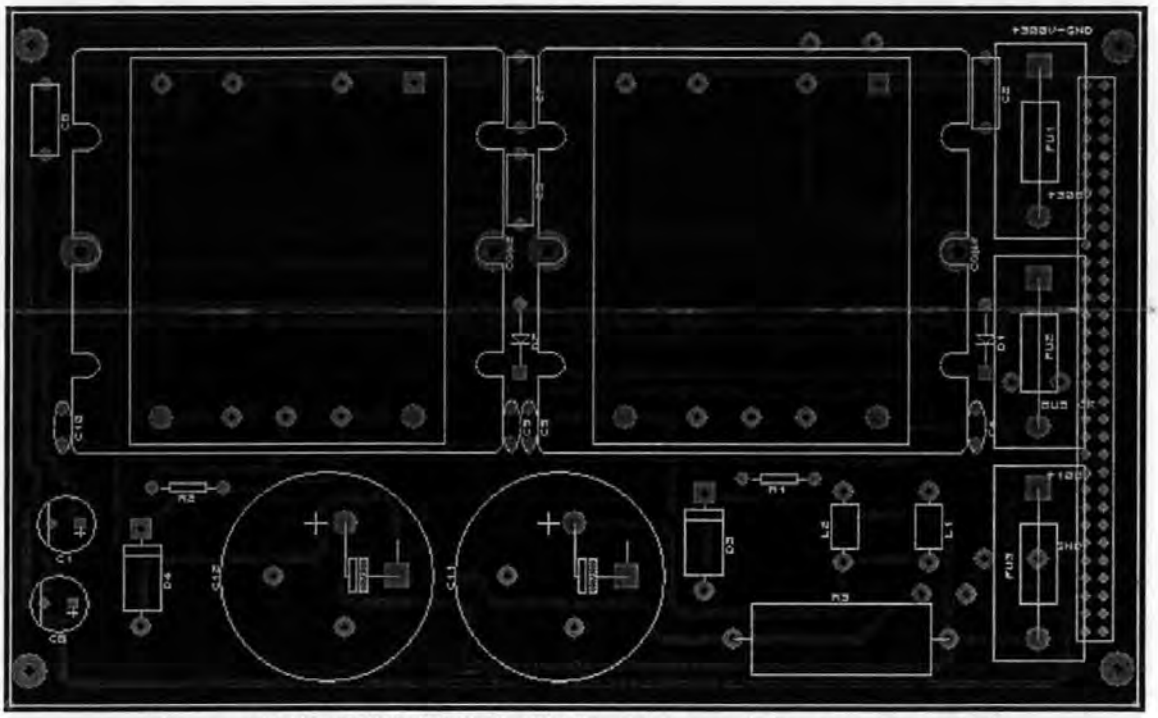

Figure A2.6 PCB2/PCB3 (±100Vdc high precision power supply)

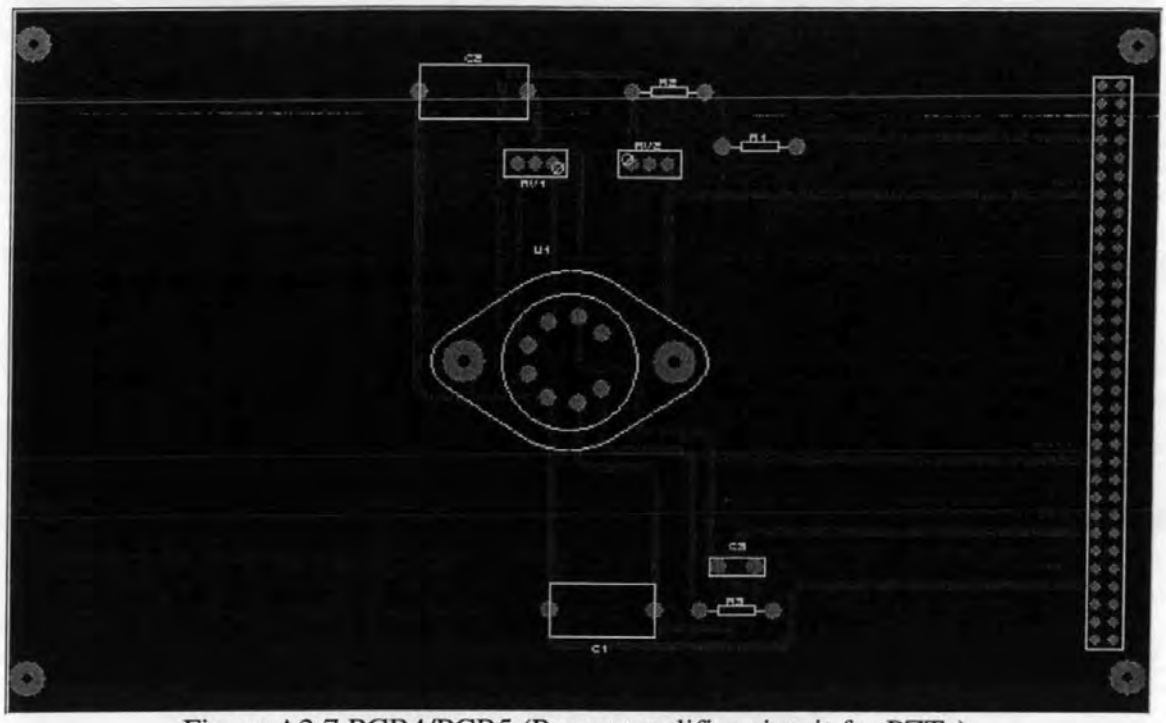

Figure A2.7 PCB4/PCB5 (Power amplifier circuit for PZTs)

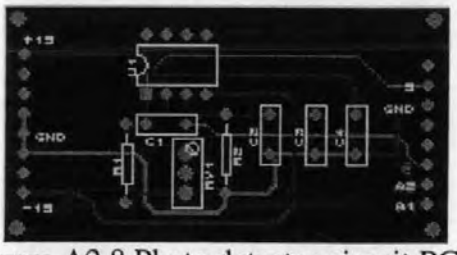

Figure A2.8 Photo detector circuit PCB

Figure A2.9 Photo detector clamping PCB

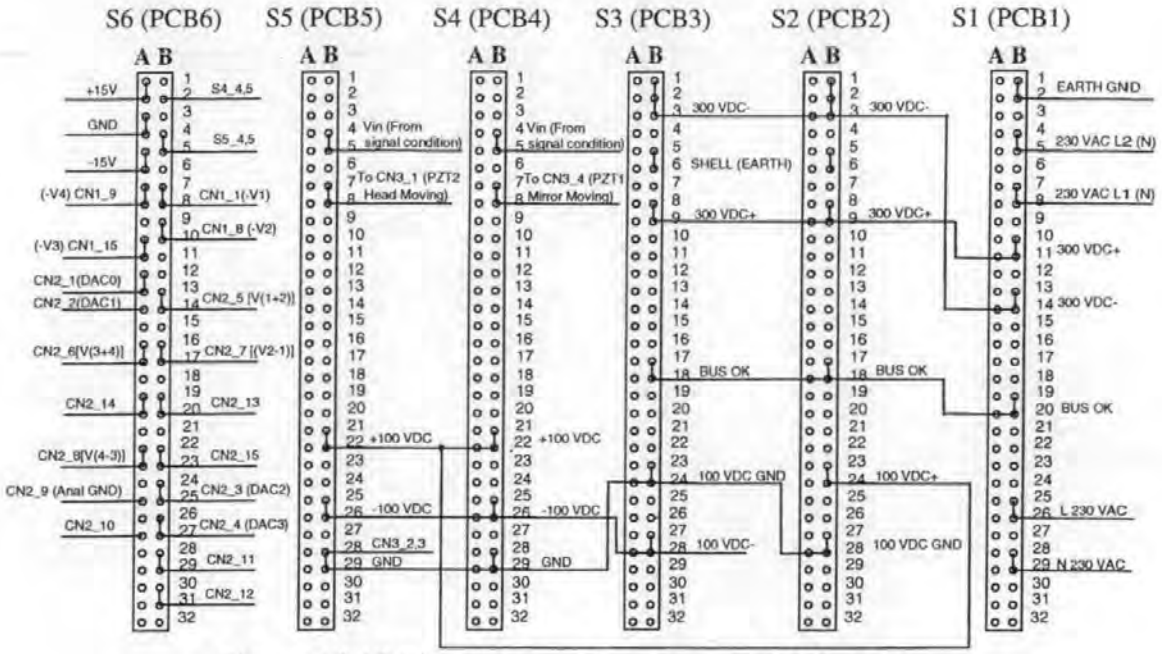

Figure A2.10 Signal connections between PCB sockets

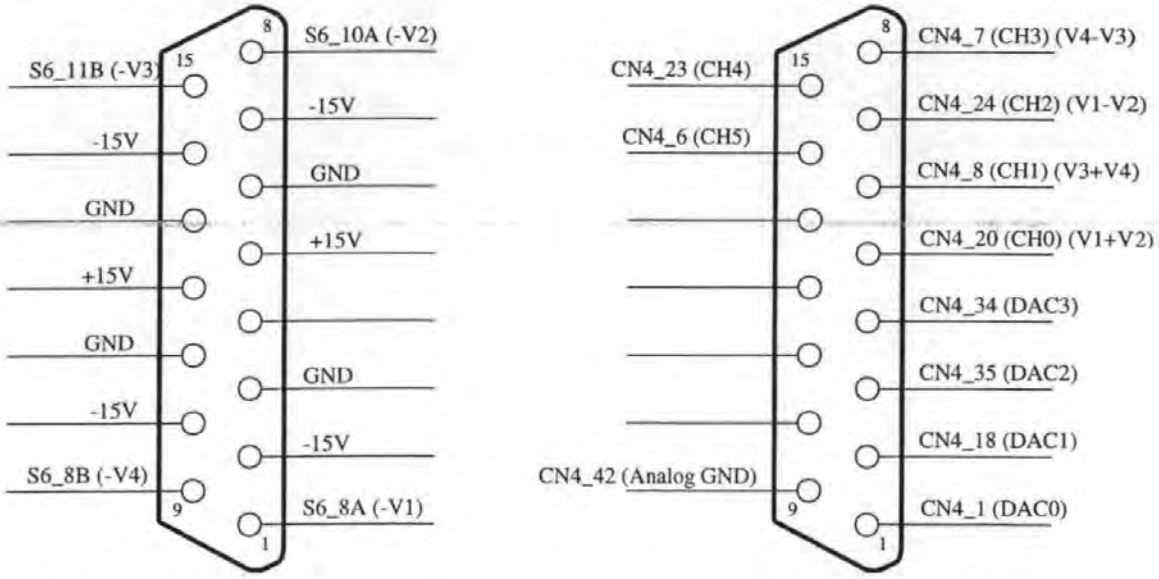

CN1: to photo detectors **CN2:** to PC-30C connector

Figure A2.11 Connector configuration (CN1 and CN2)

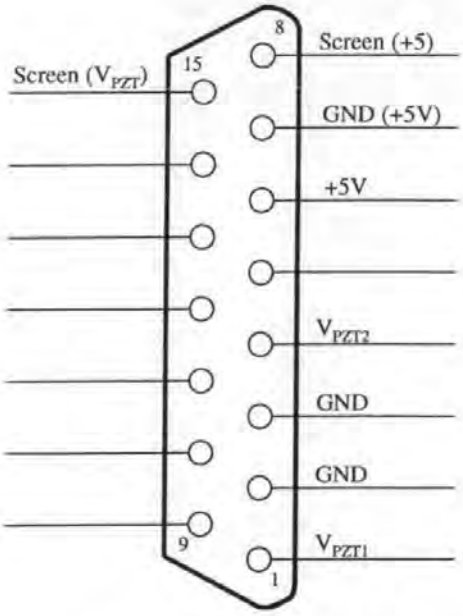

CN3: to Laser and PZTs

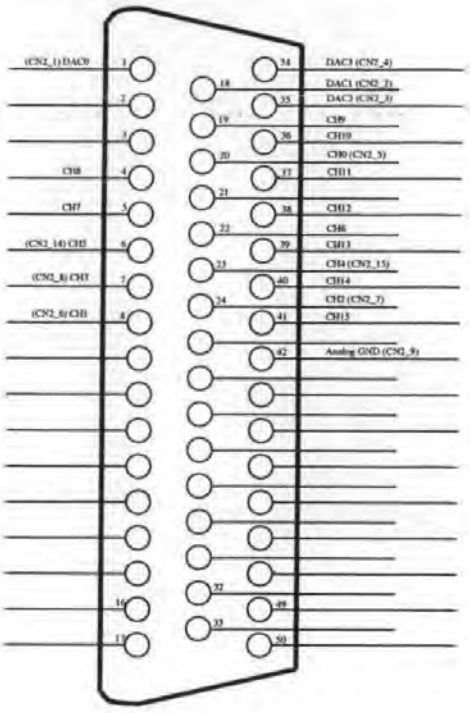

CN4: to CN2

Figure A2.12 Connector configuration (CN3 and CN4)

The electronic components used in the system can be found in the component order list below in Table A2.1—A2.3.

Stock no.	Description	Order Quantity
302-693	NE5532N, Low noise op-amp	6
262-501	1N5402, 3A, 200V, plastic encapsulated diode	6
105-509	220μF/250V capacitor	4
107-791	10000pF, 1kV, ceramic capacitor	8
214-6293	4700pF, class 'Y' 275V a.c.	8
318-042	Min. illuminated rocker switch, Red DPST	2
197-9480	Fuse clips	1(bag)
100-0051	Quick-acting Fuse, 3A, 250V	12
416-562	Quick-acting Fuse, 100mA, 250V	6
500-730	Card front, 3U, 12HP width	3
500-702	Card front, 3U, 6HP width	3
500-550	Card guide, 160mm card	14+2
500-847	Card mounting bracket	12+2
236-5719	5×20 mm fuse screw cap	1
261-5834	Chassis plug IEC Inlet, PCB mount	1
475-993	32-way plug	5
476-075	32-way skt	1
435-484	Single-sided plain copper-clad board, 100×160	5
434-267	100×160 development board	1
182-7777	0.1μF 400Vd.c. Capacitor	6
182-7783	0.22μF 400Vd.c. Capacitor	4
154-2072	100kΩ potentiometer	2
154-2050	10kΩ potentiometer	2

367-577	4 Core individually screened cable	1 reel (50m)
472-893	50-way plug, D type	1
480-153	50-way screwdown cover, D type	1

Table A2.1 Components ordered from RS

Product code	Description	Order quantity
VI-J64-CY	VI-J00 MiniMod DC-DC Converters, 50W	4
VI-FKE6-CUX	300V dc front end power supply	1
05298	Inductor, 130-150nH	4

Table A2.2 Components ordered from Vicor

Product code	Description	Order quantity
PA84	Power operational amplifier	2
MS03	Mating socket	2

Table A2.3 Components ordered from APEX Microtechnology

Appendix 3

Software C programs

This appendix contains the main body of C code written through out the whole thesis.

A3.1 Relative displacement flying height measuring method program

```
/*      File:   Displacement.c
*************************************************************************
*                                                                       *
*  Copyright (C) 1999       X. Liu.                                     *
*                                                                       *
*  The information in this document is subject to change without notice *
*  and should not be construed as a commitment.                         *
*  No responsibility is assumed for any errors that may appear in       *
*  this document or for the use or reliability of any portion of this   *
*  document or the described software.                                  *
*                                                                       *
*                                                                       *
*************************************************************************

*************************************************************************
*************************************************************************

                            MODULE FUNCTION :

*  This is the software part of the experimental system when used to make *
*  displacement measurement.                                            *
*************************************************************************

        Written : X. Liu                        September 1999.

*************************************************************************

        Language : Microsoft Visual C++ V1.0

*************************************************************************

        Other Software Required : Must be linked with C30M_X.lib

*************************************************************************

        Hardware required : IBM PC/XT/AT or compatible with 256K of memory,
        and a PC-30.

*************************************************************************

        Restrictions : None.

*************************************************************************

                            Module description :
```

```
        DAC0 is coarse input to the power amplifier for PZT1.
        DAC1 is coarse input to the power amplifier for PZT2.
        DAC2 is fine input to the power amplifier for PZT1.
        DAC3 is fine input to the power amplifier for PZT2.
        ADC0 samples V(1+2), i.e., the intensity signal (not used in this module).
        ADC1 samples V(3+4), i.e., also the intensity signal (not used in this module).
        ADC2 samples V(1-2), i.e. Cos signal.
        ADC3 samples V(4-3), i.e. Sin signal.
        The disk head-slider is moved by the PZT translator in a linear or saw-
        wave form. The output signals of the interferometric receiver are sampled
        and can be saved by the computer. Displacement (or phase-difference) is then
        derived from the Sin and Cos signals. All the signals can be displayed on
        screen if needed.

*****************************************************************************
*****************************************************************************
*****************************************************************************/
#include <graph.h>
#include <stdio.h>
#include <stdlib.h>
#include <conio.h>
#include <math.h>
#define data_30
#include "pc30.h"
#define badd  0x700
int d_a2[10000],d_a3[10000],da0_v,da1_v,da2_v,da3_v,ad0_v,ad1_v,
    ad2_v,ad3_v,max_ad2,min_ad2,start1,end1,max_ad3,min_ad3;
void main(void)
  {
  FILE *fp,*fp1;
  char ch1,file[20];
  int i,j,k,k1;
  float m,x_contract,y_contract;
  double f1,p0,p1,p_max,p_min,ang0,ang1,norm,ad2_f,ad3_f,ad2_f0,ad3_f0,
         mid_ad2,mid_ad3;
  struct _videoconfig v;
  base_30 = badd;

  j = version();
  i = j/256;
  m = (float) j - i*256;
  m = i + m/100.0F;
  printf("\nPC-30 Driver Version %5.2f", m);

again2:
  printf("\n Do you want to start (y/n): ");
  ch1=getche();
  if(ch1!='y') goto again2;

  if (diag()) printf("\n PC-30 fault.");
  else if (type_30 < found_39)
  printf("\n PC-39, PC-30B, PC-30C, PC-30D or PC-30 PG required.");
  else
    {
    init();
    dma_init();
    ad_prescaler(4);
    ad_clock(50);
    da0_v=0;
    da1_v=0;
    da2_v=0;
    da3_v=0;
    da_out(2, da2_v);
    da_out(3, da3_v);
    printf("\n Press any key to stop ");
    k=1;

/* Calibration: finding the middle value of Sin and Cos signals */
    printf("\nCALIBRATION IS CARRYING ON, PLEASE WAIT.....");
    max_ad2=0;
    min_ad2=0;
    max_ad3=0;
    min_ad3=0;
    loop0:
    while ((da0_v<2047)&&(k<20000))
      {
      da_out(0, da0_v);
      da_out(1, da1_v);
```

```
        da0_v++;
        da1_v++;
        for(i=1;i<500;i++);
        ad_in(2, &ad2_v);
        ad_in(3, &ad3_v);
        if(max_ad2<ad2_v) max_ad2=ad2_v;
        if(min_ad2>ad2_v) min_ad2=ad2_v;
        if(max_ad3<ad3_v) max_ad3=ad3_v;
        if(min_ad3>ad3_v) min_ad3=ad3_v;
        k=k+1;
        }
      while ((da0_v>0)&&(k<20000))
        {
        da_out(0, da0_v);
        da_out(1, da1_v);
        da0_v--;
        da1_v--;
        for(i=1;i<500;i++);
        ad_in(2, &ad2_v);
        ad_in(3, &ad3_v);
        if(max_ad2<ad2_v) max_ad2=ad2_v;
        if(min_ad2>ad2_v) min_ad2=ad2_v;
        if(max_ad3<ad3_v) max_ad3=ad3_v;
        if(min_ad3>ad3_v) min_ad3=ad3_v;
        k=k+1;
        }
      if (k<20000) goto loop0;
      da0_v=0;
      da1_v=0;
      da_out(0, da0_v);    /* Reset PZT2) */
      da_out(1, da1_v);  /* Reset PZT2) */
      mid_ad2=min_ad2+(max_ad2-min_ad2)/2.0;  /* Middle (zero) value of Cos signal) */
      mid_ad3=min_ad3+(max_ad3-min_ad3)/2.0;  /* Middle (zero) value of Sin signal) */
      f1=(max_ad3-min_ad3);
      f1=f1/(max_ad2-min_ad2);      /* Normalization factor of Sin and Cos signals */

      printf("\n f1,(max_ad3-min_ad3),(max_ad2-min_ad2),%f,%d,%d",f1,(max_ad3-
             min_ad3),(max_ad2-min_ad2));
      printf("\nCALIBRATION FINISHED!");
      printf("\nPLEASE PRESS ANY KEY TO CARRY ON...");

      _getch();

try:
      printf("\nKEY IN DATA FILE NAME WHICH THE Sin and Cos SIGNALS WILL BE WRITTEN IN:");
      scanf("%s",file);
      if((fp=fopen(file,"wb"))==NULL)
        {
        printf("\nCANNOT OPEN FILE, PLEASE CHECK DISK AND TRY AGAIN");
        goto try;
        }
      fwrite(&mid_ad2, sizeof(double),1,fp);
      fwrite(&mid_ad3, sizeof(double),1,fp);
      fwrite(&f1, sizeof(double),1,fp);

      da0_v=1200;     /* start point of PZT1 control voltage (range:0 to 4095) */
      da1_v=1200;     /* start point of PZT2 control voltage (range:0 to 4095) */
      da2_v=0;
      da3_v=0;
      k=1;
      /* Start measuring, Sample data in */
loop:

      if (kbhit()) goto exit;
      while ((da0_v<1240)&&(k<5000))      /* sweep between 1200 to 1240 */
        {
        /*
        da_out(0, da0_v);
        da_out(1, da1_v);
        */
        da0_v++;
        da1_v++;
        for(i=1;i<500;i++);
        ad2_f0=0.0;
        ad3_f0=0.0;
        for(i=1;i<2;i++)
          {
          ad_in(2, &ad2_v);
```

```
        ad_in(3, &ad3_v);
        ad2_f=ad2_f0+ ad2_v/1.0;      /* this filting part is no effect now */
        ad2_f0=ad2_f;
        ad3_f=ad3_f0+ ad3_v/1.0;
        ad3_f0=ad3_f;
        }
      fwrite(&ad2_f, sizeof(double),1,fp);
      fwrite(&ad3_f, sizeof(double),1,fp);
      k=k+1;
      }
    while ((da0_v>1200)&&(k<5000))
      {
      /*
      da_out(0, da0_v);
      da_out(1, da1_v);
      */
      da0_v--;
      da1_v--;
      for(i=1;i<500;i++);
      ad2_f0=0.0;
      ad3_f0=0.0;
      for(i=1;i<2;i++)
        {
        ad_in(2, &ad2_v);
        ad_in(3, &ad3_v);
        ad2_f=ad2_f0+ ad2_v/1.0;  /* this filting part is no effect now */
        ad2_f0=ad2_f;
        ad3_f=ad3_f0+ ad3_v/1.0;
        ad3_f0=ad3_f;
        }
      fwrite(&ad2_f, sizeof(double),1,fp);
      fwrite(&ad3_f, sizeof(double),1,fp);

      k=k+1;
      }
    if (k<5000) goto loop;
    fclose(fp);
    da0_v=0;
    da1_v=0;
    da_out(0, da0_v);
    da_out(1, da1_v);
again3:
    printf("\n Do you want to draw the curve (y/n): ");
    ch1=getche();
    if(ch1=='n') goto again7;
    if(ch1!='y') goto again3;
    printf("\nPLEASE INPUT DATA FILE NAME: ");
    scanf("%s",file);
    if((fp=fopen(file,"rb"))==NULL)
      {
      printf("\nCANNOT OPEN FILE\n");
      exit(1);
      }
    if( !_setvideomode( _MAXRESMODE ) )
    exit( 1 );
    _getvideoconfig( &v );
    _clearscreen(_GCLEARSCREEN);
    _setcolor(1);
    _moveto_w( 0, v.numypixels/2 );
    _lineto_w(v.numxpixels, v.numypixels/2);
    _moveto_w( 0, v.numypixels/2 );
    fread(&mid_ad2, sizeof(double),1,fp);
    fread(&mid_ad3, sizeof(double),1,fp);
    fread(&f1, sizeof(double),1,fp);

    for(k=1; k<4999; k++)
      {
      fread(&ad2_f, sizeof(double),1,fp);
      fread(&ad3_f, sizeof(double),1,fp);
      _lineto_w(k/8, v.numypixels/2-(ad2_f-2048)/10);
      }
    fclose(fp);
    if((fp=fopen(file,"rb"))==NULL)
      {
      printf("\nCANNOT OPEN FILE\n");
      exit(1);
      }
    _setcolor(2);
```

```
    _moveto_w( 0, v.numypixels/2 );
    fread(&mid_ad2, sizeof(double),1,fp);
    fread(&mid_ad3, sizeof(double),1,fp);
    fread(&f1, sizeof(double),1,fp);
    for(k=1; k<4999; k++)
      {
      fread(&ad2_f, sizeof(double),1,fp);
      fread(&ad3_f, sizeof(double),1,fp);
      _lineto_w(k/8, v.numypixels/2-(ad3_f-2048)/10);
      }
    fclose(fp);
    _getch();

again5:
    printf("\nDO YOU WANT TO REDRAW THIS CURVE (Y/N) ?");
    ch1=getche();
    if(ch1=='n') goto again7;
    if(ch1!='y') goto again5;
again6:
    printf("\nPLEASE INPUT DATA FILE NAME: ");
    scanf("%s",file);
    if((fp=fopen(file,"rb"))==NULL)
      {
    printf("\nCANNOT OPEN FILE\n");
    exit(1);
    }
  printf("\nPLEASE INPUT PLOT PARAMETER: x_contract (e.g. 16 or 32)");
  scanf("%f",&x_contract);
  printf("\nPLEASE INPUT PLOT PARAMETER: y_contract (e.g. 10)");
  scanf("%f",&y_contract);
  if( !_setvideomode( _MAXRESMODE ) )
  exit( 1 );
  _getvideoconfig( &v );
  _clearscreen(_GCLEARSCREEN);
  _setcolor(1);
  _moveto_w( 0, v.numypixels/2 );
  _lineto_w(v.numxpixels, v.numypixels/2);
  _moveto_w( 0, v.numypixels/2 );
  fread(&mid_ad2, sizeof(double),1,fp);
  fread(&mid_ad3, sizeof(double),1,fp);
  fread(&f1, sizeof(double),1,fp);
  for(k=1; k<4999; k++)
    {
    fread(&ad2_f, sizeof(double),1,fp);
    fread(&ad3_f, sizeof(double),1,fp);
    _lineto_w(k/x_contract, v.numypixels/2-(ad2_f-2048)/y_contract);

    }
  fclose(fp);
  if((fp=fopen(file,"rb"))==NULL)
    {
  printf("\nCANNOT OPEN FILE\n");
  exit(1);
    }
  _setcolor(2);
  _moveto_w( 0, v.numypixels/2 );
  fread(&mid_ad2, sizeof(double),1,fp);
  fread(&mid_ad3, sizeof(double),1,fp);
  fread(&f1, sizeof(double),1,fp);
  for(k=1; k<4999; k++)
    {
    fread(&ad2_f, sizeof(double),1,fp);
    fread(&ad3_f, sizeof(double),1,fp);
    _lineto_w(k/x_contract, v.numypixels/2-(ad3_f-2048)/y_contract);
    }
  fclose(fp);
  _getch();

    /*************************************************************************/

again7:
  printf("\nDO YOU WANT TO REDRAW THE Sin AND Cos SIGNAL CURVES WITH MODIFICATION (Y/N)
        ?");
  ch1=getche();
  if(ch1=='n') goto exit;
  if(ch1!='y') goto again7;
again8:
  printf("\nPLEASE INPUT DATA FILE NAME: ");
```

```
    scanf("%s",file);
    if((fp=fopen(file,"rb"))==NULL)
      {
      printf("\nCANNOT OPEN FILE\n");
      exit(1);
      }

    printf("\nPLEASE INPUT PLOT PARAMETER: x_contract (e.g. 0.1, 1, 16 or 32)");
    scanf("%f",&x_contract);   /* x_contract is the time the x_axis will be reduced */
    printf("\nPLEASE INPUT PLOT PARAMETER: y_contract (e.g. 10)");
    scanf("%f",&y_contract);   /* y_contract is the time the y_axis will be reduced */
    if( !_setvideomode( _MAXRESMODE ) )
    exit( 1 );
    _getvideoconfig( &v );
    _clearscreen(_GCLEARSCREEN);

  /* Draw the Cos signal */
    _setcolor(1);
    _moveto_w( 0, v.numypixels/2);
    _lineto_w(v.numxpixels, v.numypixels/2);
    _moveto_w( 0, v.numypixels/2);
    fread(&mid_ad2, sizeof(double),1,fp);
    fread(&mid_ad3, sizeof(double),1,fp);
    fread(&f1, sizeof(double),1,fp);
    for(k=1; k<4999; k++)
      {
      fread(&ad2_f, sizeof(double),1,fp);
      fread(&ad3_f, sizeof(double),1,fp);
      _lineto_w(k/x_contract, v.numypixels/2-(ad2_f-mid_ad2)/y_contract);
      }
      fclose(fp);

      if((fp=fopen(file,"rb"))==NULL)
        {
        printf("\nCANNOT OPEN FILE\n");
        exit(1);
        }

  /* Draw the Sin signal */

      _setcolor(2);
      _moveto_w( 0, v.numypixels/2);
      _lineto_w(v.numxpixels, v.numypixels/2);
      _moveto_w( 0, v.numypixels/2);
      fread(&mid_ad2, sizeof(double),1,fp);
      fread(&mid_ad3, sizeof(double),1,fp);
      fread(&f1, sizeof(double),1,fp);
      for(k=1; k<4999; k++)
        {
        fread(&ad2_f, sizeof(double),1,fp);
        fread(&ad3_f, sizeof(double),1,fp);
        _lineto_w(k/x_contract, v.numypixels/2-(ad3_f-mid_ad3)/y_contract);
        }
      fclose(fp);

      _getch();
      printf("\nDO YOU WANT TO REDRAW THE Sin AND Cos SIGNAL CURVES AFTER MODIFICATION
             (Y/N) ?");
      ch1=getche();
      if(ch1=='y') goto again8;

      /*****************************************************************
       *       Phase unwraping to derive the displacement              *
      *****************************************************************/
  again9:
      if((fp=fopen(file,"rb"))==NULL)
        {
        printf("\nCANNOT OPEN FILE\n");
        exit(1);
        }       /* Open Sin and Cos curve data file*/

  /* Draw any small part of the displacement curve */
  try1:
      printf("\nNOW A SMALL PART OF THE DISPLACEMENT WILL BE DISPLAYED");
      printf("\nPLEASE INPUT START POINT: (1 to 4999) (e.g. 1000) ");
      scanf("%d",&start1);
      printf("\nPLEASE INPUT END POINT: (2 to 4999) (e.g. 1020)");
      scanf("%d",&end1);
```

```
    printf("\nPLEASE INPUT NEW DATA FILE NAME THE DISPLACEMENT DATA WILL BE WRITTEN
            IN:");
    printf("\n(DON'T USE THE NAME OF USEFUL DATA FILES!!!!!!!)");
    scanf("%s",file);

    if((fp1=fopen(file,"wb"))==NULL)
      {
      printf("\nCANNOT OPEN FILE, PLEASE CHECK DISK AND TRY AGAIN");
      goto try1;
      }

    fread(&mid_ad2, sizeof(double),1,fp);
    fread(&mid_ad3, sizeof(double),1,fp);
    fread(&f1, sizeof(double),1,fp);

    for(k=1; k<start1; k++)
      {
      fread(&ad2_f, sizeof(double),1,fp);
      fread(&ad3_f, sizeof(double),1,fp);
      }           /* Move the data reading point to 'start1' */

    p0=0;
    p1=0;
    ang0=0;
    ang1=0;
    p_max=-6.28;
    p_min=+6.28;

    for(k=start1; k<=end1; k++)
      {
      fread(&ad2_f, sizeof(double),1,fp);
      fread(&ad3_f, sizeof(double),1,fp);

      ang1=atan2((ad3_f-mid_ad3),(f1*(ad2_f-mid_ad2)));
      if((ang1-ang0)<-3.14) p1=p0+ang1-ang0+2*3.1415926;
      else if ((ang1-ang0)> 3.14) p1=p0+ang1-ang0-2*3.1415926;
      else p1=p0+ang1-ang0;
      fwrite(&p1, sizeof(double),1,fp1);
      p0=p1;
      ang0=ang1;
      if(p_max<p1) p_max=p1;
      if(p_min>p1) p_min=p1;
      }
    fclose(fp);
    fclose(fp1);
    if(p_max>-p_min) norm=p_max;     /* norm is used to normalize the screen display*/
    else norm=-p_min;

/* Drawing Displacement-Voltage(PZT) curve */
    if((fp1=fopen(file,"rb"))==NULL)
      {
      printf("\nCANNOT OPEN FILE\n");
      exit(1);
      }       /* At this time, file is still the name of the last typed in */


    /**********************
    for(k=start1; k<=end1; k++)
      {
      fread(&p1, sizeof(double),1,fp1);
      printf("\n k,p1,%d,%f",k,p1);
      }
    fclose(fp1);
    _getch();
    ***********************/

    if((fp1=fopen(file,"rb"))==NULL)
      {
      printf("\nCANNOT OPEN FILE\n");
      exit(1);
      }     /* At this time, file is still the name of the last typed in */
    fread(&p1, sizeof(double),1,fp1);
    fclose(fp1);
    if( !_setvideomode( _MAXRESMODE ) )
    exit( 1 );
    _getvideoconfig( &v );
    _clearscreen(_GCLEARSCREEN);
```

```
    _setcolor(1);
    _moveto_w( 0, v.numypixels/2);
    _lineto_w(v.numxpixels, v.numypixels/2);
    _moveto_w( 0, v.numypixels/2-(p1-p_min)*0.4*v.numypixels/(p_max-p_min));  /* move to
                                                    the first data point to be diplayed, */

    if((fp1=fopen(file,"rb"))==NULL)
      {
      printf("\nCANNOT OPEN FILE\n");
      exit(1);
      }    /* At this time, file is still the name of the last typed in */

    for(k=start1; k<=end1; k++)
      {
      fread(&p1, sizeof(double),1,fp1);

      _lineto_w((k-start1+1)/x_contract, v.numypixels/2-(p1-
                p_min)*0.4*v.numypixels/(p_max-p_min));
      }
    fclose(fp1);
    printf("\nDisplacement_max = %f nm",p_max*670/(4*3.14));
    printf("\nDisplacement_min = %f nm",p_min*670/(4*3.14));

    _getch();

try2:
    printf("\nDO YOU WANT TO REDRAW OR DRAW A DIFFERENT PART OF THE DISPLACEMENT CURVE
           (Y/N) ?");
    ch1=getche();
    if(ch1=='n') goto exit;
    else if(ch1!='y') goto try2;
    else goto again8;

    };
exit:
  exit(0);
  }
```

A3.2 Control program for the experimental flying height testing system

```
/*      File:   Flyhight.c
*******************************************************************************
*                                                                             *
*  Copyright (C) 1999      X. Liu.                                            *
*                                                                             *
*  The information in this document is subject to change without notice       *
*  and  should  not  be  construed  as a  commitment.                         *
*  No responsibility is assumed for any errors that may appear in             *
*  this document or for the use  or  reliability  of any portion of this      *
*  document or the described software.                                        *
*                                                                             *
*                                                                             *
*******************************************************************************

*******************************************************************************
*******************************************************************************

                              MODULE FUNCTION :

        This is the software part of the experimental flying height testing
        system.

*******************************************************************************

        Written : X. Liu                        November 1999.

*******************************************************************************
```

```
        Language : Microsoft Visual C++ V1.0

*****************************************************************************

        Other Software Required : Must be linked with C30M_X.lib

*****************************************************************************

        Hardware required : IBM PC/XT/AT or compatible with 256K of memory,
        and a PC-30.

*****************************************************************************

        Restrictions : None.

*****************************************************************************

                                Module description :

        DAC0 is coarse input to the power amplifier for PZT1.
        DAC1 is coarse input to the power amplifier for PZT2.
        DAC2 is fine input to the power amplifier for PZT1.
        DAC3 is fine input to the power amplifier for PZT2.
        ADC0 samples V(1+2), i.e., the intensity signal.
        ADC1 samples V(3+4), i.e., also the intensity signal.
        ADC2 samples V(1-2), i.e. Cos signal.
        ADC3 samples V(4-3), i.e. Sin signal.
        The disk head-slider is moved by the PZT translator in a linear or saw-
        wave form. The output signals of the interferometric receiver are sampled
        and can be saved by the computer. All the signals can be displayed on
        screen if needed. Phase-difference signal is derived and can be saved to
        a data file for later use.

*****************************************************************************
*****************************************************************************/

#include <graph.h>
#include <stdio.h>
#include <stdlib.h>
#include <conio.h>
#include <math.h>
#include "pc30.h"

#define data_30
#define badd   0x700

int d_a2[10000],d_a3[10000],da0_v,da1_v,da2_v,da3_v,ad0_v,ad1_v,
    ad2_v,ad3_v,max_ad0,min_ad0,max_ad1,min_ad1,max_ad2,min_ad2,start1,end1,
    max_ad3,min_ad3;

void main(void)
  {
  FILE *fp,*fp1;
  char ch1,file[20],file1[20];
  int i,j,k,k1;
  float m,x_contract,y_contract;
  double f1,f2,p0,p1,p_max,p_min,ang0,ang1,norm,ad0_f,ad1_f,ad2_f,ad3_f,ad0_f0,ad1_f0,
  ad2_f0,ad3_f0,mid_ad0,mid_ad1,mid_ad2,mid_ad3;
  struct _videoconfig v;
  base_30 = badd;

  j = version();
  i = j/256;
  m = (float) j - i*256;
  m = i + m/100.0F;
  printf("\nPC-30 Driver Version %5.2f", m);

again2:
  printf("\n Do you want to start (y/n): ");
  ch1=getche();
  if(ch1!='y') goto again2;

  if (diag()) printf("\n PC-30 fault.");
  else if (type_30 < found_39)
  printf("\n PC-39, PC-30B, PC-30C, PC-30D or PC-30 PG required.");
  else
    {
```

```
    init();
    dma_init();
    ad_prescaler(4);
    ad_clock(10);    // ADC sampling frequency  Fs=50KHz

    //Initial output values for DAC0 ~ DAC3
    da0_v=0;   //DAC0 is the coarse input to power amplifier for PZT1
    da1_v=0;   //DAC1 is the coarse input to power amplifier for PZT2
    da2_v=0;   //DAC2 is the fine input to power amplifier for PZT1
    da3_v=0;   //DAC3 is the fine input to power amplifier for PZT2

    //The fine inputs to PZT1 and PZT2 are not activated, therefore just
    //set them to fixed value, 0.
    da_out(2, da2_v);
    da_out(3, da3_v);

    printf("\n Press any key to stop ");
    k=1;       // k here controls DAC's output points/steps

    /* ------------------------------------------------------------------
       Calibration: finding the middle value of Sin, i.e. V(4-3),
       Cos, i.e. V(1-2), V(1+2), and V(3+4) signals.
       k must be big enough so that during the calibration, at least one
       maxima and minima of each of the four signals appear.
       During the calibration, the PZT(s) will make linear or saw-wave
       movement.
    ------------------------------------------------------------------*/

    printf("\nCALIBRATION IS CARRYING ON, PLEASE WAIT.....");

    //set the initial max and min values of four signals to beyond their
    //practical value.
    max_ad0=-9999;
    min_ad0=9999;
    max_ad1=-9999;
    min_ad1=9999;
    max_ad2=-9999;
    min_ad2=9999;
    max_ad3=-9999;
    min_ad3=9999;

loop0:
    while ((da0_v<4095)&&(k<20000))   // k here controls DAC's output steps/points
      {
      da_out(0, da0_v);
      da_out(1, da1_v);
      da0_v++;
      da1_v++;

      for(i=1;i<500;i++); //Waiting a little while till the PZT translator(s) is stable

      ad_in(0, &ad0_v);       //ADC0 samples V(1+2)
      ad_in(1, &ad1_v); //ADC1 samples V(3+4)
      ad_in(2, &ad2_v); //ADC0 samples V(4-3), i.e. Sin signal
      ad_in(3, &ad3_v); //ADC0 samples V(1-2), i.e. Cos signal
      if(max_ad0<ad0_v) max_ad0=ad0_v;
      if(min_ad0>ad0_v) min_ad0=ad0_v;
      if(max_ad1<ad1_v) max_ad1=ad1_v;
      if(min_ad1>ad1_v) min_ad1=ad1_v;
      if(max_ad2<ad2_v) max_ad2=ad2_v;
      if(min_ad2>ad2_v) min_ad2=ad2_v;
      if(max_ad3<ad3_v) max_ad3=ad3_v;
      if(min_ad3>ad3_v) min_ad3=ad3_v;
      k=k+1;
      }

    while ((da0_v>0)&&(k<20000)) // k here controls the DAC's output steps/points
      {
      da_out(0, da0_v);
      da_out(1, da1_v);
      da0_v--;
      da1_v--;

      for(i=1;i<500;i++);

      ad_in(0, &ad0_v);
      ad_in(1, &ad1_v);
      ad_in(2, &ad2_v);
```

```
        ad_in(3, &ad3_v);
        if(max_ad0<ad0_v) max_ad0=ad0_v;
        if(min_ad0>ad0_v) min_ad0=ad0_v;
        if(max_ad1<ad1_v) max_ad1=ad1_v;
        if(min_ad1>ad1_v) min_ad1=ad1_v;
        if(max_ad2<ad2_v) max_ad2=ad2_v;
        if(min_ad2>ad2_v) min_ad2=ad2_v;
        if(max_ad3<ad3_v) max_ad3=ad3_v;
        if(min_ad3>ad3_v) min_ad3=ad3_v;
        k=k+1;
        }
      if (k<20000) goto loop0;
      da0_v=0;
      da1_v=0;
      da_out(0, da0_v);   // Reset the DAC0 output for PZT1
      da_out(1, da1_v); // Reset the DAC1 output for PZT2
      mid_ad0=min_ad0+(max_ad0-min_ad0)/2.0;  // Middle value of V(1+2) signal
      mid_ad1=min_ad1+(max_ad1-min_ad1)/2.0;  // Middle value of V(3+4) signal
      f1=(max_ad1-min_ad1);
      f1=f1/(max_ad0-min_ad0);  // Normalization factor for V(1+2) and V(3+4) signals
      mid_ad2=min_ad2+(max_ad2-min_ad2)/2;  // Middle value of Sin (V(4-3)) signal
      mid_ad3=min_ad3+(max_ad3-min_ad3)/2;  // Middle value of Cos (V(1-2)) signal
      f2=(max_ad3-min_ad3);
      f2=f2/(max_ad2-min_ad2);  // Normalization factor of Sin and Cos signals
      printf("\n f1,(max_ad1-min_ad1),(max_ad0-min_ad0),%f,%d,%d",f1,(max_ad1-
min_ad1),(max_ad0-min_ad0));
      printf("\n f2,(max_ad3-min_ad3),(max_ad2-min_ad2),%f,%d,%d",f2,(max_ad3-
min_ad3),(max_ad2-min_ad2));
      printf("\nCALIBRATION FINISHED!");

      printf("\nPLEASE PRESS ANY KEY TO CARRY ON...");
      _getch();

try0:
      printf("\nKEY IN DATA FILE NAME THE V(1+2) and V(3+4) WILL BE WRITTEN IN:");
      scanf("%s",file);
      if((fp=fopen(file,"wb"))==NULL)
        {
        printf("\nCANNOT OPEN FILE, PLEASE CHECK DISK AND TRY AGAIN");
        goto try0;
        }

      //save the obtained calibration parameters for later use
      fwrite(&mid_ad0, sizeof(double),1,fp);
      fwrite(&mid_ad1, sizeof(double),1,fp);
      fwrite(&f1, sizeof(double),1,fp);
      fwrite(&mid_ad2, sizeof(double),1,fp);
      fwrite(&mid_ad3, sizeof(double),1,fp);
      fwrite(&f2, sizeof(double),1,fp);

      //Initial values for DACs
      da0_v=0;     // start point of PZT1 control voltage (range:0 to 4095)
      da1_v=0;     // start point of PZT2 control voltage (range:0 to 4095)

      //The fine inputs to PZT1 and PZT2 are not activated, therefore just
      //set them to fixed value, 0.
      da2_v=0;
      da3_v=0;

      // System measurement starting
      k=1;        //k here controls the sampling points of data

loop:
      if (kbhit()) goto exit;
      while ((da0_v<4095)&&(k<10000))   //DAC output sweeps between 0 and 4095
                                        //10000 points of data will be acquired
        {
        da_out(0, da0_v);
        da_out(1, da1_v);
        da0_v++;
        da1_v++;
        for(i=1;i<500;i++);  // Wait a while for PZT(s) to be stabilised

        //Below is an averaging filter, but here it is not in effect
        ad0_f0=0.0;
        ad1_f0=0.0;
        ad2_f0=0.0;
        ad3_f0=0.0;
```

```
        for(i=1;i<2;i++)
          {
          ad_in(0, &ad0_v);
          ad_in(1, &ad1_v);
          ad_in(2, &ad2_v);
          ad_in(3, &ad3_v);
          ad0_f=ad0_f0+ ad0_v/1.0;      // this filting part is not in effect
          ad0_f0=ad0_f;
          ad1_f=ad1_f0+ ad1_v/1.0;
          ad1_f0=ad1_f;
          ad2_f=ad2_f0+ ad2_v/1.0;  // this filting part is not in effect
          ad2_f0=ad2_f;
          ad3_f=ad3_f0+ ad3_v/1.0;
          ad3_f0=ad3_f;
          }

        //Save the acquired data
        fwrite(&ad0_f, sizeof(double),1,fp);
        fwrite(&ad1_f, sizeof(double),1,fp);
        fwrite(&ad2_f, sizeof(double),1,fp);
        fwrite(&ad3_f, sizeof(double),1,fp);
        k=k+1;
        }

      while ((da0_v>0)&&(k<10000))
        {
        da_out(0, da0_v);
        da_out(1, da1_v);
        da0_v--;
        da1_v--;

        for(i=1;i<500;i++);     /* Wait a little while */

        //Below is an averaging filter, but here it is not in effect
        ad0_f0=0.0;
        ad1_f0=0.0;
        ad2_f0=0.0;
        ad3_f0=0.0;
        for(i=1;i<2;i++)
          {
          ad_in(0, &ad0_v);
          ad_in(1, &ad1_v);
          ad_in(2, &ad2_v);
          ad_in(3, &ad3_v);
          ad0_f=ad0_f0+ ad0_v/1.0;      // this filting part is not in effect
          ad0_f0=ad0_f;
          ad1_f=ad1_f0+ ad1_v/1.0;
          ad1_f0=ad1_f;
          ad2_f=ad2_f0+ ad2_v/1.0;      // this filting part is not in effect
          ad2_f0=ad2_f;
          ad3_f=ad3_f0+ ad3_v/1.0;
          ad3_f0=ad3_f;
          }
        fwrite(&ad0_f, sizeof(double),1,fp);
        fwrite(&ad1_f, sizeof(double),1,fp);
        fwrite(&ad2_f, sizeof(double),1,fp);
        fwrite(&ad3_f, sizeof(double),1,fp);
        k=k+1;
        }

    if (k<10000) goto loop;
    fclose(fp);

    //Reset PZTs outputs
    da0_v=0;
    da1_v=0;
    da_out(0, da0_v);
    da_out(1, da1_v);

again3:
    printf("\n Do you want to draw the curves (y/n): ");
    ch1=getche();
    if(ch1=='n') goto again7;
    if(ch1!='y') goto again3;

    printf("\nPLEASE INPUT DATA FILE NAME: ");
    scanf("%s",file);
    if((fp=fopen(file,"rb"))==NULL)
```

```
  {
  printf("\nCANNOT OPEN FILE\n");
  exit(1);
  }
if( !_setvideomode( _MAXRESMODE ) )
exit( 1 );
_getvideoconfig( &v );
_clearscreen(_GCLEARSCREEN);
_setcolor(1);
_moveto_w( 0, v.numypixels/2 );
_lineto_w(v.numxpixels, v.numypixels/2);
_moveto_w( 0, v.numypixels/2 );

//Read back the calibration parameters
fread(&mid_ad0, sizeof(double),1,fp);
fread(&mid_ad1, sizeof(double),1,fp);
fread(&f1, sizeof(double),1,fp);
fread(&mid_ad2, sizeof(double),1,fp);
fread(&mid_ad3, sizeof(double),1,fp);
fread(&f2, sizeof(double),1,fp);

//Read back the saved measurement data
for(k=1; k<9999; k++)
  {
  fread(&ad0_f, sizeof(double),1,fp);
  fread(&ad1_f, sizeof(double),1,fp);
  fread(&ad2_f, sizeof(double),1,fp);
  fread(&ad3_f, sizeof(double),1,fp);
  _lineto_w(k/8, v.numypixels/2-(ad0_f-2048)/10);       //Draw V(1+2) curve
  }
fclose(fp);

if((fp=fopen(file,"rb"))==NULL)
  {
  printf("\nCANNOT OPEN FILE\n");
  exit(1);
  }
_setcolor(1);
_moveto_w( 0, v.numypixels/2 );
fread(&mid_ad0, sizeof(double),1,fp);
fread(&mid_ad1, sizeof(double),1,fp);
fread(&f1, sizeof(double),1,fp);
fread(&mid_ad2, sizeof(double),1,fp);
fread(&mid_ad3, sizeof(double),1,fp);
fread(&f2, sizeof(double),1,fp);
for(k=1; k<9999; k++)
  {
  fread(&ad0_f, sizeof(double),1,fp);
  fread(&ad1_f, sizeof(double),1,fp);
  fread(&ad2_f, sizeof(double),1,fp);
  fread(&ad3_f, sizeof(double),1,fp);
  _lineto_w(k/8, v.numypixels/2-(ad1_f-2048)/10);       //Draw V(3+4) curve
  }
fclose(fp);

if((fp=fopen(file,"rb"))==NULL)
  {
  printf("\nCANNOT OPEN FILE\n");
  exit(1);
  }
_setcolor(2);
_moveto_w( 0, v.numypixels/2 );
fread(&mid_ad0, sizeof(double),1,fp);
fread(&mid_ad1, sizeof(double),1,fp);
fread(&f1, sizeof(double),1,fp);
fread(&mid_ad2, sizeof(double),1,fp);
fread(&mid_ad3, sizeof(double),1,fp);
fread(&f2, sizeof(double),1,fp);
for(k=1; k<9999; k++)
  {
  fread(&ad0_f, sizeof(double),1,fp);
  fread(&ad1_f, sizeof(double),1,fp);
  fread(&ad2_f, sizeof(double),1,fp);
  fread(&ad3_f, sizeof(double),1,fp);
  _lineto_w(k/8, v.numypixels/2-(ad2_f-2048)/10); // Draw V(1-2) curve
  }
fclose(fp);
if((fp=fopen(file,"rb"))==NULL)
```

```
    {
     printf("\nCANNOT OPEN FILE\n");
     exit(1);
    }
  _setcolor(2);
  _moveto_w( 0, v.numypixels/2 );
  fread(&mid_ad0, sizeof(double),1,fp);
  fread(&mid_ad1, sizeof(double),1,fp);
  fread(&f1, sizeof(double),1,fp);
  fread(&mid_ad2, sizeof(double),1,fp);
  fread(&mid_ad3, sizeof(double),1,fp);
  fread(&f2, sizeof(double),1,fp);
  for(k=1; k<19999; k++)
    {
    fread(&ad0_f, sizeof(double),1,fp);
    fread(&ad1_f, sizeof(double),1,fp);
    fread(&ad2_f, sizeof(double),1,fp);
    fread(&ad3_f, sizeof(double),1,fp);
    _lineto_w(k/8, v.numypixels/2-(ad3_f-2048)/10);        //Draw V(4-3) curve
    }
  fclose(fp);
  _getch();

again5:
  //The purpose of redraw the curves is just to make the curves fit the
  //screen, and look comfortable.
  printf("\nDO YOU WANT TO REDRAW THESE CURVES (Y/N) ?");
  ch1=getche();
  if(ch1=='n') goto again7;
  if(ch1!='y') goto again5;

again6:
  printf("\nPLEASE INPUT DATA FILE NAME: ");
  scanf("%s",file);
  if((fp=fopen(file,"rb"))==NULL)
    {
    printf("\nCANNOT OPEN FILE\n");
    exit(1);
    }
  printf("\nPLEASE INPUT PLOT PARAMETER: x_contract (e.g. 16 or 32)");
  scanf("%f",&x_contract);
  printf("\nPLEASE INPUT PLOT PARAMETER: y_contract (e.g. 10)");
  scanf("%f",&y_contract);
  if( !_setvideomode( _MAXRESMODE ) )
  exit( 1 );
  _getvideoconfig( &v );
  _clearscreen(_GCLEARSCREEN);
  _setcolor(1);
  _moveto_w( 0, v.numypixels/2 );
  _lineto_w(v.numxpixels, v.numypixels/2);
  _moveto_w( 0, v.numypixels/2 );
  fread(&mid_ad0, sizeof(double),1,fp);
  fread(&mid_ad1, sizeof(double),1,fp);
  fread(&f1, sizeof(double),1,fp);
  fread(&mid_ad2, sizeof(double),1,fp);
  fread(&mid_ad3, sizeof(double),1,fp);
  fread(&f2, sizeof(double),1,fp);
  for(k=1; k<9999; k++)
    {
    fread(&ad0_f, sizeof(double),1,fp);
    fread(&ad1_f, sizeof(double),1,fp);
    fread(&ad2_f, sizeof(double),1,fp);
    fread(&ad3_f, sizeof(double),1,fp);
    _lineto_w(k/x_contract, v.numypixels/2-(ad0_f-2048)/y_contract);
                                                    //Draw V(1+2) curve
    }
  fclose(fp);
  if((fp=fopen(file,"rb"))==NULL)
    {
    printf("\nCANNOT OPEN FILE\n");
    exit(1);
    }
  _setcolor(1);
  _moveto_w( 0, v.numypixels/2 );
  fread(&mid_ad0, sizeof(double),1,fp);
  fread(&mid_ad1, sizeof(double),1,fp);
  fread(&f1, sizeof(double),1,fp);
  fread(&mid_ad2, sizeof(double),1,fp);
```

```
      fread(&mid_ad3, sizeof(double),1,fp);
      fread(&f2, sizeof(double),1,fp);
      for(k=1; k<9999; k++)
        {
        fread(&ad0_f, sizeof(double),1,fp);
        fread(&ad1_f, sizeof(double),1,fp);
        fread(&ad2_f, sizeof(double),1,fp);
        fread(&ad3_f, sizeof(double),1,fp);
       _lineto_w(k/x_contract, v.numypixels/2-(ad1_f-2048)/y_contract);
                                                    //Draw V(3+4) curve
        }
      fclose(fp);
      if((fp=fopen(file,"rb"))==NULL)
        {
        printf("\nCANNOT OPEN FILE\n");
        exit(1);
        }
      _setcolor(2);
      _moveto_w( 0, v.numypixels/2 );
      fread(&mid_ad0, sizeof(double),1,fp);
      fread(&mid_ad1, sizeof(double),1,fp);
      fread(&f1, sizeof(double),1,fp);
      fread(&mid_ad2, sizeof(double),1,fp);
      fread(&mid_ad3, sizeof(double),1,fp);
      fread(&f2, sizeof(double),1,fp);
      for(k=1; k<9999; k++)
        {
        fread(&ad0_f, sizeof(double),1,fp);
        fread(&ad1_f, sizeof(double),1,fp);
        fread(&ad2_f, sizeof(double),1,fp);
        fread(&ad3_f, sizeof(double),1,fp);
        _lineto_w(k/x_contract, v.numypixels/2-(ad2_f-2048)/y_contract);
                                                    //Draw V(1-2) curve.
        }
      fclose(fp);
      if((fp=fopen(file,"rb"))==NULL)
        {
        printf("\nCANNOT OPEN FILE\n");
        exit(1);
        }
      _setcolor(2);
      _moveto_w( 0, v.numypixels/2 );
      fread(&mid_ad0, sizeof(double),1,fp);
      fread(&mid_ad1, sizeof(double),1,fp);
      fread(&f1, sizeof(double),1,fp);
      fread(&mid_ad2, sizeof(double),1,fp);
      fread(&mid_ad3, sizeof(double),1,fp);
      fread(&f2, sizeof(double),1,fp);
      for(k=1; k<9999; k++)
        {
        fread(&ad0_f, sizeof(double),1,fp);
        fread(&ad1_f, sizeof(double),1,fp);
        fread(&ad2_f, sizeof(double),1,fp);
        fread(&ad3_f, sizeof(double),1,fp);
        _lineto_w(k/x_contract, v.numypixels/2-(ad3_f-2048)/y_contract);
                                                    //Draw V(4-3) curve.
        }
      fclose(fp);
      _getch();

      /************************/

again7:
      printf("\nDO YOU WANT TO REDRAW EVERY SIGNAL CURVES WITH MODIFICATION (Y/N) ?");
      ch1=getche();
      if(ch1=='n') goto exit;
      if(ch1!='y') goto again7;

again8:
      printf("\nPLEASE INPUT DATA FILE NAME: ");
      scanf("%s",file);
      if((fp=fopen(file,"rb"))==NULL)
        {
        printf("\nCANNOT OPEN FILE\n");
        exit(1);
        }

      printf("\nPLEASE INPUT PLOT PARAMETER: x_contract (e.g. 0.1, 1, 16 or 32)");
```

```
scanf("%f",&x_contract);   // x_contract is the time the x_axis will be contracted
printf("\nPLEASE INPUT PLOT PARAMETER: y_contract (e.g. 10)");
scanf("%f",&y_contract);   // y_contract is the time the y_axis will be contracted
if( !_setvideomode( _MAXRESMODE ) )
exit( 1 );
_getvideoconfig( &v );
_clearscreen(_GCLEARSCREEN);

// Draw V(1+2) signal
_setcolor(1);
_moveto_w( 0, v.numypixels/2);
_lineto_w(v.numxpixels, v.numypixels/2);
_moveto_w( 0, v.numypixels/2);
fread(&mid_ad0, sizeof(double),1,fp);
fread(&mid_ad1, sizeof(double),1,fp);
fread(&f1, sizeof(double),1,fp);
fread(&mid_ad2, sizeof(double),1,fp);
fread(&mid_ad3, sizeof(double),1,fp);
fread(&f2, sizeof(double),1,fp);
for(k=1; k<9999; k++)
  {
  fread(&ad0_f, sizeof(double),1,fp);
  fread(&ad1_f, sizeof(double),1,fp);
  fread(&ad2_f, sizeof(double),1,fp);
  fread(&ad3_f, sizeof(double),1,fp);
  _lineto_w(k/x_contract, v.numypixels/2-(ad0_f-mid_ad0)/y_contract);
  }
fclose(fp);

if((fp=fopen(file,"rb"))==NULL)
  {
  printf("\nCANNOT OPEN FILE\n");
  exit(1);
  }

// Draw V(3+4) signal
_setcolor(1);
_moveto_w( 0, v.numypixels/2);
_lineto_w(v.numxpixels, v.numypixels/2);
_moveto_w( 0, v.numypixels/2);
fread(&mid_ad0, sizeof(double),1,fp);
fread(&mid_ad1, sizeof(double),1,fp);
fread(&f1, sizeof(double),1,fp);
fread(&mid_ad2, sizeof(double),1,fp);
fread(&mid_ad3, sizeof(double),1,fp);
fread(&f2, sizeof(double),1,fp);
for(k=1; k<9999; k++)
  {
  fread(&ad0_f, sizeof(double),1,fp);
  fread(&ad1_f, sizeof(double),1,fp);
  fread(&ad2_f, sizeof(double),1,fp);
  fread(&ad3_f, sizeof(double),1,fp);
  _lineto_w(k/x_contract, v.numypixels/2-(ad1_f-mid_ad1)/y_contract);
  }
fclose(fp);

if((fp=fopen(file,"rb"))==NULL)
  {
  printf("\nCANNOT OPEN FILE\n");
  exit(1);
  }

//Draw V(1-2) signal
_setcolor(2);
_moveto_w( 0, v.numypixels/2);
_lineto_w(v.numxpixels, v.numypixels/2);
_moveto_w( 0, v.numypixels/2);
fread(&mid_ad0, sizeof(double),1,fp);
fread(&mid_ad1, sizeof(double),1,fp);
fread(&f1, sizeof(double),1,fp);
fread(&mid_ad2, sizeof(double),1,fp);
fread(&mid_ad3, sizeof(double),1,fp);
fread(&f2, sizeof(double),1,fp);
for(k=1; k<9999; k++)
  {
  fread(&ad0_f, sizeof(double),1,fp);
  fread(&ad1_f, sizeof(double),1,fp);
  fread(&ad2_f, sizeof(double),1,fp);
```

```
      fread(&ad3_f, sizeof(double),1,fp);
      _lineto_w(k/x_contract, v.numypixels/2-(ad2_f-mid_ad2)/y_contract);
      }
    fclose(fp);

    if((fp=fopen(file,"rb"))==NULL)
      {
      printf("\nCANNOT OPEN FILE\n");
      exit(1);
      }

    //Draw V(4-3) signal
    _setcolor(1);
    _moveto_w( 0, v.numypixels/2);
    _lineto_w(v.numxpixels, v.numypixels/2);
    _moveto_w( 0, v.numypixels/2);
    fread(&mid_ad0, sizeof(double),1,fp);
    fread(&mid_ad1, sizeof(double),1,fp);
    fread(&f1, sizeof(double),1,fp);
    fread(&mid_ad2, sizeof(double),1,fp);
    fread(&mid_ad3, sizeof(double),1,fp);
    fread(&f2, sizeof(double),1,fp);
    for(k=1; k<9999; k++)
      {
      fread(&ad0_f, sizeof(double),1,fp);
      fread(&ad1_f, sizeof(double),1,fp);
      fread(&ad2_f, sizeof(double),1,fp);
      fread(&ad3_f, sizeof(double),1,fp);
      _lineto_w(k/x_contract, v.numypixels/2-(ad3_f-mid_ad3)/y_contract);
      }
    fclose(fp);
    _getch();

    printf("\nDO YOU WANT TO REDRAW EVERY SIGNAL CURVES AFTER MODIFICATION (Y/N) ?");
    ch1=getche();
    if(ch1=='y') goto again8;

    /***************
    Phase unwraping to derive the phase-difference between the two beams
    ***************/
    again9:
    if((fp=fopen(file,"rb"))==NULL)
      {
      printf("\nCANNOT OPEN FILE\n");
      exit(1);
      }    // Open V(1+2),V(2+3),V(1-2) and V(4-3) data file

    // Draw any small part of the intensity and phase-difference curves
try1:
    printf("\n NOW A SMALL PART OF THE PHASE-DIFFERENCE CURVE WILL BE DISPLAYED");
    printf("\nPLEASE INPUT START POINT: (between 1 and 9998) (e.g. 1000) ");
    scanf("%d",&start1);
    printf("\nPLEASE INPUT END POINT: (between 2 to 9999) (e.g. 1020)");
    scanf("%d",&end1);
    printf("\nPLEASE KEY IN NEW DATA FILE NAME THE PHASE DATA WILL BE WRITTEN IN:");
    printf("\n(DON'T USE THE NAME OF USEFUL DATA FILES!!!!!!!)");
    scanf("%s",file1);

    if((fp1=fopen(file1,"wb"))==NULL)
      {
      printf("\nCANNOT OPEN FILE, PLEASE CHECK DISK AND TRY AGAIN");
      goto try1;
      }

    fread(&mid_ad0, sizeof(double),1,fp);
    fread(&mid_ad1, sizeof(double),1,fp);
    fread(&f1, sizeof(double),1,fp);
    fread(&mid_ad2, sizeof(double),1,fp);
    fread(&mid_ad3, sizeof(double),1,fp);
    fread(&f2, sizeof(double),1,fp);

    for(k=1; k<start1; k++)
      {
      fread(&ad0_f, sizeof(double),1,fp);
      fread(&ad1_f, sizeof(double),1,fp);
      fread(&ad2_f, sizeof(double),1,fp);
      fread(&ad3_f, sizeof(double),1,fp);
      }       // Move the data reading point to 'start1'
```

```
   p0=0;
   p1=0;
   ang0=0;
   ang1=0;
   p_max=-6.28;
   p_min=+6.28;

   for(k=start1; k<=end1; k++)
     {
     fread(&ad0_f, sizeof(double),1,fp);
     fread(&ad1_f, sizeof(double),1,fp);
     fread(&ad2_f, sizeof(double),1,fp);
     fread(&ad3_f, sizeof(double),1,fp);

     ang1=atan2((ad3_f-mid_ad3),(f1*(ad2_f-mid_ad2)));
     p1=ang1;
     /*
     if((ang1-ang0)<-3.14) p1=p0+ang1-ang0+2*3.1415926;
     else if ((ang1-ang0)> 3.14) p1=p0+ang1-ang0-2*3.1415926;
     else p1=p0+ang1-ang0;
     */
     //Save the phase-difference value of this point
     fwrite(&p1, sizeof(double),1,fp1);
  /*
     p0=p1;
     ang0=ang1;
  */
     if(p_max<p1) p_max=p1;
     if(p_min>p1) p_min=p1;
     }
  fclose(fp);
  fclose(fp1);
  if(p_max>-p_min) norm=p_max;      // norm is used to normalize the screen display
  else norm=-p_min;

  //Draw the Intensity-Voltage(PZT) and Phase-Voltage curves
  if((fp1=fopen(file1,"rb"))==NULL)
    {
    printf("\nCANNOT OPEN FILE\n");
    exit(1);
    }

  //******** for testing purpose ************
  for(k=start1; k<=end1; k++)
    {
    fread(&p1, sizeof(double),1,fp1);
    printf("\n k,p1,%d,%f",k,p1);
    }
  fclose(fp1);
  _getch();
  //*********************************/

  if((fp=fopen(file,"rb"))==NULL)
    {
    printf("\nCANNOT OPEN FILE\n");
    exit(1);
    }

  // Draw V(3+4), i.e. the intensity curve
  if( !_setvideomode( _MAXRESMODE ) )
  exit( 1 );
  _getvideoconfig( &v );
  _clearscreen(_GCLEARSCREEN);
  _setcolor(1);
  _moveto_w( 0, v.numypixels/2);
  _lineto_w(v.numxpixels, v.numypixels/2);
  _moveto_w( 0, v.numypixels/2);
  fread(&mid_ad0, sizeof(double),1,fp);
  fread(&mid_ad1, sizeof(double),1,fp);
  fread(&f1, sizeof(double),1,fp);
  fread(&mid_ad2, sizeof(double),1,fp);
  fread(&mid_ad3, sizeof(double),1,fp);
  fread(&f2, sizeof(double),1,fp);

  for(k=1; k<start1; k++)
    {
    fread(&ad0_f, sizeof(double),1,fp);
```

```
      fread(&ad1_f, sizeof(double),1,fp);
      fread(&ad2_f, sizeof(double),1,fp);
      fread(&ad3_f, sizeof(double),1,fp);
      }           // Move the data reading point to 'start1'

    for(k=start1; k<end1; k++)
      {
      fread(&ad0_f, sizeof(double),1,fp);
      fread(&ad1_f, sizeof(double),1,fp);
      fread(&ad2_f, sizeof(double),1,fp);
      fread(&ad3_f, sizeof(double),1,fp);
      _lineto_w((k-start1+1)/x_contract, v.numypixels/2-(ad1_f-mid_ad1)/y_contract);
      }
    fclose(fp);

    // Draw the phase-difference curve
    if((fp1=fopen(file1,"rb"))==NULL)
      {
      printf("\nCANNOT OPEN FILE\n");
      exit(1);
      }
    // At this point, file1 is still the last one    being used.
    fread(&p1, sizeof(double),1,fp1);
    fclose(fp1);

    _setcolor(2);
    _moveto_w( 0, v.numypixels/2);
    _lineto_w(v.numxpixels, v.numypixels/2);
    _moveto_w( 0, v.numypixels/2-(p1-p_min)*0.4*v.numypixels/(p_max-p_min));
                                  //  Move to the first data point to be displayed.

    if((fp1=fopen(file1,"rb"))==NULL)
      {
      printf("\nCANNOT OPEN FILE\n");
      exit(1);
      }
    // At this point, file1 is still the last one    being used
    for(k=start1; k<=end1; k++)
      {
      fread(&p1, sizeof(double),1,fp1);
      _lineto_w((k-start1+1)/x_contract, v.numypixels/2-(p1-
p_min)*0.4*v.numypixels/(p_max-p_min));
      }
    fclose(fp1);
    printf("\nPhase-difference_max = %f nm",p_max);
    printf("\nPhase-difference_min = %f nm",p_min);
    _getch();

try2:
    printf("\nDO YOU WANT TO REDRAW OR DRAW A DIFFERENT PART OF THE DISPLACEMENT CURVE
(Y/N) ?");
    ch1=getche();
    if(ch1=='n') goto exit;
    else if(ch1!='y') goto try2;
    else goto again8;

    };
exit:
  exit(0);
  }
```

A3.3 Program for extracting optical constants of the head-slider and initial phase difference from experimental data

To save pages, the header files are not listed here.

```
/*      File:   FL_POWELL.C
*************************************************************************
*                                                                       *
*  Copyright (C) 1999      X. Liu.                                      *
*                                                                       *
*  The information in this document is subject to change without notice *
*  and should not be construed as a commitment.                         *
*  No responsibility is assumed for any errors that may appear in       *
*  this document or for the use or reliability of any portion of this   *
*  document or the described software.                                  *
*                                                                       *
*                                                                       *
*************************************************************************

*************************************************************************
*************************************************************************

                              MODULE FUNCTION :

This is the main rutine for extracting the optical constants and initial phase
difference by using Powell method

*************************************************************************

       Written : X. Liu                        November 1999.

*************************************************************************

       Language : Microsoft Visual C++ V1.0

*************************************************************************
*************************************************************************

                              Module description :


*************************************************************************
*************************************************************************/

#include <stdio.h>
#include <math.h>
#include "nr1.h"
#include "nrutil1.h"
#define NRANSI
#define NDIM 3          /* Number of parameters to be estimated */
#define FTOL 1.0e-12

int N,N1,start1, end1, sample_1;
double Immax,Immin,Im[800],Qm[800];   /* Im[] and Qm[] are measured intensity and phase
                                         difference. Immax and Immin are the maxima and
                                         minima of the measured intensity curve */

/*-----------------------------------------------------------------

Function:                       Ifunc

Input Parameters: (θ0, n, k)→ x[], and 4πn0h/λ → h

Output Parameters: none

Return Parameter: Theoretical intensity value

Description: Theoretical intensity calculation
```

```
-----------------------------------------------------------------*/

double Ifunc(double x[],double h)
{
double pt12=((1.0-SQR(x[2])-SQR(x[3]))*sin(h)-2.0*x[3]*cos(h))*
(SQR(1.0+x[2])+SQR(x[3])+0.2*(1.0-SQR(x[2])-SQR(x[3]))*cos(h)+
0.4*x[3]*sin(h));

double pt13=(0.2*SQR(1.0+x[2])+0.2*SQR(x[3])+(1.0-SQR(x[2])-SQR(x[3]))*
cos(h)+2.0*x[3]*sin(h))*(0.2*(1.0-SQR(x[2])-SQR(x[3]))*sin(h)-
0.4*x[3]*cos(h));

double pt14=SQR(SQR(1.0+x[2])+SQR(x[3])+0.2*(1.0-SQR(x[2])-SQR(x[3]))*
cos(h)+0.4*x[3]*sin(h))+SQR(0.2*(1.0-SQR(x[2])-SQR(x[3]))*sin(h)-
0.4*x[3]*cos(h));

double pt22=(0.2*SQR(1.0+x[2])+0.2*SQR(x[3])+(1.0-SQR(x[2])-SQR(x[3]))*
cos(h)+2.0*x[3]*sin(h))*(SQR(1.0+x[2])+SQR(x[3])+0.2*(1.0-SQR(x[2])-
SQR(x[3]))*cos(h)+0.4*x[3]*sin(h));

double pt23=((1.0-SQR(x[2])-SQR(x[3]))*sin(h)-2.0*x[3]*cos(h))*
(0.2*(1.0-SQR(x[2])-SQR(x[3]))*sin(h)-0.4*x[3]*cos(h));

double pt24=SQR(SQR(1.0+x[2])+SQR(x[3])+0.2*(1.0-SQR(x[2])-SQR(x[3]))*
cos(h)+0.4*x[3]*sin(h))+SQR(0.2*(1.0-SQR(x[2])-SQR(x[3]))*sin(h)-
0.4*x[3]*cos(h));

double MM=SQR((pt12-pt13)/pt14)+SQR((pt22+pt23)/pt24);

return MM;      /* Theoretical intensity value */
}

/*-----------------------------------------------------------------

Function:                    func

Input Parameters: (θ0, n, k)→ x[]

Output Parameters: none

Return Parameter: The value of merit function

Description: Calculation of merit function

-----------------------------------------------------------------*/

double func(double x[])
{
int i;
double Q1=atan(2.0*x[3]/(1.0-SQR(x[2])-SQR(x[3])));  /*Phase shift on reflection */
double Imin=Ifunc(x,Q1);       /* Minima of theoretical intensity curve */
double Imax=Ifunc(x,Q1+3.14159265);   /* Maxima of theoretical intensity curve */
double x1,It_norm,pt11,pt12,pt13,pt14,pt21,pt22,pt23,pt24,It;
double M,mm1,mm2,mm3,Qmr;
M=0.0;
for (i=1;i<=N;i++)      /* Calculate the value of merit function */
  {
  Qmr=-Qm[i];
  mm3=(25.0*SQR(x[2])*SQR(cos(Qmr-x[1]))+72.0*SQR(x[3])-
  97.0*SQR(x[2])+36.0+72.0*SQR(x[2])*SQR(x[3])+36.0*SQR(SQR(x[3]))+
  36.0*SQR(SQR(x[2])));

  mm1=6.0*SQR(x[2])*cos(Qmr-x[1])-6.0*cos(Qmr-x[1])+
  6.0*SQR(x[3])*cos(Qmr-x[1])+13.0*sin(Qmr-x[1])*x[3]+
  1.0*sqrt(25.0*SQR(x[2])*SQR(cos(Qmr-x[1]))+72.0*SQR(x[3])-
  97.0*SQR(x[2])+36.0+72.0*SQR(x[2])*SQR(x[3])+36.0*SQR(SQR(x[3]))+
  36.0*SQR(SQR(x[2])));

  mm2=-4.0*sin(Qmr-x[1])-12.0*x[3]*cos(Qmr-x[1])+
  9.0*sin(Qmr-x[1])*SQR(x[3])+9.0*sin(Qmr-x[1])*SQR(x[2]);

  double x1=2.0*(3.1415926-atan(mm1/mm2)); /*x1 represents 4πh/λ. here it is derived
                                             from the measured phase difference */

  pt11=((Im[i]-Immin)*(Imax-Imin)/(Immax-Immin)+Imin)*sin(Qmr-x[1]); /* not used here */
```

```
    pt12=((1.0-SQR(x[2])-SQR(x[3]))*sin(x1)-2.0*x[3]*cos(x1))*
    (SQR(1.0+x[2])+SQR(x[3])+0.2*(1.0-SQR(x[2])-SQR(x[3]))*cos(x1)+
    0.4*x[3]*sin(x1));

    pt13=(0.2*SQR(1.0+x[2])+0.2*SQR(x[3])+(1.0-SQR(x[2])-SQR(x[3]))*
    cos(x1)+2.0*x[3]*sin(x1))*(0.2*(1.0-SQR(x[2])-SQR(x[3]))*sin(x1)-
    0.4*x[3]*cos(x1));

    pt14=SQR(SQR(1.0+x[2])+SQR(x[3])+0.2*(1.0-SQR(x[2])-SQR(x[3]))*
    cos(x1)+0.4*x[3]*sin(x1))+SQR(0.2*(1.0-SQR(x[2])-SQR(x[3]))*sin(x1)-
    0.4*x[3]*cos(x1));

    pt21=((Im[i]-Immin)*(Imax-Imin)/(Immax-Immin)+Imin)*cos(Qmr-x[1]); /* not used here */

    pt22=(0.2*SQR(1.0+x[2])+0.2*SQR(x[3])+(1.0-SQR(x[2])-SQR(x[3]))*cos(x1)+
    2.0*x[3]*sin(x1))*(SQR(1.0+x[2])+SQR(x[3])+0.2*(1.0-SQR(x[2])-SQR(x[3]))*
    cos(x1)+0.4*x[3]*sin(x1));

    pt23=((1.0-SQR(x[2])-SQR(x[3]))*sin(x1)-2.0*x[3]*cos(x1))*
    (0.2*(1.0-SQR(x[2])-SQR(x[3]))*sin(x1)-0.4*x[3]*cos(x1));

    pt24=SQR(SQR(1.0+x[2])+SQR(x[3])+0.2*(1.0-SQR(x[2])-SQR(x[3]))*cos(x1)+
    0.4*x[3]*sin(x1))+SQR(0.2*(1.0-SQR(x[2])-SQR(x[3]))*sin(x1)-0.4*x[3]*cos(x1));

    It=SQR((pt12-pt13)/pt14)+SQR((pt22+pt23)/pt24);
    It_norm=(It-Imin)*(Immax-Immin)/(Imax-Imin)+Immin;
    M=M+SQR(Im[i]-It_norm);
    if (mm3<0) M=10000000.0; /*set a large number to M */
    }

  return M;       /* M is the value of the merit function */
  }

  int main(void)
  {
  int i,iter,j;
  double fret,**xi;
  static double p[]={0.0,0.0,2.0,0.1};  /* Initial estimation for {θ0, n, k} */
  N1=1;           /* N1 >= 0, sample data are selected every N1+1 saved data point */
  N=100;  /* Number of sampling points being used for estimation */
  start1=500;     /* start point of the sampling data from the beginnig of the saved
                     data point to get the minima and maxima of the measured intensity
                     curve Immin and Immax */
  end1=1100;      /* end point of sampling data to get minima and maxima of the measured
                     intensity curve Immin and Immax */
  calib();
  printf("\nImmax, Immin,%f %fn",Immax,Immin);
  sample_1=500;  /* The start sampling data point from the beginning
                          of the data file to be used for estimation */
  gdata();

  xi=matrix(1,NDIM,1,NDIM);
  for (i=1;i<=NDIM;i++)
  for (j=1;j<=NDIM;j++)
  xi[i][j]=(i == j ? 1.0 : 0.0);
  powell(p,xi,NDIM,FTOL,&iter,&fret,func);
  printf("Iterations: %3d\n\n",iter);
  printf("Minimum found at: \n");
  for (i=1;i<=NDIM;i++) printf("%12.6f,",p[i]);
  printf("\n\nMinimum function value = %12.6f \n\n",fret);
  printf("The last searching direction matrix used is:\n");
  for (i=1;i<=NDIM;i++)
    {printf("\n");
    for (j=1;j<=NDIM;j++)
    printf("%12.6f",xi[i][j]);
    }
  free_matrix(xi,1,NDIM,1,NDIM);
  return 0;
  }
  #undef NRANSI
```

FL_CALIB.C

```
#include <graph.h>
#include <stdio.h>
```

```
#include <stdlib.h>
#include <conio.h>
#include <math.h>
#include <string.h>

extern int start1, end1;
extern double Immin, Immax;    /* Immin and Immax will be used by other functions */

void calib(void)
{
FILE *fp;
char file[20];
int j;
double f1,f2,ad0_f,ad1_f,ad2_f,ad3_f,mid_ad0,mid_ad1,mid_ad2,mid_ad3;

strcpy(file,"h-data"); /* The data file was obtained by using Flyhight.c in Section
                          A3.2, and the name should be changed to "h-data" to be used
                          here. */

/* Calibration start */

Immax=-9999.0;
Immin=9999.0;

/* The following part is to get the minima and maxima of the intensity curve */
fp=fopen(file,"rb");
fread(&mid_ad0, sizeof(double),1,fp);
fread(&mid_ad1, sizeof(double),1,fp);
fread(&f1, sizeof(double),1,fp);
fread(&mid_ad2, sizeof(double),1,fp);
fread(&mid_ad3, sizeof(double),1,fp);
fread(&f2, sizeof(double),1,fp);

for(j=1; j<start1; j++)
  {
  fread(&ad0_f, sizeof(double),1,fp);
  fread(&ad1_f, sizeof(double),1,fp);
  fread(&ad2_f, sizeof(double),1,fp);
  fread(&ad3_f, sizeof(double),1,fp);
  }          /* Move the data reading point to 'start1' */

for(j=start1; j<=end1; j++)
  {
  fread(&ad0_f, sizeof(double),1,fp);
  fread(&ad1_f, sizeof(double),1,fp);
  fread(&ad2_f, sizeof(double),1,fp);
  fread(&ad3_f, sizeof(double),1,fp);

  if(Immax<ad1_f) Immax=ad1_f;
  if(Immin>ad1_f) Immin=ad1_f;
  }  /* get the minima and maxima of the intensity curve */
fclose(fp);

/* printf("\n Immax,Immin,%f,%f",Immax,Immin);

printf("\nCALIBRATION FINISHED!");
printf("\nPLEASE PRESS ANY KEY TO CARRY ON...");

_getch(); */

}
```

GETDATA.C

```
#include <stdio.h>
#include <stdlib.h>
#include <conio.h>
#include <math.h>
#include <string.h>
extern int N,N1,sample_1;
extern double Im[800], Qm[800]; /* Define large enough vectors to store Im[] and Qm[]
                                   data. Im[] are measured intensity, Qm[] are measured
                                   phase difference */
void gdata(void)
{
FILE *fp;
char file[20];
```

```
  int j,j1;

  double f1,f2,ad0_f,ad1_f,ad2_f,ad3_f,mid_ad0,mid_ad1,mid_ad2,mid_ad3;
  strcpy(file,"h-data");
  fp=fopen(file,"rb");
  fread(&mid_ad0, sizeof(double),1,fp);
  fread(&mid_ad1, sizeof(double),1,fp);
  fread(&f1, sizeof(double),1,fp);
  fread(&mid_ad2, sizeof(double),1,fp);
  fread(&mid_ad3, sizeof(double),1,fp);
  fread(&f2, sizeof(double),1,fp);

  for(j=1; j<sample_1; j++)
    {
    fread(&ad0_f, sizeof(double),1,fp);
    fread(&ad1_f, sizeof(double),1,fp);
    fread(&ad2_f, sizeof(double),1,fp);
    fread(&ad3_f, sizeof(double),1,fp);
    }          /* Move the data reading point to 'start1' */

  /* get the sample data */
  for(j=1;j<=N;j++)
    {
    fread(&ad0_f, sizeof(double),1,fp);
    fread(&ad1_f, sizeof(double),1,fp);
    fread(&ad2_f, sizeof(double),1,fp);
    fread(&ad3_f, sizeof(double),1,fp);
    Im[j]=ad1_f; /*measured intensity */
    Qm[j]=atan2((ad3_f-mid_ad3),(f1*(ad2_f-mid_ad2))); /* Measured phase difference */

    for(j1=1;j1<=N1;j1++)       /* N1 >= 0, sample data are selected every N1+1 saved
                                   data point. */
      {
      fread(&ad0_f, sizeof(double),1,fp);
      fread(&ad1_f, sizeof(double),1,fp);
      fread(&ad2_f, sizeof(double),1,fp);
      fread(&ad3_f, sizeof(double),1,fp);
      }  /* Move to the next sampling point */
    }
  fclose(fp);

  printf("\n Sample Data Have Been Got");

  }
```

F1DIM1.C

```
#define NRANSI
#include "nrutil1.h"

extern int ncom;
extern double *pcom,*xicom,(*nrfunc)(double []);

double f1dim(double x)
{
int j;
double f,*xt;

xt=vector(1,ncom);
for (j=1;j<=ncom;j++) xt[j]=pcom[j]+x*xicom[j];
f=(*nrfunc)(xt);
free_vector(xt,1,ncom);
return f;
}
#undef NRANSI
/* (C) Copr. 1986-92 Numerical Recipes Software . */
```

LINMIN1.C

```
#define NRANSI
#include "nrutil1.h"
#define TOL 2.0e-4

int ncom;
double *pcom,*xicom,(*nrfunc)(double []);

void linmin(double p[], double xi[], int n, double *fret, double (*func)(double []))
{
```

```
double brent(double ax, double bx, double cx,
double (*f)(double), double tol, double *xmin);
double f1dim(double x);
void mnbrak(double *ax, double *bx, double *cx, double *fa, double *fb,
double *fc, double (*func)(double));
int j;
double xx,xmin,fx,fb,fa,bx,ax;

ncom=n;
pcom=vector(1,n);
xicom=vector(1,n);
nrfunc=func;
for (j=1;j<=n;j++)
  {
  pcom[j]=p[j];
  xicom[j]=xi[j];
  }
ax=0.0;
xx=1.0;
mnbrak(&ax,&xx,&bx,&fa,&fx,&fb,f1dim);
*fret=brent(ax,xx,bx,f1dim,TOL,&xmin);
for (j=1;j<=n;j++)
  {
  xi[j] *= xmin;
  p[j] += xi[j];
  }
free_vector(xicom,1,n);
free_vector(pcom,1,n);
}
#undef TOL
#undef NRANSI
/* (C) Copr. 1986-92 Numerical Recipes Software . */


NRUTIL1.C

#if defined(__STDC__) || defined(ANSI) || defined(NRANSI) /* ANSI */

#include <stdio.h>
#include <stddef.h>
#include <stdlib.h>
#include <malloc.h>
#define NR_END 1
#define FREE_ARG char*

void nrerror(char error_text[])
/* Numerical Recipes standard error handler */
{
fprintf(stderr,"Numerical Recipes run-time error...\n");
fprintf(stderr,"%s\n",error_text);
fprintf(stderr,"...now exiting to system...\n");
exit(1);
}

double *vector(long nl, long nh)
/* allocate a double vector with subscript range v[nl..nh] */
{
double *v;

v=(double *)malloc((size_t) ((nh-nl+1+NR_END)*sizeof(double)));
if (!v) nrerror("allocation failure in vector()");
return v-nl+NR_END;
}

int *ivector(long nl, long nh)
/* allocate an int vector with subscript range v[nl..nh] */
{
int *v;

v=(int *)malloc((size_t) ((nh-nl+1+NR_END)*sizeof(int)));
if (!v) nrerror("allocation failure in ivector()");
return v-nl+NR_END;
}

unsigned char *cvector(long nl, long nh)
/* allocate an unsigned char vector with subscript range v[nl..nh] */
{
unsigned char *v;
```

```
v=(unsigned char *)malloc((size_t) ((nh-nl+1+NR_END)*sizeof(unsigned char)));
if (!v) nrerror("allocation failure in cvector()");
return v-nl+NR_END;
}

unsigned long *lvector(long nl, long nh)
/* allocate an unsigned long vector with subscript range v[nl..nh] */
{
unsigned long *v;

v=(unsigned long *)malloc((size_t) ((nh-nl+1+NR_END)*sizeof(long)));
if (!v) nrerror("allocation failure in lvector()");
return v-nl+NR_END;
}

double *dvector(long nl, long nh)
/* allocate a double vector with subscript range v[nl..nh] */
{
double *v;

v=(double *)malloc((size_t) ((nh-nl+1+NR_END)*sizeof(double)));
if (!v) nrerror("allocation failure in dvector()");
return v-nl+NR_END;
}

double **matrix(long nrl, long nrh, long ncl, long nch)
/* allocate a double matrix with subscript range m[nrl..nrh][ncl..nch] */
{
long i, nrow=nrh-nrl+1,ncol=nch-ncl+1;
double **m;

/* allocate pointers to rows */
m=(double **) malloc((size_t)((nrow+NR_END)*sizeof(double*)));
if (!m) nrerror("allocation failure 1 in matrix()");
m += NR_END;
m -= nrl;

/* allocate rows and set pointers to them */
m[nrl]=(double *) malloc((size_t)((nrow*ncol+NR_END)*sizeof(double)));
if (!m[nrl]) nrerror("allocation failure 2 in matrix()");
m[nrl] += NR_END;
m[nrl] -= ncl;

for(i=nrl+1;i<=nrh;i++) m[i]=m[i-1]+ncol;

/* return pointer to array of pointers to rows */
return m;
}

double **dmatrix(long nrl, long nrh, long ncl, long nch)
/* allocate a double matrix with subscript range m[nrl..nrh][ncl..nch] */
{
long i, nrow=nrh-nrl+1,ncol=nch-ncl+1;
double **m;

/* allocate pointers to rows */
m=(double **) malloc((size_t)((nrow+NR_END)*sizeof(double*)));
if (!m) nrerror("allocation failure 1 in matrix()");
m += NR_END;
m -= nrl;

/* allocate rows and set pointers to them */
m[nrl]=(double *) malloc((size_t)((nrow*ncol+NR_END)*sizeof(double)));
if (!m[nrl]) nrerror("allocation failure 2 in matrix()");
m[nrl] += NR_END;
m[nrl] -= ncl;

for(i=nrl+1;i<=nrh;i++) m[i]=m[i-1]+ncol;

/* return pointer to array of pointers to rows */
return m;
}

int **imatrix(long nrl, long nrh, long ncl, long nch)
/* allocate a int matrix with subscript range m[nrl..nrh][ncl..nch] */
{
long i, nrow=nrh-nrl+1,ncol=nch-ncl+1;
```

```
int **m;

/* allocate pointers to rows */
m=(int **) malloc((size_t)((nrow+NR_END)*sizeof(int*)));
if (!m) nrerror("allocation failure 1 in matrix()");
m += NR_END;
m -= nrl;


/* allocate rows and set pointers to them */
m[nrl]=(int *) malloc((size_t)((nrow*ncol+NR_END)*sizeof(int)));
if (!m[nrl]) nrerror("allocation failure 2 in matrix()");
m[nrl] += NR_END;
m[nrl] -= ncl;

for(i=nrl+1;i<=nrh;i++) m[i]=m[i-1]+ncol;

/* return pointer to array of pointers to rows */
return m;
}

double **submatrix(double **a, long oldrl, long oldrh, long oldcl, long oldch,
long newrl, long newcl)
/* point a submatrix [newrl..][newcl..] to a[oldrl..oldrh][oldcl..oldch] */
{
long i,j,nrow=oldrh-oldrl+1,ncol=oldcl-newcl;
double **m;

/* allocate array of pointers to rows */
m=(double **) malloc((size_t) ((nrow+NR_END)*sizeof(double*)));
if (!m) nrerror("allocation failure in submatrix()");
m += NR_END;
m -= newrl;

/* set pointers to rows */
for(i=oldrl,j=newrl;i<=oldrh;i++,j++) m[j]=a[i]+ncol;

/* return pointer to array of pointers to rows */
return m;
}

double **convert_matrix(double *a, long nrl, long nrh, long ncl, long nch)
/* allocate a double matrix m[nrl..nrh][ncl..nch] that points to the matrix
declared in the standard C manner as a[nrow][ncol], where nrow=nrh-nrl+1
and ncol=nch-ncl+1. The routine should be called with the address
&a[0][0] as the first argument. */
{
long i,j,nrow=nrh-nrl+1,ncol=nch-ncl+1;
double **m;

/* allocate pointers to rows */
m=(double **) malloc((size_t) ((nrow+NR_END)*sizeof(double*)));
if (!m) nrerror("allocation failure in convert_matrix()");
m += NR_END;
m -= nrl;

/* set pointers to rows */
m[nrl]=a-ncl;
for(i=1,j=nrl+1;i<nrow;i++,j++) m[j]=m[j-1]+ncol;
/* return pointer to array of pointers to rows */
return m;
}

double ***f3tensor(long nrl, long nrh, long ncl, long nch, long ndl, long ndh)
/* allocate a double 3tensor with range t[nrl..nrh][ncl..nch][ndl..ndh] */
{
long i,j,nrow=nrh-nrl+1,ncol=nch-ncl+1,ndep=ndh-ndl+1;
double ***t;

/* allocate pointers to pointers to rows */
t=(double ***) malloc((size_t)((nrow+NR_END)*sizeof(double**)));
if (!t) nrerror("allocation failure 1 in f3tensor()");
t += NR_END;
t -= nrl;

/* allocate pointers to rows and set pointers to them */
t[nrl]=(double **) malloc((size_t)((nrow*ncol+NR_END)*sizeof(double*)));
if (!t[nrl]) nrerror("allocation failure 2 in f3tensor()");
```

```
t[nrl] += NR_END;
t[nrl] -= ncl;

/* allocate rows and set pointers to them */
t[nrl][ncl]=(double *) malloc((size_t)((nrow*ncol*ndep+NR_END)*sizeof(double)));
if (!t[nrl][ncl]) nrerror("allocation failure 3 in f3tensor()");
t[nrl][ncl] += NR_END;
t[nrl][ncl] -= ndl;

for(j=ncl+1;j<=nch;j++) t[nrl][j]=t[nrl][j-1]+ndep;
for(i=nrl+1;i<=nrh;i++)
  {
  t[i]=t[i-1]+ncol;
  t[i][ncl]=t[i-1][ncl]+ncol*ndep;
  for(j=ncl+1;j<=nch;j++) t[i][j]=t[i][j-1]+ndep;
  }

/* return pointer to array of pointers to rows */
return t;
}

void free_vector(double *v, long nl, long nh)
/* free a double vector allocated with vector() */
{
free((FREE_ARG) (v+nl-NR_END));
}

void free_ivector(int *v, long nl, long nh)
/* free an int vector allocated with ivector() */
{
free((FREE_ARG) (v+nl-NR_END));
}

void free_cvector(unsigned char *v, long nl, long nh)
/* free an unsigned char vector allocated with cvector() */
{
free((FREE_ARG) (v+nl-NR_END));
}

void free_lvector(unsigned long *v, long nl, long nh)
/* free an unsigned long vector allocated with lvector() */
{
free((FREE_ARG) (v+nl-NR_END));
}

void free_dvector(double *v, long nl, long nh)
/* free a double vector allocated with dvector() */
{
free((FREE_ARG) (v+nl-NR_END));
}

void free_matrix(double **m, long nrl, long nrh, long ncl, long nch)
/* free a double matrix allocated by matrix() */
{
free((FREE_ARG) (m[nrl]+ncl-NR_END));
free((FREE_ARG) (m+nrl-NR_END));
}

void free_dmatrix(double **m, long nrl, long nrh, long ncl, long nch)
/* free a double matrix allocated by dmatrix() */
{
free((FREE_ARG) (m[nrl]+ncl-NR_END));
free((FREE_ARG) (m+nrl-NR_END));
}

void free_imatrix(int **m, long nrl, long nrh, long ncl, long nch)
/* free an int matrix allocated by imatrix() */
{
free((FREE_ARG) (m[nrl]+ncl-NR_END));
free((FREE_ARG) (m+nrl-NR_END));
}

void free_submatrix(double **b, long nrl, long nrh, long ncl, long nch)
/* free a submatrix allocated by submatrix() */
{
free((FREE_ARG) (b+nrl-NR_END));
}
```

```
void free_convert_matrix(double **b, long nrl, long nrh, long ncl, long nch)
/* free a matrix allocated by convert_matrix() */
{
free((FREE_ARG) (b+nrl-NR_END));
}

void free_f3tensor(double ***t, long nrl, long nrh, long ncl, long nch,
        long ndl, long ndh)
/* free a double f3tensor allocated by f3tensor() */
{
free((FREE_ARG) (t[nrl][ncl]+ndl-NR_END));
free((FREE_ARG) (t[nrl]+ncl-NR_END));
free((FREE_ARG) (t+nrl-NR_END));
}

#else /* ANSI */
/* traditional - K&R */

#include <stdio.h>
#include <malloc.h>
#define NR_END 1
#define FREE_ARG char*

void nrerror(error_text)
char error_text[];
/* Numerical Recipes standard error handler */
{
void exit();

fprintf(stderr,"Numerical Recipes run-time error...\n");
fprintf(stderr,"%s\n",error_text);
fprintf(stderr,"...now exiting to system...\n");
exit(1);
}

double *vector(nl,nh)
long nh,nl;
/* allocate a double vector with subscript range v[nl..nh] */
{
double *v;

v=(double *)malloc((unsigned int) ((nh-nl+1+NR_END)*sizeof(double)));
if (!v) nrerror("allocation failure in vector()");
return v-nl+NR_END;
}

int *ivector(nl,nh)
long nh,nl;
/* allocate an int vector with subscript range v[nl..nh] */
{
int *v;

v=(int *)malloc((unsigned int) ((nh-nl+1+NR_END)*sizeof(int)));
if (!v) nrerror("allocation failure in ivector()");
return v-nl+NR_END;
}

unsigned char *cvector(nl,nh)
long nh,nl;
/* allocate an unsigned char vector with subscript range v[nl..nh] */
{
unsigned char *v;

v=(unsigned char *)malloc((unsigned int) ((nh-nl+1+NR_END)*sizeof(unsigned char)));
if (!v) nrerror("allocation failure in cvector()");
return v-nl+NR_END;
}

unsigned long *lvector(nl,nh)
long nh,nl;
/* allocate an unsigned long vector with subscript range v[nl..nh] */
{
unsigned long *v;

v=(unsigned long *)malloc((unsigned int) ((nh-nl+1+NR_END)*sizeof(long)));
if (!v) nrerror("allocation failure in lvector()");
return v-nl+NR_END;
}
```

```
double *dvector(nl,nh)
long nh,nl;
/* allocate a double vector with subscript range v[nl..nh] */
{
double *v;

v=(double *)malloc((unsigned int) ((nh-nl+1+NR_END)*sizeof(double)));
if (!v) nrerror("allocation failure in dvector()");
return v-nl+NR_END;
}

double **matrix(nrl,nrh,ncl,nch)
long nch,ncl,nrh,nrl;
/* allocate a double matrix with subscript range m[nrl..nrh][ncl..nch] */
{
long i, nrow=nrh-nrl+1,ncol=nch-ncl+1;
double **m;

/* allocate pointers to rows */
m=(double **) malloc((unsigned int)((nrow+NR_END)*sizeof(double*)));
if (!m) nrerror("allocation failure 1 in matrix()");
m += NR_END;
m -= nrl;

/* allocate rows and set pointers to them */
m[nrl]=(double *) malloc((unsigned int)((nrow*ncol+NR_END)*sizeof(double)));
if (!m[nrl]) nrerror("allocation failure 2 in matrix()");
m[nrl] += NR_END;
m[nrl] -= ncl;

for(i=nrl+1;i<=nrh;i++) m[i]=m[i-1]+ncol;

/* return pointer to array of pointers to rows */
return m;
}

double **dmatrix(nrl,nrh,ncl,nch)
long nch,ncl,nrh,nrl;
/* allocate a double matrix with subscript range m[nrl..nrh][ncl..nch] */
{
long i, nrow=nrh-nrl+1,ncol=nch-ncl+1;
double **m;

/* allocate pointers to rows */
m=(double **) malloc((unsigned int)((nrow+NR_END)*sizeof(double*)));
if (!m) nrerror("allocation failure 1 in matrix()");
m += NR_END;
m -= nrl;

/* allocate rows and set pointers to them */
m[nrl]=(double *) malloc((unsigned int)((nrow*ncol+NR_END)*sizeof(double)));
if (!m[nrl]) nrerror("allocation failure 2 in matrix()");
m[nrl] += NR_END;
m[nrl] -= ncl;

for(i=nrl+1;i<=nrh;i++) m[i]=m[i-1]+ncol;

/* return pointer to array of pointers to rows */
return m;
}

int **imatrix(nrl,nrh,ncl,nch)
long nch,ncl,nrh,nrl;
/* allocate a int matrix with subscript range m[nrl..nrh][ncl..nch] */
{
long i, nrow=nrh-nrl+1,ncol=nch-ncl+1;
int **m;

/* allocate pointers to rows */
m=(int **) malloc((unsigned int)((nrow+NR_END)*sizeof(int*)));
if (!m) nrerror("allocation failure 1 in matrix()");
m += NR_END;
m -= nrl;


/* allocate rows and set pointers to them */
m[nrl]=(int *) malloc((unsigned int)((nrow*ncol+NR_END)*sizeof(int)));
```

```
if (!m[nrl]) nrerror("allocation failure 2 in matrix()");
m[nrl] += NR_END;
m[nrl] -= ncl;

for(i=nrl+1;i<=nrh;i++) m[i]=m[i-1]+ncol;

/* return pointer to array of pointers to rows */
return m;
}

double **submatrix(a,oldrl,oldrh,oldcl,oldch,newrl,newcl)
double **a;
long newcl,newrl,oldch,oldcl,oldrh,oldrl;
/* point a submatrix [newrl..][newcl..] to a[oldrl..oldrh][oldcl..oldch] */
{
long i,j,nrow=oldrh-oldrl+1,ncol=oldcl-newcl;
double **m;

/* allocate array of pointers to rows */
m=(double **) malloc((unsigned int) ((nrow+NR_END)*sizeof(double*)));
if (!m) nrerror("allocation failure in submatrix()");
m += NR_END;
m -= newrl;

/* set pointers to rows */
for(i=oldrl,j=newrl;i<=oldrh;i++,j++) m[j]=a[i]+ncol;

/* return pointer to array of pointers to rows */
return m;
}

double **convert_matrix(a,nrl,nrh,ncl,nch)
double *a;
long nch,ncl,nrh,nrl;
/* allocate a double matrix m[nrl..nrh][ncl..nch] that points to the matrix
declared in the standard C manner as a[nrow][ncol], where nrow=nrh-nrl+1
and ncol=nch-ncl+1. The routine should be called with the address
&a[0][0] as the first argument. */
{
long i,j,nrow=nrh-nrl+1,ncol=nch-ncl+1;
double **m;

/* allocate pointers to rows */
m=(double **) malloc((unsigned int) ((nrow+NR_END)*sizeof(double*)));
if (!m) nrerror("allocation failure in convert_matrix()");
m += NR_END;
m -= nrl;

/* set pointers to rows */
m[nrl]=a-ncl;
for(i=1,j=nrl+1;i<nrow;i++,j++) m[j]=m[j-1]+ncol;
/* return pointer to array of pointers to rows */
return m;
}

double ***f3tensor(nrl,nrh,ncl,nch,ndl,ndh)
long nch,ncl,ndh,ndl,nrh,nrl;
/* allocate a double 3tensor with range t[nrl..nrh][ncl..nch][ndl..ndh] */
{
long i,j,nrow=nrh-nrl+1,ncol=nch-ncl+1,ndep=ndh-ndl+1;
double ***t;

/* allocate pointers to pointers to rows */
t=(double ***) malloc((unsigned int)((nrow+NR_END)*sizeof(double**)));
if (!t) nrerror("allocation failure 1 in f3tensor()");
t += NR_END;
t -= nrl;

/* allocate pointers to rows and set pointers to them */
t[nrl]=(double **) malloc((unsigned int)((nrow*ncol+NR_END)*sizeof(double*)));
if (!t[nrl]) nrerror("allocation failure 2 in f3tensor()");
t[nrl] += NR_END;
t[nrl] -= ncl;

/* allocate rows and set pointers to them */
t[nrl][ncl]=(double *) malloc((unsigned int)((nrow*ncol*ndep+NR_END)*sizeof(double)));
if (!t[nrl][ncl]) nrerror("allocation failure 3 in f3tensor()");
t[nrl][ncl] += NR_END;
```

```
    t[nrl][ncl] -= ndl;

    for(j=ncl+1;j<=nch;j++) t[nrl][j]=t[nrl][j-1]+ndep;
    for(i=nrl+1;i<=nrh;i++)
      {
      t[i]=t[i-1]+ncol;
      t[i][ncl]=t[i-1][ncl]+ncol*ndep;
      for(j=ncl+1;j<=nch;j++) t[i][j]=t[i][j-1]+ndep;
      }

    /* return pointer to array of pointers to rows */
    return t;
    }

    void free_vector(v,nl,nh)
    double *v;
    long nh,nl;
    /* free a double vector allocated with vector() */
    {
    free((FREE_ARG) (v+nl-NR_END));
    }

    void free_ivector(v,nl,nh)
    int *v;
    long nh,nl;
    /* free an int vector allocated with ivector() */
    {
    free((FREE_ARG) (v+nl-NR_END));
    }

    void free_cvector(v,nl,nh)
    long nh,nl;
    unsigned char *v;
    /* free an unsigned char vector allocated with cvector() */
    {
    free((FREE_ARG) (v+nl-NR_END));
    }

    void free_lvector(v,nl,nh)
    long nh,nl;
    unsigned long *v;
    /* free an unsigned long vector allocated with lvector() */
    {
    free((FREE_ARG) (v+nl-NR_END));
    }

    void free_dvector(v,nl,nh)
    double *v;
    long nh,nl;
    /* free a double vector allocated with dvector() */
    {
    free((FREE_ARG) (v+nl-NR_END));
    }

    void free_matrix(m,nrl,nrh,ncl,nch)
    double **m;
    long nch,ncl,nrh,nrl;
    /* free a double matrix allocated by matrix() */
    {
    free((FREE_ARG) (m[nrl]+ncl-NR_END));
    free((FREE_ARG) (m+nrl-NR_END));
    }

    void free_dmatrix(m,nrl,nrh,ncl,nch)
    double **m;
    long nch,ncl,nrh,nrl;
    /* free a double matrix allocated by dmatrix() */
    {
    free((FREE_ARG) (m[nrl]+ncl-NR_END));
    free((FREE_ARG) (m+nrl-NR_END));
    }

    void free_imatrix(m,nrl,nrh,ncl,nch)
    int **m;
    long nch,ncl,nrh,nrl;
    /* free an int matrix allocated by imatrix() */
    {
    free((FREE_ARG) (m[nrl]+ncl-NR_END));
```

```
free((FREE_ARG) (m+nrl-NR_END));
}

void free_submatrix(b,nrl,nrh,ncl,nch)
double **b;
long nch,ncl,nrh,nrl;
/* free a submatrix allocated by submatrix() */
{
free((FREE_ARG) (b+nrl-NR_END));
}

void free_convert_matrix(b,nrl,nrh,ncl,nch)
double **b;
long nch,ncl,nrh,nrl;
/* free a matrix allocated by convert_matrix() */
{
free((FREE_ARG) (b+nrl-NR_END));
}

void free_f3tensor(t,nrl,nrh,ncl,nch,ndl,ndh)
double ***t;
long nch,ncl,ndh,ndl,nrh,nrl;
/* free a double f3tensor allocated by f3tensor() */
{
free((FREE_ARG) (t[nrl][ncl]+ndl-NR_END));
free((FREE_ARG) (t[nrl]+ncl-NR_END));
free((FREE_ARG) (t+nrl-NR_END));
}

#endif /* ANSI */
```

MNBRAK1.c

```
#include <math.h>
#define NRANSI
#include "nrutil1.h"
#define GOLD 1.618034
#define GLIMIT 100.0
#define TINY 1.0e-20
#define SHFT(a,b,c,d) (a)=(b);(b)=(c);(c)=(d);

void mnbrak(double *ax, double *bx, double *cx, double *fa, double *fb, double *fc,
            double (*func)(double))
{
double ulim,u,r,q,fu,dum;

*fa=(*func)(*ax);
*fb=(*func)(*bx);
if (*fb > *fa)
  {
  SHFT(dum,*ax,*bx,dum)
  SHFT(dum,*fb,*fa,dum)
  }
*cx=(*bx)+GOLD*(*bx-*ax);
*fc=(*func)(*cx);
while (*fb > *fc)
  {
  r=(*bx-*ax)*(*fb-*fc);
  q=(*bx-*cx)*(*fb-*fa);
  u=(*bx)-((*bx-*cx)*q-(*bx-*ax)*r)/
    (2.0*SIGN(FMAX(fabs(q-r),TINY),q-r));
  ulim=(*bx)+GLIMIT*(*cx-*bx);
  if ((*bx-u)*(u-*cx) > 0.0)
    {
    fu=(*func)(u);
    if (fu < *fc)
      {
      *ax=(*bx);
      *bx=u;
      *fa=(*fb);
      *fb=fu;
      return;
      }
    else if (fu > *fb)
      {
      *cx=u;
      *fc=fu;
```

```
        return;
        }
      u=(*cx)+GOLD*(*cx-*bx);
      fu=(*func)(u);
      }
    else if ((*cx-u)*(u-ulim) > 0.0)
      {
      fu=(*func)(u);
      if (fu < *fc)
        {
        SHFT(*bx,*cx,u,*cx+GOLD*(*cx-*bx))
        SHFT(*fb,*fc,fu,(*func)(u))
        }
      }
    else if ((u-ulim)*(ulim-*cx) >= 0.0)
      {
      u=ulim;
      fu=(*func)(u);
      }
    else
      {
      u=(*cx)+GOLD*(*cx-*bx);
      fu=(*func)(u);
      }
    SHFT(*ax,*bx,*cx,u)
    SHFT(*fa,*fb,*fc,fu)
    }
  }
  #undef GOLD
  #undef GLIMIT
  #undef TINY
  #undef SHFT
  #undef NRANSI
  /* (C) Copr. 1986-92 Numerical Recipes Software . */


  BRENT1.C

  #include <math.h>
  #define NRANSI
  #include "nrutil1.h"
  #define ITMAX 100
  #define CGOLD 0.3819660
  #define ZEPS 1.0e-10
  #define SHFT(a,b,c,d) (a)=(b);(b)=(c);(c)=(d);

  double brent(double ax, double bx, double cx, double (*f)(double), double tol,
        double *xmin)
  {
  int iter;
  double a,b,d,etemp,fu,fv,fw,fx,p,q,r,tol1,tol2,u,v,w,x,xm;
  double e=0.0;

  a=(ax < cx ? ax : cx);
  b=(ax > cx ? ax : cx);
  x=w=v=bx;
  fw=fv=fx=(*f)(x);
  for (iter=1;iter<=ITMAX;iter++)
    {
    xm=0.5*(a+b);
    tol2=2.0*(tol1=tol*fabs(x)+ZEPS);
    if (fabs(x-xm) <= (tol2-0.5*(b-a))) {
    *xmin=x;
    return fx;
    }
  if(fabs(e) > tol1)
    {
    r=(x-w)*(fx-fv);
    q=(x-v)*(fx-fw);
    p=(x-v)*q-(x-w)*r;
    q=2.0*(q-r);
    if (q > 0.0) p = -p;
    q=fabs(q);
    etemp=e;
    e=d;
    if(fabs(p) >= fabs(0.5*q*etemp) || p <= q*(a-x) || p >= q*(b-x))
    d=CGOLD*(e=(x >= xm ? a-x : b-x));
    else
```

```
        {
        d=p/q;
        u=x+d;
        if (u-a < tol2 || b-u < tol2)
        d=SIGN(tol1,xm-x);
        }
      }
    else
      {
      d=CGOLD*(e=(x >= xm ? a-x : b-x));
      }
    u=(fabs(d) >= tol1 ? x+d : x+SIGN(tol1,d));
    fu=(*f)(u);
    if(fu <= fx)
      {
      if (u >= x) a=x; else b=x;
      SHFT(v,w,x,u)
      SHFT(fv,fw,fx,fu)
      }
    else
      {
      if (u < x) a=u; else b=u;
      if (fu <= fw || w == x)
        {
        v=w;
        w=u;
        fv=fw;
        fw=fu;
        }
      else if (fu <= fv || v == x || v == w)
        {
        v=u;
        fv=fu;
        }
      }
  }
  nrerror("Too many iterations in brent");
  *xmin=x;
  return fx;
  }
  #undef ITMAX
  #undef CGOLD
  #undef ZEPS
  #undef SHFT
  #undef NRANSI
  /* (C) Copr. 1986-92 Numerical Recipes Software . */


  POWELL1.C

  #include <math.h>
  #define NRANSI
  #include "nrutil1.h"
  #define ITMAX 200

  void powell(double p[], double **xi, int n, double ftol, int *iter, double *fret,
              double (*func)(double []))
  {
  void linmin(double p[], double xi[], int n, double *fret,
              double (*func)(double []));
  int i,ibig,j;
  double del,fp,fptt,t,*pt,*ptt,*xit;

  pt=vector(1,n);
  ptt=vector(1,n);
  xit=vector(1,n);
  *fret=(*func)(p);
  for (j=1;j<=n;j++) pt[j]=p[j];
  for (*iter=1;;++(*iter))
    {
    fp=(*fret);
    ibig=0;
    del=0.0;
    for (i=1;i<=n;i++)
      {
      for (j=1;j<=n;j++) xit[j]=xi[j][i];
      fptt=(*fret);
      linmin(p,xit,n,fret,func);
```

```
            if(fabs(fptt-(*fret)) > del)
              {
              del=fabs(fptt-(*fret));
              ibig=i;
              }
            }
          if(2.0*fabs(fp-(*fret)) <= ftol*(fabs(fp)+fabs(*fret)))
            {
            free_vector(xit,1,n);
            free_vector(ptt,1,n);
            free_vector(pt,1,n);
            return;
            }
          if (*iter == ITMAX) nrerror("powell exceeding maximum iterations.");
          for (j=1;j<=n;j++)
            {
            ptt[j]=2.0*p[j]-pt[j];
            xit[j]=p[j]-pt[j];
            pt[j]=p[j];
            }
          fptt=(*func)(ptt);
          if(fptt < fp)
            {
            t=2.0*(fp-2.0*(*fret)+fptt)*SQR(fp-(*fret)-del)-del*SQR(fp-fptt);
            if (t < 0.0)
              {
              linmin(p,xit,n,fret,func);
              for (j=1;j<=n;j++)
                {
                xi[j][ibig]=xi[j][n];
                xi[j][n]=xit[j];
                }
              }
            }
        }
    }
}
#undef ITMAX
#undef NRANSI
/* (C) Copr. 1986-92 Numerical Recipes Software . */
```

References

[1] [Abraham,1996] Abraham D. W., Praino A. P., Re M. E., and Wickramasinghe H. K., "Method and apparatus for detecting asperities on magnetic disk using thermal proximity imaging," U.S. patent 5527110, June 18, 1996.

[2] [Archard & Kirk, 1961] Archard J. F., and Kirk M. T., "Lubrication at point contacts," Proc. Roy. Soc. (London) A261, 532-550, 1961.

[3] [Aruga et al., 1986] Aruga K., Mizoshita Y., Yamada T., and Yaneoka S., "Spacing fluctuation of flying head sliders in track accessing (forced vibration analysis using finite element method)," Tribology and Mechanics of Magnetic Storage System, vol.3, (B. Bhushan, and N. S. Eiss, eds.), pp.79-86, SP-21, ASLE, Park Ridge, Illinois, 1986.

[4] [Azzam & Bashara, 1987] Azzam R. M. A. and Bashara N. M., *Ellipsometry and Polarized Light,* North-Holland, 1987.

[5] [Best, 1987] Best G. L., "Comparison of optical and capacitive measurements of slider dynamics," IEEE Transactions on Magnetics, Vol.23, pp.3453-3455, 1987.

[6] [Best et al.,1986] Best G. L., Horne D. E., Chiou A., and Sussner H., "Precise optical measurement of slider dynamics," IEEE Transactions on Magnetics, Vol.22, pp.1017-1019, 1986.

[7] [Bhushan, 1996] Bhushan Bharat, *Tribology and Mechanics of Magnetic Storage Devices*, 2nd edition, Springer, 1996.

[8] [Bogy & Talke, 1985] Bogy D. B., and Talke F. E., "Laser Doppler interferometry on magnetic recording systems," IEEE Transactions on Magnetics, Vol.21, pp.1332-1337, 1984.

[9] [Born & Wolf, 1989] Born M. and Wolf E., *Principle of optics*, Pergamon Press, Oxford, 1989.

[10] Bouchard G., Miu D. K., Bogy D. B., and Talke F. E., "On the dynamics of Winchester and 3370-type sliders used in magnetic recording disk files," in Tribology and Mechanics of Magnetic Storage Systems, Vol.1 (B. Bhushan et al., eds.), pp.85-89, SP-16, ASLE, Park Ridge, Illinois, 1984.

[11] Bouchard G., Bogy D. B., and Talke F. E., "An experimental comparison of the head/disk interface dynamics in $5\frac{1}{4}$ and 8-inch disk drives," IBM J. Res. Develop. Vol.29, pp.316-323, 1985

[12] [Bouchard et al., 1985] Bouchard G., Bogy D. B., and Talke F. E., "Use of a laser Doppler anemometer for studying in-plane motions of sliders in magnetic disk files," in Tribology and Mechanics of Magnetic Storage Systems, Vol.2 (B. Bhushan and N. S. Eiss, eds.), pp.87-89, SP-19, ASLE, Park Ridge, Illinois, 1985.

[13] Briggs G. R., and Herkart P. G., "Unshielded capacitor probe technique for determining disk file ceramic slider flying characteristics," IEEE Transactions on Magnetics, Vol.7, pp.428-, 1971.

[14] [Briggs & Talke, 1989] Briggs C. A. and Talke F. E., "An investigation of the IBM 3380 K slider using laser doppler interferometry," IEEE Transactions on Magnetics, Vol.25, No.5, pp.3707-3709, 1989.

[15] [Cameron & Gohar, 1966] Cameron A., and Gohar R., "Theoretical and experimental studies of the oil film in lubricated point contacts," Proc. Roy. Soc. (London) A291, 520-536, 1966.

[16] Cha Ellis, Chiang Chisin, Enguero Jorge, Lee Jerry J. K., "Effect of temperature and altitude on flying height," IEEE Transactions on Magnetics, Vol.32, No.5, Pt.1, pp 3729-3731, Sep., 1996.

[17] [Crook, 1958] Crook A. W., "the lubrication of rollers," Pro. Roy. Soc. (London), Phil. Trans. A250, 387-409, 1958.

[18] [Crook, 1961] Crook A. W., "Elastohydrodynamic lubrication of rollers," Nature 190, 1182-1183, 1961.

[19] Dahlgren R. P., "Calibration standards for flying height testers," U.S. Patent, No.4624564, Nov., 1986.

[20] [de Groot 1996] de Groot Peter, "Optical gap measuring apparatus and method," U.S. patent 5557399, September 1996.

[21] [de Groot et al., 1996a] de Groot P.; Deck L.; Sobbitsky J.; Biegen J. "Polarization interferometer for measuring the flying height of magnetic read-write heads," Optics Letters Vol.21, No.6, pp.441-443, March,1996.

[22] [de Groot et al., 1996b] de Groot P. D., Deck L., Soobitsky J., Biegen J., "Optical flying-height testing of magnetic read-write heads," Proceedings of the SPIE, Vol.2782, pp.47-57, 1996.

[23] [de Groot, 1998a] de Groot Peter, "Determining the optical constants of read-write sliders during flying height testing," Applied. Optics, Vol.37, pp.5116-5125, 1998.

[24] [de Groot, 1998b] de Groot Peter, "Birefringence in rapidly-rotating glass disk," Journal of Optics Society of America, A15, pp.1202-1211, 1998.

[25] Duran Carlos A, "Error analysis of a multiwavelength dynamic flying height tester," IEEE Transactions on Magnetics Vol.32, No.5, Pt.1, pp.3720-3722, Sep., 1996.

[26] Deng Y., Tsai H., and Nixon B. J., "Drive-level flying height measurements and altitude effects," IEEE Transactions on Magnetics Vol.30, No.6, pp.4191-4193, 1994.

[27] [Eaton & Baldwinson, 1997] Eaton R., and Baldwinson M., "Imaging of media lubricant spacing contributions by readback signal analysis," IEEE Transactions on Magnetics Vol.33, No.1, pp.974-977, 1997.

[28] [Erickson & Lauer, 1997] Erickson T. E. and Lauer J. P., "Multiplexed laser interferometer for non-dispersed spectrum detection in a dynamic flying height tester," US Patent, No.5673110, Sep.30, 1997.

[29] [Feliss & Talke, 1977] "Capacitance probe study of rotating head/tape interface," IBM J. Res. Develop. Vol.21, pp.289-293, 1977.

[30] [Fleisher & Lin, 1974] Fleisher J. M. and Lin C., "Infrared laser interferometer for measuring air-bearing separation," IBM Journal of Research and Development, Vol.18, No.6, pp.529-533, 1974.

[31] [Foored et al., 1969-1970] Foored C. A., Wedevan L. D., Westlake F. J., and Cameron A., "Optical elastohydrodynamics," Proc. Inst. Mech. Engrs., 184, Part I, 1969-1970.

[32] [Fridge & Miller, 1986] Fridge D. A. and Miller K. A., U.S. Patent, No.4593368, June 3, 1986.

[33] Fukuzawa Tadashi, Hisano Teiji, Watabe Hiroshi, "Glass disk distortion effect in an optical flying height tester," IEEE Transactions on Magnetics, Vol.32, No.5, Pt.1, pp.3690-3692, Sep., 1996.

[34] [Fukuzawa et al, 1996] Fukuzawa T., Hisano T., Morita T. and Ikarugi K., "Method and apparatus for measuring flying height of a magnetic head above a disk surface at three wavelength," U.S. Patent, No. 5502565, Mar., 1996.

[35] Guerra J. M., and Plummer W. T., "Optical proximity imaging method and apparatus," U.S. Patent, No.4681451, July, 1987.

[36] [Guerra, 1998] Guerra J. M., "Dark field, photon tunnelling imaging system and methods for measuring flying height of read/write heads," U.S. Patent, No.5719677, Feb., 1998.

[37] [Hariharan, 1985] Hariharan P., *Optical Interferometry*, Academic Press, Orlando, Florida, 1985.

[38] Hegde S. G., Scranton R. A., and Yarmchuk E. J., "Capacitive measurement and control of the flying height of a recording slider," U.S. Patent, No.4931887, June 5, 1990.

[39] [Hendriks, 1988] Hendriks F., "A design tool for steady gas bearings using finite elements," Tribology and Mechanics of Magnetic Storage System, vol.5, (B. Bhushan and N. S. Eiss, eds.), pp.124-129, SP-25, ASLE, Park Ridge, Illinois, 1988.

[40] Henze D., Mui P., Clifford G. and Davidson R. J., "Multi-channel interferometer measurments of slider flying height and pitch," IEEE Transactions on Magnetics, Vol.25, No.5, pp.3710-3712, 1989.

[41] [Hoagland and Monson, 1991] Hoagland A. S., and Monson J. E., *Digital Magnetic Recording*, 2nd edition, John Wiley & Sons, Inc., 1991.

[42] [Hu & Bogy, 1997] Hu Y. And Bogy D. B., "Dynamic stability and spacing modulation of sub-25 nm fly height sliders," Journal of Tribology, Transactions of ASME, Vol.119, pp.646-652, 1997.

[43] Klaassen K. B. and van Peppen J. C. L., "Method and circuitry for in-situ measurement of transducer and transducer magnetic instability," U.S. Patent, No.5130866, July 14, 1992.

[44] [Klaassen & van Peppen, 1994] Klaassen K. B. and van Peppen J. C. L., "Slider-disk clearance measurements in magnetic disk drives using the readback transducer," IEEE Transactions on Instrumentation and Measuement, Vol.43, No.2, pp.121-126, 1994.

[45] [Lacey et al., 1992] Lacey, C., Adams, J. A., Ross, E. W., Cormier, A., "A new method for measuring flying height dynamically," Phase Metrics communication , 1992.

[46] [Lacey et al, 1993] Lacey C., Shelor R., Cormier A., and Talke F. E., "Interferometric measurement of disk/slider spacing: the effect of phase shift on reflection," IEEE Transactions on Magnetics, Vol.29, No.6, 1993.

[47] [Lacey & Ross, 1995] Lacey C., Ross E., "Method and apparatus to calibrate intensity and determine fringe order for interferometric measurement of small spacings," U.S. Patent, No. 5457534, 1995.

[48] Lacey C., and Womack K., "Imaging polarimeter detector for measurement of small spacing," U.S. Patent, No.5638178, June, 1997.

[49] [Lee & Wu, 1995] Lee C. K., Wu T. W., "Differential laser interferometer for nanometer displacement measurements," AIAA Journal, Vol.33, No.9, pp.1675-1680, Sept., 1995.

[50] [Li et al, 2001] Li A, Liu X, Jenkins D, Clegg W, Davey P., "Parameter estimation method for real time flying height detection of hard disk drives," presented at the IEEE/AIP 8th Joint MMM-Intermag Conference, San Antonio, Texas, January 7-11, 2001.

[51] Li Y, Menon A. K., Goglia P., "The development and implementation of a flying height tester calibration standard," IEEE Transactions on Magnetics, Vol.30, Vol.6, Pt.1, pp.4131-4133, Nov., 1994.

[52] Li Y, and Menon A. K., "On the flying height determination of film-coated magnetic heads," Adv. Info. Storage Syst., Vol.6, pp.55-67, 1995

[53] Li Y., Menon A. K., Goglia P., "Flat-head/bump-disk apparatus for evaluating the accuracy of a flying height tester," IEEE Transactions on Magnetics, Vol.32, No.5, Pt.1, pp.3678-3680, Sep., 1996.

[54] [Li et al, 1996] Li Y., Menon A. K., Goglia P. "Evaluations of diamond-like-carbon film optical constants and their effects on flying height determination," Transactions of the ASME, Journal of Tribology, Vol.118, No.4, pp.767-773, Oct., 1996.

[55] [Li & Menon, 1996] Li Y., Menon A. K., "Flying height measurement metrology for ultra-low spacing in rigid magnetic recording," IEEE Transactions on Magnetics, Vol.32, No.1, pp.129-134, Jan., 1996.

[56] [Li, 1997] Li Y., "Flying height measurement on Al_2O_3 film of a magnetic slider," Journal of Tribology, Vol.119, pp.681-686, 1997.

[57] Li Y., and Wang G., "In-situ alumina recession and protrusion measurement on a magnetic head," IEEE Transactions on Magnetics, Vol.34, No.4, pp.1771-1776, July, 1996.

[58] [Licht, 1968] Licht L., "An experimental study of self-acting foil bearings," J. Lub. Tech., Trans. ASME90, 199-220, 1968.

[59] [Lin, 1973] Lin C., "Techniques for the measurement of air bearing separation - a review," IEEE Transactions on Magnetics, V9, 4, pp673-677, 1973.

[60] Lin C., and Sullivan R. F., "An application of white light interferometry in thin film measurements," IBM Journal of Research and Development, Vol.16, No.3, pp.269-276, 1972.

[61] [Liu et al., 1999] Liu B, Zhu Y, Li Y, Hua W, Leng Q, Sheng G. "An experimental study of slider vibration in nanometer spaced head-disk interface," IEEE Transactions on Magnetics, Vol.35, No.5, pp.2463-2465, 1999.

[62] [Liu et al., 2000] Liu X. Q., Clegg W. W., and Liu B., "Ultra low head disk spacing measurement using dual beam polarisation interferometry," Accepted for publication on Optics & Laser technology, 2000.

[63] Lo J. L., and Sides P. J., "Measurement of flying height by scattered total internal reflection," J. Appl. Phys., Vol.81, No.8, pp.5381-5383, 1997.

[64] [Lue & Lacey, 1994] Lue K., Lacey C., Talke F.E. "Measurement of flying height with carbon overcoated sliders," IEEE Transactions on Magnetics, Vol.30, No.6, pp.4167-4169, Nov. 1994.

[65] Mager M., "Method and apparatus for calibration of optical flying height testers," U.S. Patent, No.5220408, June, 1993.

[66] Mallinson J. C., *The Foundations of Magnetic Recording*, 2nd edition, Academic press, 1993.

[67] [McMillan &Talke, 1994] McMillan T. C.; Talke F. E., "Ultra low flying height measurements using monochromatic and phase demodulated laser interferometry," IEEE Transactions on Magnetics, Vol.30, No.6, pp.4173-4175, Nov., 1994.

[68] [Mee & Daniel, 1995] Mee C. Denis and Eric D. Daniel, *Magnetic Recording Technology*, 2nd edition, McGraw-Hill, 1995

[69] [Millman, 1986] Millman S. E., Hoyt R. F., Horne D. E., and Beye B., "Motion pictures of in-situ air bearing dynamics," IEEE Transactions on Magnetics, Vol.22, pp1031-1033, 1986.

[70] Mitsuya Y., Mitsui A., Kawabe Y., Lunde L., "Three-dimensional measurement of head flying height and attitude using image processing of fringe patterns formed by Michelson laser interferometry," Transactions of the ASME, Journal of Tribology, Vol.118, No.3, pp.564-70, July 1996.

[71] Mitsuya Y., and Ohkubo T., "High knudsen number rarefaction effects in gas-lubricated slider bearings for computer flying heads," SME Journal of Tribology, Vol.109, No.2, pp.276-282, 1987.

[72] [Miu et al., 1984] Miu D. K., Bouchard G., Bogy D.B., and Talke F. E. "Dynamic response of a winchester-type slider measured by laser doppler interferometry," IEEE Transactions on Magnetics, Vol.20, pp.927-929, 1984.

[73] [Miu & Bogy, 1986-a] Miu D. K., and Bogy D. B., "Dynamics of gas-lubricated slider bearings in magnetic recording disk files - part I: experimental observation," ASME Journal of Tribology, Vol.108, No.4, pp.584-588. 1986.

[74] [Miu & Bogy, 1986b] Miu D. K., and Bogy D. B., "Dynamics of gas-lubricated slider bearings in magnetic recording disk files - part II: Numerical Simulation," ASME Journal of Tribology, Vol.108, No.4, pp.589-593. 1986.

[75] [Mizoshita et al., 1985] Mizoshita Y., Aruga K., and Yamada T., "Dynamic characteristics of a magnetic head slider," IEEE Transactions on Magnetics, Vol.21, pp.1509-1511, 1985.

[76] [Moller, 1988] Moller K. D., *Optics*, University Science Books, 1988.

[77] Muranushi F., Tanaka K. and Takeuchi Y., "Estimation of the zero-spacing error duo to a phase shift of reflected light in measuring a magnetic head slider's flying height by light interference," Adv. Info. Storage Syst., Vol.4, pp.371-379, 1992.

[78] Muranushi F., Tanaka K. and Takeuchi Y. "The ultraviolet light interference method to measure sliding flying height," ASME press, Adv. Info. Storage Syst., Vol.5, pp.435-450, 1993.

[79] [Nigam, 1982] Nigam A., "A visible laser interferometer for air bearing seperation measurement to submicron accuracy," ASME Journal of Lubrication Technology, Vol.104, No.1, pp.60-65, 1982.

[80] [Novotny & Hsiao, 1998] Novotny V. J. and Hsiao M. J., "Sensitive magnetic readback head-disk spacing measurements in recording drives," IEEE Transactions on Magnetics, Vol.34, No.4, pp1762-1764, 1998.

[81] [NR, 1992] *Numerical Recipes in C: The Art of Scientific Computing*, Cambridge University Press, 1992.

[82] [Ohkubo & Kishigami, 1988] Ohkubo T., and Kishigami J., "Accurate measurement of gas-lubricated slider bearing separation using visible laser interferometry," ASME Journal of Tribology, Vol.110, No. 1, pp. 148-155. 1988.

[83] Ohtsubo Y., Kawashima N., and Marumo H., "Measurement method for the spacing fluctuation of a head slider in a magnetic disk drive," IEEE Transactions on Magnetics, Vol.23, pp.3450-3452, 1987.

[84] [Riener, 1988] Riener Timothy A., Goding Adrian C., and Talke Frank E., "Measurement of head/disk spacing modulation using a two channel fiber optic laser doppler vibrometer," IEEE Transactions on Magnetics, Vol.24, No.6, pp.2745-2747, 1988.

[85] [Riener & Talke, 1988] Riener T. A., and Talke F. E., "Dynamics of magnetic recording sliders using laser doppler interferometry," Jour. of Precision Eng., Vol.10, No.3, pp.131-140, 1988.

[86] [Schardt, 1998] Schardt B. C., Schrech E., and Sonnenfeld R., "Flying height measurement while seeking in hard disk drives," IEEE Transactions on Magnetics, Vol.34, No.4, pp.1765-1767, 1998.

[87] Schilling Robert J., and Harris Sandra L., *Applied Numerical Methods for Engineers –using Matlab and C*, Brooks/Cole, Thomson Learning 1999.

[88] [Shi et al., 1987] Shi W. K., Zhu L. Y., and Bogy D. B., "Use of readback signal modulation to measure head/disk spacing variations in magnetic disk files," IEEE Transactions on Magnetics, Vol.23, pp.233-240, 1987.

[89] [Smith, 1999] Smith G., "Dynamic in-situ measurements of head-to-disk spacing," IEEE Transactions on Magnetics, Vol.35, No.5, pp.2346-2351, 1999.

[90] Smith P. W., Ganapathi S. K., Veillard D. H., "Measurement of head-disk spacing using laser heterodyne interferometry-part II: simulation and experiments," IEEE Transactions on Magnetics, Vol.29, No.6, Pt.2, pp.3912-3914, Nov., 1993.

[91] Sommargren G., "Distance measuring interferometer and method of use," U.S. Patent, No.4,606,638, 1986.

[92] Sommargren G, "Flying height and topography measuring interferometer," U.S. Patent, No.5,218,424, 1993.

[93] [Sonnenfield, 1993] Sonnenfield R., "Capacitance methods in head-disk interface studies," IEEE Transactions on Magnetics Vol.29, No.2, pp.247-252, Nov., 1993.

[94] [Staudenmann, 1998] Staudenmann M. "A new laser interferometer system for investigation of the dynamics at the head/disk interface," IEEE Transactions on Magnetics, Vol.34, No.4, pp.1696-1698. 1998.

[95] Suk M., Ishii T. and Bogy D. B., "Comparison of flying height measurement between multi-channel laser interferometer and the capacitance probe slider," IEEE Transactions on Magnetics, Vol.27, No.6, 1991.

[96] [Sundaram et al., 1999] Sundaram R., Yao W., Ku R. C. and Kuo D., "Study of head/disk interface dynamics using a thermal asperity sensor," IEEE Transactions on Magnetics, Vol.35, No.5, pp.2481-2483, 1999.

[97] Takeuchi Yoshinori, Tanaka Katsuyuki, Odaka Toshiko, Muranushi Fumitaka, "Examination of flying height of magnetic head slider between simulations and measurements taking into account zero-spacing error," Transactions of the Japan Society of Mechanical Engineers, Part C 60 576, pp.2547-2553, Aug., 1994.

[98] [Tanaka et al., 1984] Tanaka K., Takeuchi Y., Terashima S., Odaka T., and Saitoh Y., "Measurements of transient motion of magnetic disk slider," IEEE Transactions on Magnetics, Vol.20, pp.924-926, 1984.

[99] Tsai Youping, Nixon Hsiao-chu, Brian J., "Drive-level flying height measurements and altitude effects," IEEE Transactions on Magnetics, Vol.30, No.6, Pt.1, pp.4191-4193, Nov., 1994.

[100] Veillard Dominque H., Ganapathi S. K., Smith Paul W., "Real-time tracking of the head-disk separation using laser heterodyne interferometry, part I: Instrumentation," IEEE Transactions on Magnetics, Vol.29, No.6, Pt.2, pp.3909-3911, Nov., 1993.

[101] [Walker & Sides, 2000] Walker K. C. and Sides P. J., "Absolute calibration of SCATIR with comparison to measurements of flying height on the DFHT II," Paper FB-05, InterMag 2000, Toronto, Canada, 2000.

[102] [Wallace, 1951] Wallace Jr. R. L., "The reproduction of magnetically recorded signals," The Bell System Technical Journal, 30, pp.1145-1173, 1951.

[103] [Wang & Taratorin, 1999] Wang Shan X., and Taratorin, Alexander M., *Magnetic Information Storage Technology*, Academic press, 1999

[104] [White 1984] White J. W., "Flying characteristics of the 3370-type slider on a $5\frac{1}{4}$-inch disk–Part I: Static analysis," Tribology and Mechanics of Magnetic Storage System, vol.1, (B. Bhushan, et al., eds.), pp.72-76, SP-16, ASLE, Park Ridge, Illinois, 1984.

[105] [White & Nigam, 1980] White J. W., and Nigam A., "A factored implicit scheme for the numerical solution of the Reynolds equation at very low spacing," J. Lub. Tech., Transactions on, ASME, vol.102, pp80-85, 1980.

[106] Womack K. H., and Butler A., "In-situ n & k phase compensation in an interferometric flying height tester," IEEE Transactions on Magnetics, Vol.34, No.2, pp.459-461, 1998.

[107] [Yamada et al., 1986] Tamada T., Mizoshita Y., and Aruga K., "Spacing fluctuation of flying height head sliders in track accessing (measurement using optical interferometer)," Tribology and Mechanics of Magnetic Storage System, vol.3, (B. Bhushan and N. S. Eiss, eds.), pp.87-94, SP-21, ASLE, Park Ridge, Illinois, 1986.

[108] [Zhu et al., 1998] Zhu J., Carr T., and Varsanofiev D., "A digital sampling technique for amplitude and pulse width measurement," IEEE Transactions on Magnetics, Vol.34, No.4, pp.2027-2029, 1998.

[109] Zhu L. Y., Hallamasek D. K., Bogy D. B., "Measurement of head/disk spacing with a laser interferometer," IEEE Transactions on Magnetics, Vol.24, No.6, pp.2739-2741, 1988.

Publications

1. Warwick Clegg, Xinqun Liu, Bo Liu, and Amei Li, "Normal incidence polarization interferometry flying height testing," IEEE Transactions on Magnetics, vol. 37, no. 4I, pp.1941-1943, 2001.

2. Xinqun Liu, Warwick Clegg, and Bo Liu, "Ultra low head disk spacing measurement using dual beam polarization interferometry," Optics & Laser technology, vol.32, no.4, pp.287-291, 2000.

3. Xinqun Liu, Warwick Clegg, David Jenkins, and Bo Liu, "Polarisation interferometer for measuring small displacement," IEEE Transactions on Instrumentation and Measurement, vol50, no.4, pp.868-871, 2001.

4. Xinqun Liu, Warwick Clegg, Bo Liu, and Chongtow Chong, "Improved intensity interferometry method for measuring head-disk spacing down to contact," IEEE Transactions on Magnetics, vol. 36, no. 5, pp.2674-2676, 2000.

5. Xinqun Liu, Warwick Clegg, and Bo Liu, "Normal incidence polarisation interferometer for measuring flying height of magnetic heads," IEEE Transactions on Magnetics, vol. 35, no. 5, 1999.

6. Xinqun Liu, Warwick Clegg, and Bo Liu, "Interferometry method for measuring head-disk spacing down to contact," Proceedings of SPIE - The International Society for Optical Engineering, v 3740, pp. 598-60, 1999.

Normal Incidence Polarization Interferometry Flying Height Testing

Warwick Clegg, Xinqun Liu, Bo Liu, Amei Li, and Chongtow Chong

Abstract—**In this paper, a dual-beam normal incidence polarization interferometer is presented to measure the flying height or head-disk spacing. It has the advantages of both the intensity interferometry method and the oblique incidence polarization interferometry method. With this polarization interferometer, not only can the flying height be measured down to contact without losing accuracy, but also the pitch and roll of the head-slider can be detected dynamically. The optical parameters of the head-slider can also be determined. Design details and experimental results are given.**

Index Terms– **Flying height, head-disk-interface, polarization interferometry, slider dynamics.**

I. Introduction

Flying height or spacing between the read-write head-slider and the magnetic medium is a critical parameter in rigid disk design. The flying height is below 50 nm for most current disk drives. It is believed that the technology will move to 5~10 nm head-disk spacing within the next year or two. Currently, the data storage industry relies mainly on optical testers for quantifying the head-slider's flying height in both new product design and manufacturing of the head-slider [1]. These optical testers employ a rotating transparent glass disk in place of the magnetic disk, and determine the flying height by analyzing the interference phenomena between the slider and the glass disk [2]-[3].

Up to now, the methods that are widely accepted by the industry are intensity interferometry and polarization interferometry. A detailed analysis of the characteristics of these two methods has been given in [4]. A schematic of a modern flying height tester based on intensity interferometry is shown in Fig. 1, in which a normal incidence beam is usually employed. At the slider-disk interface, the light beam actually experiences a multi-reflection. In such a case, the intensity of the interfered light reflected from the slider-disk interface is formulated by the standard thin-film equation [5].

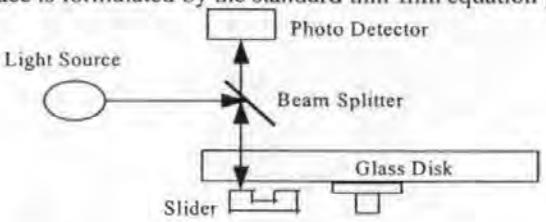

Fig. 1. Schematic of a flying height tester based on intensity interferometry

Using the intensity interferometry technique, the flying height can be measured down to 20 nm or even 10 nm with acceptable precision. However, because of the nature and shape of the intensity signal curve with respect to the flying height, when the spacing is reduced to under 10 nm, the sensitivity of this intensity-based technique worsens considerably. In addition, to determine the optical constants of the slider, a separate ellipsometer will inevitably be needed [6].

To cope with the fundamental limit of the above-mentioned intensity-based technique, a polarization interferometry flying height tester was developed [7], which is shown in Fig. 2.

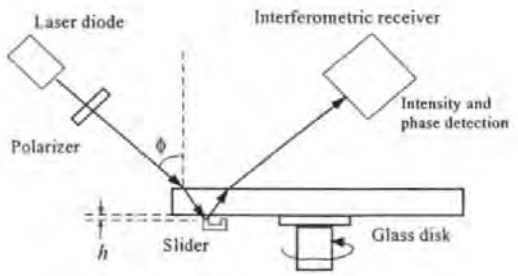

Fig. 2. Schematic of a polarization interferometry flying height tester

In this method, about 50° oblique incidence is adopted to make the best use of the phase information. The oblique incident laser beam defines two orthogonal polarization components s and p, where p polarization is parallel to the plane of incidence. The combined reflections from the slider-disk interface modify the polarizing state of the beam. The intensity of the interfered light and the phase difference between the two polarization components can be detected by the interferometric receiver. What is important about the intensity and phase information is that they are

Manuscript received February 7, 2000. This joint research is supported in part by the British Council (Singapore).

Warwick Clegg is with the Centre for Research in Information Storage Technology, University of Plymouth, PL4 8AA, UK (telephone: 44-1752-232576, e-mail: wclegg@plymouth.ac.uk).

Xinqun Liu is with the Centre for Research in Information Storage Technology, University of Plymouth, PL4 8AA, UK (telephone: 44-1752-232623, e-mail: xliu@plymouth.ac.uk).

Bo Liu is with the Data Storage Institute, National University of Singapore, Singapore 119260 (telephone: 65-96866474, e-mail: dsiliubo@dsi.nus.edu.sg).

Amei Li is with the Centre for Research in Information Storage Technology, University of Plymouth, PL4 8AA, UK (telephone: 44-1752-232579, e-mail: A.Li-1@plymouth.ac.uk).

Chongtow Chong is with the Data Storage Institute, Singapore 117608 (telephone: 65-8745248, e-mail: towchong@dsi.nus.edu.sg).

complementary. When the intensity signal curve has a steep slope, the phase is fairly constant; when the intensity is nearly constant, the phase is changing rapidly. Using both curves together means that there always exists a way to measure flying height with good sensitivity.

However, one disadvantage of this method is that its light beam is obliquely incident on the glass disk. As a result, the sensitivity of its intensity channel is reduced by a factor of $1/\cos\phi$ compared with that of the normal incidence.

In addition to the disadvantages mentioned, because only one point measurement is performed at one time, neither of the above methods can perform dynamic measurement of the slider's pitch and roll, which is very important for the study of the slider's dynamics. To deal with these problems, we developed a normal incidence polarization interferometer, which is described below.

II. Deal-beam Normal Incidence Polarization Interferometer for Flying Height Testing

The dual-beam normal incidence polarization interferometer is shown in Fig. 3, which is a further development of the system described earlier [4].

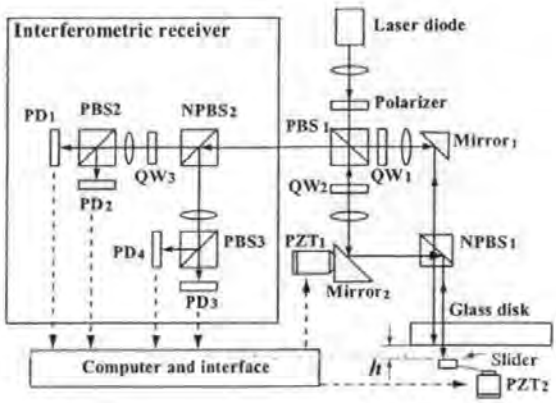

Fig. 3. Dual-beam normal incidence polarization interferometer

Instead of using a Wollaston prism to split into a deal-beam, here we employ a more flexible beam-splitter and mirror configuration. The main part of the interferometer utilizes a polarization beam splitter, two quarter-wave plates, two mirrors, and a non-polarizing beam splitter as both a beam splitter and phase shifter. A 670 nm laser diode is still used as the light source. The laser beam passes through the polarizer and enters the polarizing beam splitter. Then the p-polarized component passes through and is finally focused onto the slider air-bearing surface. The s-polarized component is coupled out and reflected by Mirror1 and focused on an adjacent point on the glass disk or slider air-bearing surface. Mirror2 is driven by a PZT translator (PZT1) to perform phase shifting, which can be used for system calibration and phase compensation. It can also be moved by hand by a micrometer to adjust the spacing of the two orthogonally polarized beams. The returning beam enters the interferometric receiver, which is used to measure the intensity and phase difference between the two polarization components of the returned beam. The interferometric receiver consists of a non-polarizing beam splitter, a quarter-wave plate, two polarization beam splitters, and four photo detectors. The detected voltage signals are sampled in by the computer through an A/D converter board. The PZT translators are also controlled by the computer through a D/A converter board and a high voltage amplifier.

A. Flying Height Measurement

When making the flying height measurement, the p-polarized beam is focused on the slider air-bearing surface, and the s-polarized beam on an adjacent point on the glass disk. According to [4], The intensity I and the phase difference θ between the two polarization components of the returned beams are given as:

$$I = I_{p0}\left|\frac{r_{p20} + r_{p01}\exp(i4\pi n_0 h/\lambda)}{1 + r_{p20}r_{p01}\exp(i4\pi n_0 h/\lambda)}\right|^2 + I_{s0}|r_{s20}|^2 \qquad (1)$$

$$\theta = \arg(r_{s20}) - \arg\left(\frac{r_{p20} + r_{p01}\exp(i4\pi n_{03} h/\lambda)}{1 + r_{p20}r_{p01}\exp(i4\pi n_0 h/\lambda)}\right) - \theta_0 \qquad (2)$$

where $r_{p20} = r_{s20} = \dfrac{n_2 - n_0}{n_2 + n_0}$, $r_{p01} = \dfrac{n_0 - (n_1 + ik_1)}{n_0 + (n_1 + ik_1)}$, θ_0 is the initial phase difference between the two polarized beams, I_{p0} and I_{s0} are the intensities of the two incident beams, λ is the wavelength, h is the flying height, and n_2, n_0 and $(n_1 + ik_1)$ are the refractive indices of glass, air, and slider material respectively. From (1) and (2), the intensity and the phase curves, $I(h)$ and $\theta(h)$, are plotted in Fig.4 where we choose the refractive index of the slider as $n_1 + ik_1 = 2.2 + 0.4i$.

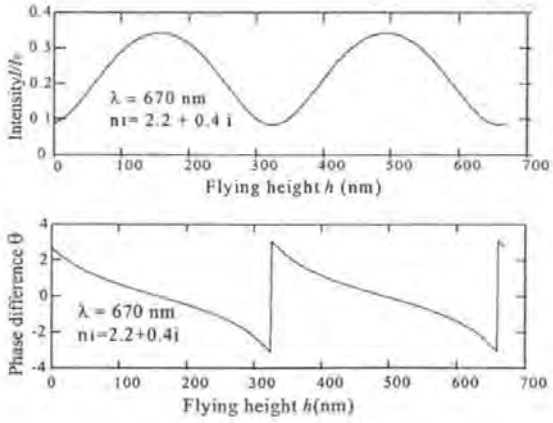

Fig. 4. Intensity and phase difference as functions of flying height

From Fig. 4, it can be seen that the phase curve has good sensitivity when the intensity curve is getting flat, particularly around the near contact area.

B. Slider's Pitch And Roll Measurement

When measuring the slider's pitch and roll, the two beams are focused on two different points on the slider air-bearing

surface. In this case, the reflective coefficients of both the beams are determined by the same thin film equation [4]. After the flying height has been determined, by measuring the phase difference between the two beams, the slider's pitch and roll can be determined dynamically.

III. EXPERIMENTAL RESULTS

To test the ability and effectiveness of this interferometer, we make the following experiments. A 3 mm thick glass disk is held in stationary state. A PZT translator (PZT2) is used to move the head-slider in saw-wave form to simulate the head-disk spacing variation. A 12-bit D/A converter is used to control a 0~10V voltage output applying to PZT2.

With the measured intensity and phase information, the flying height can be determined in a number of ways. First, analytically, we can use the phase value only to determine the flying height all the way down to contact since the whole phase curve has a fairly good sensitivity. Second, we can use the intensity value in the area where its sensitivity is high, and in the area where its sensitivity is low, we use phase value. Third, we can also calculate the flying height by minimizing the difference between measured and theoretical values of both the intensity and phase [4].

Here we use the measured phase information only to derive the flying height change according to (2). The measured head-disk spacing changes are plotted in Fig.5 and Fig.6, where the optical constants of the head-slider are predetermined to be n=2.79, and k=0.0998, and the initial phase difference θ_0 is measured to be 0.16° and 2.13° respectively in the two experiments.

When measuring the slider's pitch and roll, we use the measured phase information only. To determine it qualitatively, we can take the relationship between the phase difference and the slider's pitch or roll as quasi-linear. To determine it quantitatively, we need to first measure the flying height, so the changing rate of the height at this point can be determined. The slider's pitch or roll can then be determined linearly from the measured phase difference value by using this changing rate.

With the measured intensity and phase information, we can also use a similar method as in [1] to determine the optical constants of the slider, which is necessary to determine the flying height.

IV. CONCLUSION

Design details of a dual-beam normal incidence polarization interferometric flying height tester and its practical set-up are presented. Numerical analysis and experimental results show that the proposed method can be used for flying height measurement down to contact with greatly improved accuracy at small head-disk spacing compared to the existing intensity method, and with improved intensity channel sensitivity compared with the existing polarization interferometry method. It also shares the additional advantage with the oblique incidence polarization

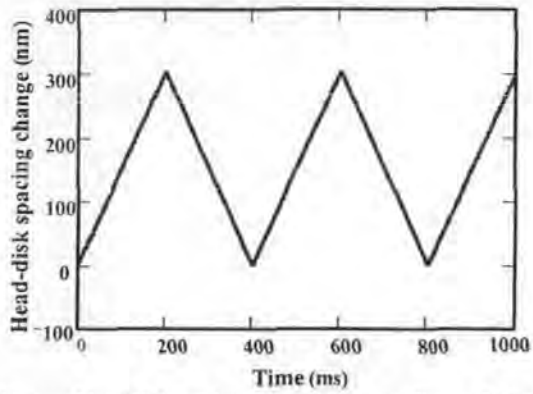

Fig. 5. Measured head-disk spacing change with an amplitude of about 300 nm

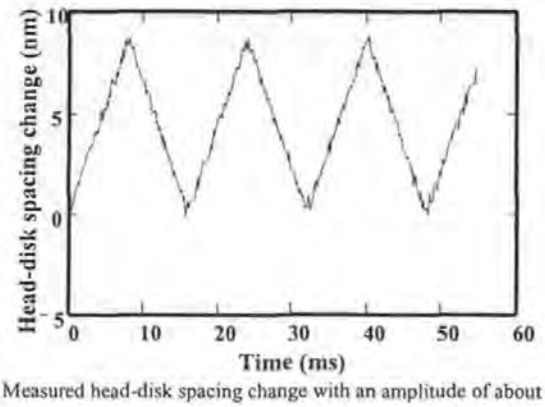

Fig. 6. Measured head-disk spacing change with an amplitude of about 8.5 nm

interferometer that the complex refractive index of the slider can be determined in-situ during the flying height testing which is an indispensable step for flying height measurement. The slider's pitch and roll can also be measured dynamically, which is impossible by using other types of traditional flying height testers.

V. REFERENCES

[1] P. de Groot, "Determining the optical constants of read-write sliders during flying height testing", *Applied. Optics*., vol. 37, pp. 5116-5125, 1998.

[2] C. Lacey, J. Adams, E. Ross, and A. Cormier, "A new method for measuring flying height dynamically", *Phase Metrics communication*, 1992.

[3] P. de Groot, L. Deck, J. Sobbitsky, and J. Biegen, "Polarization interferometer for measuring the flying height of magnetic read-write heads", *Optics Letters* vol. 21 (6), pp. 441-443, March, 1996.

[4] X. Liu, W. Clegg, and B. Liu, "Normal incidence polarization interferometer for measuring flying height of magnetic heads. *IEEE Transactions on Magnetics*, vol. 6, pp. 2457-2459, 1999.

[5] M. Born, E. Wolf, *Principles of Optics*, Pergamon Press, Oxford, 1989.

[6] Y. Li, A. Menon, and P. Goglia, "Evaluations of diamond-like-carbon film optical constants and their effects on flying height determination",*Trans. ASME. Journal of Tribology*, vol. 118 (4), pp. 767-773, Oct. 1996.

[7] P. de Groot, L. Deck, J. Soobitsky, and J. Biegen, "Optical flying-height testing of magnetic read-write heads", *Proceedings of the SPIE*, Vol. 2782, pp. 47-57, 1996.

ELSEVIER

Optics & Laser Technology 32 (2000) 287–291

Optics & Laser Technology

www.elsevier.com/locate/optlastec

Ultra low head–disk spacing measurement using dual beam polarisation interferometry

Xinqun Liu[a,*], Warwick Clegg[a], Bo Liu[b]

[a]*Centre for Research in Information Storage Technology, University of Plymouth, Devon PL4 8AA, UK*
[b]*Data Storage Institute, National University of Singapore, Singapore 119260*

Received 8 June 2000; accepted 26 July 2000

Abstract

In this paper, a dual-beam normal incidence polarisation interferometer is proposed to measure the flying height or head–disk spacing. Using this interferometer, the head–disk spacing can be measured both in magnetic real disk condition and in glass disk condition. It has the advantage of both the currently popular intensity interferometry method and the oblique incidence polarisation interferometry method. With this polarisation interferometer, not only the flying height can be measured down to contact without losing accuracy, but the pitch and roll of the head-slider can also be detected dynamically. The optical parameters of the head-slider can also be determined. Design details and experimental study are presented. © 2000 Elsevier Science Ltd. All rights reserved.

Keywords: Dual-beam polarisation interferometry; Head–disk spacing; Flying height; Displacement measurement

1. Introduction

The need for ever-greater storage capacity has resulted in the data-storage recording densities of magnetic hard disk drives growing at a rate of about 60% every year in the past decade. In order to support with these developments, work has been undertaken in parallel to improve the heads, media, channel, and electronics. However, one of the most critical and effective parameters in increasing areal density is the flying height or spacing between the read–write head and the recording disk medium. Although it is very desirable to reduce the head–disk spacing or flying height to increase the recording areal density, head–disk contact is undesirable during disk operation since that will deteriorate the tribological performance of the head–disk interface and its reliability. Since 1990, flying height has been reduced from above 140 nm to under 20 nm for the leading-edge products of the magnetic recording industry. It is expected that the head–disk spacing will reduce from the current value of 25–35 nm to a level of 5–10 nm, as the technology moves from the current 10 Gb/in^2 areal density to beyond 40 Gb/in^2 areal density of commercial hard disk drives by the year 2004 [1]. Therefore, it becomes more and more important and necessary to make high accurate head–disk spacing measurement and characterisation both in new read–write head product development and on the manufacturing line.

Optical interferometry has been the major means for measuring head–medium separation. Considering the measurement condition of whether a real magnetic disk or a special glass disk is used, we divide the methods into relative displacement measuring (RDM) method and direct spacing measuring (DSM) method. In RDM method, real magnetic disk and head-slider are employed. The head–disk spacing is determined by measuring the relative motion between the head-slider and the disk by using dual-beam interferometry [2–5]. In DSM method, a special transparent glass disk is used in place of the real magnetic disk, and the flying height is determined by analysing the interference phenomena between the slider and the rotating glass disk [6–8]. The DSM method has the advantage that the absolute head–disk spacing can be directly measured, while the RDM method has the advantage of using the real magnetic disk. It will be highly advantageous if a testing instrument can be used in the above two methods. Based on this consideration, we proposed a dual-beam polarisation interferometry which has this preferred ability.

* Corresponding author. Tel.: +44-1752-232623; fax: +44-1752-232583.
E-mail address: xliu@plymouth.ac.uk (X. Liu).

PII: S0030-3992(00)00072-4

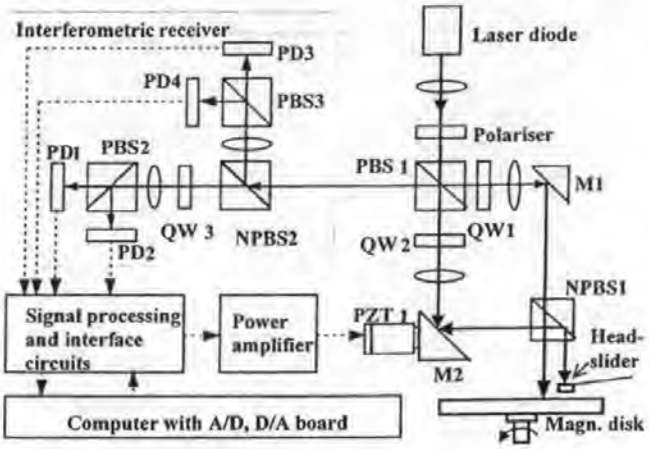

Fig. 1. Dual-beam polarisation interferometer.

2. Dual-beam polarisation interferometer

Our dual-beam polarisation interferometer for head–disk spacing measurement is as shown in Fig. 1. Instead of using one or more acousto-optical modulators (AOM), this polarisation interferometer configuration utilises two orthogonally polarised light beams to remove the directional ambiguity of the flying height change.

The main part of the interferometer utilises a polarising beam splitter PBS1, two-quarter-wave plates QW1 and QW2, two mirrors M1 and M2, and a non-polarising beam splitter NPBS1 as both a beam splitter and phase shifter.

The use of a polarising beam splitter PBS1 is to make the most use of the laser beam and prevent the returning beam from feeding back to the laser diode. Mirror M2 is driven by a piezoelectric translator PZT1, which can be used to perform system calibration. M2 can also be micro-positioned manually to adjust the spacing of the two measurement points. A 670 nm wavelength laser diode is used as the light source. The laser beam passes through the polariser and enters the polarising beam splitter PBS1. Then the s-polarised component is coupled out and reflected by mirror M1 and focused on the reference point (disk surface). The p-polarised component passes through and is focused onto the measurement point (back surface of the head-slider). The returning beam enters the interferometric receiver, which is used to measure the intensity and phase difference between the two polarised beams. The interferometric receiver consists of a non-polarising beam splitter NPBS2, two polarising beam splitters PBS2 and PBS3, a quarter-wave plate QW3 and four photo-detectors. The detected voltage signals are amplified and equalised, then sampled in by the computer through a 12-bit A/D converter board. The sampling rate of the A/D converter will determine the measurement bandwidth of the system. The A/D converter board with a sampling rate of 5 MS/s is commercially available at present and that is fast enough to measure the dynamics of the head–disk spacing. The piezoelectric translator is also controlled by the computer through a 12-bit D/A converter board and a high-voltage amplifier.

The interferometric receiver is the key part of this interferometer to obtain the intensity and phase information of the returned beam so as to determine the head–disk spacing.

We take the electric field of the two orthogonally polarised components of the returned beam to be

$$E_p = A_p \exp(i(\omega t)), \tag{1}$$

$$E_s = A_s \exp(i(\omega t + \theta + \theta_0)), \tag{2}$$

where ω is the angular frequency of the radiation, A_p and A_s are the amplitudes of E_p and E_s, respectively, θ_0 is the initial phase difference between the two polarised beams, and θ is the phase difference which will be used to determine the head–disk spacing. The combined beam, $E_p + E_s$, after passing through NPBS2 and QW3, and incident upon PBS2 and PBS3, is split into four orthogonal beams with a phase difference of $\pi/2$ between them. The wave intensities being received by the four photo-detectors (P_{PD1}–P_{PD4}) are proportional to the square of the electric field and can be formulated by [9]

$$P_{PD1} = K(b - a\sin(\theta + \theta_0)), \tag{3}$$

$$P_{PD2} = K(b + a\sin(\theta + \theta_0)), \tag{4}$$

$$P_{PD3} = K(b + a\cos(\theta + \theta_0)), \tag{5}$$

$$P_{PD4} = K(b - a\cos(\theta + \theta_0)), \tag{6}$$

where K is the photoelectric conversion factor of the photodetector, b represent the DC components, and a represent the magnitudes of the AC components. So the quadrature signals ($P_{PD2} - P_{PD1}$) and ($P_{PD3} - P_{PD4}$) are obtained. These two signals are sampled by the computer through two channels of the A/D converter board. The phase difference ($\theta + \theta_0$) is then determined by phase evaluation and unwrapping [10]. The intensity signal ($P_{PD1} + P_{PD2} + P_{PD3} + P_{PD4}$) is also sampled in by the computer for use in the DSM method.

3. In relative displacement measuring method

3.1. Theory

When this dual-beam interferometer is used in RDM method, real magnetic disk is used. The measurement beam is focused on the back surface of the head-slider and the reference beam is focused on an adjacent point on the disk, which is shown in Fig. 2, where h is the head–disk spacing to be measured.

The head–disk spacing h has a simple relationship with the phase difference ϕ detected by the interferometric receiver:

$$4\pi h/\lambda + \theta_0 = \phi, \tag{7}$$

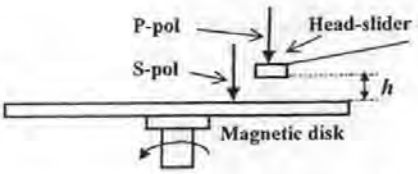

Fig. 2. Relative displacement measuring method.

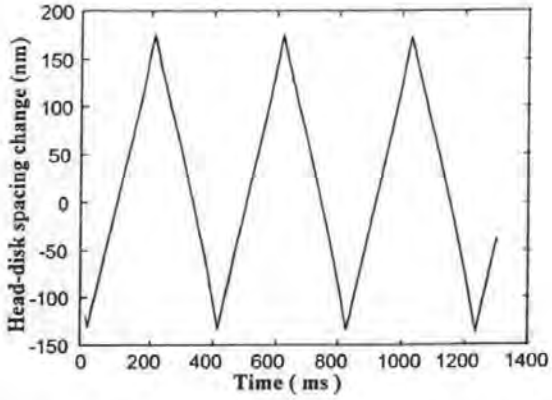

Fig. 3. Measured head–disk spacing change with an amplitude of about 300 nm in RDM method.

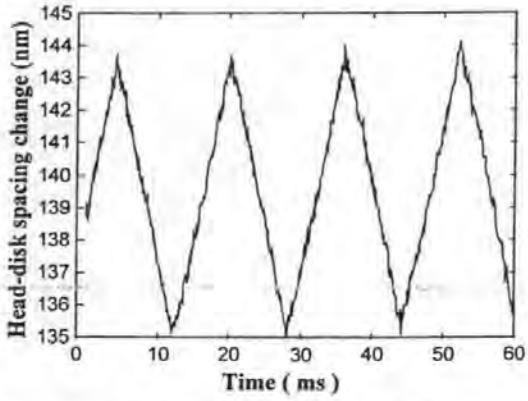

Fig. 4. Measured head–disk spacing change with an amplitude of about 8.5 nm in RDM method.

where λ is the wavelength of the laser and θ_0 is the initial phase difference between the two beams.

3.2. Experimental study

We made several experimental simulations to test the ability and effectiveness of this interferometer. We used another piezoelectric translator PZT2 to move the head-slider vertically to the disk. The PC computer controls 0 –10 V voltage output applying to PZT2 through another channel of the 12-bit D/A converter board. Two experimental results are shown as in Figs. 3 and 4 where the head-slider was moved in a saw-wave form with two different amplitudes of 300 and 8.5 nm, respectively.

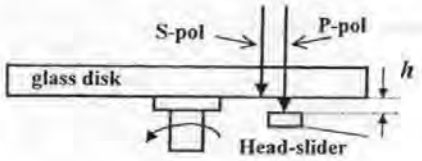

Fig. 5. Direct spacing measuring method.

4. In direct spacing measuring method

4.1. Theory

RDM method is a good way to measure the head–disk spacing because a real magnetic disk can be used. However, although a special glass disk must be used, DSM method sometimes is more popular because the absolute head–disk spacing can be observed and measured directly, especially in the case where it is difficult for the light beam to 'spot' the back surface of the head-slider. When our dual-beam interferometer is used in DSM method, a glass disk with anti-reflection coating on top surface is employed. The measurement beam (p-polarised beam) is focused on the air bearing surface of the head-slider and the reference beam (s-polarised beam) is focused on an adjacent point on the glass disk, which is shown in Fig. 5 where h still represents the head–disk spacing to be measured.

According to the standard thin-film equation [11], the reflection coefficient of the p-polarised beam is

$$r_p = \frac{r_{p20} + r_{p01}\exp(i\beta_p)}{1 + r_{p20}r_{p01}\exp(i\beta_p)}, \tag{8}$$

where $r_{p20}=(n_2-n_0)/(n_2+n_0)$, $r_{p01}=(n_0-(n_1+ik_1))/(n_0+(n_1+ik_1))$, $\beta_p=(4\pi/\lambda)n_0h$, λ is the wavelength, h is the head–disk spacing, and n_2, n_0 and (n_1+ik_1) are the refractive indices of the glass disk, air, and slider material, respectively. So the intensity I and the phase difference ϕ between the two polarisation components detected by the interferometric receiver are

$$I = I_{p0}\left|\frac{r_{p20} + r_{p01}\exp(i\beta_p)}{1 + r_{p20}r_{p01}\exp(i\beta_p)}\right|^2 + I_{s0}|r_{s20}|^2, \tag{9}$$

$$\phi = \arg(r_{s20}) - \arg\left(\frac{r_{p20} + r_{p01}\exp(i\beta_p)}{1 + r_{p20}r_{p01}\exp(i\beta_p)}\right) + \theta_0, \tag{10}$$

where $r_{s20}=(n_2-n_0)/(n_2+n_0)$, I_{p0} and I_{s0} are the intensities of the incident p polarised and s polarised beams. From (9) and (10), the intensity I and the phase difference $\theta=(\phi-\theta_0)$ as functions of head–disk spacing h are plotted in Fig. 6 where the refractive index of the slider is chosen as $n_1+ik_1=2.2+0.4i$.

With the measured intensity and phase information, the head–disk spacing can be determined in a number of ways. First, analytically, we can use the phase value only to determine the flying height all the way down to contact, since the whole phase curve has a fairly good sensitivity.

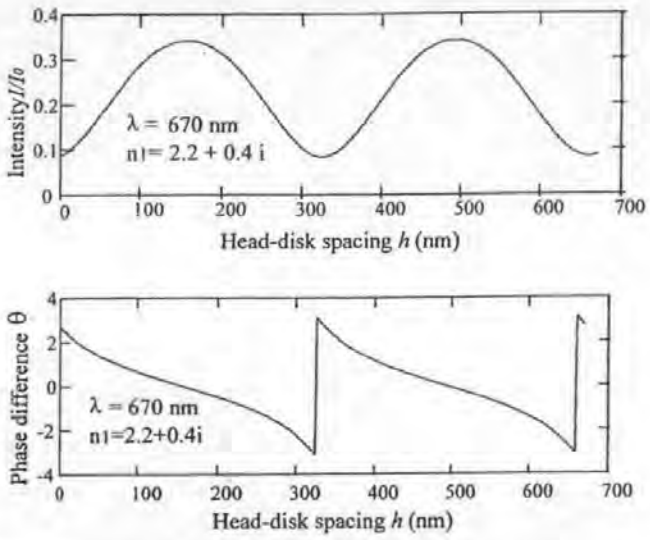

Fig. 6. Intensity and phase difference as functions of head–disk spacing.

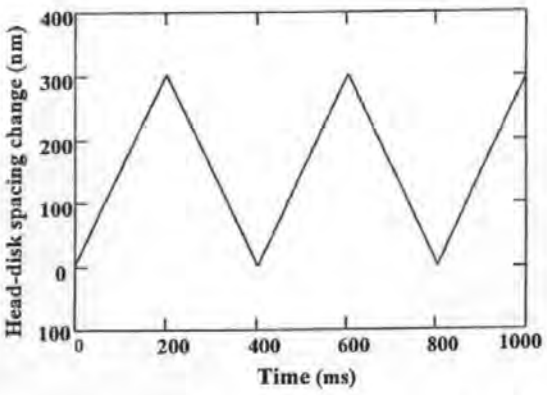

Fig. 7. Measured head–disk spacing change with an amplitude of about 300 nm in DSM method.

Second, we can use the intensity value in the area where its sensitivity is high, and in the area where its sensitivity is low, we use phase value. Third, we can also calculate the flying height by minimising the difference between measured and theoretical values of both the intensity and phase [12].

4.2. Experimental study

Again, to test the ability and effectiveness of this interferometer, we make the following experimental simulation. A 3 mm thick glass disk is held in stationary state. A PZT translator (PZT2) is still used to move the head-slider in saw-wave form to simulate the head–disk spacing variation. Here we use the measured phase information only to derive the flying height change according to (10). The measured head–disk spacing changes are plotted in Figs. 7 and 8, where the optical constants of the head-slider are

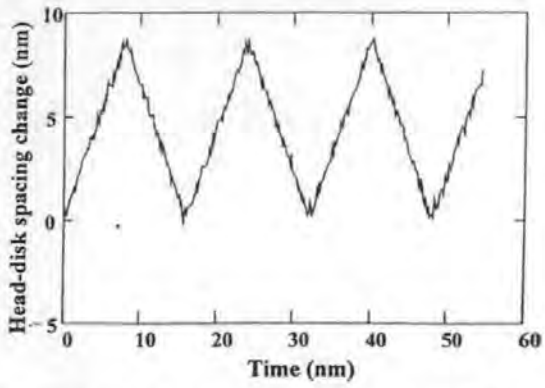

Fig. 8. Measured head–disk spacing change with an amplitude of about 8.5 nm in DSM method.

predetermined to be $n=2.79$, and $k=0.0998$, and the initial phase difference θ_0 is measured to be 0.16 and 2.13°, respectively, in the two experiments.

5. Discussions and conclusions

From the experimental results, it can be seen that the head–disk spacing change can be measured with subnanometer accuracy in both the RDM and DSM methods by using this dual-beam polarisation inteferometer. The system measurement error mainly comes from the noises which result from background and mechanical vibration, air current disturbances and thermal drift. Noises from laser diode, photo detectors, and the system's electronics also produce measurement errors. We can carefully refine every part of these to further improve the system's measurement precision and accuracy.

Since the dual-beam configuration, this interferometer can also be used to dynamically measure the head-slider's pitch and roll, which is very important to study the head-slider's dynamics. This cannot be performed by using ordinary single beam interferometry flying height testers. In addition, when this interferometer is used in DSM method, with the measured intensity and phase information, we can use a similar method as in [6] to determine the optical constants of the head-slider material, which is an indispensable step in measuring the head–disk spacing.

References

[1] Liu B, Zhu Y, Li Y, Hua W, Leng Q, Sheng G. An experimental study of slider vibration in nanometer spaced head–disk interface. IEEE Trans Magn 1999;35(5):2463–5.

[2] Staudenmann M. A new laser interferometer system for investigation of the dynamics at the head/disk interface. IEEE Trans Magn 1998;34(4):1696–8.

[3] McMillan T, Talke F. Ultra low flying height measurements using monochromatic and phase demodulated laser interferometry. IEEE Trans Magn 1994;30(6):4173–5.

[4] Lee C-K, Wu T-W. Differential laser interferometer for nanometer displacement measurements. AIAA J 1995;33(9):1675–80.

[5] Briggs C, Talke F. An investigation of the IBM 3380 K slider using laser doppler interferometry. IEEE Trans Magn 1989;25(5):3707–9.
[6] de Groot P. Determining the optical constants of read–write sliders during flying height testing. Appl Opt 1998;37:5116–25.
[7] Lacey C, Adams J, Ross E, Cormier A. A new method for measuring flying height dynamically. Phase Metrics communication, 1992.
[8] Ohkubo T, Kishigami J. Accurate measurement of gas-lubricated slider bearing separation using visible laser interferometry. ASME J Tribol 1988;110(1):148–55.
[9] Peng G, Wu C, Huang Y. The displacement measurement of a shaker in an accelerometer caliberation system. Proc SPIE 1996;2868:285–9.
[10] Malacara D. Optical shop testing, 2nd ed. New York: Wiley, 1992.
[11] Born M, Wolf E. Principles of optics, 6th ed. Oxford: Pergamon Press, 1989.
[12] de Groot P, Deck L, Sobbitsky J, Biegen J. Polarization interferometer for measuring the flying height of magnetic read–write heads. Opt Lett 1996;21(6):441–3.

Polarization Interferometer for Measuring Small Displacement

Xinqun Liu+, Warwick Clegg+, David Jenkins+, and Bo Liu*

+Centre for Research in Information Storage Technology, University of Plymouth, PL4 8AA, UK.
*Data Storage Institute, 10 Kent Ridge Crescent, Singapore 119260

Abstract

A homodyne polarization laser interferometer is presented for high speed measurement of small displacements. No modulation technique is used, so the opto-mechanical set-up is relatively simple. The dual beam arrangement enables the displacement to be measured whilst the use of polarization interferometry enables the determination of the directional nature of the displacement. Another feature of this interferometer lies in the fact that it is also suitable for the measurement of head-media spacing of a hard disk drive. Combined with the electronics used at present, sub-nanometre resolution is achievable. Its measurement bandwidth is limited only by the sampling rate of the A/D board being used.

1. Introduction

Optical interferometry is a well established technique for precise and non-contact measurement. Various kinds of interferometry, such as heterodyne interferometry [1]-[3], sinusoidal phase modulating interferometry [4]-[5], and phase-shifting interferometry [6]-[7], have been developed to make high resolution measurement of small displacements. However, apart from the complexity of the system construction, these existing methods are generally feasible only for low speed measurement applications. When a high speed measurement is needed, it is difficult to find a suitable technique if the measurement accuracy requirement is high. The speed limitation in these displacement measurement interferometers is mainly due to the use of slow modulation or scanning techniques [8]. In this paper, we propose a homodyne polarization interferometer, which can be used for high speed measurement of small displacements with sub-nanometre resolution and accuracy.

2. Dual beam polarization interferometer

Our dual beam polarization interferometer for displacement measurement is as shown in Fig 1. Instead of using one or more acousto-optical modulators (AOM), this polarization interferometer configuration utilizes two orthogonally-polarized light beams to remove the directional ambiguity of the displacement. The main part of the interferometer utilises a polarizing beam splitter PBS1, two quarter-wave plates QW1 and QW2, two mirrors M1 and M2, and a non-polarizing beam splitter NPBS1 as both a beam splitter and phase shifter.

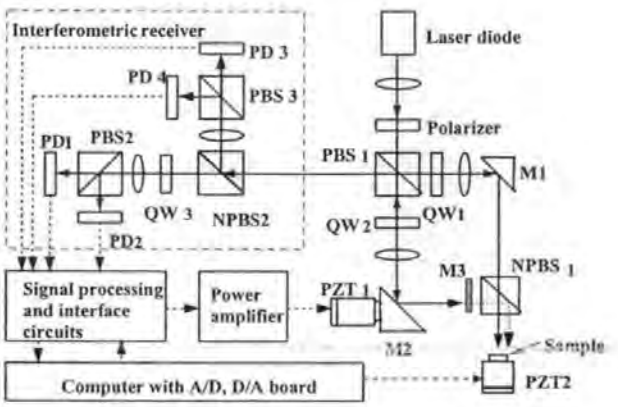

Fig 1 Dual-beam polarization interferometer

The use of a polarizing beam splitter PBS1 is to make the most use of the laser beam and prevent the returning beam from feeding back to the laser diode. Mirror M2 is driven by a piezoelectric translator PZT1, which can be used to perform system calibration. Mirror M3 is used as a reference plane when single point displacement is measured. When the system is used to measure the relative displacement of two adjacent points, such as the vertical movement of the hard-disk read/write head relative to the disk surface, M3 is removed and the reference beam is coupled out by $NPBS_1$ to the second measurement point. Mirror M2 can also be micro-positioned manually to adjust the spacing of the two measurement points. A 670 nm wavelength laser diode is used as the light source. The laser beam passes through the polarizer and enters the polarizing beam splitter PBS1. Then the s-polarized component is coupled out and

0018-9464/00$10.00 © 2001 IEEE

reflected by mirror M1 and focused on the measurement point on the sample. The p-polarized component passes through and is focused onto the reference mirror or another measurement point. The returning beam enters the interferometric receiver, which is used to measure the intensity and phase difference between the two polarized beams. The interferometric receiver consists of a non-polarizing beam splitter NPBS2, two polarizing beam splitters PBS2 and PBS3, a quarter-wave plate QW3 and four photo-detectors. The detected voltage signals are amplified and equalized, then sampled in by the computer through a 12-bit A/D converter board. The sampling rate of the A/D converter will determine the measurement speed of the system. The A/D converter board with a sampling rate of 20MS/s is commercially available at present. The piezoelectric translators are also controlled by the computer through a 12-bit D/A converter board and a high voltage amplifier.

We take the electric field of the two orthogonally polarized beams to be:

$$E_p = A_p \exp(i(\omega t)) \tag{1}$$

$$E_s = A_s \exp(i(\omega t + \phi)) \tag{2}$$

where ω is the angular frequency of the radiation, A_p and A_s are the amplitudes of E_p and E_s respectively, and

$$\phi = 4\pi(d + \Delta d)/\lambda \tag{3}$$

In equation (3), λ is the wavelength of the laser beam, d is the static optical path difference between the two polarized beams and Δd is the displacement to be measured. The combined beam, $E_p + E_s$, after passing through NPBS2 and QW3, and incident upon PBS2 and PBS3, is split into four orthogonal beams with a phase difference of $\pi/2$ between them. The wave intensities being received by the four photo-detectors (P_{PD1} to P_{PD4}) are proportional to the square of the electric field and can be formulated by [9]:

$$P_{PD1} = K(b_1 - a_1 \sin(4\pi(d + \Delta d)/\lambda) \tag{4}$$

$$P_{PD2} = K(b_2 + a_2 \sin(4\pi(d + \Delta d)/\lambda) \tag{5}$$

$$P_{PD3} = K(b_3 + a_3 \cos(4\pi(d + \Delta d)/\lambda) \tag{6}$$

$$P_{PD4} = K(b_4 - a_4 \cos(4\pi(d + \Delta d)/\lambda) \tag{7}$$

where K is the photoelectric conversion factor of the photo-detector, b_1 to b_4 represent the DC components, and a_1 to a_4 represent the magnitudes of the AC components. By simple signal conditioning and processing, quadrature signals $(P_{PD2} - P_{PD1} b_2 / b_1)$ and $(P_{PD3} - P_{PD4} b_3 / b_4)$ are obtained. These two signals are sampled by the computer through two channels of the A/D converter board. The displacement Δd is then determined by phase evaluation and unwrapping [10].

3. Experimental results

To test the ability and effectiveness of this interferometer, several experiments have been conducted. We use another piezoelectric translator PZT2 to move the sample. A 12-bit D/A converter is used to control a 0 – 10V voltage output applying to PZT2. We first make an experiment to test the general noise level of the system or the system measurement error. In this experiment, PZT1 and PZT2 are both held stationary. The sampling rate of the A/D converter is set to 50KHz. The measurement result is as shown in Fig. 2.

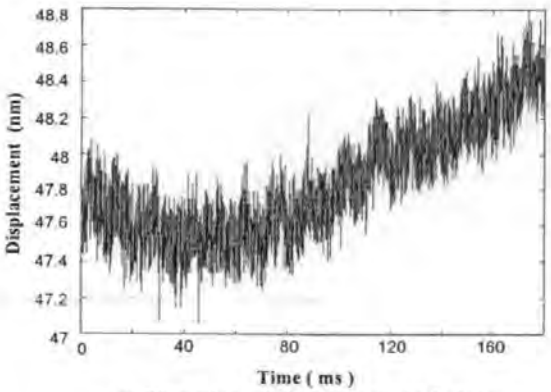

(a) The plot of 9000 sampled data

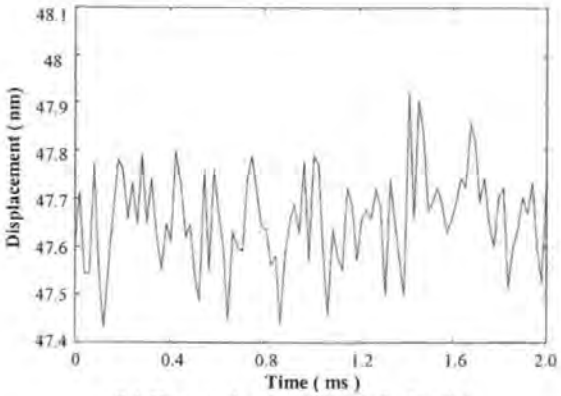

(b) Expanded version of plot (a)

Fig. 2 System measurement error and general noise level

From Fig. 2, we can see that the system measurement error is composed of both low and high frequency components. The low-frequency noise can be observed from Fig. 2 (a), which most likely results from background vibration, thermal drift, air current disturbances etc. The magnitude of noise level caused by these can be well above 1 nm. In fast changing displacement measurement cases, this low frequency noise can be eliminated by simple signal processing. The high frequency noise comes from the laser diode, the photo-detector, and the system's electronics. The magnitude of this noise level is about 0.3 nm, which can be seen from Fig. 2 (b).

We now conduct further experiments in which we use PZT2 to move the sample in a saw-wave form with several different amplitudes from about 4.75μm down to 1 nm. The measurement results are shown in Fig. 3 to Fig. 7 for successively smaller displacements.

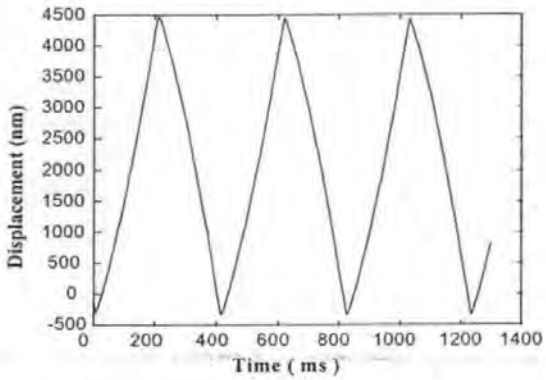

Fig. 3 Measurement result for displacement amplitude of about 4.75 μm

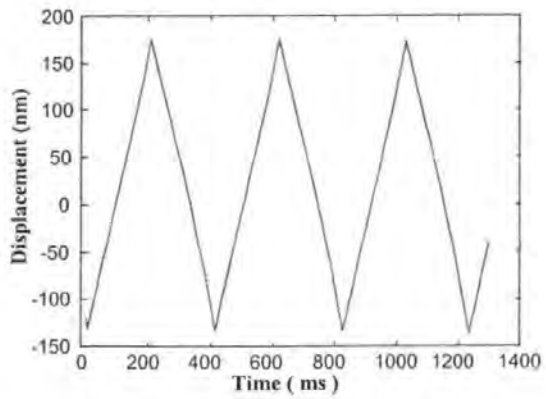

Fig. 4 Measurement result for displacement amplitude of about 300 nm

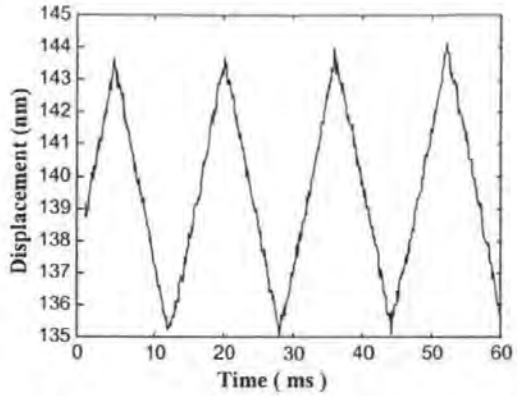

Fig. 5 Measurement result for displacement amplitude of about 8.5 nm

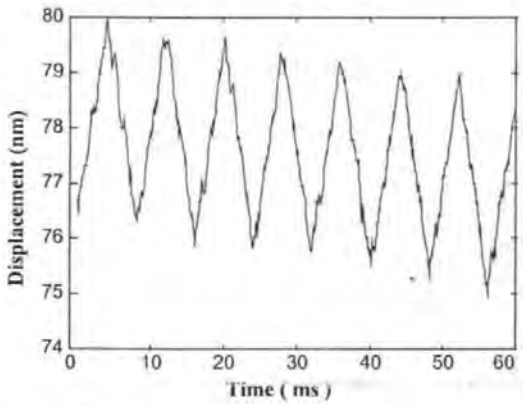

Fig. 6 Measurement result for displacement amplitude of about 3.5 nm

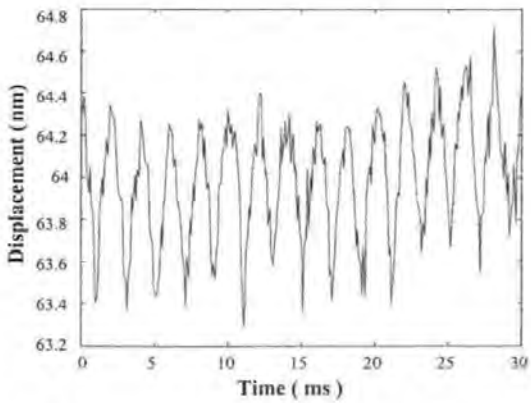

Fig. 7 Measurement result for displacement amplitude of about 0.8 nm

From the experimental results shown above, it can be seen that the displacements with different magnitudes are measured with rather satisfying precision.

4. Conclusions

The homodyne polarization laser interferometer proposed here can be used for the accurate measurement of small displacements, and is especially suitable for the measurement of high speed displacements. Theoretically, a 12-bit A/D converter can provide a measurement resolution higher than $\lambda/4096$. However, because of the system noise, especially the electrical noise, the system in its present configuration has a general measurement resolution of about 0.5 nm. This will be further improved by carefully refining of the system's electronics and mechanics. This dual beam interferometer is particularly suitable for the characterisation of the head-media spacing of hard disk drives [11]. The system's measurement bandwidth can also be increased by choosing a higher sampling rate A/D board.

5. References

[1] G. E. Sommargren, "Optical heterodyne profilometry," *Applied. Optics*. Vol. 20, pp. 610-618, 1981.

[2] K. Tatsuno and Y. Tsunoda, "Diode laser direct modulation heterodyne interferometer," *Applied. Optics*. Vol. 26, pp. 37-40, 1987

[3] X. Dai and K. Seta, "High-accuracy absolute distance measurement by means of wavelength scanning heterodyne interferometry", *Meas. Sci. Technol*, No.9, pp. 1031-1035, 1998.

[4] O. Sasaki, K. Takahashi, and T. Suzuki, "Sinusoidal phase modulating interferometer with a feedback control system to eliminate external disturbance", *Optical Engineering*, Vol. 29, pp. 1511-1515, 1990a.

[5] X. Wang, O. Sasaki, Y. Takebayashi, T. Suzuki, and T. Maruyama, "Sinusoidal phase-modulating Fizeau interferometer using self-pumped phase conjugator for surface profile measurements, *Optical Engineering*, Vol. 33, pp. 2670-2674, 1994.

[6] K Creath, "Phase measurement interferometry techniques," *Progress in Optics*, Vol. 27, pp 273-359, 1990.

[7] P. Hariharan, "Phase-stepping interferometry with laser diodes: effect of changes in laser power with output wavelength," *Applied. Optics*. Vol. 28, pp. 27-28, 1989.

[8] R. Li, and T. Aruga, "An interferometer system scheme for the fast measurement of small displacement", *Proceedings of SPIE*, Vol. 3482, pp. 908-913, 1998.

[9] G. Peng, C. Wu, and Y. Huang, "The displacement measurement of a shaker in an accelerometer caliberation system", *Proceedings of SPIE*, Vol. 2868, pp. 285-289, 1996.

[10] D. Malacara, *Optical Shop Testing, 2nd edition*, John Wiley & Sons, Inc., New York, 1992

[11] W. Clegg, X. Liu, and B. Liu, "Dual beam normal incidence polarization interferometry flying height testing", *IEEE International Conference on Magnetics*, paper CP-04, April 2000, Toronto, Canada.

Improved Intensity Interferometry Method for Measuring Head–Disk Spacing Down to Contact

Xinqun Liu, Warwick Clegg, Bo Liu, and Chongtow Chong

***Abstract*—In this paper, we give a detailed analysis of the working principle, application limits, and potential problems of the intensity interferometry flying height testing, one of the most popularly-used flying height testing techniques. Then, phase-shift methods are proposed to improve the sensitivity of this technique when the head–disk spacing is below 10 nm or near contact. This is based on fabricating the glass testing disk to have a specified thickness, or having it coated with a specified thickness thin carbon film. Theoretical analysis, numerical evaluation, and experimental considerations are presented.**

***Index Terms*—Flying height, glass disk, head disk spacing, intensity interferometry, phase shift.**

I. Introduction

With the development of the magnetic disk storage industry, the capacity of a single hard disk is getting larger and larger. While the disk size is unchanged or even getting smaller, the recording areal density increases tremendously every year. In recent years, the areal density has grown at a rate of more than 50% per year. In order to support with these developments, work has been undertaken in parallel to improve the heads, media, channel, and electronics. However, one of the most critical and effective parameters in increasing areal density is the flying height or spacing between the read-write head slider and the recording disk medium. In the past few years since 1990, flying height has been reduced from above 140 nm to under 20 nm for the leading-edge products of the magnetic recording industry. It is believed that the technology will move to 5~10 nm head–disk spacing to achieve 40 Gb/in^2 areal density within the next year or two.

Although it is very desirable to reduce the head–disk spacing or flying height to increase the recording areal density, head disk contact is undesirable during disk operation since it will deteriorate the tribological performance of the head disk interface and its reliability. Therefore, it is necessary to make accurate ultra-low flying height measurements both in new product development and on the manufacturing line [1], [2].

Optical interferometry has been the major means for measuring head/medium separation. Laser Doppler Interferometry (LDI) and Phase Demodulated Laser Interferometry (PDLI) can be used to determine the head–disk spacing by measuring the relative motion between the head slider and the disk [3], [4]. However, with the decreasing size of the head slider, accessing to the back of the slider by the optical beam becomes difficult. Hence, current optical testers employ a rotating transparent disk in place of the magnetic disk, and determine the flying height by analyzing the interference phenomena between the slider and the glass disk. One of these flying height testing methods used by the industry is intensity interferometry [5], [6], which we will describe in the following.

Manuscript received February 7, 2000. This work was supported in part by the British Council (Singapore).

X. Liu and W. Clegg are with the Centre for Research in Information Storage Technology, University of Plymouth, PL4 8AA, UK (e-mail: {xliu; wclegg}@plymouth.ac.uk).

B. Liu and C. Chong are with the Data Storage Institute, Singapore 117608 (e-mail: {dsiliubo; towchong}@dsi.nus.edu.sg).

Publisher Item Identifier S 0018-9464(00)09051-8.

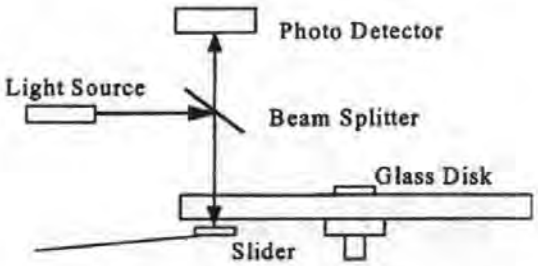

Fig. 1. Schematic of an intensity interferometry flying height tester

II. Intensity Interferometry Flying Height Testing

This method is used by the majority of the industry to determine the absolute flying height. A schematic of an intensity interferometry flying height tester is shown in Fig. 1 in which a normal incidence beam is usually employed. At the slider-disk interface, the light beam actually experiences a multi-reflection. In such an instance, the intensity of the interfered light reflected from the slider-disk interface is given by the standard thin-film equation [7] as below

$$I_s = I_0 \frac{r_{20}^2 + |r_{01}|^2 + 2r_{20}|r_{01}|\cos(\delta + \phi_s)}{1 + r_{20}^2|r_{01}|^2 + 2r_{20}|r_{01}|\cos(\delta + \phi_s)} \tag{1}$$

where

$$\delta = \frac{4\pi h}{\lambda}, \quad \phi_s = \pi - \tan^{-1}\left(\frac{2n_0k_1}{n_0^2 - n_1^2 - k_1^2}\right),$$
$$r_{20} = \frac{n_2 - n_0}{n_2 + n_0}, \quad r_{01} = \frac{n_0 - (n_1 + ik_1)}{n_0 + (n_1 + ik_1)},$$

h is the flying height, λ is the light wavelength, n_0, $(n_1 + ik_1)$, n_2 are refractive indices of the air, slider and glass respectively, r_{20} is the reflection coefficient of the glass-air boundary, r_{01} is of the air-slider boundary, I_0 is the intensity of the light incident to the slider-disk interface, and I is the intensity of the light reflected from the slider-disk interface, Taking the effective index of the slider as $n_1 + ik_1 = 2.2 + 0.4i$ for example, we give the

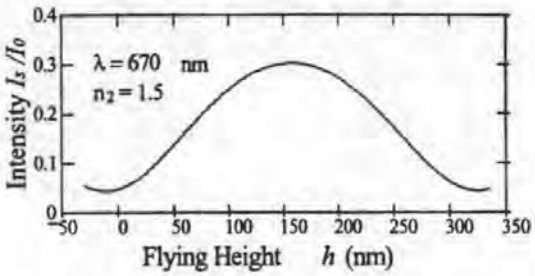

Fig. 2. Reflected intensity as a function of flying height.

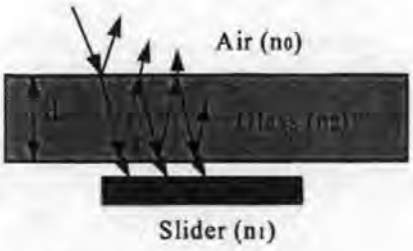

Fig. 3. Two-layer reflection consideration.

plot of the normalized intensity I_S/I_0 as a function of flying height h in Fig. 2.

From Fig. 2, it can be seen that using this intensity interferometry technique, the flying height can be measured down to around 10 nm with acceptable precision. However, when the spacing is reduced to under 10 nm, the sensitivity of this intensity-based technique worsens considerably, even in the presence of phase change on reflection phenomenon (PCOR).

III. Methods to Improve the Sensitivity Near Contact

Since the intensity based technique is a simple and accurate flying height testing method and has been widely employed by the disk industry, it is useful to determine if ways can be found to increase the sensitivity near contact. To deal with this problem, we find that if the phase of the intensity curve is shifted, the sensitivity around the near contact area can be improved. Here we give two methods to achieve this.

A. Using Glass Disks of Specified Thickness

If we use long coherence length light source, e.g., laser diode, in the intensity-based tester, and use a glass disk without any anti-reflection coating as the testing disk, the light beam will experience a two-layer reflection as shown in Fig. 3 [8]. The intensity of the interfered beam reflected from the slider disk interface will be formulated as the following expression

$$I = I_0 \left| \frac{r_{02} + r_{l1} \exp(i4\pi n_2 d/\lambda)}{1 + r_{02} r_{l1} \exp(i4\pi n_2 d/\lambda)} \right|^2 \qquad (2)$$

where $r_{l1} = (r_{20} + r_{01} \exp(i4\pi n_0 h/\lambda)/1 + r_{20} r_{01} \exp(i4\pi n_0 h/\lambda))$, $r_{02} = (n_0 - n_2/n_0 + n_2)$, d is the glass disk thickness. From (2), we can see that the intensity of the interfered light beam is not only dependent on the head disk spacing h, but also dependent on the glass disk thickness d. By numerical evaluation, we find that if the glass disk is manufactured or modified to have a thickness within $(\lambda/4n_2)(2m + 1.3)$ to $(\lambda/4n_2)(m + 1.8)$, *m is an integer*, the intensity curve of the two-layer reflections, according to (2), is advantageously phase-shifted relative to the intensity curve of the single layer reflections, and can be used for determining the head–disk spacing down to contact. This is shown in Fig. 4 where the glass disk thickness is $(\lambda/4n_2)(2m + 1.5)$. We can see from Fig. 4 that when the intensity curve I_s is getting flat where the flying height is below 10 nm, the intensity curve I_d has very good sensitivity. Since for present technology, it is difficult to manufacture a glass disk with small enough thickness tolerance, e.g. ±2 nm, for the whole disk, a better way to apply this method is by utilizing small areas of the disk where the thickness can be controlled and measured accurately.

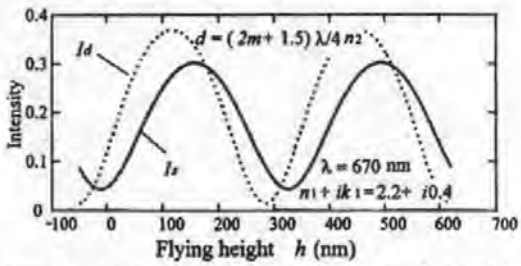

Fig. 4. Intensity curve as a function of flying height. I_s is of single layer reflections, I_d is of two-layer reflections and can be used to determine the head–disk spacing down to contact.

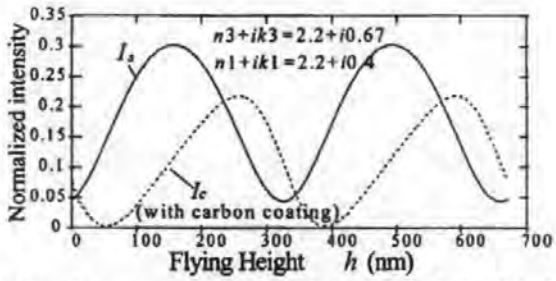

Fig. 5. Intensity curve as a function of flying height. I_s is of single layer reflections, and Ic is of using carbon coating glass disk, with $d_1 = 23$ nm.

B. Using a Glass Disk with Carbon-Coating

In this method, we utilize a glass disk with antireflection coating on one side and carbon coating on the other side (working surface). In this case, the light beam will experience two-layer reflections as well, and the intensity of the returned beam from the slider-disk interface is given to be:

$$I_c = I_0 \left| \frac{r_{23} + r_{l2} \exp(i4\pi n_3 d_1/\lambda)}{1 + r_{23} r_{l2} \exp(i4\pi n_3 d_1/\lambda)} \right|^2 \qquad (3)$$

where $r_{l2} = (r_{30} + r_{01} \exp(i4\pi n_0 h/\lambda)/1 + r_{30} r_{01} \exp(i4\pi n_0 h/\lambda))$, $r_{23} = (n_2 - (n_3 + ik_3)/n_2 + (n_3 + ik_3))$, $r_{30} = (n_3 + ik_3 - n_0/n_3 + ik_3 + n_0)$, d_1 is thickness of the carbon coating film, and $(n_3 + ik_3)$ is the refractive index of the carbon coating layer. Again by numerical evaluation, we found if the carbon coating thickness d_1 is selected from 0.03λ to 0.08λ the intensity curve will also be advantageously phase-shifted relative to the intensity curve of the single layer reflections, and can also be used to determine the head–disk spacing down to contact. This is shown in Fig. 5 where the carbon coating thickness is 0.035λ. This method can be used for the whole disk, since making a

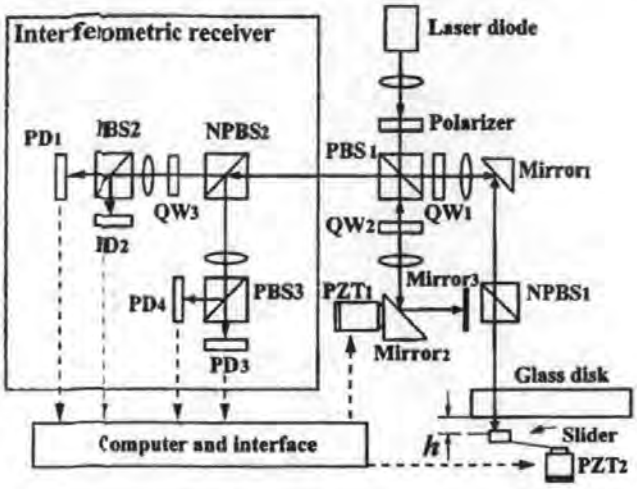

Fig. 6. Expeimental set-up to measure the glass disk thickness

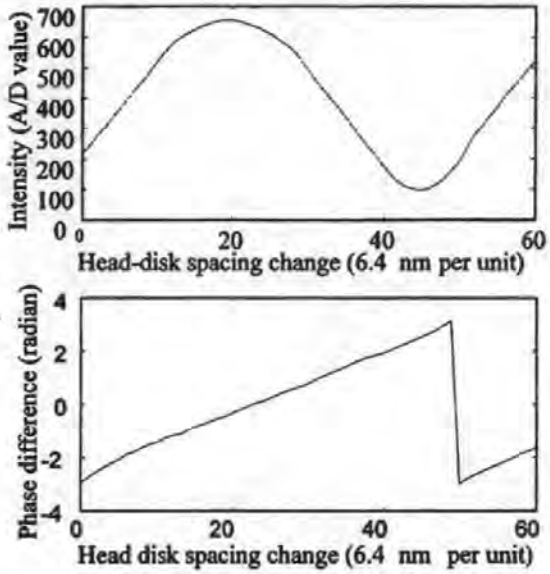

Fig. 7. Measured intensity and phase difference $(\theta + \theta_0)$ with respect to the head–disk spacing change

carbon coating with thickness tolerance of ± 2 nm is quite practical, and in this case, the maximum flying height error caused will be 0.8 nm by calculation.

IV. Experimental Consideration

Since carbon coating is quite a common practice, there will be no problem putting this method into practical use. Hence we have conducted experiments to verify the practical feasibility of the first method-using glass disk of specified thickness. Since we do not know the exact thickness of the glass disk, what we do experimentally is to find the thickness of the disk and examining its effect on the reflected beam. To determine the glass disk thickness, we need two equations. One is the intensity expression (2). The other is the phase equation which is given by:

$$\theta = \arg\left(\frac{r_{02} + r_{l1}\,\exp(i4\pi n_2 d/\lambda)}{1 + r_{02} r_{l1}\,\exp(i4\pi n_2 d/\lambda)}\right) \tag{4}$$

Theoretically, two different head disk spacing values with their corresponding intensity and phase values result in four equations, with which the disk thickness can be determined. The method we use here is different from this. We use a similar method as used in determining the optical constants of the slider in [2]. The experimental set-up is shown in Fig. 6, which is similar to the one used in [9]. The intensity and phase difference $(\theta + \theta_0)$between the two polarized beams can be measured by the interferometric receiver. θ_0 is the initial phase difference. Using PZT2 to make a continuous head–disk spacing change, we get the measured intensity and phase curves as shown in Fig. 7. From the measured data, the glass disk thickness is determined to be $(\lambda/4n_2)(2m + 0.89)$.

V. Conclusion

After a detailed analysis, numerical evaluation, and experimental testing, we conclude that the proposed phase-shifting methods using glass disk with certain thickness range or with certain carbon coating thickness range, can be used for the flying height measurement down to contact with greatly improved sensitivity without changing the opto-mechanical set-up of the traditional intensity based tester.

References

[1] Y. Li and A. Menon, "Flying height measurement metrology for ultra-low spacing in rigid magnetic recording," *IEEE Trans. Magn.*, vol. 32, pp. 129–134, 1996.

[2] P. de Groot, "Determining the optical constants of read-write sliders during flying height testing," *Appl. Opt.*, vol. 37, pp. 5116–5125, 1998.

[3] T. Riener, A. Goding, and F. Talke, "Measurement of head/disk spacing modulation using a two channel fiber optic laser doppler vibrometer," *IEEE Trans. Magn.*, vol. 24, pp. 2745–2747, 1988.

[4] D. Veillard, S. Ganapathi, and P. Smith, "Real-time tracking of the head–disk separation using laser heterodyne interferometry. Part one: instrumentation," *IEEE Trans. Magn.*, vol. 29, pp. 3909–3911, 1993.

[5] Y. Li, A. Menon, and P. Goglia, "Evaluations of diamond-like-carbon film optical constants and their effects on flying height determination," *Trans. ASME. J. Tribo.*, vol. 118, pp. 767–773, 1996.

[6] C. Lacey, J. Adams, E. Ross, and A. Cormier, "A new method for measuring flying height dynamically," in *Phase Metrics Communication*, 1992.

[7] M. Born and E. Wolf, *Principle of Optics*. Oxford: Pergamon, 1989.

[8] X. Liu, W. Clegg, and B. Liu, "Interferometry method for measuring head–disk spacing down to contact," *Proc. SPIE*, vol. 3740, pp. 598–601, 1999.

[9] W. Clegg, X. Liu, and B. Liu, "Deal beam normal incidence polarization interferometry flying height testing," in *IEEE Intermag 2000 Conf.*, Toronto, Canada, April 2000, paper-CP-04.

Normal Incidence Polarization Interferometer for Measuring Flying Height of Magnetic Heads

Xinqun Liu and Warwick Clegg
Centre for Research in Information Storage Technology, University of Plymouth, Devon, PL4 8AA, UK.

Bo Liu
Data Storage Institute, National University of Singapore, Singapore 119260

Abstract— **In this paper, we give a brief review and analysis to the two currently most powerful methods for flying height testing of magnetic heads - intensity interferometry and polarization interferometry. Then a dual-beam normal incidence polarization interferometry method is proposed to compromise the disadvantages of the above two methods. The proposed method not only has the advantages of both the above methods, but also can be used to measure the pitch and roll of the head-slider dynamically. Design details and analysis of the relationship between the optical parameters of the tester and its testing accuracy are given.**

Index Term— **Flying height, head-disk-interface, normal incidence polarization interferometry, slider dynamics.**

I. Introduction

A critical parameter in rigid disk design is the height or spacing between the read-write head-slider and the magnetic medium. The flying height is below 50 nm for most current disk drives. It is believed that the technology will move to 5~10 nm head-disk spacing by the year 2002~3. Currently, the data storage industry relies mainly on optical testers for quantifying the head-slider's flying height in both new product design and manufacturing of the head-slider [1]. These optical testers employ a rotating transparent glass disk in place of the magnetic disk, and determine the flying height by analysing the interference phenomena between the slider and the glass disk [2]-[4].

Up to now, the methods that are widely accepted by the industry are intensity interferometry and polarization interferometry.

A. Intensity Interferometry

This method is used by the majority of the industry to determine the absolute flying height. A schematic of a modern flying height tester based on intensity interferometry is shown in Fig. 1 in which a normal incidence beam is usually employed. At the slider-disk interface, the light beam actually experiences a multi-reflection. In such an instance, the intensity of the interfered light reflected from the slider-disk interface is given by the standard thin-film

Manuscript received February 20, 1999.
Xinqun Liu, 44-1752-232623, fax 44-1752-232583, xliu@plymouth.ac.uk; Warwick Clegg, 44-1752-232576, fax 44-1752-232583, wclegg@ plymouth .ac.uk; Bo Liu, 65-96866474, fax 65-778-2968, dsiliubo@ dsi.nus.edu.sg
This joint research is supported by the British Council (Singapore).

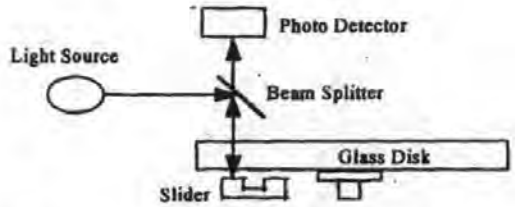

Fig. 1. Schematic of a flying height tester based on intensity interferometry

equation [5] as below

$$I = I_0 \frac{r_1^2 + |r_2|^2 + 2r_1|r_2|\cos(\delta + \phi_s)}{1 + r_1^2|r_2|^2 + 2r_1|r_2|\cos(\delta + \phi_s)} \quad (1)$$

where $\delta = \frac{4\pi h}{\lambda}$, $\phi_s = \pi - \tan^{-1}\left(\frac{2n_0 k_1}{n_0^2 - n_1^2 - k_1^2}\right)$, $r_1 = \frac{n_2 - n_0}{n_2 + n_0}$, $r_2 = \frac{n_0 - (n_1 + ik_1)}{n_0 + (n_1 + ik_1)}$, h is the flying height, λ is the light wavelength, n_0, $(n_1 + ik_1)$, n_2 are refractive indices of the air, slider and glass respectively, r_1 is the reflection coefficient of the glass-air boundary, r_2 is of the air-slider boundary, I_0 is the intensity of the light incident to the slider-disk interface, and I is the intensity of the light reflected from the slider-disk interface. Note that the parameter $(n_1 + ik_1)$ here is the "effective" refractive index of the slider which needs a separate ellipsometer to determine in this intensity based tester [6]. Taking the effective index of the slider as $n_1 + ik_1 = 2.2 + 0.4i$ for example, we give the plot of the normalized intensity I / I_0 as a function of flying height h in Fig. 2.

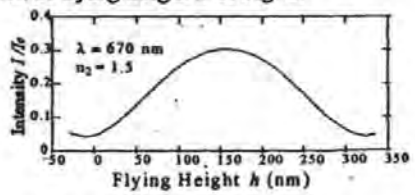

Fig. 2. Reflected intensity as a function of flying height

From Fig. 2 it can be seen that the best sensitivity (defined as dI / dh) occurs around h = 60 nm, and calculations show that the sensitivity is reduced to half the maximum value at

about h = 10 nm, and continues to worsen below this height even in the presence of phase change on reflection phenomenon (PCOR).

B. Polarization Interferometry

To cope with the fundamental limit of the above-mentioned intensity-based technique, a polarization interferometry flying height tester was developed [7] which is shown in Fig. 3. In this method, about 50° oblique incidence is

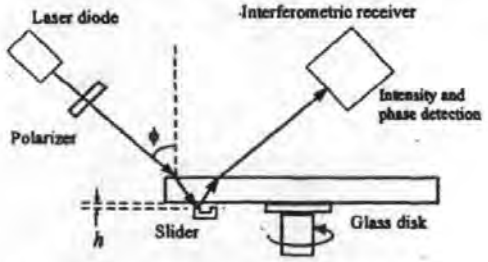

Fig. 3. Schematic of a modern polarization interferometry flying height tester

adopted to make the best use of the phase information. The oblique incident laser beam defines two orthogonal polarization components s and p, where p polarization is parallel to the plane of incidence. The combined reflections from the slider-disk interface modify the polarization state of the beam. The intensity of the interfered light I and the phase difference θ between the two polarization components have the following relationship with the flying height h:

$$I(h) = I_{p0}\left|r_p(\beta)\right|^2 + I_{s0}\left|r_s(\beta)\right|^2 \qquad (2)$$

$$\theta(h) = \arg\left[r_s(\beta)\right] - \arg\left[r_p(\beta)\right] \qquad (3)$$

where $\beta = 4\pi h\cos(\phi)/\lambda$, $I_{p0} = I_{s0} = I_0$, λ is the wavelength of the laser beam, ϕ is the incident angle, I_{p0} and I_{s0} are the intensities of the incident p polarized and s polarized light to the slider-disk interface, and r_p and r_s are the effective reflectivities of the slider-disk combination. From (2) and (3), the intensity I and the phase difference θ as functions of flying height can be drawn as in Fig. 4. What is important about the intensity and phase curves is that they are complementary. When the intensity curve has a steep slope, the phase is fairly constant; when the intensity is nearly constant, the phase is changing rapidly. Using both curves together means that there always exists a way to measure flying height with good sensitivity.

However, one disadvantage of this method is that its light beam is obliquely incident on the glass disk. As a result, the sensitivity of its intensity channel is reduced by a factor of $1/\cos\phi$ compared with that of the normal incidence. This can also be seen in Fig. 5.

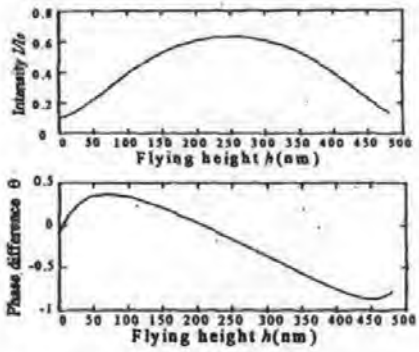

Fig. 4. Intensity curve and phase difference curve

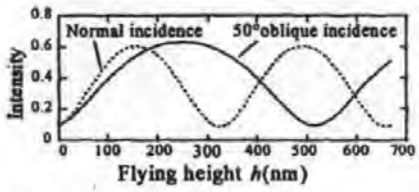

Fig. 5. Intensity curves with different beam incidence conditions

In addition to the disadvantages mentioned, because they only perform one point measurement at one time, neither of the above methods can perform dynamic measurement of the slider's pitch and roll, which is very important for the study of the slider's dynamics. To deal with these problems, we propose the following method.

II. Normal Incidence Polarization Interferometer for Flying Height Testing

We propose a dual-beam normal incidence polarization interferometry method which is shown in Fig. 6.

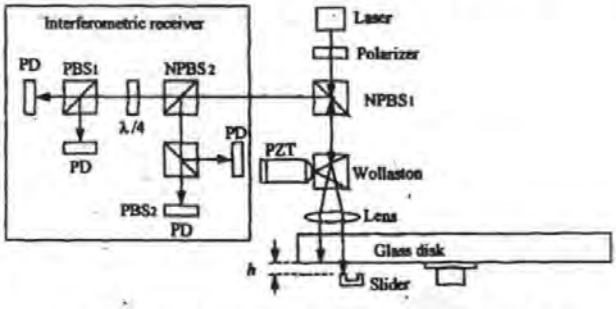

Fig. 6. Dual-beam normal incidence polarization interferometry

A 670 nm laser diode is used as the light source. The laser beam passes through a polarizer and a beam splitter. The exiting beam then passes through a Wollaston prism which splits the light into two orthogonally-polarized beams. The lens focuses these two beams on two close but distinct points on the slider air bearing surface and the glass disk. The reflected beams then pass through the Wollaston prism again and recombine to a single beam. This returning beam finally

enters the interferometric receiver which is used to measure the intensity and phase difference between the two polarization components of the returned beam. The interferometric receiver consists of a non-polarising beam splitter, a quarter-wave plate, two polarising beam splitters, and four photo detectors. The PZT translator is used to move the Wollaston prism so as to adjust the phase difference between the two polarization components.

A. Flying height measurement

When making the flying height measurement, the p-polarized beam is focused on the slider air-bearing surface, and the s-polarized beam on an adjacent point on the glass disk. According to the standard thin-film equation, the reflection coefficient of the p-polarized beam is

$$r_p = \frac{r_{p20} + r_{p01}\exp(i\beta_p)}{1 + r_{p20}\, r_{p01}\exp(i\beta_p)} \tag{4}$$

where $r_{p20} = \dfrac{n_2 - n_0}{n_2 + n_0}$, $r_{p01} = \dfrac{n_0 - (n_1 + ik_1)}{n_0 + (n_1 + ik_1)}$,

$\beta_p = \dfrac{4\pi}{\lambda} n_0 h$, λ is the wavelength, h is the flying height, and n_2, n_0 and $(n_1 + ik_1)$ are the refractive indices of glass, air, and slider material respectively. So the intensity I and the phase difference θ between the two polarization components detected by the interferometric receiver are:

$$I = I_{p0}\left|\frac{r_{p20} + r_{p01}\exp(i\beta_p)}{1 + r_{p20} r_{p01}\exp(i\beta_p)}\right|^2 + I_{s0}\left|r_{s20}\right|^2 \tag{5}$$

$$\theta = \arg(r_{s20}) - \arg\left(\frac{r_{p20} + r_{p01}\exp(i\beta_p)}{1 + r_{p20} r_{p01}\exp(i\beta_p)}\right) \tag{6}$$

where $r_{s20} = \dfrac{n_2 - n_0}{n_2 + n_0}$, I_{p0} and I_{s0} are the intensities of the incident p polarized and s polarized beams. From (5) and (6), the intensity I and the phase difference θ as functions of flying height are plotted in Fig. 7 where we choose the refractive index of the slider as $n_1 + ik_1 = 2.2 + 0.4i$. From Fig. 7, it can be seen that the phase curve has good sensitivity when the intensity curve is getting flat, particularly around the near contact area.

B. Slider's pitch and roll measurement

When measuring the slider's pitch and roll, the two beams are focused on two different points on the slider air-bearing surface. In this case, the reflective coefficients of both the beams are determined by the same thin film equation as (4). After the flying height has been determined, through measuring the phase difference between the two beams with the interferometric receiver, we can determine the slider's pitch and roll dynamically.

As to the birefringence effect resulting from the stress in the glass disk when it is rotating, it is easy to measure and compensate the phase change arising from it when using this flying height testing system.

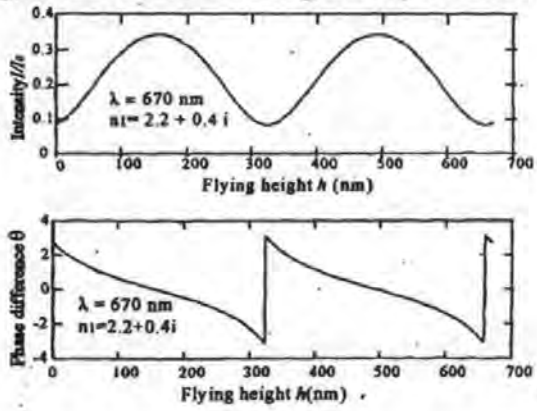

Fig. 7. Intensity and phase difference as functions of flying height

III. Conclusion

Design details of the dual-beam normal incidence polarization interferometric flying height tester and its practical set-up are presented. Theoretical analysis and numerical results show that the proposed method can be used for the flying height measurement down to contact with greatly improved accuracy at small head-disk spacing compared to the existing intensity method, and with improved intensity channel sensitivity compared with the existing polarization interferometry method. It also shares the additional advantage with the oblique incidence polarization interferometer that the complex refractive index of the slider can be determined in-situ during the flying height testing which is an indispensable step for flying height measurement.

References

[1] P. de Groot, "Determining the optical constants of read-write sliders during flying height testing", *Appl. Opt.*, Vol. 37, pp. 5116-5125, 1998.

[2] T. Ohkubo, and J. Kishigami, "Accurate measurement of gas-lubricated slider bearing separation using visible laser interferometry", *ASME Journal of Tribology*, Vol. 110 (1), pp. 148-155, 1988.

[3] C. Lacey, J. Adams, E. Ross, A. Cormier, "A new method for measuring flying height dynamically", *Phase Metrics communication*, 1992.

[4] P. de Groot, L. Deck, J. Sobbitsky, J. Biegen, "Polarization interferometer for measuring the flying height of magnetic read-write heads", *Optics Letters* Vol. 21 (6), pp. 441-443, March, 1996.

[5] M. Born, E. Wolf, *Principles of Optics*, Pergamon Press, Oxford, 1989.

[6] Y. Li; A. Menon, P. Goglia, "Evaluations of diamond-like-carbon film optical constants and their effects on flying height determination", *Trans. ASME. Journal of Tribology*, Vol. 118 (4), pp. 767-773, Oct. 1996.

[7] P. de Groot, L. Deck, J. Soobitsky, J. Biegen, "Optical flying-height testing of magnetic read-write heads", *Proceedings of the SPIE*, Vol. 2782, pp. 47-57, 1996.

Interferometry method for measuring head-disk spacing down to contact

Xinqun Liu*[a], Warwick Clegg[a], Bo Liu[b]

[a] Centre for Research in Information Storage Technology, University of Plymouth, PL4 8AA, UK.

[b] Data Storage Institute, National University of Singapore, Singapore

ABSTRACT

In this paper, we give a detailed analysis of the working principle, application limits, and potential problems of the intensity interferometry flying height testing, one of the most popularly used flying height testing techniques. Then, a phase-shift method is proposed to improve the sensitivity of this technique when the head-disk spacing is below 10 nm or near contact, based on manufacturing the glass testing disk to have a thickness within specified tolerances. Theoretical analysis and numerical evaluation are presented.

Keywords: Intensity interferometry, head-disk spacing, flying height, flying height measurement, phase-shift.

1. INTRODUCTION

With the development of the magnetic disk storage industry, the capacity of a single hard disk is getting larger and larger. While the disk size is unchanged or even getting smaller, the recording areal density increases tremendously every year. In recent years, the areal density has grown at a rate of more than 50% per year. In order to support with these developments, work has been undertaken in parallel to improve the heads, media, channel, and electronics. However, one of the most critical and effective parameters in increasing areal density is the flying height or spacing between the read-write head slider and the recording disk medium. In the past few years since 1990, flying height has been reduced from above 140 nm to under 20 nm for the leading-edge products of the magnetic recording industry. It is believed that the technology will move to 5~10 nm head-disk spacing to achieve 40 Gb/in^2 areal density by the year 2002~3.

Although it is very desirable to reduce the head-disk spacing or flying height to increase the recording areal density, head disk contact is undesirable during disk operation since that will deteriorate the tribological performance of the head disk interface and its reliability. Therefore, it is necessary to make accurate ultra-low flying height measurement both in new product development and on the manufacturing line[1,2].

2. HEAD-DISK SPACING MEASUREMENT TECHNIQUES

Different methods have been developed and utilised to measure the head-disk spacing or flying height. These can be classified into two general categories: electrical methods and optical interferometry methods. Among the electrical methods, the capacitance probe technique[3] requires that the disk head slider be modified with a conductive element to act as the probe, and as a result, the slider's dynamics may probably be changed. Another electrical method is the readback transducer method[4]. Since a variation in head-disk spacing produces a proportional variation in pulse width, by detection of the pulse width of the read transducer output, the flying height can be determined to some extent. Because these are all indirect measuring methods, other precise direct measuring methods must be used to calibrate them. Therefore their applications are limited.

* Correspondence: Email: xliu@plymouth.ac.uk ; Telephone: +44-1752-232623; Fax: +44-1752-232583.

Part of the OSJ/SPIE Conference on Optical Engineering for Sensing and Nanotechnology (ICOSN '99) • Yokohama, Japan • June 1999
SPIE Vol. 3740 • 0277-786X/99/$10.00

Optical interferometry has been the major means for measuring head/medium separation. Although Laser Doppler Interferometry (LDI) and Phase Demodulated Laser Interferometry (PDLI) can be used to determine the head-disk spacing by measuring the relative motion between the head slider and the disk[5,6], the most popular flying height testing technique used by the industry is intensity interferometry[7,8,9,10]. A schematic of an intensity interferometry flying height tester is shown in Figure 1. Its popularity is based on its accuracy, no modification to the head slider, and ability to view the complete air-bearing surface. The operating principle of this technique is straightforward: A mechanism loads the head slider onto a rotating glass disk, the light source (laser beam or monochromatic light) illuminates a measurement point on the slider, and the thin-film effect modulates the reflected light. By measuring the reflected beam's intensity, the flying height is determined. In the next part of this paper, we will give a detailed analysis of the working principle, application limits and potential problems of this intensity interferometry technique. Then, a phase-shift method is proposed to improve the sensitivity of this technique when the head-disk spacing is below 10 nm or near contact.

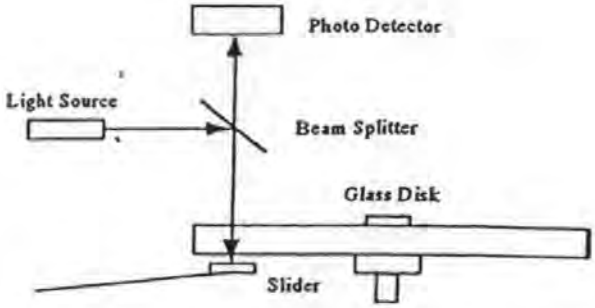

Figure 1. Schematic of an intensity interferometry flying height tester

3. THEORETICAL ANALYSIS OF INTENSITY INTERFEROMETRY

3.1. Theoretical Basis

In intensity interferometry flying height testers, a normal incidence beam is usually employed. At the slider-disk interface, the light beam experiences a multi-reflection as shown in Figure 2. In such an instance, the intensity of the interfered light reflected from the slider-disk interface is given by the standard thin-film equation[11] as below

$$I = I_0 \frac{r_{20}^2 + |r_{01}|^2 + 2r_{20}|r_{01}|\cos(\delta+\phi_s)}{1 + r_{20}^2|r_{01}|^2 + 2r_{20}|r_{01}|\cos(\delta+\phi_s)} \qquad (1)$$

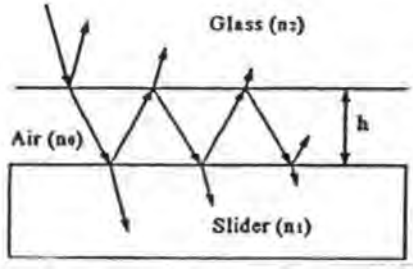

Figure 2. Beam multi-reflection at slider-disk interface

where $\delta = \frac{4\pi h}{\lambda}$, $\phi_s = \pi - \tan^{-1}\left(\frac{2n_0k_1}{n_0^2 - n_1^2 - k_1^2}\right)$, $r_{20} = \frac{n_2 - n_0}{n_2 + n_0}$, $r_{01} = \frac{n_0 - (n_1 + ik_1)}{n_0 + (n_1 + ik_1)}$, h is the flying height, λ is the light wavelength in vacuum, n_0, $(n_1 + ik_1)$, n_2 are the refractive indices of the air, slider and glass respectively, r_{20} is the reflection coefficient of the glass-air boundary, r_{01} is of the air-slider boundary, I_0 is the intensity of the incident light to the slider-disk interface, and I is the intensity of the light reflected from the slider-disk interface. Equation (1) is the theoretical basis and working principle of all modern intensity interferometry flying height testers.

3.2. Potential Problems

From the last section, we have seen that, only reflections at the slider-disk interface are considered, that is, only a single layer reflection effect is taken into account. This may not be sufficient, especially when a laser is used as the light source in which case the light's coherence length is much longer. Consider the slider and glass disk interface again in Figure 3, the glass disk is about 3 mm thick. If the coherence length of the light beam is longer

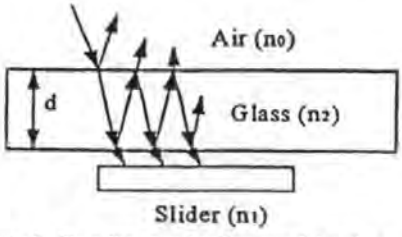

Figure 3. Two-layer reflection consideration

than a few times the double thickness of the glass disk, the two-layer reflection effect should be considered. In this case, the intensity of the returned beam from the glass disk is given as:

$$I(N) = I_0 \left| r_{02} + t_{02} t_{20} r(h) \exp(i \frac{4\pi n_2 d}{\lambda}) \sum_{m=2}^{N-2} [r_{20}{}^m r^m(h) \exp(i \cdot m \frac{4\pi n_2 d}{\lambda})] \right|^2 \quad (2)$$

where $r(h) = \dfrac{r_{20} + r_{01} \exp(i \frac{4\pi h}{\lambda})}{1 + r_{20} r_{01} \exp(i \frac{4\pi h}{\lambda})}$ is the reflectivity of the slider-disk interface according to the standard thin film equation, $r_{02} = \dfrac{n_0 - n_2}{n_0 + n_2}$, $t_{02} = \dfrac{2n_0}{n_0 + n_2}$, $t_{20} = \dfrac{2n_2}{n_0 + n_2}$, d is the thickness of the glass disk, and N is the reflection cycles the beam is assumed to have experienced between the two surfaces of the glass disk within its coherence length. From (2), we can see that the interfered beam returned from the glass disk is not only dependent on the head-disk spacing h, but also dependent on the glass disk thickness d. Figure 4 shows the plots of the intensities as functions of flying height where the glass disk thickness d is chosen to be three different values. From Figure 4, we notice that the intensity curve of the returned beam from the glass disk, when multi-reflection happens between the two glass-disk surfaces, is totally different from the one when only single layer reflection is considered. This is true especially when a laser is used as the light source, in which case the coherence length of the light beam is longer than a few times the double thickness of the glass disk. To deal with this problem, an effective way is to make an efficient anti-reflection coating at the top surface of the glass disk, so that the effect of multi-reflection between the two glass-disk surfaces can be neglected, and the single layer reflection equation (1) can be employed.

3.3. Method to Improve the Sensitivity Near Contact

From the above analysis, we conclude that the single layer reflection equation (1) can be employed to be the theoretical basis to determine the head-disk spacing if the effect of multi-layer reflections can be eliminated. From the intensity curve I_s in Figure 4, we notice that using this intensity interferometry technique, the flying height can be measured down to about 15 nm with acceptable precision. However, when the spacing is reduced to under 10 nm, the sensitivity of this intensity-based technique worsens considerably. To deal with this problem, we find that if the phase of the intensity curve is shifted, the sensitivity around the near contact area can be improved. Again from the intensity curves in Figure 4,

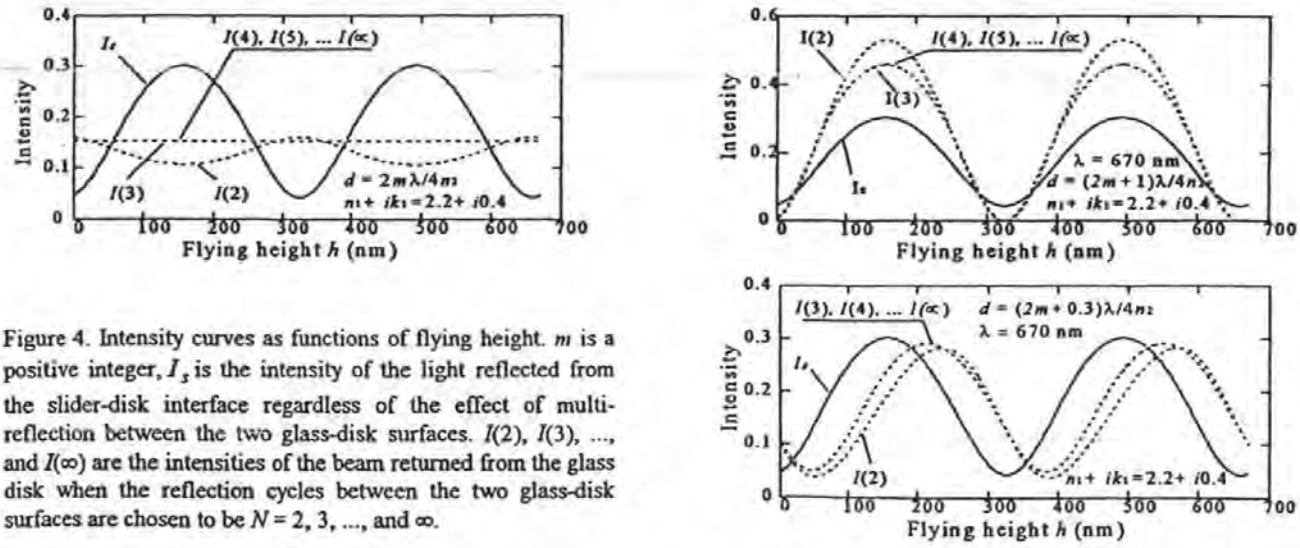

Figure 4. Intensity curves as functions of flying height. m is a positive integer, I_s is the intensity of the light reflected from the slider-disk interface regardless of the effect of multi-reflection between the two glass-disk surfaces. $I(2)$, $I(3)$, ..., and $I(\infty)$ are the intensities of the beam returned from the glass disk when the reflection cycles between the two glass-disk surfaces are chosen to be $N = 2, 3, ...,$ and ∞.

we see that the effect of the multi-reflection between the two glass-disk surfaces has already performed this function

if a light source of long coherence length, e.g., laser, is used. In fact, we find that if the glass disk is manufactured or modified to have a thickness within $\frac{\lambda}{4n_2}(2m+1.3)$ to $\frac{\lambda}{4n_2}(m+1.7)$, the intensity curve of the two-layer reflections according to (2) is advantageously phase-shifted relative to the intensity curve of the single layer reflections, and can be used to determine the head-disk spacing down to contact. This is shown in Figure 5 where the disk thickness is $\frac{\lambda}{4n_2}(2m+1.5)$. We can see from Figure 5 that when the intensity curve I_s is getting flat where the flying height is below 10 nm, the curve I_d has very good sensitivity because of its strong rate of change with flying height.

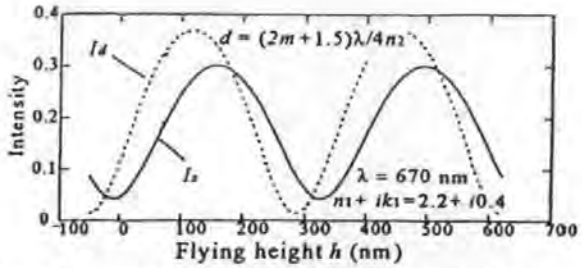

Figure 5. Intensity curve as a function of flying height. I_s is of single layer reflections, I_d is of two-layer reflections and can be used to determine the head-disk spacing down to contact.

4. CONCLUSIONS

After a detailed analysis and numerical evaluation of the intensity interferometry flying height testing technique, we find that when using light of long coherence length, e.g. laser, as the light source, an anti-reflection coating must be applied to the top surface of the glass disk to eliminate the effect of multi-reflections between the two surfaces of the glass disk. In addition, if a light source of long coherence length is employed, a specially made or modified glass disk can be used to improve the sensitivity of this technique when the flying height is down to near contact.

ACKNOWLEDGEMENTS

The support of the British Council (Singapore) in facilitating this joint research is gratefully acknowledged.

REFERENCES

1. Y. Li, and A. Menon, "Flying height measurement metrology for ultra-low spacing in rigid magnetic recording", *IEEE Transactions on Magnetics*, Vol. 32, 1, pp. 129-134, 1996.
2. P. de Groot, "Determining the optical constants of read-write sliders during flying height testing", *Appl. Opt.*, Vol. 37, pp. 5116-5125, 1998.
3. R. Sonnenfield, "Capacitance methods in head-disk interface studies", *IEEE Transactions on Magnetics*, Vol. 29, 2, pp. 247-252, 1993.
4. W. Shi, L. Zhu and D. Bogy, "Use of readback signal modulation to measure head/disk spacing variations in magnetic disk files", *IEEE Transactions on Magnetics*, Vol. 23, pp. 233-240, 1987.
5. T. Riener, A. Goding, and F. Talke, "Measurement of head/disk spacing modulation using a two channel fibre optic Laser Doppler Vibrometer, *IEEE Transactions on Magnetics*, Vol. 24, 6, pp. 2745-2747, 1988.
6. D. Veillard, S. Ganapathi, P. Smith, "Real-time tracking of the head-disk separation using laser heterodyne interferometry. part one: Instrumentation", *IEEE Transactions on Magnetics*, Vol. 29, 6, pp. 3909-3911, 1993.
7. Y. Li, A. Menon, P. Goglia, "Evaluations of diamond-like-carbon film optical constants and their effects on flying height determination", *Transactions of the ASME. Journal of Tribology*, Vol. 118, 4, pp. 767-773, 1996.
8. K. Lue, C. Lacey, and F. Talke, "Measurement of flying height with carbon overcoated sliders", *IEEE Transactions on Magnetics*, Vol. 30, 6, pp. 4167-4169, 1994.
9. C. Lacey, J. Adams, E. Ross, A. Cormier, "A new method for measuring flying height dynamically", *Phase Metrics Communication* , 1992.
10. T. Ohkubo, and J. Kishigami, "Accurate measurement of gas-lubricated slider bearing separation using visible laser interferometry", *ASME Journal of Tribology*, Vol. 110, 1, pp. 148-155, 1988.
11. M. Born, E. Wolf, *Principle of optics*, Pergamon Press, Oxford, 1989.